

Development and evaluation of a library of thiazoline-sugar based inhibitors

by

Isaac Seo

B.Sc., Simon Fraser University, 2012

Thesis Submitted in Partial Fulfillment of the
Requirements for the Degree of
Master of Science

in the
Department of Chemistry
Faculty of Science

© Isaac Seo 2017

SIMON FRASER UNIVERSITY

Spring 2017

All rights reserved.

However, in accordance with the *Copyright Act of Canada*, this work may be reproduced, without authorization, under the conditions for Fair Dealing. Therefore, limited reproduction of this work for the purposes of private study, research, education, satire, parody, criticism, review and news reporting is likely to be in accordance with the law, particularly if cited appropriately.

Approval

Name: Isaac Kippum Seo
Degree: Master of Science (Chemistry)
Title: *Development and evaluation of a library of thiazoline-sugar based inhibitors*
Examining Committee: **Chair:** Hogan Yu
Professor

David J. Vocadlo
Senior Supervisor
Professor

Andrew J. Bennet
Supervisor
Professor

Tim Storr
Supervisor
Associate Professor

Nabyl Merbouh
Supervisor
Senior Lecturer

Robert Young
Internal Examiner
Professor

Date Defended/Approved: April 20, 2017

Abstract

Cell active inhibitors of glycoside processing enzymes are valuable research tools that aid understanding the physiological roles of this diverse class of enzymes. *endo-N*-Acetylglucosaminidases have emerged as playing important roles in both mammals and human pathogens, however, metabolically stable cell active inhibitors of these enzymes are lacking. Here we describe a divergent synthetic strategy involving elaboration of a thiazoline core scaffold. We illustrate the potential of this approach by using the copper catalysed azide-alkyne click (CuAAC) reaction, in combination with a suitable catalyst to avoid poisoning by the thiazoline moiety, to generate a targeted panel of candidate inhibitors of *endo-N*-Acetylglucosaminidases and chitinases.

Acknowledgements

“Knowledge in the end is based on acknowledgement.” – Wittgenstein *On Certainty*

Prof. David Vocadlo, for his invaluable mentorship and support. I consider my time under his guidance an outstanding success if, over the past few years, I was able to glean a small fraction of his patient leadership and passion for elegant science.

Prof. Andrew Bennet, Prof. Tim Storr, and Prof. Nabyl Merbouh, for their supervisory care and thoughtful feedback. As iron sharpens iron, my committee members have given me focus and provided a model which I strive to emulate. Prof. Merbouh deserves a further personal thanks for taking me under his wing, both inside and outside of academia.

Prof. Robert Young, my internal examiner, for taking time to nurture my scientific endeavors and challenge me to reach new heights.

Prof. Yue Qian, for being my personal cheerleader and/or slave driver whenever I needed encouragement or admonishment.

Past and current members of the Vocadlo and Bennet Lab, with whom I have had the great pleasure of sharing times of excitement and disappointment. Who have seen my many character flaws, yet embraced me as a brother. Among this group of amazing people, I would like to especially thank a few who have gone above and beyond the call of duty:

Dr. Samy Cecioni, for exceptional guidance in chemical synthesis and the occasional remark on the social normative.

Dr. Yanping Zhu, for reminding me that the future of badminton is in the hands of China and for holding my hand through the tumultuous waters of molecular biology.

Dr. Dustin King, for his patience and knowledge in enzyme kinetics, hockey, and golf – only one of which I have been able to understand.

Dr. John Pal Adabala, for his friendship and aid in chemical synthesis - both having been fostered over many enjoyable beverages.

Tom Clark, for his mastery of spectroscopy and mental stimulation.

David Shen, for his scientific input and willingness to share investment ideas.

Zarina Madden, for providing molecular biology / biochemistry safety training and ensuring the maintenance of the lab.

Esther Woo, for her enthusiastic willingness to work on any task given that appropriate compensation is provided.

Table of Contents

Approval.....	ii
Abstract.....	iii
Acknowledgements.....	iv
Table of Contents.....	vi
List of Tables.....	viii
List of Figures.....	ix
List of Schemes.....	xii
Glossary.....	xiii

Chapter 1. Introduction	1
1.1. Carbohydrates and their roles in living systems.....	1
1.1.1. Carbohydrate structure and nomenclature.....	2
1.1.2. Biosynthesis of carbohydrates.....	7
1.1.3. <i>N</i> -Acetylglucosamine polysaccharides in biology.....	9
1.2. Enzymes and their biological functions.....	11
1.2.1. Methods of studying enzyme activity.....	12
1.2.2. Carbohydrate processing enzymes.....	12
1.2.3. Endo-acting <i>N</i> -acetylglucosaminidases.....	16
1.2.4. ENGase virulence factors.....	16
1.3. Enzymology.....	19
1.3.1. Michaelis-Menten kinetics.....	20
1.3.2. Enzyme inhibition.....	24
1.3.3. Inhibitors of <i>N</i> -acetylhexosaminidases.....	26
1.3.4. Approaches to develop selective inhibitors.....	27
1.3.5. Spectroscopic methods to measuring enzyme activity.....	28
1.4. Synthetic procedures in carbohydrate chemistry.....	29
1.4.1. Selective reactivity in carbohydrates.....	29
1.4.2. Synthetic challenges in thiazoline chemistry.....	31
1.5. Aims of thesis.....	32

Chapter 2. Synthesis and evaluation of a library of inhibitors for endo-acting <i>N</i>-acetylglucosaminidases	33
2.1. Contributions.....	33
2.2. Abstract.....	34
2.3. Introduction.....	35
2.3.1. The rise of antibacterial resistance.....	35
2.3.2. Targeting endo- β - <i>N</i> -acetylglucosaminidases for antivirulence.....	36
2.3.3. Endo D is an established virulence factor in <i>Streptococcus pneumoniae</i> that is required for immunal detection.....	37
2.3.4. Auto, a virulence-associated peptidoglycan hydrolase in <i>Listeria monocytogenes</i> , is required for intracellular entry.....	38
2.3.5. FlgJ is required for flagella maturation in <i>Salmonella enterica</i>	38
2.3.6. Click chemistry as a means for the rapid development of a library of inhibitors.....	39

2.4.	Results and discussion	42
2.4.1.	Design and synthesis of 4-OH modified NAG-thiazoline	42
2.4.2.	Kinetic properties and inhibition assay for Endo D	49
2.4.3.	Limitations of thiazoline-sugars inhibiting Auto and FlgJ	52
2.5.	Conclusions	53
2.6.	Experimental	54
2.6.1.	General procedures	54
2.6.2.	Synthetic procedures for chemical compounds	55
2.6.3.	Gene expression and enzyme purification	121
2.6.4.	Kinetic analysis of enzymes	122
2.6.5.	Standard analysis of water content	122
Chapter 3.	Rational design and synthesis of an inhibitor of Hex D to explore enzyme function.....	123
3.1.	Contributions	123
3.2.	Abstract	124
3.3.	Introduction.....	125
3.4.	Results and discussion	127
3.4.1.	Design and synthesis of 3-OH modified galactose-thiazoline.....	127
3.4.2.	Inhibition assays of Hex D shows loss of inhibition potential	128
3.5.	Conclusions and future prospects.....	129
3.6.	Experimental	130
3.6.1.	Synthetic procedures for chemical compounds.....	130
References	144

List of Tables

Table 2.1.	Azides used and inhibitors synthesized.....	45
Table 3.1.	K_i values of inhibitors developed for Hex D	128

List of Figures

Figure 1.1.	D-Glucose can be drawn in various ways to highlight various aspects of carbohydrate structure. Fischer projections emphasize the stereochemistry found in different sugars. Haworth projections illustrate the ring structure. Chair conformations underscore favourable conformations of sugars in solution.....	3
Figure 1.2.	Fischer projections show showing the configuratory stereocentre in determining D and L configurations of Glucose.....	3
Figure 1.3.	Nucleophilic attack of a hydroxyl at the anomeric centre from the re face (reaction towards the right to obtain the β -anomer) or si face (reaction towards the left to obtain the α -anomer).....	4
Figure 1.4.	Common hexose sugars found in biological systems.	4
Figure 1.5.	Selected symbols for illustrating saccharides.	6
Figure 1.6.	A. Cellulose is composed of β 1-4 linked glucose. B. Starch is composed of α 1-4 linked glucose. C. Glycogen is composed of α 1-4 linked glucose with α 1-6 linked branches starting new polymer chains. These three compounds are the most common forms of polymeric glucose found in nature.	8
Figure 1.7.	A. Chitin B. Chitosan These biopolymers play an important structural role in many invertebrates and insects.....	10
Figure 1.8.	Structure of peptidoglycan.....	10
Figure 1.9.	Blood group antigens found in human blood. From left to right O, A, and B blood types. The AB blood type contains both A and B antigens.	11
Figure 1.10.	Activated sugar substrates for glycosyltransferases include Leloir nucleotide phosphate sugars and non-Leloir sugar phosphate or sugar polyprenol phosphate substrates.	13
Figure 1.11.	Inverting mechanism of β -glycoside hydrolases involves an enzyme stabilized transition state resulting in inversion of stereochemistry at the anomeric position.	13
Figure 1.12.	Retaining mechanism of β -glycoside hydrolases involves the formation of a covalent enzyme substrate intermediate followed by hydrolysis, resulting in retention of stereochemistry at the anomeric position.	14
Figure 1.13.	Neighbouring <i>N</i> -acetyl group participation hydrolysis mechanism involves the nucleophilic attack of the acetamido moiety of the aminosugar, displacing the aglycon and forming an oxazoline intermediate, which is hydrolyzed by water to result in the overall retention of stereochemistry at the anomeric position.....	15

Figure 1.14.	The mechanism of substrate assisted glycoside hydrolases involves an oxazoline/oxazolinium type transition state. Pictured here is the charged oxazolinium.	15
Figure 1.15.	Structure of a glycan on the F _C portion of IgG	17
Figure 1.16.	F _C portion of an IgG illustrating the physical presence of the glycan which is needed for the antibody to adapt its proper structure.	18
Figure 1.17.	The non-linear dependence of rate on substrate concentration for an enzymatic reaction	21
Figure 1.18.	Carbohydrate based inhibitors of <i>N</i> -acetyl hexosaminidases, many of which are transition state charge and/or shape mimics.	26
Figure 1.19.	Nitrophenolic GalNAc substrates such as <i>para</i> -nitrophenyl 2-acetamido-2-deoxy galactopyranoside absorb weakly at 405 nm and only the liberated nitrophenolate absorbs strongly at this wavelength permitting the amount of product to be conveniently monitored.	28
Figure 1.20.	Dynamic mutarotation of carbohydrates.	29
Figure 1.21.	The anomeric effect can be rationalized using two different models: hyperconjugation, which stabilize the axial orbital via electron donation, or dipole minimization, which disfavours aligned dipoles.	30
Figure 1.22.	The reactivity of hydroxyl groups generally associated with aldohexopyranose sugars.	30
Figure 1.23.	Degradation pathways of thiazoline sugars.	32
Figure 2.1.	Early proposed CuAAC mechanism based on DFT calculations.	40
Figure 2.2.	Introduction of a second Cu atom lowers the transition state energy and may account for the kinetics observed in CuAAC reactions.	41
Figure 2.3.	A. The coordination of tris(triazoyl)amine ligands bind to copper during CuAAC, stabilizing the intermediate and allowing for more efficient click chemistry. B. 2-(4-((bis((1-(<i>tert</i> -butyl)-1H-1,2,3-triazol-4-yl)methyl)amino)methyl)-1H-1,2,3-triazol-1-yl)acetic acid (BTAA) is a water-soluble tris-triazoyl ligand that also maintains copper in the Cu (I) oxidation state and protects the reagents from oxidative damage during the reaction.	42
Figure 2.4.	Graph of initial velocities measured by light absorbance at 405 nm with 3F4NP-GlcNAc (2 mM) substrate versus Endo D concentration. This graph shows two distinct areas of linear activity below 100 nM and above 200 nM, which is consistent with dimerization kinetics.	51
Figure 2.5.	The pH dependence of Auto and FlgJ shows activity in acidic media.	52

Figure 3.1.	Co-crystal structure of Gal-thiazoline bound to Hex D shows a large binding pocket vicinal to the 3-OH position of Gal-thiazoline	126
Figure 3.2.	Synthesized Gal-thiazoline inhibitors of Hex D.	127

List of Schemes

Scheme 2.1.	Synthesis of 3- <i>O</i> - <i>tert</i> -butyldiphenylsilyl-6- <i>O</i> -pivaloyl-NAG-thiazoline.....	43
Scheme 2.2.	Synthesis of 4- <i>O</i> -propargyl-NAG-thiazoline via stepwise alkylation and deprotection	43
Scheme 2.3.	Synthesis of 4- <i>O</i> -propargyl-NAG-thiazoline and use of CuAAC for the rapid development of various inhibitors (See Table 2.1 for azides)	44
Scheme 2.4.	Synthesis of 4- <i>O</i> -allyl-NAG-thiazoline	45
Scheme 2.5.	Synthesis of 4- <i>O</i> -benzyl-NAG-thiazoline	45
Scheme 3.1.	Synthesis of 3-OH functionalized Gal-thiazoline.....	127

Glossary

[E]	Enzyme concentration
[ES]	Enzyme-substrate complex concentration
[P]	Product concentration
[S]	Substrate concentration
34DNP	3,4-dinitrophenol
3F4NP	3-fluoro-4-nitrophenol
3PG	3-phosphoglycerate
4MU	4-methylumbelliferone
4NP	4-nitrophenol
ATP	Adenosine triphosphate
BTTAA	2-(4-((bis((1-(<i>tert</i> -butyl)-1H-1,2,3-triazol-4-yl)methyl)amino)methyl)-1H-1,2,3-triazol-1-yl)acetic acid
CAZy	Carbohydrate active enzyme database
CD	Circular dichroism
CFG	Consortium for functional glycomics
CHES	<i>N</i> -cyclohexyl-2-aminoethanesulfonic acid
ChiA	Chitinase A
CRISPR	Clustered regularly interspaced short palindromic repeats
CSA	Camphor sulfonic acid
CuAAC	Copper-catalyzed azide-alkyne cycloaddition reaction
DCM	Dichloromethane
DDQ	2,3-Dichloro-5,6-dicyano-1,4-benzoquinone
DMF	<i>N,N'</i> -dimethylformamide
DMSO	Dimethylsulfoxide
DNA	Deoxyribonucleic acid
E	Enzyme
Endo F2	Endohexosaminidase F2; cleaves chitobiose core of biantennary mannose structures
Endo H	Endohexosaminidase H; cleaves chitobiose core of high mannose structures
EndoD	Endohexosaminidase D

ENGase	Endo- <i>N</i> -acetylglucosaminidase
ES	Enzyme-substrate complex
EtOAc	Ethyl acetate
FlgJ	Flagellar peptidoglycan hydrolase
G3P	Glyceraldehyde-3-phosphate
GalNAc	<i>N</i> -acetylgalactosamine
GH	Glycoside hydrolase
GlcNAc	<i>N</i> -acetylglucosamine
GNPNAT1	Glucosamine-phosphate <i>N</i> -acetyltransferase 1
GST	Glutathione <i>S</i> -transferase
GT	Glycosyltransferase
HEPES	2-[4-(2-hydroxyethyl)piperazin-1-yl]ethanesulfonic acid
Hex A	Hexosaminidase A
Hex B	Hexosaminidase B
Hex D	Hexosaminidase D
IC ₅₀	Half maximal inhibitory concentration
iNOS	Inducible nitric oxide synthase
IPTG	Isopropyl β-D-1-thio-galactopyranoside
k_{cat}	Catalytic constant
k_{cat}/K_M	Second-order rate constant; catalytic efficiency
K_i	Inhibitory constant; affinity of an enzyme for an inhibitor
K_M	Michaelis constant; measures enzyme affinity for substrate
LB	Lysogeny broth
MeCN	Acetonitrile
NADP ⁺ /NADPH	Nicotinamide adenine dinucleotide phosphate
NAG	<i>N</i> -acetylglucosamine
n.d.	Not determined
NagZ	<i>Escherichia coli</i> β- <i>N</i> -acetylglucosaminidase
NMR	Nuclear magnetic resonance
OGA	O-GlcNAcase β- <i>N</i> -acetylglucosaminidase
P	Product
PDB	Protein data bank
<i>p</i> TSA	<i>para</i> -Toluenesulfonic acid

qNMR	Quantitative nuclear magnetic resonance
RCSB	Research collaboratory for structural bioinformatics
RNase B	Ribonuclease B, a high mannose <i>N</i> -glycoprotein used as a positive control for endoglycosidases.
S	Substrate
SpGH85	Truncated form of Endo D, containing the catalytic residues of the hydrolase
TALEN	Transcription activator-like effector nucleases
TEA	Triethylamine
TBAF	Tetra- <i>n</i> -butylammonium fluoride
TBDPS	<i>tert</i> -butyldiphenylsilyl ether
THF	Tetrahydrofuran
TMS	Trimethylsilyl or tetramethylsilane
v	Rate of product formation
v_0	Initial rate of product formation
V_{\max}	Maximal rate of product formation

Chapter 1.

Introduction

1.1. Carbohydrates and their roles in living systems

Scientists often recognize that biological processes provide some of the most complex, yet elegantly ordered methods of accomplishing a chemical transformation. The chemistry of life itself, though immensely complicated, can be thought of as principally being governed by interactions between four major building blocks: carbohydrates, proteins, nucleic acids, and lipids. Of these four, carbohydrates are the most abundant, accounting for up to half of the world's dry biomass. Despite the widespread presence of these molecules, they are arguably the least studied of the four biological building blocks. This is due to the intrinsic complexity found in even short oligomers. To illustrate this complexity, it can be insightful to compare different forms of biological materials. Genetic information is encoded by long chains of four different monomers in DNA (Adenine, Thymine, Guanine, and Cytosine), but allows for the diversity seen in biology. Proteins, with 20 basic monomers, can account for many of the amazing functions that drives processes within the body. Though these classic biopolymers exemplify natural diversity, it would be a great mistake to sidestep the complexity presented by carbohydrates. For even a short chain composed of six basic units, the number of all linear and branched isomers is on the order of 10^{12} (Varki, 1999). Though simply a theoretical limit, this almost unfathomable number of possible permutations represent many times more complexity than what can be done using any other building block. This chapter is a concise introduction to the nature and role of carbohydrates as well as the study of enzymes responsible for their addition and cleavage.

1.1.1. Carbohydrate structure and nomenclature

The term carbohydrate describes a molecule consisting of carbon, hydrogen and oxygen. Although the morpheme 'hydrate' would imply a hydrogen-oxygen ratio of 2:1 giving an empirical formula of $(\text{CH}_2\text{O})_n$, many exceptions can be found (Varki, 1999). A common example is deoxyribose, which has the empirical formula of $\text{C}_5\text{H}_{10}\text{O}_4$ and is found in the sugar-phosphate backbone of DNA. Structurally, it is more instructive to view most biological carbohydrate units as polyhydroxy aldehydes (aldoses) or polyhydroxy ketones (ketoses) because they generally bear such a functionality that can enable their cyclization.

Saccharide, a term often used synonymously with carbohydrate, comes from the latin word *saccharum*, referring to 'sweet'. Simple sugars, or monosaccharides, are fundamental units of carbohydrates that cannot be further hydrolyzed. These compounds are typically colourless, water-soluble solids that often invoke a sweet taste when consumed. Monosaccharides can be classified by the number of carbon backbone atoms they contain: diose (2), triose (3), tetrose (4), pentose (5), hexose (6), heptose (7), and so on.

Carbohydrates can be drawn in a number of different ways as illustrated by Figure 1.1. Historically, the Fischer projection was used to draw and characterize sugars and thus, much nomenclature in carbohydrate chemistry stems from characterizations derived from the Fischer projection. The same compounds can also be drawn in Haworth projection, which allows for the visualization of the 3-dimensional structure on paper. Although the Haworth projection allowed for some representation of the 3D structure, the six membered rings do not exist in a planar form, but take the form of a chair or boat conformation. Though this chair conformation most accurately describes the innate structure of carbohydrates, Fischer and Haworth projections are sometimes used to emphasize distinct structural components such as stereocentres or ring structures (Soderberg, 2016).

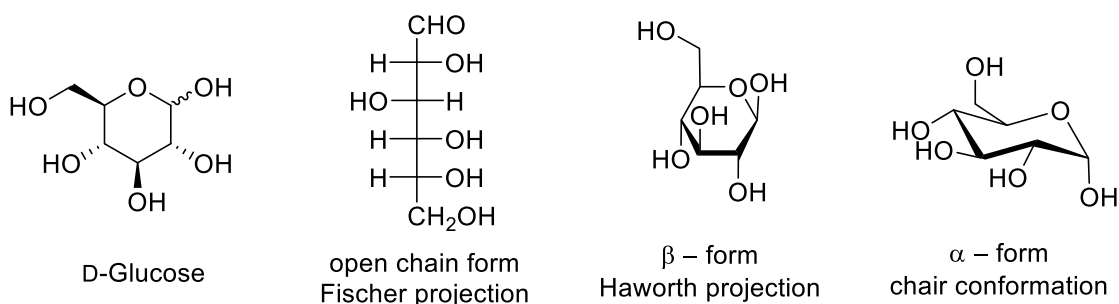


Figure 1.1. D-Glucose can be drawn in various ways to highlight various aspects of carbohydrate structure. Fischer projections emphasize the stereochemistry found in different sugars. Haworth projections illustrate the ring structure. Chair conformations underscore favourable conformations of sugars in solution.

The absolute configuration of all monosaccharides are noted as being either D or L sugars. This notation is defined by the stereocentre at the highest-numbered centre of chirality. If that centre's hydroxyl group is on the right when drawn according to the Fischer projection, it is a D-sugar. Conversely, if that centre's hydroxyl group is on the left, it is an L-sugar. The same sugar in D and L forms are enantiomers or mirror images of each other, while the configurations of other hydroxyls define the individual sugars themselves (McNaught, 1997).

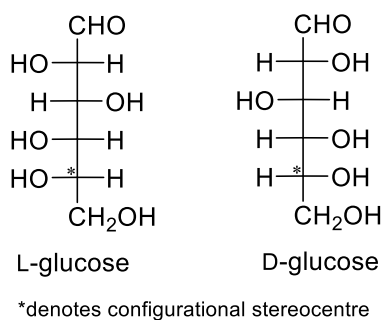


Figure 1.2. Fischer projections show showing the configurational stereocentre in determining D and L configurations of Glucose.

If the aldose or ketose contains sufficient numbers of carbon atoms in its backbone, they can cyclize to form a 6-membered ring (pyranose) or a 5-membered ring (furanose) via nucleophilic attack of a hydroxyl on either the *re* or *si* face of the carbonyl. This attack results in the formation of two possible diastereomers that are referred to as anomers in carbohydrate chemistry; the resulting hemiacetal carbon is referred to as the anomeric centre. The configuration of the anomeric centre is denoted by α - or β - in

reference to the aforementioned configurational stereocentre. If, when drawn in Fischer projection, the anomeric hydroxyl is on the same side as the oxygen of the configurational carbon, it is an α -anomer. Conversely, if the anomeric hydroxyl is on the opposite side as the oxygen of the configurational carbon when drawn in Fischer projection, it is a β -anomer (McNaught, 1997).

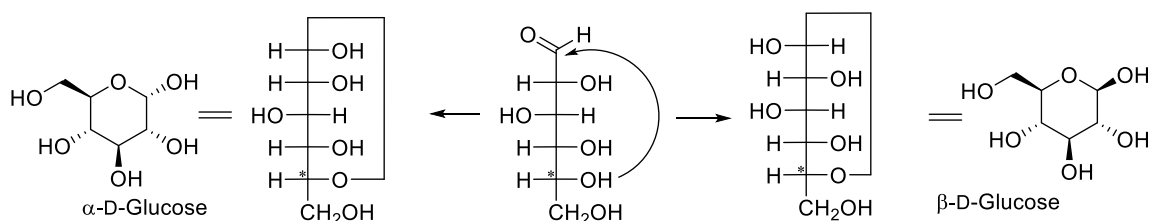


Figure 1.3. Nucleophilic attack of a hydroxyl at the anomeric centre from the re face (reaction towards the right to obtain the β -anomer) or si face (reaction towards the left to obtain the α -anomer).

The most common hexose is β -glucose, composed of exclusively equatorial hydroxyls. However, other hexoses can be made by modifying or replacing a hydroxyl group. Some of the most common monosaccharide units found in nature are shown in Figure 1.4. One particular functionality central to this thesis is that of the 2-acetamido group found in 2-acetamido-2-deoxy-D-glucopyranose (GlcNAc) and *N*-acetylgalactosamine (GalNAc).

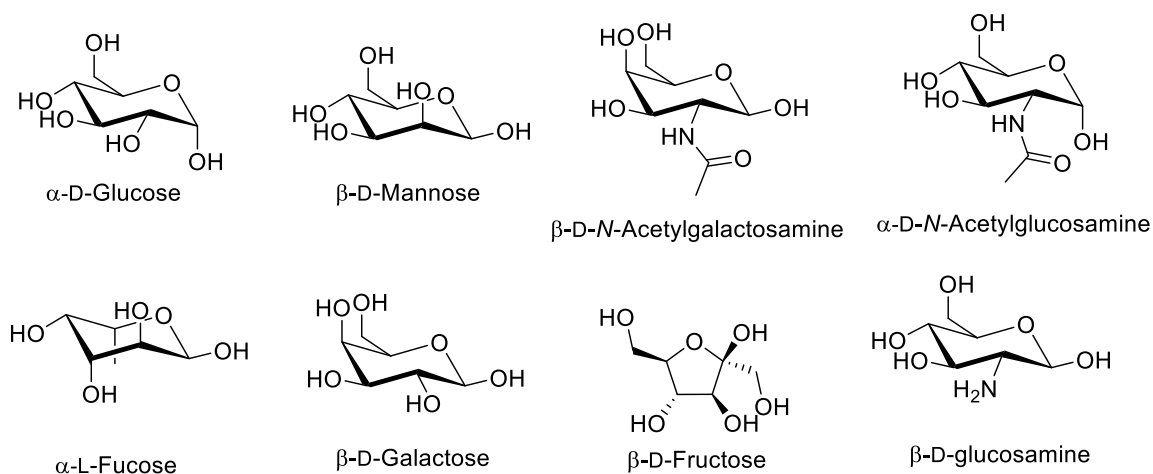


Figure 1.4. Common hexose sugars found in biological systems.

Saccharides are often classified according to the number of monosaccharides they contain. As previously mentioned, monosaccharides are the simplest forms of sugars. The

prefix di-, tri-, tetra-, and so on, are used to describe more complex carbohydrates formed by the dehydration synthesis of two hydroxyls of simpler saccharides. The term oligosaccharide is used to describe a saccharide polymer containing between 3 to 10 monosaccharide units, while the term polysaccharide is used to describe polymers of over 10 such units.

Because of the complexity inherently present in many oligosaccharides, it is sometimes desirable to use simpler symbols to illustrate common monosaccharides. The Consortium for Functional Glycomics (CFG) established a set of symbols, shown in Figure 1.5, that visually depict oligosaccharides in readily recognizable forms. Pentoses are depicted as stars, hexoses as circles, *N*-acetylhexosamines as squares, hexosamines as squares divided diagonally and acidic sugars as diamonds (Varki, 2009).

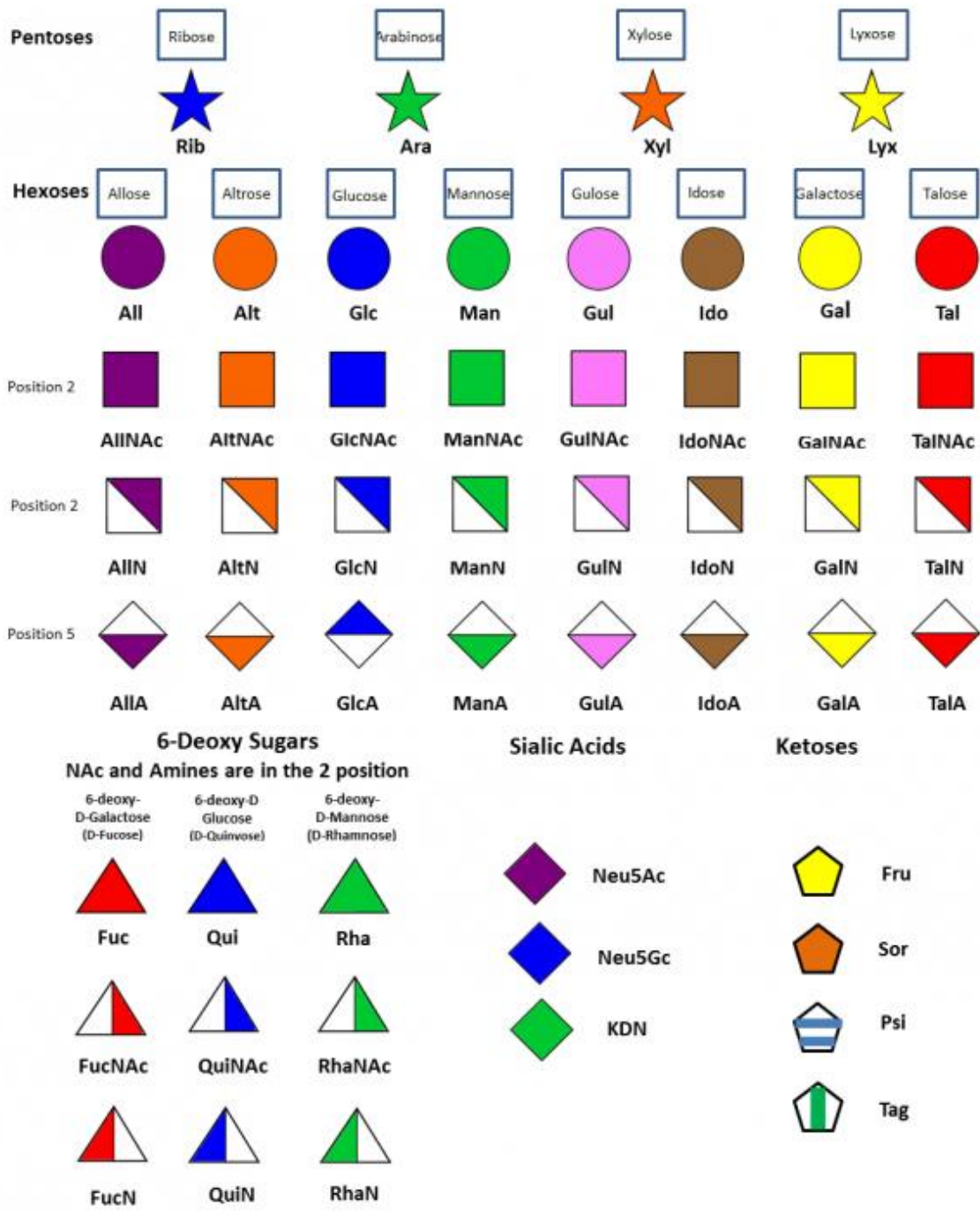


Figure 1.5. Selected symbols for illustrating saccharides.
 Developed by the CFG (Perez, 2016)

1.1.2. Biosynthesis of carbohydrates

As a prevalent type of natural organic compound, carbohydrate biosynthesis must involve ubiquitous processes. One example is found in the case of photosynthesis, where plants and some bacteria use the energy found in sunlight to activate ATP (the major source of energy utilized in biological systems) via photophosphorylation while splitting water via photolysis into oxygen, hydrogen ions, and free electrons. These ions react with NADP^+ , reducing it to NADPH. ATP and NADPH are then used to reduce CO_2 to give 3-phosphoglycerate - the main biological feedstock used in a variety of biosynthetic pathways. This process is light dependent, but all biological systems are still able to function in the absence of light. This is due to the fact that excess glyceraldehyde-3-phosphate and ATP energy can be stored in the form of glucose via gluconeogenesis. Plants are able to store large amounts of energy in the form of polysaccharides such as starch (α 1-4 linked glucose) or utilize the rigid polymer cellulose (β 1-4 linked glucose) for structural support (see Figure 1.6). Because of the polymeric nature of carbohydrates, they act as a convenient means of storing energy in biological systems. (Nelson, 2008)

Animals and other organisms do not have the ability to undergo photosynthesis and instead, digest some of these polysaccharides as rich sources of energy to convert them to elementary building blocks such as pyruvate. Pyruvate can be incorporated into a plethora of compounds, most centrally, glucose-6-phosphate, which can further be stored as glycogen, a highly branched polysaccharide of α 1-4 linked glucose with α 1-6 linked branches. The glycolysis of glucose yields pyruvate, producing a net energy excess (two molecules of ATP), and is the process all organisms use to generate energy for powering the cellular machinery (Nelson, 2008).

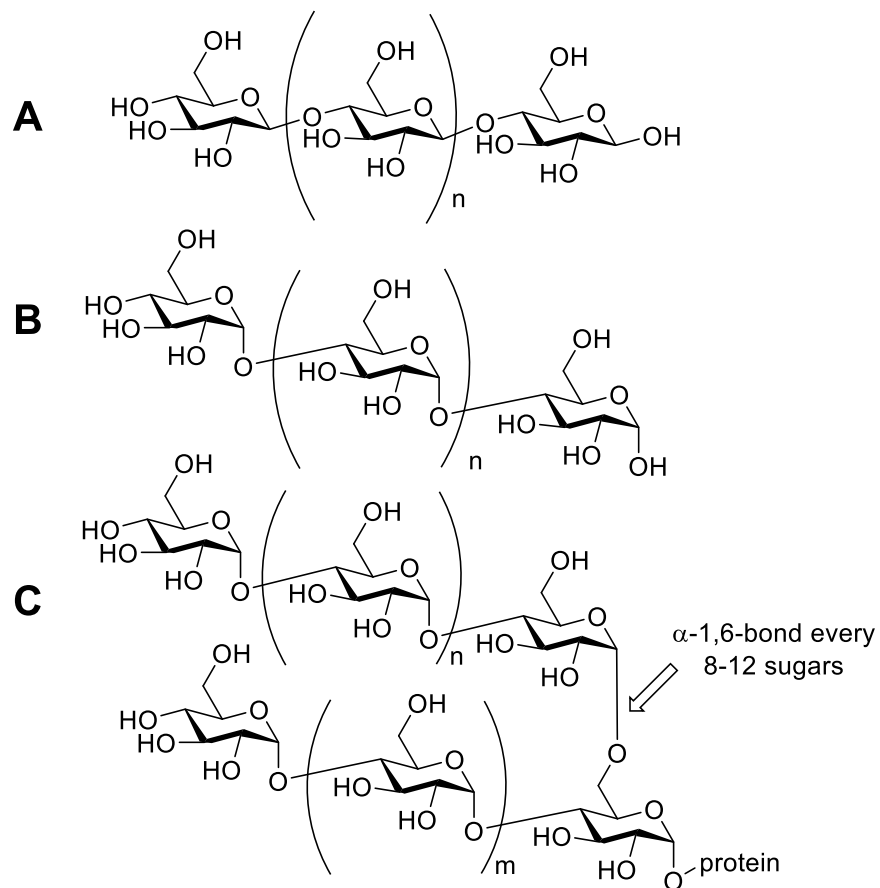


Figure 1.6. A. Cellulose is composed of β 1-4 linked glucose. B. Starch is composed of α 1-4 linked glucose. C. Glycogen is composed of α 1-4 linked glucose with α 1-6 linked branches starting new polymer chains. These three compounds are the most common forms of polymeric glucose found in nature.

The activated glucose-6-phosphate transfer to create glycogen is a prime example of the sorts of chemical group transfer reactions that are possible via the action of glycosyltransferases on non-Leloir sugar donors. Although the glycosyltransferases and sugar donors will be revisited in further detail later in this thesis, it is sufficient to say that polysaccharides and oligosaccharides are built up one unit by one unit through the transfer of one activated sugar onto a growing saccharide chain.

Though glucose may be the most prevalent sugar found in nature, modifications to the various positions gives rise to other vital sugars. One very important modification is the *N*-acetyl modification at the C2 position that results in the formation of *N*-

acetylglucosamine (GlcNAc). This is biosynthesized by the amination of fructose-6-phosphate using glutamine as the source of ammonia in the first step of the hexosamine biosynthetic pathway, followed by *N*-acetylation by glucosamine-phosphate *N*-acetyltransferase 1 (GNPNAT1) (Munkley, 2016). These sugars, with *N*-Acetyl modifications at the 2 position, will be the focus of this thesis.

1.1.3. *N*-Acetylglucosamine polysaccharides in biology

In mammals, *O*-GlcNAc and *N*-GlcNAc modifications play a vital role in various diseases, protein stability, and signaling (Bond, 2015; Hanover, 2010; Zhu, 2016). However, the vast majority of GlcNAc found in nature comes from the structural components of fungi, insects, and crustaceans. These structural components, polymers of β 1-4 linked GlcNAc known as chitin, are essential to invertebrates and affords them protection and structural rigidity. The nature of chitin, when folded back on itself to form antiparallel chains, has numerous hydrogen bonds that form an immensely strong substance, tougher than any other molecule in nature and weight-for-weight stronger than bone or steel (Merzendorfer, 2003). Chitin can be further processed by chitin deacetylases to create copolymers of GlcNAc with varying amounts of 2-amino-2-deoxy-D-glucopyranose (GlcNH₂), which is known as chitosan. The modification of chitin into chitosan is thought to make it more elastic and to also protect it from the action of hostile chitinases (Lenardon, 2010). Chitin is also known to be involved in various vectors of human disease such as mosquitoes, sand flies, ticks, and snails (Lenardon, 2010).

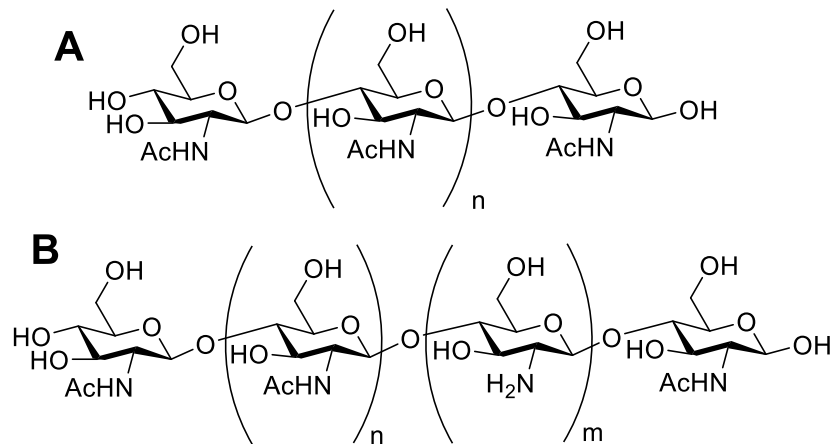


Figure 1.7. A. Chitin
B. Chitosan
These biopolymers play an important structural role in many invertebrates and insects.

The ubiquitous presence of carbohydrates is also found in prokaryotes, where peptidoglycan, a polymer consisting of β -(1-4) linked *N*-acetylglucosamine and *N*-acetylmuramic acid cross-linked with an oligopeptide, is heavily used in the cell wall. This polymer makes up 90% of the dry weight for Gram-positive bacteria and 10% for Gram-negative bacteria. Further surrounding the cell membrane in some bacteria is the glycocalyx, which consists of a polysaccharide network that aids in immune evasion and adhesion (Costerton, 1981).

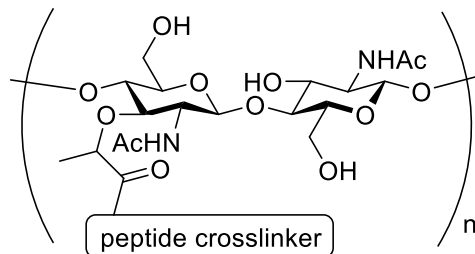


Figure 1.8. Structure of peptidoglycan

Although most forms of carbohydrates are found as polysaccharides such as starch, cellulose or chitin, many other biologically relevant oligosaccharides are synthesized and used in a number of ways that include signaling, protein folding, and adhesion (Varki, 1993). One of the best examples that highlights the importance of oligosaccharides in human biology is the case of human A/B/O blood types where the presence or absence of galactose (Gal) or *N*-acetylgalactosamine (GalNAc) on the

terminus of the antigens covering the surface of red blood cells give rises to the different blood types. These subtle differences in oligosaccharide structure being distinguished by the body underscores the importance of saccharides in biology (Berg, 2006).

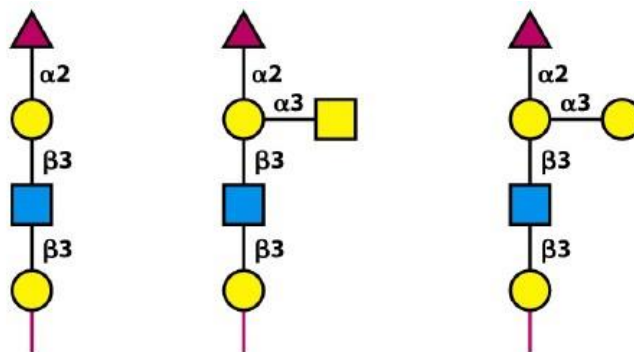


Figure 1.9. Blood group antigens found in human blood. From left to right O, A, and B blood types. The AB blood type contains both A and B antigens.

1.2. Enzymes and their biological functions

Enzymes are biological catalysts that increase the rate of specific biochemical reactions. These biomolecules catalyze such reactions by stabilizing the high-energy transition state of a reaction, typically resulting in rate increases of 10^{10} to 10^{15} fold over the uncatalyzed reaction (Schramm, 1998). In rare instances, enzyme-catalyzed reactions are so efficient that the kinetics of the reaction reaches the diffusion limit (Zhou, 1982).

Almost all biologically relevant chemical reactions require the use of an enzyme. Otherwise, most reactions would take too long, require too much energy, or release too much sudden energy to their surroundings. Because these enzymes are required for life, the dysregulation or misregulation of these enzymes can cause disease or death. Given their importance, a great deal of research has been undertaken to understand the mechanisms by which enzymes operate and develop strategies to modulate their activity (Bertozzi, 2001).

1.2.1. Methods of studying enzyme activity

Enzyme activity can be studied in a variety of different ways, including for example: genetic, crystallographic, spectroscopic and computer modeling techniques. The use of genetic knockout or knockdown techniques offer insights into specific roles that a given enzyme may play in a biological system. Additionally, site directed mutagenesis allows for the mutation of a specific amino acid residue, which may reveal catalytic mechanisms and modes of substrate or transition state binding (McCarter, 1994). More recently, clustered regularly interspaced short palindromic repeats (CRISPRs) (Yang, 2013) and transcription activator-like effector nucleases (TALENs) (Joung, 2013) have been used for *in situ* genome editing to study the roles of various proteins. Crystallographic techniques have been used to obtain 3D X-ray structures of enzymes with or without a substrate, product or inhibitor (Shi, 2014). This method can give insight into the catalytic mechanism and allow for the rational design of better inhibitors. However, such solid state X-ray structures should be used with the limitations of resolution, solvent effects, and enzyme dynamics in mind as such structures may or may not always be an accurate representation of the enzyme behaviour in solution. For studying solution dynamics, spectroscopic methods such as multidimensional NMR (Yuzwa, 2014) or circular dichroism (Greenfield, 2006) are better suited as they are able to monitor and report on changes in enzyme structure in the solution phase. Computer modelling techniques have been used to predict different protein conformations, analyze enzyme interactions and develop inhibitors (Ganem, 1996). Though all of these methods have aided understanding of enzyme function, the most prevalent and widely utilized technique is to use kinetic analysis. This technique will be further elaborated in section 1.3.

1.2.2. Carbohydrate processing enzymes

Carbohydrate processing enzymes are responsible for the addition, modification and cleavage of sugars to or from a protein, lipid or other glycan. Glycosyltransferases (GT) transfer activated sugars, such as Leloir nucleotide sugars or non-Leloir phosphates (Figure 1.10), onto a nucleophilic glycosyl acceptor molecule. Glycoside hydrolases (GH) act to reverse the action of glycosyltransferases, taking a glycoside modified substrate

and hydrolyzing the glycosidic bond (Shaikh, 2008; Love, 2005). Both GTs and GHs (by nature of their reversibility) are also utilized in synthesis of various oligosaccharides or glycoproteins (Vocadlo, 2008).

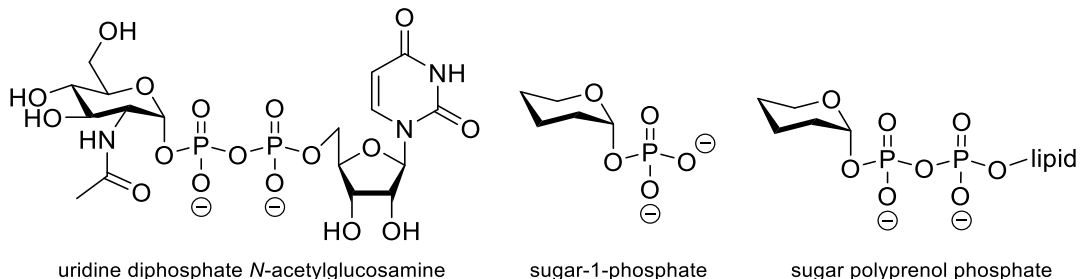


Figure 1.10. Activated sugar substrates for glycosyltransferases include Leloir nucleotide phosphate sugars and non-Leloir sugar phosphate or sugar polyprenol phosphate substrates.

Glycoside hydrolases can be categorized based on the stereospecificity of the hydrolysis product. Inverting glycoside hydrolases utilize two enzymatic residues that allows for the nucleophilic attack of water at the anomeric position, thereby resulting in the overall inversion of stereochemistry at the anomeric position (Figure 1.11). Retaining glycoside hydrolases hydrolyze glycosidic bonds with overall retention of stereochemistry at the anomeric position. This is typically achieved through a two-step mechanism involving the formation of a glycosyl enzyme intermediate (Figure 1.12).

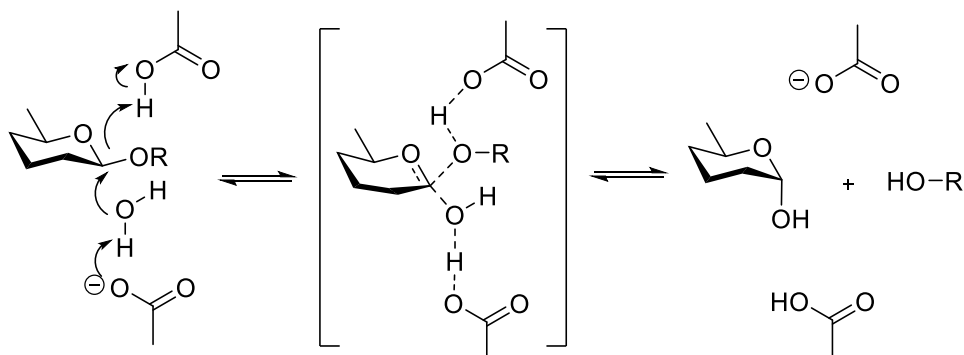


Figure 1.11. Inverting mechanism of β -glycoside hydrolases involves an enzyme stabilized transition state resulting in inversion of stereochemistry at the anomeric position.

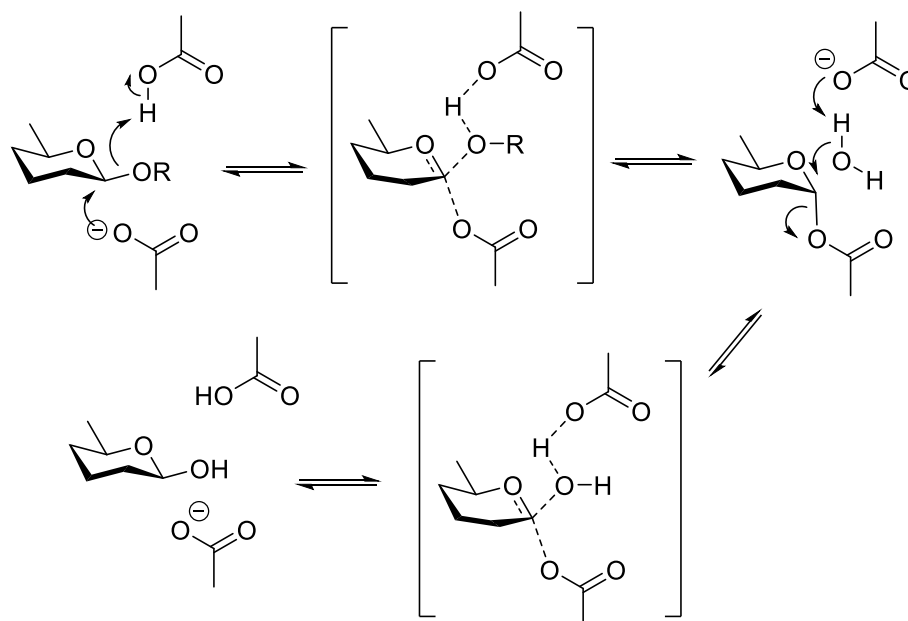


Figure 1.12. Retaining mechanism of β -glycoside hydrolases involves the formation of a covalent enzyme substrate intermediate followed by hydrolysis, resulting in retention of stereochemistry at the anomeric position.

It is to be noted that the first-formed hemiacetal product of both retaining and inverting glycoside hydrolases will mutarotate to form a mixture of diastereomers, the case of which depends on a number of factors including the anomeric effect (described in detail in section 1.4.1). Observation by NMR spectroscopy of the stereochemical outcome can be used to gain insights into the retaining or inverting nature of the enzyme mechanism.

An alternative mechanism resulting in retention of stereochemistry is used by some β -*N*-acetylhexosaminidases, where the *N*-acetyl group is involved as shown in Figure 1.13.

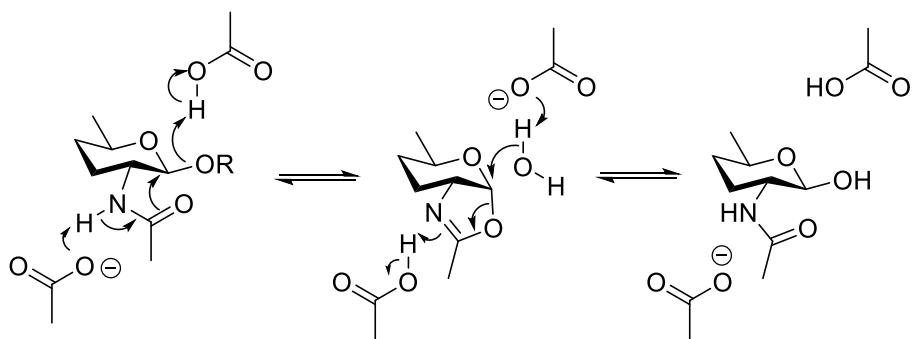


Figure 1.13. Neighbouring *N*-acetyl group participation hydrolysis mechanism involves the nucleophilic attack of the acetamido moiety of the aminosugar, displacing the aglycon and forming an oxazoline intermediate, which is hydrolyzed by water to result in the overall retention of stereochemistry at the anomeric position.

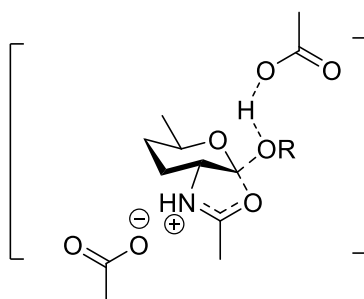


Figure 1.14. The mechanism of substrate assisted glycoside hydrolases involves an oxazoline/oxazolinium type transition state. Pictured here is the charged oxazolinium.

This mechanism involves the formation of an oxazoline intermediate (Figure 1.14) that is hydrolyzed by the near microscopic reverse of the first step and results in the overall conservation of stereochemistry at the anomeric position. Not all β -*N*-acetyl hexosaminidases use this mechanism. For example, the Carbohydrate Active enZyme (CAZy) database outlines glycoside hydrolase family 3 and 22 that utilizes a double displacement mechanism (Vocadlo, 2005), while family 19 utilizes an inverting mechanism (Iseli, 1996). However, this substrate assisted catalysis mechanism has been proven for glycoside hydrolase family 18, 20, 25, 56, 73, 84 and 85 enzymes (Mark, 2001; Macauley, 2005; Terwisscha van Sheltinga, 1995).

1.2.3. Endo-acting *N*-acetylglucosaminidases

Endo-acting *N*-acetylglucosaminidases (ENGases) are glycoside hydrolases that cleave an internal glycosidic bond of an oligosaccharide or polysaccharide. This is in contrast to exo-acting glucosaminidases that only cleave the terminal saccharide off of an oligosaccharide or protein. Many of these endo-acting glucosaminidases have important roles in degrading chitin in insects and fungi, or as virulence factors in pathogenic bacteria. In humans, exo-acting glucosaminidases have been shown to play an important role in several physiological processes. Misregulation of these processes is implicated in diseases. Though some ENGase substrates such as chitin does not exist in humans, chitinases are present in the human genome and is induced in asthma (Zhu, 2004).

1.2.4. ENGase virulence factors

Many endo-acting hexosaminidases are established bacterial virulence factors. Auto, an enzyme from *Listeria monocytogenes* (a intracellular bacteria) digests peptidoglycan and is involved in the initial entry into a host cell. When genetic knockout studies were used to silence Auto, the pathogen had low *in vivo* invasiveness in mice (Bublitz, 2009; Cabanes, 2004). A *Listeria monocytogenes* chitinase (ChiA) is involved in downregulating inducible nitric oxide synthase (iNOS) and connected to the suppression of host innate immunity, suggesting a link between chitinases and pathogenesis (Chandhuri, 2013). Endohexosaminidase D (EndoD) from *Streptococcus pneumoniae* is responsible for cleaving the glycan on immunoglobulins, thereby compromising its detection by the adaptive immune system (Abbott, 2009; Fang, 2016; Anthony, 2010, 2011 & 2012). Peptidoglycan hydrolase FlgJ (FlgJ) from *Salmonella enterica* is involved in digesting the peptidoglycan cell wall near the flagellum, which is required to exert the flagellum (Herlihey, 2014; Nambu, 1999). The structures of the substrates of some of these enzymes are illustrated in Figures 1.8 and 1.15. These enzymes will be discussed in further detail in Section 2.3.

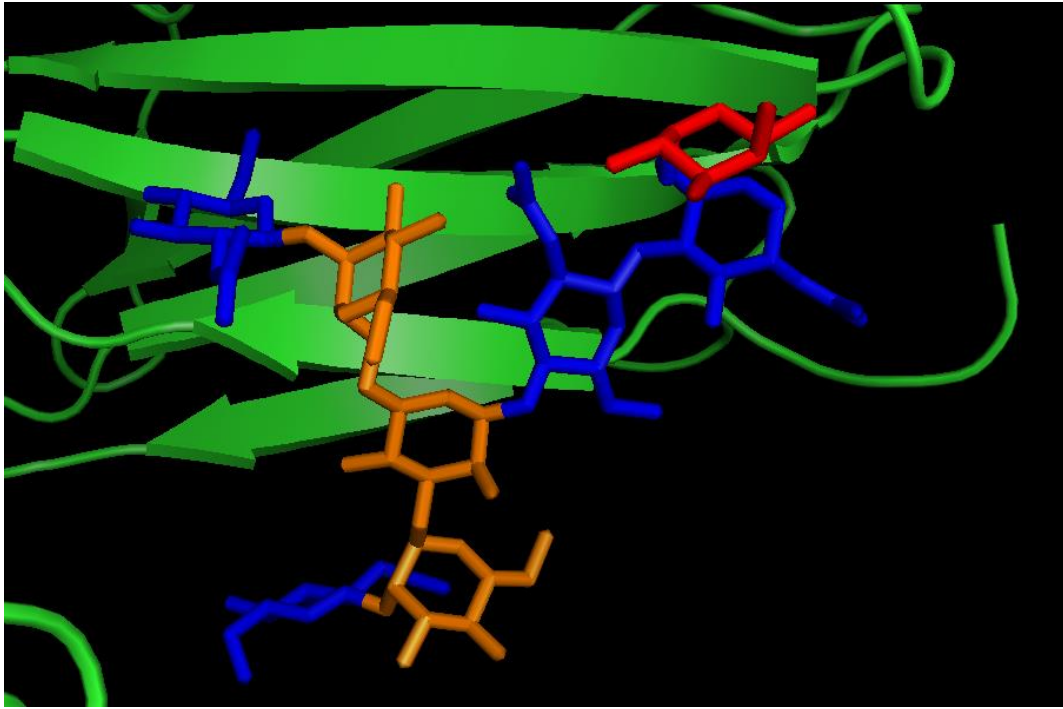


Figure 1.15. Structure of a glycan on the F_c portion of IgG

Accessed from the Research Collaboratory for Structural Bioinformatics (RCSB) protein data bank (PDB) structure 3AVE (Fang, 2016)

Protein shown as a ribbon in green

GlcNAc shown as stick form in blue

Man shown as stick form in orange

Fuc shown as stick form in red



Figure 1.16. Fc portion of an IgG illustrating the physical presence of the glycan which is needed for the antibody to adapt its proper structure.

Accessed from RCSB PDB structure 3AVE (Fang, 2016)

Protein shown as a ribbon in green

Glycans shown as stick form in yellow

As strains of antibiotic resistant bacteria become more prevalent in modern society, treating of bacterial infections is becoming increasingly difficult (Reardon, 2014). It is theorized that resistance arises through a number of different possible mechanisms, but they all arise from the huge selective pressure imparted by having a drug target being a factor essential for survival. One method of relieving much of that pressure is to target non-essential virulence factors (Beckham, 2014). This is an attractive strategy since the virulence inhibitor does not hinder bacterial proliferation, but only affects either bacterial invasion or persistence within the host. Much research in this field is being pursued and we can eagerly look forward to future anti-virulence therapeutics adept at combating antibiotic resistant bacterial strains, arising from these efforts (Guo, 2015; Seeberger, 2014). This topic will be revisited in further detail in section 2.3.

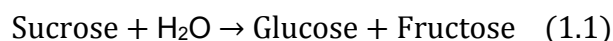
1.3. Enzymology

Although a variety of enzyme assays have been developed to allow for the study of different types of enzymes under numerous conditions, they all share the need for changes in the levels of products or substrates being readily measured. The most commonly used reporters include fluorescent substrates, which allows for the study of enzyme kinetics via continuous assays, typically with low background levels. Further structural modifications to the enzyme (via site directed mutagenesis) or using synthetic substrates or inhibitors can give insights into enzyme mechanisms (Çetinbaş, 2006, Abbott, 2009, Alteen, 2016). Special attention will be given to kinetic behavior as first described by Leonor Michaelis and Maude Menten.

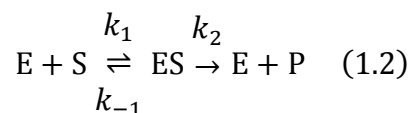
1.3.1. Michaelis-Menten kinetics

Kinetics is a field of chemistry involved with the study of reaction rates. In its simplest form, reaction rates for an elementary step are proportional to the concentration of reactants to the power of its reaction order - the overall reaction rate generally being equal to the slowest, or rate determining step. With the addition of an enzyme, the mechanism and kinetics for a reaction change drastically.

One of the first scientists to formalize this study of enzyme kinetics was Adrian Brown in 1902, who investigated the rate of hydrolysis of sucrose (refined table sugar, a disaccharide composed of glucose and fructose) into the monosaccharides glucose and fructose catalyzed by β -fructofuranosidase (Brown, 1902).



Brown noted that when the concentration of sucrose was much higher than the enzyme concentration, the overall reaction rate became independent of the sucrose concentration. Thus, he proposed the combining of free enzyme (E) and substrate (S) to form an enzyme substrate complex (ES) that can either dissociate back to regenerate free enzyme and substrate (governed by rate constant k_{-1}), or react to form the product (P) and free enzyme (governed by rate constant k_2). In this scheme shown in equation 1.2, the overall initial rate of formation (v_0) is governed by the product of a rate constant (k_2) and concentration of the enzyme substrate complex ([ES]).



$$v_0 = \frac{d[\text{P}]}{dt} = k_2[\text{ES}] \quad (1.3)$$

Equation 1.3 would explain the overall rate of sucrose hydrolysis by β -fructofuranosidase being essentially independent of changes in sucrose concentration when large. Alternatively, when the concentration of substrate is much less than that of enzyme, one can envision a state where not all enzyme is bound to form an enzyme

substrate complex and an increase in substrate influences the concentration of the complex. Thus, the initial velocity, v_0 , appears to be dependent on the concentration of substrate in a first order manner. This relationship is illustrated graphically in Figure 1.17.

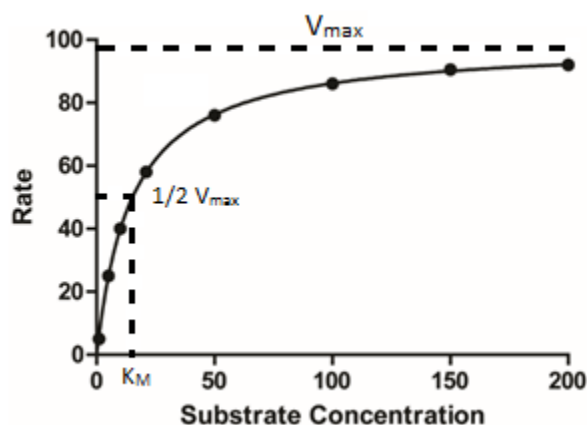


Figure 1.17. The non-linear dependence of rate on substrate concentration for an enzymatic reaction

The overall rate of production of the enzyme substrate complex can be defined as:

$$\frac{d[ES]}{dt} = k_1[E][S] - k_{-1}[ES] - k_2[ES] \quad (1.4)$$

This equation however, cannot be integrated unless two simplifying assumptions are made: that E and S are in rapid equilibrium with the ES complex and that the rate of formation of the ES complex is exactly matched by its rate of breakdown. Many of these kinetics were rigorously studied by Michaelis and Menten (Michaelis, 1913, translated into English by Johnson, 2011). This assumption is known as the steady state assumption and is mathematically illustrated by Equation 1.5. To be of experimental use, kinetic expressions must be formulated in terms of experimentally measurable quantities. The quantities [E] and [ES] are not directly measurable, but the total concentration of enzyme $[E]_T$ is equal to the sum of [E] and [ES].

$$\frac{d[ES]}{dt} = 0 \quad (1.5)$$

$$[E]_T = [E] + [ES] \quad (1.6)$$

Combining (1.4), (1.5) and (1.6), the rate equation for enzymatic reactions where such assumptions hold true can be derived (1.7).

$$k_1([E]_T - [ES])[S] = (k_{-1} + k_2)[ES] \quad (1.7)$$

Upon rearrangement and solving for [ES], equation (1.8) defines [ES] in measurable quantities where K_M , the Michaelis constant for a reaction, is defined by equation (1.9). K_M can be viewed under certain conditions as an equilibrium constant that can reflect the affinity of an enzyme for its substrate. The smaller the K_M value, the higher the affinity of the enzyme for its substrate.

$$[ES] = \frac{[E]_T[S]}{K_M + [S]} \quad (1.8)$$

$$K_M = \frac{k_{-1} + k_2}{k_1} \quad (1.9)$$

Substituting our expression for unmeasurable [ES] using measurable factors (1.8) into the original rate expression (1.3), a rate equation governed by enzyme and substrate concentrations can be derived (1.10).

$$v = \frac{d[P]}{dt} = k_2[ES] = \frac{k_2[E]_T[S]}{K_M + [S]} \quad (1.10)$$

$$[S] \gg K_M \quad v_0 = V_{max} = k_2[E]_T = k_{cat}[E]_T \quad (1.11)$$

$$v_0 = \frac{V_{max}[S]}{K_M + [S]} \quad (1.12)$$

$$K_M \gg [S] \quad v_0 = \frac{k_2[E]_T[S]}{K_M} \quad (1.13)$$

As the value of [S] reaches infinity, the rate asymptotically approaches a maximum value mathematically reduced to (1.11) as K_M becomes negligible. As this rate represents the maximum rate of the enzyme catalyzed reaction, this maximal rate is given the designation of V_{max} and equation (1.10) can also be written in terms of V_{max} to give (1.12),

which is called the Michaelis-Menten equation. Conversely, if K_M is much greater than $[S]$, equation (1.10) approximates to (1.13). Again, these equations fit the first order dependence on substrate when $[S]$ is low, and zero order dependence when $[S]$ is high (illustrated in Figure 1.17). These equations are best used when measuring initial rates, where there is an absence of complicating factors such as product inhibition, reversible reactions, and progressive inactivation of the enzyme.

The Michaelis-Menten equation is the basic equation used to describe most standard cases of enzyme kinetics. According to this equation, when $K_M = [S]$, then $v = V_{max}/2$. Thus, K_M is also be defined as the substrate concentration at which the rate of the reaction is half of the maximum. It follows that enzymes having small K_M values achieves maximal catalytic efficiency at lower substrate concentrations than do enzymes with higher K_M values.

Although the arguably simplest method to find the Michaelis constant is to find the substrate concentration at one half of V_{max} , a number of complications may arise. We have established that at very high substrate concentrations, the initial reaction rate asymptotically approaches V_{max} . In practice, it is often difficult to accurately assess V_{max} as very high substrate concentrations are sometimes limited by substrate solubility or availability. An alternative approach was proposed by Hans Lineweaver and Dean Burke using equation (1.14), the reciprocal form of the Michaelis-Menten equation (Lineweaver, 1934).

$$\frac{1}{v_0} = \left(\frac{K_M}{V_{max}}\right) \frac{1}{[S]} + \frac{1}{V_{max}} \quad (1.14)$$

Using (1.14), a plot of $1/v_0$ vs $1/[S]$ can be graphed where the slope is equal to K_M/V_{max} , the Y-intercept is equal to $1/V_{max}$ and the extrapolated X-intercept is equal to $-1/K_M$. This type of plot is referred to as a Lineweaver-Burke plot or a double-reciprocal plot. However, this method also has a number of disadvantages: the requirement for a number of experiments that require relatively high levels of $[S]$ leads to data points crowding the left side of the graph, small errors in v_0 for smaller values of $[S]$ will lead to larger errors when taking the reciprocal of the value, and gives unequal weighting in the range of substrate concentration or reaction rate (Dowd, 1965). Although this plot still

remains as an efficient means of graphically presenting data, linear regression methods have largely been superseded by computer generated nonlinear regression models directly analyzing Michaelis-Menten plots (Dixon, 1953; Wilkinson, 1961).

In the Michaelis-Menten model, the rate constant in (1.11) is referred to as the catalytic constant, k_{cat} . Using this term in the Michaelis-Menten equation (1.12) at very low [S] and assuming very low steady state levels of [ES], the initial rate simplifies to (1.15).

$$v_0 \approx \left(\frac{k_{cat}}{K_M} \right) [E][S] \quad (1.15)$$

The term k_{cat}/K_M is known as the second-order rate constant and defines the catalytic efficiency of the enzyme. It is an apparent second-order rate constant for the simplified reaction $E + S \rightarrow E + P$.

1.3.2. Enzyme inhibition

Developing enzyme inhibitors is a useful way to study the effect a particular enzyme has on a given biological system. At the outset, the answers to questions regarding the physiological roles of enzymes may seem to be readily discerned by using either pharmacological inhibitors or genetic manipulation. However, even in the absence of off-target effects of inhibitors, the cellular consequences of eliminating an enzyme may not be the same as inhibiting catalytic activity (Weiss, 2007). Many enzymes are known to participate in protein-protein interactions and removing a given enzyme may influence cell function through many pathways. Only by demonstration of a consistent cellular phenotype when using both genetic methods and selective small molecule inhibition can one conclude a causal relationship exists between a given enzyme and the observed phenotype.

The potency of enzyme inhibitors are usually reported as IC_{50} or K_i values. An IC_{50} value indicates the concentration of inhibitor required to reduce the activity of an enzyme to half of its activity using a standard assay. In practice, IC_{50} values are most commonly reported when comparing similar types of inhibitors, such as inhibitors having the same

scaffold. IC_{50} values are often used when assaying many inhibitors because they only require one constant substrate concentration, with varying concentrations of inhibitor, and data is therefore easier to collect. One major drawback in comparing different IC_{50} values drawn from the literature stems from the fact that IC_{50} values differ depending on the substrate concentration used. K_i values, on the other hand, describe the dissociation of the inhibitor bound enzyme complex and requires multiple kinetic measurements in a range of substrate concentrations against one concentration of inhibitor - repeated multiple times with different amounts of inhibitor added (Burlingham, 2003). This information is pooled and K_i is determined by non-linear regression to determine both the K_i value and the mode of inhibition (competitive, uncompetitive, non-competitive, or mixed). The relationship between K_i and IC_{50} for competitive inhibitors can be described mathematically by the Cheng-Prusoff relationship given in equation (1.16).

$$IC_{50} = K_i \left(1 + \frac{[S]}{K_M} \right) \quad (1.16)$$

Although Cheng and Prusoff also described relationships between K_i and IC_{50} values for other modes of inhibition (non-competitive, uncompetitive, and mixed inhibition; Cheng 1973), previous work has demonstrated that the inhibitors used in this research bind to the enzymes of interest in a competitive manner.

Given the importance of enzyme inhibitors, there are many approaches to developing, finding or enhancing inhibitors. Strategies for high-throughput screening and structure-activity relationships are well documented and many excellent reviews exist (Gloster, 2012; Csermely, 2013; Harvey, 2015). Complementary to such strategies is to develop inhibitors through rational design, which draws insight from an understanding of the structure and function of a given enzymatic process.

1.3.3. Inhibitors of *N*-acetylhexosaminidases

Because of the critical role of *N*-acetylhexosaminidases in a variety of physiological and pathological processes, a variety of carbohydrate based inhibitors have been developed, a sample of which are shown here (Figure 1.18). These inhibitors can be charge and/or shape mimics of either the oxocarbenium ion-like transition state or the oxazoline intermediate (Gloster, 2010; Dorfmueller, 2006; Whitworth, 2007; Lenzen, 2008; Cekic, 2016).

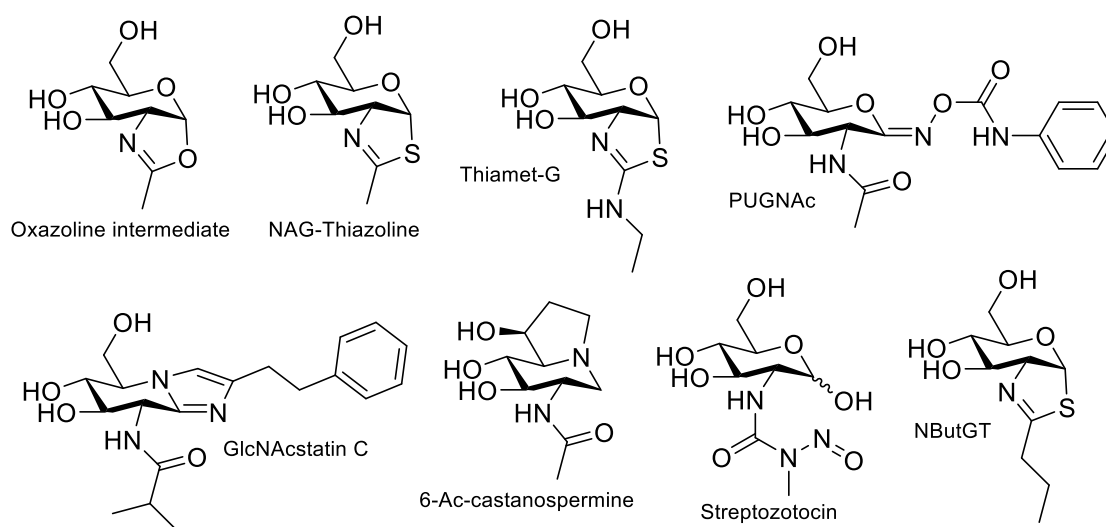


Figure 1.18. Carbohydrate based inhibitors of *N*-acetyl hexosaminidases, many of which are transition state charge and/or shape mimics.

Such classes of inhibitors, often termed transition state analogs, are of particular interest because transition state analogs are exceptionally potent – binding to enzymes much more tightly than the natural substrate. This is possible because enzymes catalyze a reaction by binding and stabilizing the high energy transition state. Such inhibitors were first proposed by Linus Pauling, and have since been validated several times (Lillelund, 2002).

Several transition state analogues have been developed that inhibit hexosaminidases (Figure 1.18). NAG-Thiazoline is a synthetic sugar that effectively

mimics the oxazoline-type transition state (Whitworth, 2007). The longer carbon-sulfur bond of NAG-Thiazoline mimics the carbon-oxygen bond formation found on the way to the oxazoline/oxazolinium intermediate; the more polarized electronic distribution associated with the less electronegative sulfur also is proposed to mimic the charged oxazolinium (Whitworth, 2007).

1.3.4. Approaches to develop selective inhibitors

Because of the wide range of *N*-acetylhexosaminidases that use substrate assisted catalysis, NAG-thiazoline is a non-selective inhibitor of many *N*-acetylglucosaminidases. The promiscuity of NAG-thiazoline towards numerous enzymes makes it difficult to study the specific biological role of one particular enzyme. Thus, the development of selective hexosaminidase inhibitors is necessary to further our understanding of these enzymes' function *in vivo* and in cells.

Selective inhibition of specific enzymes can be achieved based on subtle structural differences between hexosaminidase isoforms. Modifications at the 2' position of NAG-thiazoline have been explored extensively by Vocadlo *et al.* resulting in the development of NButGT, Thiamet-G and related compounds (Yuzwa, 2008; Cekic, 2016). These compounds are selective inhibitors of OGA over lysosomal HexA and HexB enzymes (Yuzwa, 2008; Macauley, 2010; Kong, 2015). The selectivity in this case is attributed to the availability of a deeper pocket in the active site of OGA. Thiamet-G was found to be even more potent because of the exocyclic amine, which increases its basicity making it protonated at physiological pH and able to form an ion-pair in the active site (Vocadlo, 2012; Cekic, 2016).

Similarly, modification of the 6 position has been studied by Kren *et al.* with particular emphasis on triazole linked dimers aimed at targeting potential multivalency effects, but these compounds showed weak inhibition towards multiple *N*-acetylhexosaminidases (Krenjzova, 2014).

The work presented in this thesis presents my work in developing thiazoline-sugar based inhibitors with modifications at the 3 and 4 positions. Towards this goal, various protecting groups and the inherent reactivity of the hydroxyl groups of hexoses were used to synthesize parent compounds which may be further derivatized to form a library of compounds to be screened as potential inhibitors.

1.3.5. Spectroscopic methods to measuring enzyme activity

The use of continuous spectrophotometric assays in testing inhibition of enzymes by inhibitors is a standard procedure that is easily performed by using a chromogenic or fluorogenic substrate (Eisenthal, 2002). Nitrophenol based substrates have commonly been used to measure enzyme activity and inhibition (Yagi, 1989, Alteen, 2016, & Abbott, 2009). These substrates exploit the different spectroscopic properties of nitrophenolates as compared to the intact ethers (Figure 1.19). Enzymatic reactions using such substrates can be monitored by a spectrophotometer and the absorbance measurements can give insights into the aforementioned kinetic properties of enzymes.

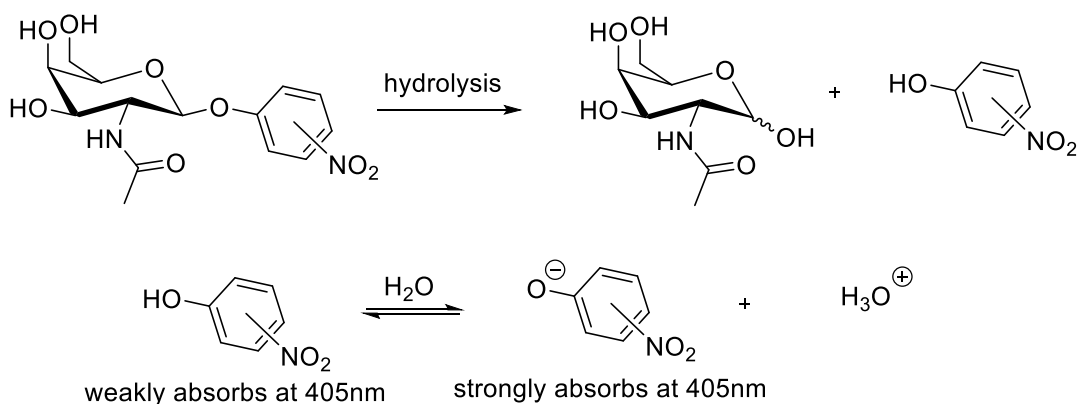


Figure 1.19. Nitrophenolic GalNAc substrates such as *para*-nitrophenyl 2-acetamido-2-deoxy galactopyranoside absorb weakly at 405 nm and only the liberated nitrophenolate absorbs strongly at this wavelength permitting the amount of product to be conveniently monitored.

1.4. Synthetic procedures in carbohydrate chemistry

The synthesis of mono- and oligosaccharide derivatives presents many synthetic challenges due to the inherent structural properties of carbohydrates. The chemical environment surrounding each hydroxyl group, and the inherent differences in reactivity depends on the specific monosaccharide, which can make such chemistry challenging.

1.4.1. Selective reactivity in carbohydrates

Carbohydrates in solution are known to mutarotate to form the acyclic open chain form which then cyclizes to form the opposite anomer (Figure 1.20). This process leads to a mixture of anomers dictated by the stability of the equatorial and axial positions of the anomeric hydroxyl group. The stability of equatorial versus axial hydroxyls at the anomeric position draws on steric 1,3-diaxial interactions as well as the stereoelectronic anomeric effect, which explains the stability of the axial anomeric hydroxyl (Romers, 1969). The exact basis of the anomeric effect is still unclear, but is generally explained using hyperconjugation and dipole minimization models (Figure 1.21)

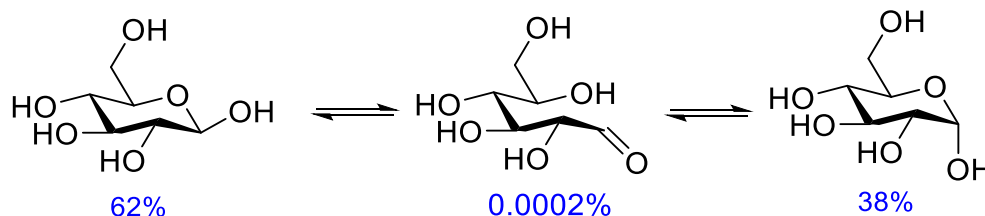


Figure 1.20. Dynamic mutarotation of carbohydrates.

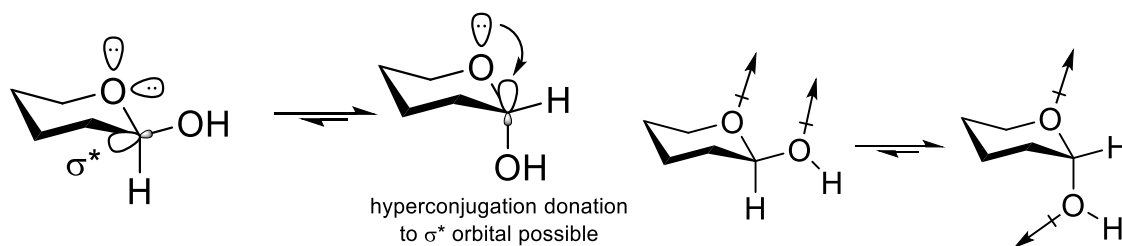


Figure 1.21. The anomeric effect can be rationalized using two different models: hyperconjugation, which stabilize the axial orbital via electron donation, or dipole minimization, which disfavours aligned dipoles.

The presence of multiple hydroxyl groups in carbohydrates requires special attention being dedicated to selective protection. Numerous methods have been developed to allow for selective protection and manipulation of carbohydrate hydroxyls based on the intrinsic reactivity of each hydroxyl. In general, the reactivity of hydroxyl groups is illustrated in Figure 1.22.

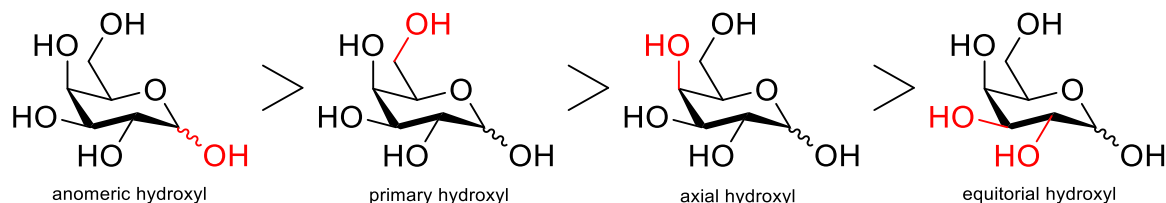


Figure 1.22. The reactivity of hydroxyl groups generally associated with aldohexopyranose sugars.

Common alcohol protecting groups include esters, ethers and silyl ethers (Wuts, 2006). Esters, such as acetates or benzoates are among the most common protecting groups; they are installed in mild, neutral conditions, and are cleaved using basic or acidic conditions. However, smaller esters are known to migrate easily. Ethers such as benzyl ethers are typically installed via nucleophilic displacement of the halide of corresponding benzyl halides using an alkoxide. These ethers are typically reductively cleaved using hydrogenolysis or DDQ. Various silyl ethers were developed to be stable towards a wide

range of conditions by having different alkyl or phenyl groups attached to the silicon atom. Trimethylsilyl (TMS) ethers are the most labile of the silyl ethers, while *tert*-butyldiphenylsilyl ethers are relatively stable in a great deal of conditions. All silyl ethers are readily cleaved using a source of fluoride ions.

It is particularly efficient to utilize diol protecting groups that can selectively protect two nearby hydroxyls (Wuts, 2006). Benzylidene type protecting groups are efficient at selectively protecting the 4 and 6 hydroxyl positions of a hexose by forming a new 6 membered ring. A further advantage of such protecting groups is the established methods of selective ring opening by using various reducing agents with or without a coordinating Lewis acid to yield a single free hydroxyl in a regioselective manner.

1.4.2. Synthetic challenges in thiazoline chemistry

The sensitivity of thiazolines towards acidic, reductive or oxidative conditions limits much of the chemistry that can be done to these compounds. Figure 1.23 illustrates many of the possible degradation pathways that thiazolines may undergo. Thiazolines are known to be hydrolyzed below pH 6.0 in protic solvents by protonation to form an easily hydrolyzed thiazolium (Knapp, 2002). The N=C double bond is sensitive to reductive/radical conditions and the sulfur is sensitive to oxidative conditions. These properties limit the chemistry that can be performed in the presence of thiazolines (Gaumont, 2009; Chen, 2014; Knapp, 2007). Because of the sensitivity of thiazolines, the choice of chemically orthogonal protecting groups is very important.

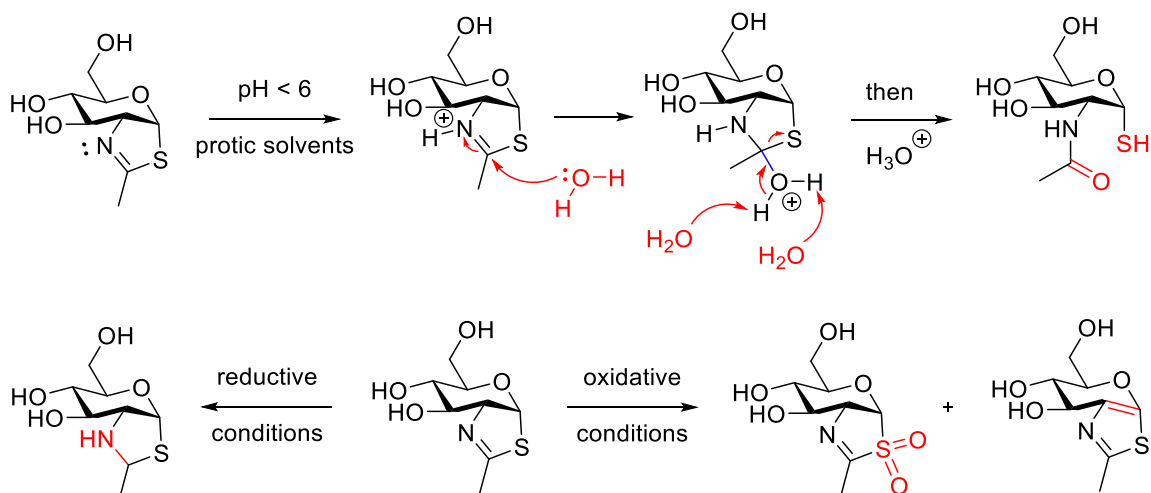


Figure 1.23. Degradation pathways of thiazoline sugars.

1.5. Aims of thesis

This thesis reports on effects to develop the methodology towards the synthesis of a library of inhibitors of glycoside hydrolases that use a substrate assisted hydrolysis mechanism. Towards this goal, modifications to transition state analog sugar-thiazoline inhibitors were made at the 3 and 4-hydroxyl positions. The development of such inhibitors could allow for insights and proof-of-concept studies of a number of interesting enzymes that include virulence factors, chitinases and primary screens for biological function. The synthetic challenges overcome from working with sensitive functional groups builds our understanding of protecting groups and synthetic organic chemistry (Slemove, 2013).

Chapter 2.

Synthesis and evaluation of a library of inhibitors for endo-acting *N*-acetylglucosaminidases

2.1. Contributions

The Endo D project builds on previous work done by Prof. Matthew Macauley in collaboration with Prof. Alisdair Boraston from the University of Victoria. Kinetic analysis of these enzymes were done by Isaac Seo and Esther Woo. Enzyme expression and purification of the full length protein was done by Dr. Joanne Hobbs at the University of Victoria. SpGH85, a truncated form of Endo D containing the catalytic GH85 module, was expressed and purified by Isaac Seo.

The Auto project was done in collaboration with Prof. Brian Mark from the University of Manitoba. Assay development was done by Isaac Seo. Enzyme expression and purification was done by Dr. Veronica Larmour at the University of Manitoba.

The FlgJ project was in collaboration with Prof. Brian Mark from the University of Manitoba. Assay development was done by Isaac Seo. Enzyme expression and purification was done by Patryk Zaloba at the University of Manitoba.

Chemical synthesis and characterization was done by Isaac Seo and Esther Woo. Assay development was done by Isaac Seo. Some non-commercial azides and catalyst reagents were purchased from Dr. Lars Nordstroem and Prof. Peng Wu at the Scripps Research Institute.

2.2. Abstract

Thiazoline-sugar based inhibitors are known transition state analog inhibitors of *N*-acetylhexosaminidases that utilize a substrate assisted catalysis mechanism. Although selective inhibitors have been developed with modifications at the 2-OH and 6-OH positions, modifications at the 3-OH and 4-OH positions have not been explored. Many endo-*N*-acetylglucosaminidases that act on oligosaccharide or polysaccharide substrates comprised of monosaccharides glycosylated at the 4-OH position have fascinating roles in disease. A library of inhibitors were developed by selectively alkylating the 4-OH position of NAG-thiazoline and tested for inhibition against bacterial virulence factors Endo D, Auto, and FlgJ. These thiazoline based inhibitors were found ineffective in inhibiting Endo D and unsuited to the acidic pH profile of Auto and FlgJ.

2.3. Introduction

2.3.1. The rise of antibacterial resistance

The discovery of penicillin by Fleming revolutionized the 20th century and even played a major role in the planning of historic events such as D-Day in World War II. These events provided the historic push required to motivate its large scale production and use in replacing the traditional bacteriostatic sulfonamides (Brandt, 2013; Alharbi, 2014). Although antibiotics are largely seen only as treatments for bacterial infections, the impact of these important drugs goes far beyond this application. Antibiotics are critical in enhancing our ability to perform medical surgeries, are used in livestock food supplies, and their use can be important during immunosuppressant therapy. It can be argued that without Fleming's Nobel-prize winning discovery, much advancement in medicine would have been delayed by decades (Aldridge, 1999).

Despite penicillin's initial label as a miracle drug, as early as 1945 Fleming himself warned that the misuse of this discovery could lead to the selective propagation of resistant bacteria (Fleming, 1945). Unfortunately, this warning was ignored as businesses took the opportunity to introduce large amounts of penicillin into over-the-counter salves, lozenges, and even cosmetic creams. This caused widespread resistance to develop in various bacterial pathogens. This rapid spread of resistance was in part accelerated by the ability of bacteria to transfer resistance genes laterally via plasmids (Juhas, 2015). The alarming rise of antibiotic resistant and multi-drug resistant pathogens is a highly concerning issue. Loss of effective antibacterials would create immense societal and economic problems (Eliopoulos, 2003).

One can imagine that the emergence of resistance factors within drug resistant bacteria would require increased energy and compromise fitness, thereby giving selection pressure for non-drug resistant bacteria in the absence of antibiotic use. Unfortunately, this is not the case. Many strains of drug resistant pathogens have ameliorated these deleterious parts of resistance mechanisms by subsequent secondary mutations (Gillespie, 2001). This results in pathogenic strains that have diminished or eliminated

costs of resistance, further highlighting the constant challenge in combating pathogens (Lenski, 2010; zur Wiesch, 2010).

A number of methods for combating bacterial diseases have been proposed, they include mining for new antibiotics from novel culturing environments (Fenical, 2006), using antimicrobial peptides (Zaslhoff, 2002), targeting mechanisms of drug resistance (Stubbs, 2007), managing gut microbiota (Round, 2009), and developing inhibitors of virulence factors (Ahmad, 2008). Of these strategies, inhibiting virulence factors is thought to apply less selective pressure for the development of bacterial resistance. This is because traditional bactericidal or bacteriostatic methods are aimed at killing bacteria or hindering their proliferation instead of disarming them (Rasko, 2010). This approach includes the inhibition of various virulence factors involved in adherence, invasion, biofilm development, quorum sensing, virulence gene expression and toxin secretion (Mühlen, 2015). Targeting pathogenicity enables clearance by the host immune system and alleviates the pressure on the pathogen to develop resistance by affecting only the pathogenicity associated with a particular virulence factor. Furthermore, such anti-virulence targeting will not modify or damage the natural gut microbiota, which has important functions in human health (Cegelski, 2008).

2.3.2. Targeting endo- β -*N*-acetylglucosaminidases for antivirulence

Although numerous anti-virulence targets have been explored, a number of important endo- β -*N*-acetylglucosaminidase (ENGase) virulence factors have not held the spotlight in literature and only limited research has been done on its inhibition (Frederiksen, 2013; Rico-Lastres, 2015; Santana, 2016). ENGases are a group of endoglycosidases that hydrolyze β -1,4-glycosidic bonds in the *N,N'*-diacetylchitobiose core of glycans in glycoproteins. These enzymes are widely found in nature and play a role in glycoprotein metabolism, many use a substrate assisted catalysis mechanism (Cekic, 2016).

Because of the species specific nature of many virulence factor ENGases, ultra-narrow spectrum inhibitors are able to be developed. Inhibiting these species specific virulence factors minimize the development of lateral resistance transfer for multi-drug resistant bacteria (Molohon, 2016).

Because ENGases are known to have varied and strict substrate specificity, many other ENGases, such as Endo-H and Endo-F2 are frequently used as tools for structural characterization and analysis of the various glycans in glycoproteins (Freeze, 2008). Notably, some ENGases have been engineered and exploited for biosynthesis of glycoproteins by using large oligosaccharide oxazolines (Noguchi, 2015).

2.3.3. Endo D is an established virulence factor in *Streptococcus pneumoniae* that is required for immunal detection

Streptococcus pneumoniae was one of the earliest pathogens discovered (first isolated in 1881 by Louis Pasteur) and is responsible for bacterial pneumonia along with a host of other illnesses such as meningitis, bronchitis, and conjunctivitis (Siemieniuk, 2011). Though we have access to antibiotics and vaccines to combat this scourge, pneumococcal infections still play a large role in human health, especially with the recent rise of drug resistant strains (Nuermberger, 2004). As these strains become more prevalent, the requirement for better drug targets increase.

Endo D is a periplasmic ENGase expressed by *S. pneumoniae*. As an established virulence factor, Endo D is responsible for cleaving a conserved glycan off of immunoglobulin G (IgG) molecules that facilitate foreign body recognition as part of the adaptive immune response (Robb, 2015; Hava, 2002; Chen, 2008; Orihuela, 2004; Muramatsu, 2001; Yamamoto, 2005). Without this conserved glycan, downstream recognition of IgGs by subsequent immune response mechanisms is compromised and allows for immune evasion by *S. pneumoniae*. Endo D is able to cleave glycan motifs ranging from $\text{Man}_3\text{GlcNAc}_2$ to $\text{Man}_5\text{GlcNAc}_2$ off of proteins (Robb, 2017). As a glycoside hydrolase, Endo D is a part of the GH85 family within the CAZy database. This family of hydrolases uses a substrate assisted catalysis mechanism, but even amongst these, Endo

D is particular in that it may use the imide tautomeric form of Asparagine 335 as a catalytic general base (Abbott, 2009).

2.3.4. Auto, a virulence-associated peptidoglycan hydrolase in *Listeria monocytogenes*, is required for intracellular entry

Listeria monocytogenes is responsible for modern food poisoning as it is able to grow at typical refrigeration temperatures and is motile even at freezing temperatures (Grundling, 2004). It further evades many forms of immune surveillance because it is an intracellular bacterium.

Auto, a virulence factor found in *L. monocytogenes*, is involved in the initial entry of the bacterium into a host cell (Bublitz, 2009) as well as flagellar function (Roure, 2012). Many bacterial surface proteins are responsible for interacting with the host cell and each step in infection requires different virulence factors on the bacterial cell surface. Thus, reshaping the surface of *L. monocytogenes* by Auto is essential to its virulence. Biochemically, Auto is an *N*-acetylglucosaminidase belonging to the GH73 family of the CAZy database, which is proposed to use substrate assisted catalysis to hydrolyze peptidoglycan.

2.3.5. FlgJ is required for flagella maturation in *Salmonella enterica*

Salmonella enterica is a foodborne pathogen responsible for salmonellosis in foods such as poultry, pork, beef, fish, and unpasteurised dairy. Like *L. monocytogenes*, *S. enterica* is also able to proliferate at refrigeration temperatures and produces various toxins that induce food poisoning when ingested. One major virulence factor of *S. enterica* is its flagellum that allows it to be motile.

During biosynthesis of the flagella, various proteins must be extruded from the flagellar basal body and must pass through the inner membrane, periplasmic space, and outer membrane. Thus, its formation requires targeted hydrolysis of the peptidoglycan

layer by FlgJ (Nambu, 1999, Zaloba, 2016). This enzyme is was recently found to by an *N*-acetylglucosaminidase belonging to the GH73 family of the CAZy database, which is again, proposed to use the substrate assisted hydrolysis mechanism (Herlihey, 2014).

As expected from GH85 and GH73 families of enzymes that use a substrate assisted catalysis mechanism, many of these enzymes can be inhibited by sugar-thiazoline based inhibitors (Knapp, 1996; Mark, 2001). When NAG-thiazoline, a monosaccharide based inhibitor, is used to inhibit an oligosaccharide processing enzyme that binds large oligosaccharide substrates, one would expect only weak inhibitory activity. This is indeed what is observed for many ENGases (Hauser, 2005; Abbott, 2009). More effective inhibitors of ENGases have been developed by Withers *et al.* utilizing chitobiose and chitotriose scaffolds (Macdonald, 2010), but such inhibitors have a caveat when used *in vivo*. Such oligosaccharide based inhibitors are susceptible to the hydrolysis actions of various endo or exo acting glycoside hydrolases. To overcome these limitations, we planned to modify the 4 position of NAG-thiazoline with a propargyl group to allow for rapid access to a number of potential inhibitors via click chemistry. These compounds should be stable within cells and could bind better than the monosaccharide.

2.3.6. Click chemistry as a means for the rapid development of a library of inhibitors.

The copper-catalyzed azide-alkyne cycloaddition (CuAAC) is a chemical transformation that efficiently connects an azide and alkyne by forming a triazole ring (Amblard, 2009). This widely used reaction was first studied by Huisgen, but in the absence of a catalyst, required high temperatures and long reaction times (Huisgen, 1963). The discovery of copper (I) as a catalyst of this cycloaddition has been a major advance and the reaction is chemically orthogonal in reactivity to a wide variety of functional groups, spectator ions, and solvents (Spiteri, 2010). In fact, the addition of copper (I) salts allows for the increase in rates by a factor of 10^7 relative to the thermal process (Hein, 2010). Sharpless used the term “click chemistry” to describe this “near-perfect” bond forming reaction as it can be used to easily generate intended products in high yields with little or no byproducts (Kolb, 2001).

Although copper (I) salts can be used directly to couple azides and alkynes, particular attention has to be made to keep reaction conditions free of oxygen, as the reaction can be plagued by the formation of oxidative coupling byproducts (Hein, 2010). Sodium ascorbate was first introduced as a convenient alternative to strict oxygen-free conditions. Ascorbate acts as a mild reductant towards copper (II) sulfate, forming *in situ* copper (I), while also reducing dissolved dioxygen. This typically results in the CuAAC transformation occurring in near quantitative yields without the need for other additives even in complex environments (McKay, 2014).

The mechanism of the CuAAC reaction was initially proposed as a simple cyclization reaction shown in Figure 2.1, which was derived from early DFT calculations (Himo, 2005). However, these calculations could not reconcile the theoretical energy levels to the greater rate observed in the reaction. Today, the most generally accepted mechanism is more complex, involving a binuclear Cu(I) mechanism with the second copper centre aiding the coordination and activation of the acetylene as shown in Figure 2.2 (Hein, 2010).

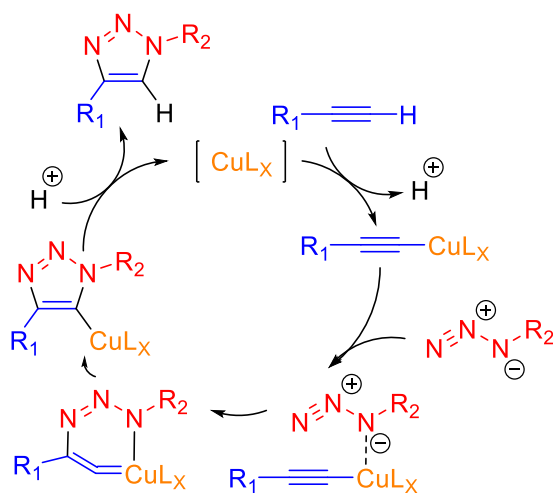


Figure 2.1. Early proposed CuAAC mechanism based on DFT calculations.

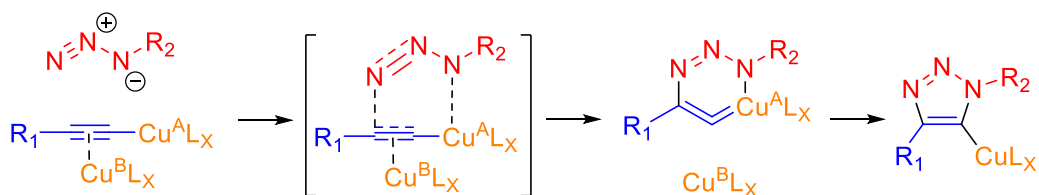


Figure 2.2. Introduction of a second Cu atom lowers the transition state energy and may account for the kinetics observed in CuAAC reactions.

Although the CuAAC reaction is hailed as one of the most efficient transformations, it still suffers from poisoning effects of closely coordinating soft ligands. Most metal catalysts are often known to be influenced by the effects of sulfur compounds (Oudar, 1980). Sulfur is known to coordinate strongly with metal ions, inhibiting their use as effective catalysts. Thiazoline based compounds also cause such metal catalyst poisoning (Brands, 2003) and therefore require the use of an appropriate catalyst for efficient use.

Many tris(triazoyl)amine ligands are added to CuAAC reactions as additives to stabilize the Cu(I) oxidation state in aqueous mixtures. Due to the chelating nature of these catalysts as shown in Figure 2.3A, they are able to bind to Cu(I), masking it from potential poisoning. Although many different ligands have been developed for CuAAC, a balance must be maintained between too strongly and too weakly binding ligands. If the ligand is too strong, the binding could tie up the copper coordination sites and effectively reduce the Cu(I) available for reaction. If the ligand is too weak, it may not prevent Cu aggregates from forming. Tris(triazoyl)amine ligands combine both strong and weak donor ligands by combining a strong central nitrogen donor with weaker peripheral donors (Besanceney-Webler, 2011; Soriano del Amo, 2010). These ligand 2-(4-((bis((1-(*tert*-butyl)-1H-1,2,3-triazol-4-yl)methyl)amino)methyl)-1H-1,2,3-triazol-1-yl)acetic acid (BTAA) shown in Figure 2.3B, is able to stabilize Cu(I) while providing electron density to the metal for catalysis.

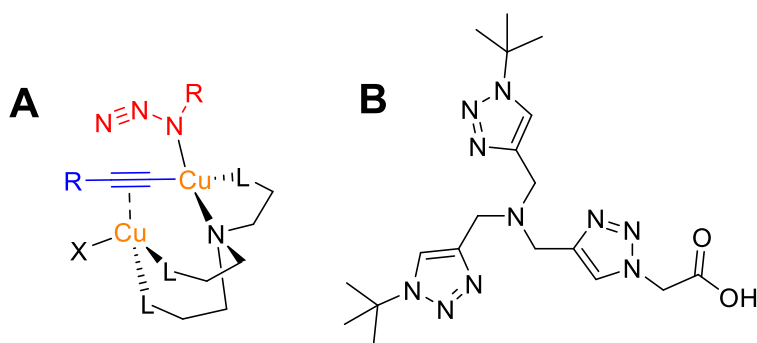


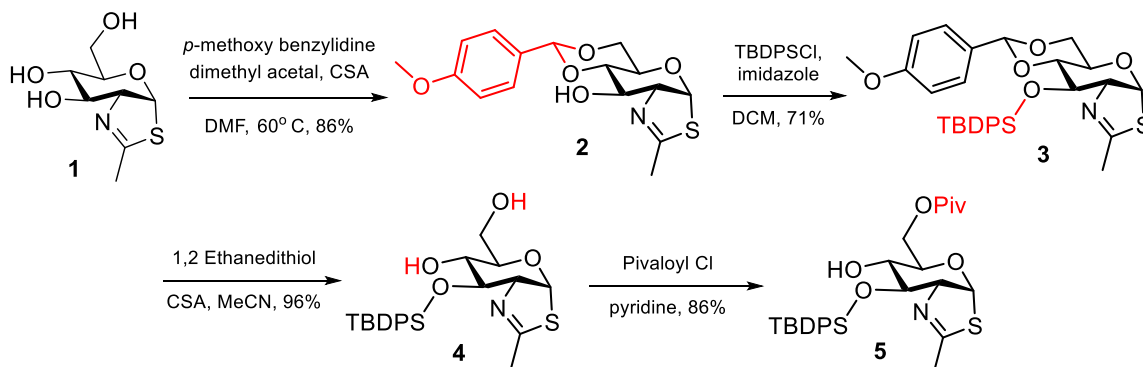
Figure 2.3. **A.** The coordination of tris(triazolyl)amine ligands bind to copper during CuAAC, stabilizing the intermediate and allowing for more efficient click chemistry.
B. 2-(4-((bis((1-(*tert*-butyl)-1H-1,2,3-triazol-4-yl)methyl)amino)methyl)-1H-1,2,3-triazol-1-yl)acetic acid (BTAA) is a water-soluble tris-triazolyl ligand that also maintains copper in the Cu (I) oxidation state and protects the reagents from oxidative damage during the reaction.

2.4. Results and discussion

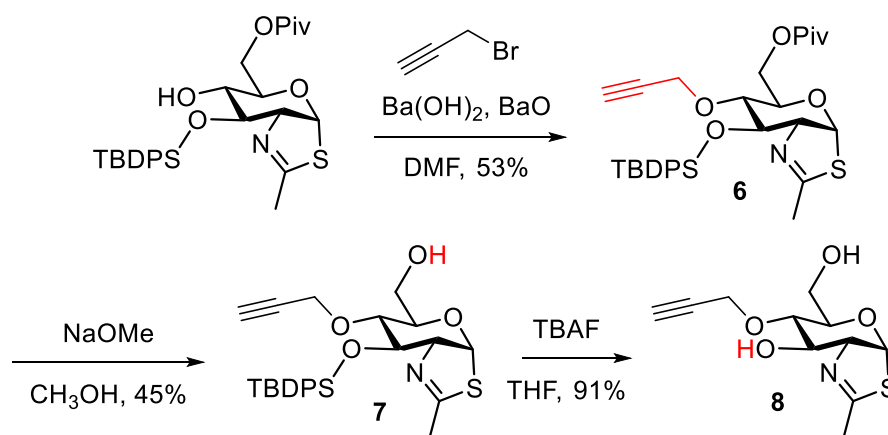
2.4.1. Design and synthesis of 4-OH modified NAG-thiazoline

Building off the initial studies on the inhibition of Endo D (Abbott, 2009), we set out to selectively modify the 4-hydroxyl group of NAG-thiazoline. Accomplishing this goal required the selective protection of NAG-thiazoline at the 3 and 6 positions. This was done by first synthesizing NAG-thiazoline according to literature procedure in six steps with overall yield of 29% (Knapp, 1996) and selectively protecting the 4 and 6 positions using *p*-methoxybenzylidene (Ritter, 2001). This was followed by selective protection of the 3 position using *tert*-butyl(chloro)diphenylsilane to yield fully protected NAG-thiazoline. Unfortunately, after many unsuccessful attempts at selective deprotection of the benzylidene under oxidative, reductive, and acidic conditions, we opted for complete removal of the benzylidene under mild acidic conditions in the presence of a cation scavenger. The primary hydroxyl was selectively esterified over the 4 position using the bulky pivaloyl chloride yielding the free alcohol at the 4 position of NAG-thiazoline as illustrated in Scheme 2.1. This intermediate was alkylated at low temperature to yield protected 4-O-alkyl-NAG-thiazolines. After subsequent deprotections, 4-O-propargyl-

NAG-Thiazoline, 4-O-benzyl-NAG-thiazoline and 4-O-allyl-NAG-thiazoline were synthesized according to Schemes 2.2, 2.4 and 2.5.



Scheme 2.1. Synthesis of 3-O-tert-butylidiphenylsilyl-6-O-pivaloyl-NAG-thiazoline

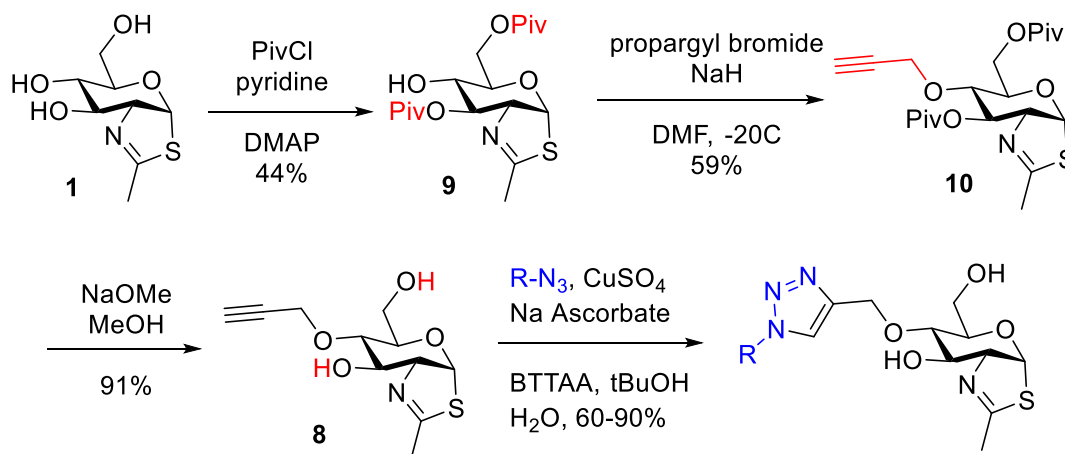


Scheme 2.2. Synthesis of 4-O-propargyl-NAG-thiazoline via stepwise alkylation and deprotection

An alternative approach to synthesizing 4-O-alkyl-NAG-thiazolines was found by esterification of NAG-thiazoline with 2.5 equivalents of pivaloyl chloride and TEA in DCM. This resulted in equimolar amounts of 4,6-di-O-pivaloyl-NAG-thiazoline and 3,6-di-O-pivaloyl-NAG-thiazoline that could both be separated and purified by silica gel flash column chromatography. The undesired 4,6-di-O-pivaloyl-NAG-thiazoline could be recycled by saponification with a methanolic solution of sodium methoxide to yield free NAG-thiazoline. 3,6-di-O-pivaloyl-NAG-thiazoline could be alkylated at low temperatures with sodium hydride in DMF to yield the corresponding 4-O-alkyl-3,6-di-O-pivaloyl-NAG-

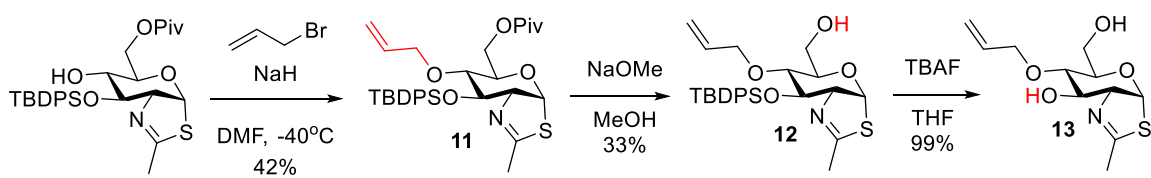
thiazoline. After methanolysis in sodium methoxide, the 4-*O*-alkyl-NAG-thiazoline could be easily isolated.

The rapid preparation of a number of inhibitors used the copper (I) catalyzed azide alkyne click reaction between 4-*O*-propargyl-NAG-thiazoline and various azides. The general scheme involved addition of the azide to the alkyne sugar in a solution of water/*tert*-butanol with copper (II) sulfate, sodium ascorbate and BTAA. This resulted in a targeted panel of inhibitors shown in Table 2.1.

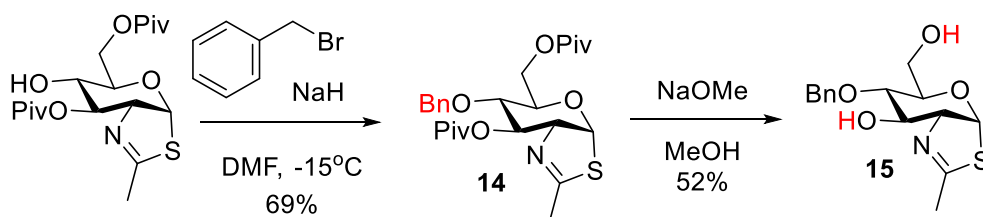


Scheme 2.3. Synthesis of 4-*O*-propargyl-NAG-thiazoline and use of CuAAC for the rapid development of various inhibitors (See Table 2.1 for azides)

Other methods of preparing NAG-thiazoline inhibitors such as rapid fuctionalization via metathesis and thiol-ene click chemistry were explored using 4-*O*-allyl-NAG-thiazoline. Unfortunately, Grubbs-type metathesis reactions were only possible with stoichiometric quantities of Grubbs II catalyst. Radical and UV light induced thiol-ene reaction conditions resulted in no reaction or degradation of starting material. However, the 4-*O*-allyl-NAG-thiazoline could potentially be useful as a functionalized inhibitor. In addition, 4-*O*-benzyl-NAG-thiazoline was prepared to compare the enzymatic active site tolerance towards the conserved triazole linker in inhibitors developed through CuAAC. These compound were synthesized in similar conditions to the 4-*O*-propargyl-NAG-thiazoline and are illustrated in Scheme 2.4 and Scheme 2.5.



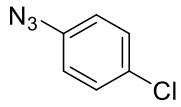
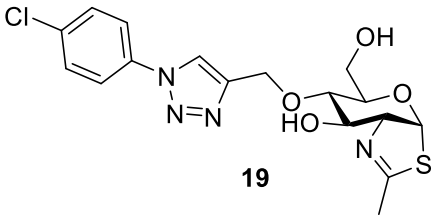
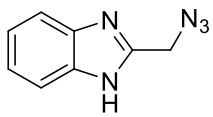
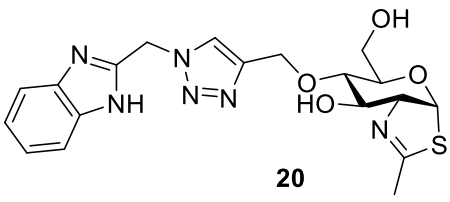
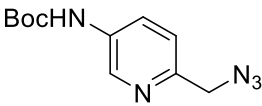
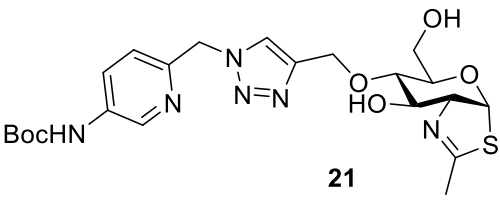
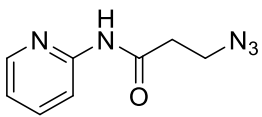
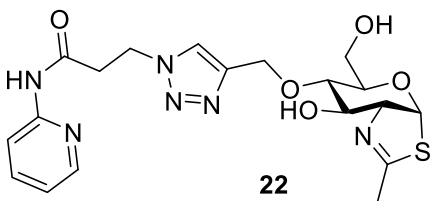
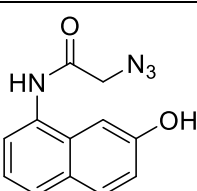
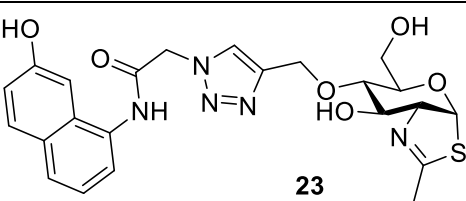
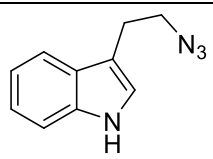
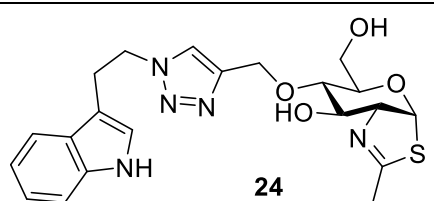
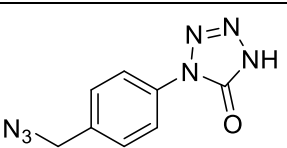
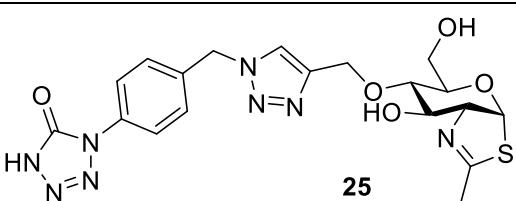
Scheme 2.4. Synthesis of 4-O-allyl-NAG-thiazoline

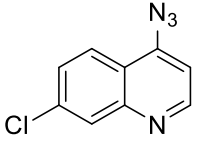
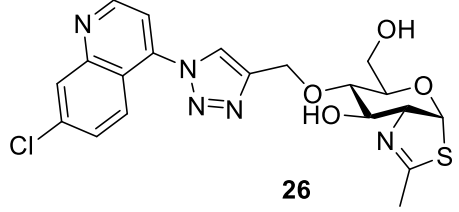
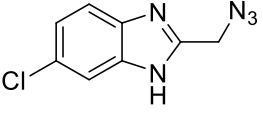
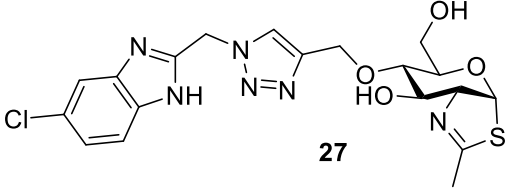
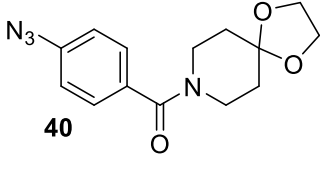
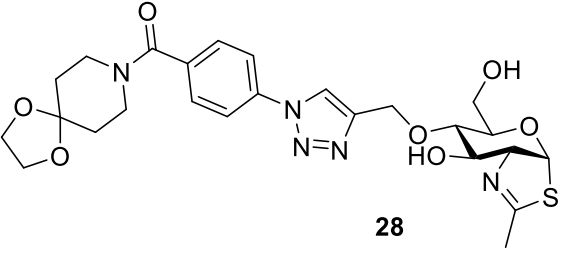
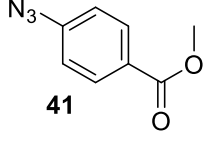
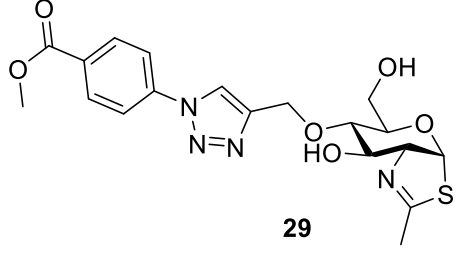
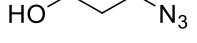
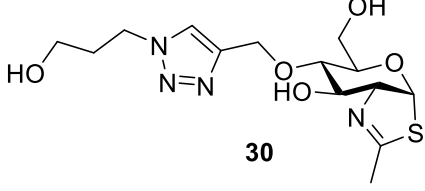
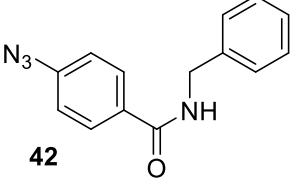
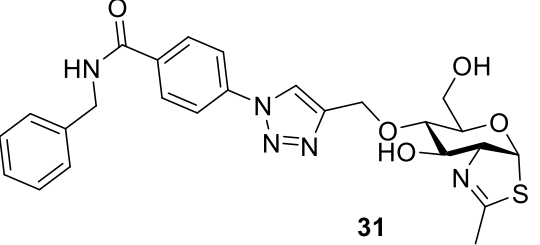


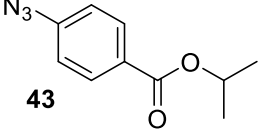
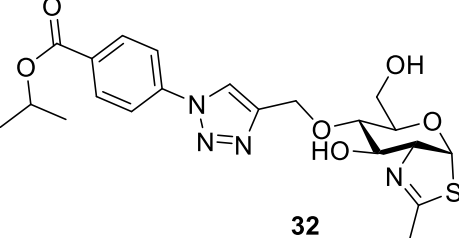
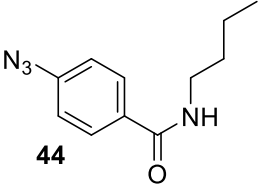
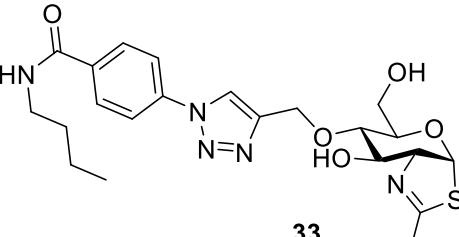
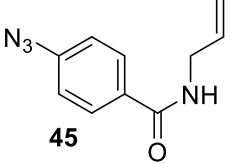
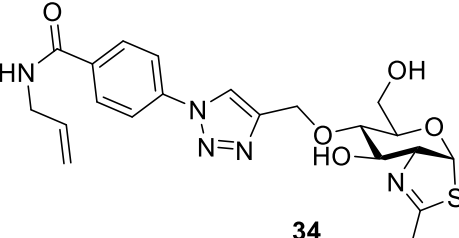
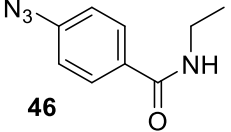
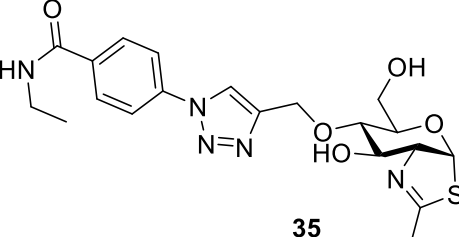
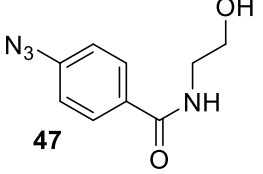
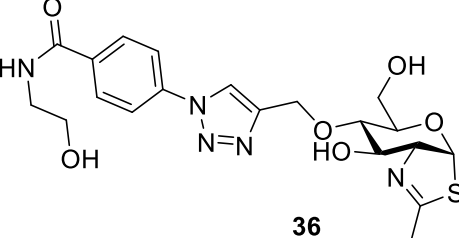
Scheme 2.5. Synthesis of 4-O-benzyl-NAG-thiazoline

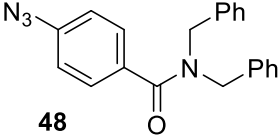
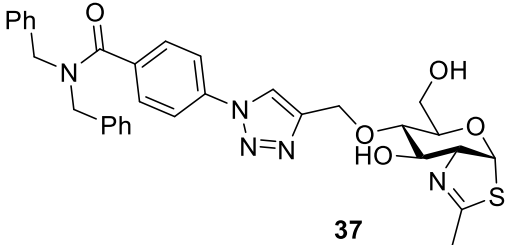
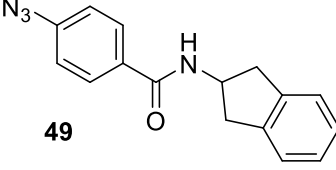
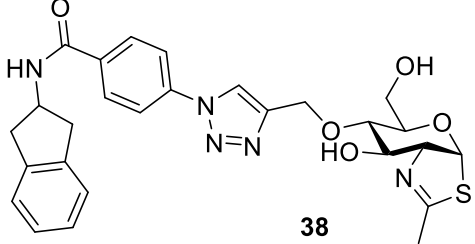
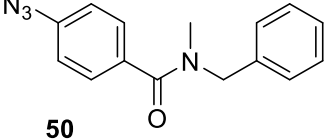
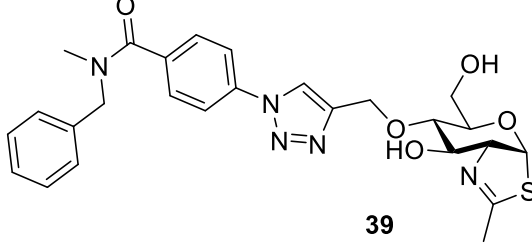
Table 2.1. Azides used and inhibitors synthesized

Azide	Compound synthesized
	 16
	 17
	 18

Azide	Compound synthesized
	 <p style="text-align: center;">19</p>
	 <p style="text-align: center;">20</p>
	 <p style="text-align: center;">21</p>
	 <p style="text-align: center;">22</p>
	 <p style="text-align: center;">23</p>
	 <p style="text-align: center;">24</p>
	 <p style="text-align: center;">25</p>

Azide	Compound synthesized
	 <p style="text-align: center;">26</p>
	 <p style="text-align: center;">27</p>
 <p style="text-align: center;">40</p>	 <p style="text-align: center;">28</p>
 <p style="text-align: center;">41</p>	 <p style="text-align: center;">29</p>
	 <p style="text-align: center;">30</p>
 <p style="text-align: center;">42</p>	 <p style="text-align: center;">31</p>

Azide	Compound synthesized
 <p>43</p>	 <p>32</p>
 <p>44</p>	 <p>33</p>
 <p>45</p>	 <p>34</p>
 <p>46</p>	 <p>35</p>
 <p>47</p>	 <p>36</p>

Azide	Compound synthesized
 <p>48</p>	 <p>37</p>
 <p>49</p>	 <p>38</p>
 <p>50</p>	 <p>39</p>

2.4.2. Kinetic properties and inhibition assay for Endo D

SpGH85, the catalytic protein domain of Endo D which includes amino acids 159 - 807, was unable to hydrolyze substrates such as 4-nitrophenyl *N*-acetyl- β -D-glucosaminide (4NP-GlcNAc), 3-Fluoro-4-nitrophenyl *N*-acetyl- β -D-glucosaminide (3F4NP-GlcNAc), 3,4-dinitrophenyl *N*-acetyl- β -D-glucosaminide (34DNP-GlcNAc) and 4-methylumbelliferyl *N*-acetyl- β -D-glucosaminide (4MU-GlcNAc) when tested in phosphate, HEPES, tris and citrate/phosphate/CHES buffers at various pH ranges of 6 to 8 which covers the reported range of Endo D activity.

When collaborators produced SpGH85 and tested its activity on RNase B, an *N*-glycan, no glycosidase activity was found. Only when the full length Endo D, which consists of an extra 135 amino acids at the N-terminus and an extra 847 amino acids at

the C-terminus, was expressed and purified could glycosidase activity be observed on RNase B.

When tested for activity against the synthetic substrate 3,4DNP-GlcNAc, this full length Endo D showed hydrolytic activity with a K_M of about 15-40 μ M depending on the concentration of enzyme used. It is commonly thought that K_M is not dependant on enzyme concentration, but this only applies to situations where the catalytic efficiency of an enzyme is independent of its concentration. Figure 2.4 shows the reaction velocity versus enzyme concentration, where an abrupt change in kinetic activity is observed between 100 to 200 nM of Endo D. This data is more consistent with concentration dependant dimerization of enzymes, which can influence activity.

The discrepancy between previously published data showing SpGH85 can cleave β -D-glycosamides and is inhibited by NAG-thiazoline (Abbott, 2009) and this study, in which we observe no inhibition by NAG-thiazoline, may arise from either difficulties in reproducibly expressing the shorter domain construct of SpGH85 or from potential enzyme impurities such as NagZ, which is able to hydrolyze 3F4NP-GlcNAc substrates. Although because this enzyme does not use substrate assisted catalysis (Stubbs, 2013; Vocadlo, 2000) this scenario seems unlikely. Perhaps the full length Endo D construct for which I observe activity on β -D-glycosamides has a different active site architecture and is not efficiently inhibited by NAG-thiazoline. NAG-thiazoline may also bind to SpGH85 in the solid state, but this current study shows that inhibition of SpGH85 cannot be observed by kinetic hydrolysis of nitrophenolic substrates.

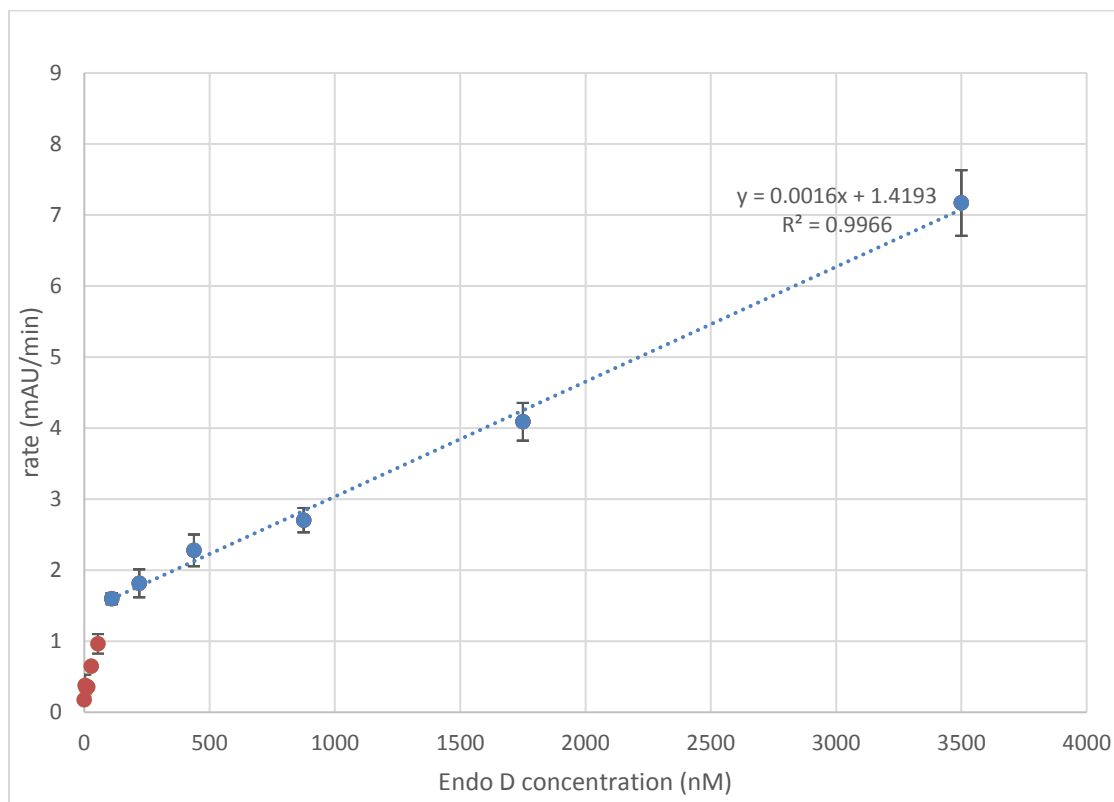


Figure 2.4. Graph of initial velocities measured by light absorbance at 405 nm with 3F4NP-GlcNAc (2 mM) substrate versus Endo D concentration. This graph shows two distinct areas of linear activity below 100 nM and above 200 nM, which is consistent with dimerization kinetics.

Though many interesting biological reasons may account for this observed abrupt change in activity depending on enzyme concentration, inhibition assays were performed with a preliminary screen of 25 inhibitors. However, none of the 25 inhibitors showed any inhibition of Endo D at multiple different concentrations of inhibitors (200 μ M to 500 nM) in multiple concentrations of enzyme (400 nM, 200 nM, 100 nM and 40 nM) in a buffer solution of 50 mM CHES, 50 mM citrate, 50 mM phosphate and 100 mM sodium chloride at pH 7.5 or PBS. Perplexed by these results that were exacerbated by indications that the positive control inhibitor NAG-thiazoline had no measureable inhibition at up to 200 μ M concentrations, even though inhibition of SpGH85 by NAG-thiazoline was reported at concentrations below 50 μ M, PUGNAc, a known non-specific inhibitor of *N*-acetylglucosaminidases, was tested for inhibitions at concentrations up to 200 μ M.

Unfortunately, this compound also showed no inhibitory action against Endo D. Kinetic characterization of full length Endo D is not available in previous literature and the data presented in this study suggests that Endo D is not inhibited by traditional GH85 inhibitors.

2.4.3. Limitations of thiazoline-sugars inhibiting Auto and FlgJ

Both Auto and FlgJ are *N*-acetylglucosaminidases that degrade peptidoglycan and as such, are most suited to assay via turbidometric activity on preparations of insoluble peptidoglycan. However, the pH dependence of both Auto and FlgJ shows they are most active in acidic media, with catalytic activity dropping rapidly above pH 5.0 for Auto and 4.0 for FlgJ (Bublitz, 2009, Herlihey, 2014). In these conditions, thiazoline-sugar inhibitors rapidly decompose to the acyclic *N*-acetyl-thiol-sugar. Comparatively, the pK_a of thiazoline sugar NButGT is 5.17 (Cekic, 2016) and NAG-thiazoline is known to hydrolyze below pH 6 (Knapp, 2002).

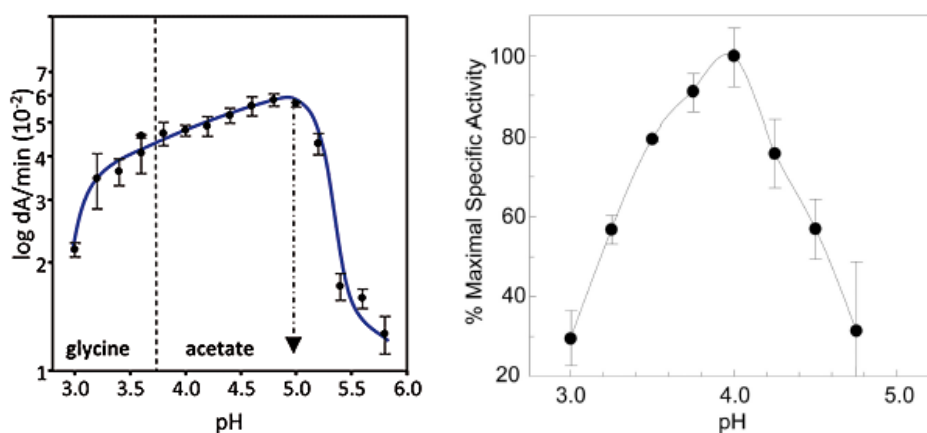


Figure 2.5. The pH dependence of Auto and FlgJ shows activity in acidic media. Figures adapted from Bublitz 2009 and Herlihey 2014

2.5. Conclusions

A number of NAG-thiazoline derivatives were synthesized and tested for inhibition against Endo D (SpGH85 and full length). Several of these compounds (15, 17, 38, 44, 45, 47, 48 and 49) will need to be revisited for complete characterization to obtain ^{13}C NMR spectra. During the course of kinetic characterization of Endo D, it was found that its activity depended on its concentration, suggesting that there may be dimerization of the enzyme that results in diminished activity. Furthermore, NAG-thiazoline, its derivatives, along with other inhibitors, were unable to inhibit Endo D despite observing X-ray crystal structures of NAG-thiazoline bound to SpGH85. This suggests that more specific interactions may be involved in the mechanism of Endo D.

Auto and FlgJ were both tested for inhibition by thiazoline based inhibitors, but due to their low pH optimum, thiazoline degradation in the inhibitors was observed. It was found that in all cases, thiazoline-sugar inhibitors were not appropriately suited to inhibit these enzymes. It is possible that other, more acid tolerant inhibitors, such as 4-functionalized amino-thiazoline sugars, could be used to probe inhibition of enzymes such as Auto and FlgJ.

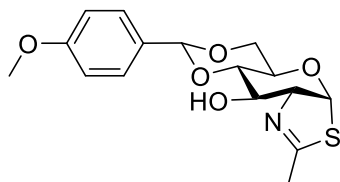
Though the enzymatic studies presented in this chapter was limited to enzymes that were not well suited for inhibition by thiazoline sugars, the same methodology and inhibitors can be applied to various other chitinases and hydrolases from CAZy database GH 18, 20, 73, 84 or 85 due to their shared hydrolysis mechanism (Horn 2006; Piszkiwicz 1967; Piszkiwicz 1968a; Piszkiwicz 1968b; Macauley 2009; Fujita 2007). Enzymes with an acidic pH optimum could potentially be inhibited by amino-thiazoline sugars, which are more stable in acidic conditions as double protonation is required for thiazolinium formation. Comparatively, the pKa of NButGT (Figure 1.18), a related thiazoline sugar inhibitor selective for OGA, is 5.17 (Cekic, 2016).

2.6. Experimental

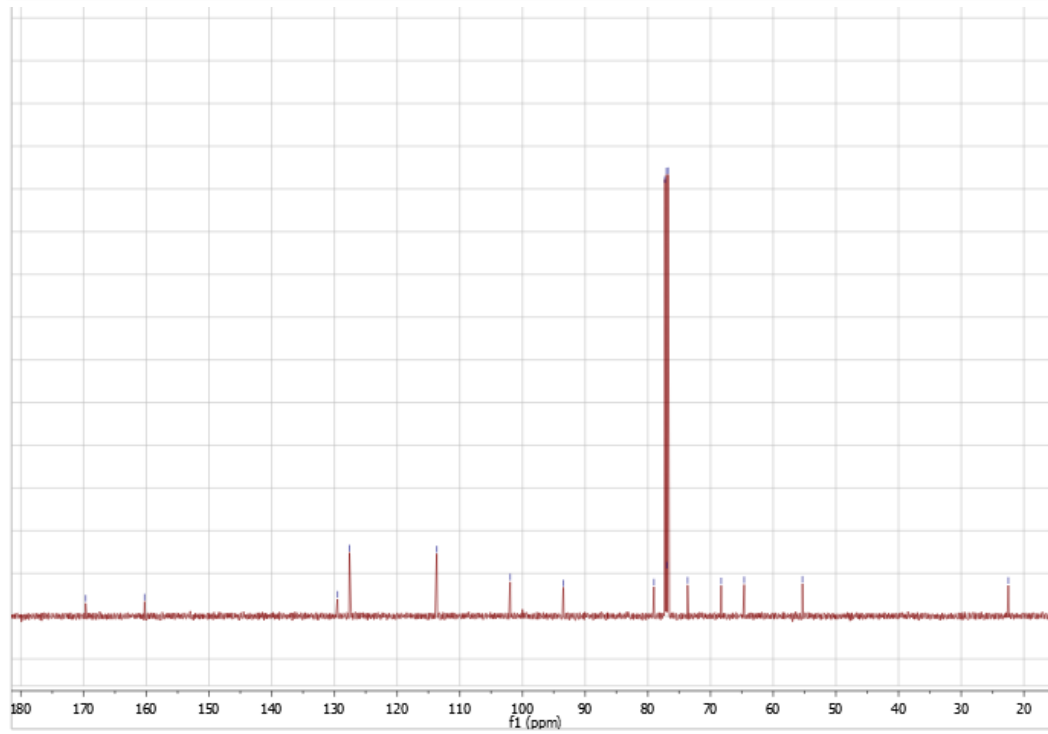
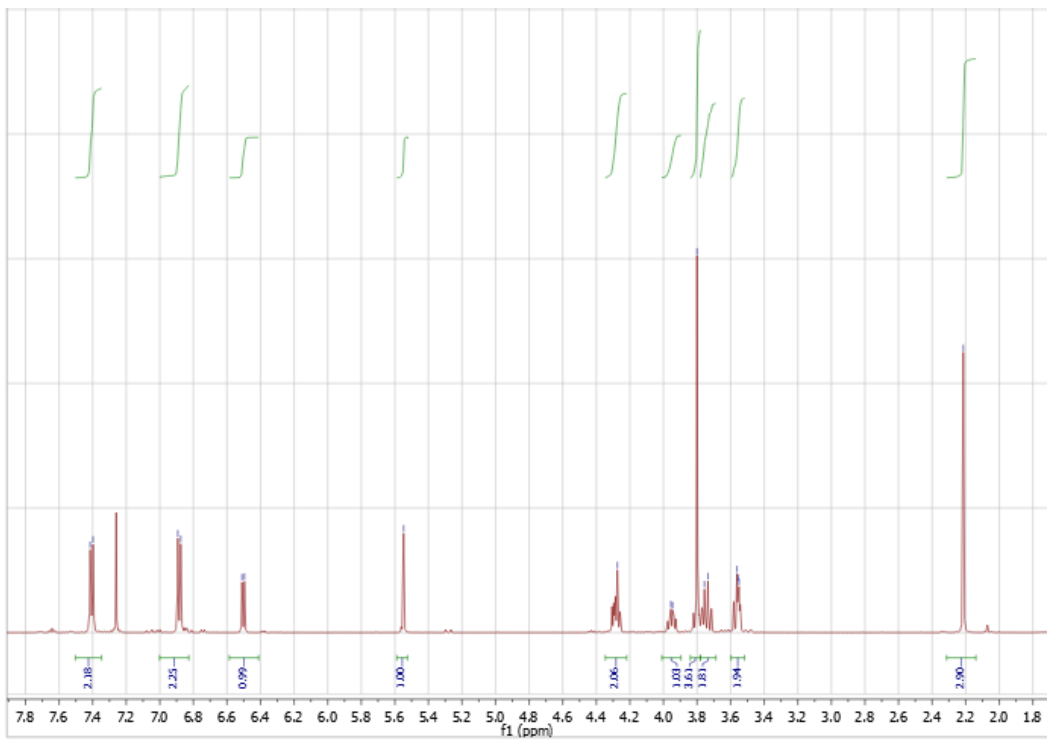
2.6.1. General procedures

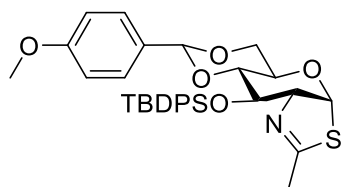
All chemicals were purchased from Sigma-Aldrich, Alfa Aesar, Carbosynth, or TCI and used without further purification unless specifically noted. All dry solvents and buffer salts were purchased from Sigma-Aldrich, VWR, or BioShop and used without further purification. The progress of all reactions were monitored via thin layer chromatography on Merck pre-coated silica gel plates using ethyl acetate/hexanes, ethyl acetate/dichloromethane, methanol/dichloromethane, or acetone/hexanes solvent elution systems. Flash chromatography was performed under positive pressure using Fisher Scientific silica gel (230-400 mesh) where spots were visualized under ultraviolet light (254 nm) and staining with KMnO_4 with gentle heating. Proton (^1H) and carbon (^{13}C) spectra were obtained on either a Bruker AVANCE 500 (500 MHz for ^1H , 125 MHz for ^{13}C) or Bruker AVANCE 400 (400MHz for ^1H , 100 MHz for ^{13}C) unless otherwise specified. NMR samples were dissolved in deuterated chloroform, methanol, or DMSO from Cambridge Isotope Laboratories. High resolution mass spectroscopy data was obtained using a Bruker maXis TOF LC/MS/MS instrument. Enzyme concentrations were obtained using a Nanodrop₂₀₀₀ using the appropriate extinction coefficient and the optical density at 280 nm. Enzyme kinetic reactions were determined by absorbance measurements at 405 nm or 600 nm using a Molecular Devices Spectramax i3x reader. Data was graphed on Microsoft Excel and kinetic parameters were determined using GraphPAD Prism 3.

2.6.2. Synthetic procedures for chemical compounds

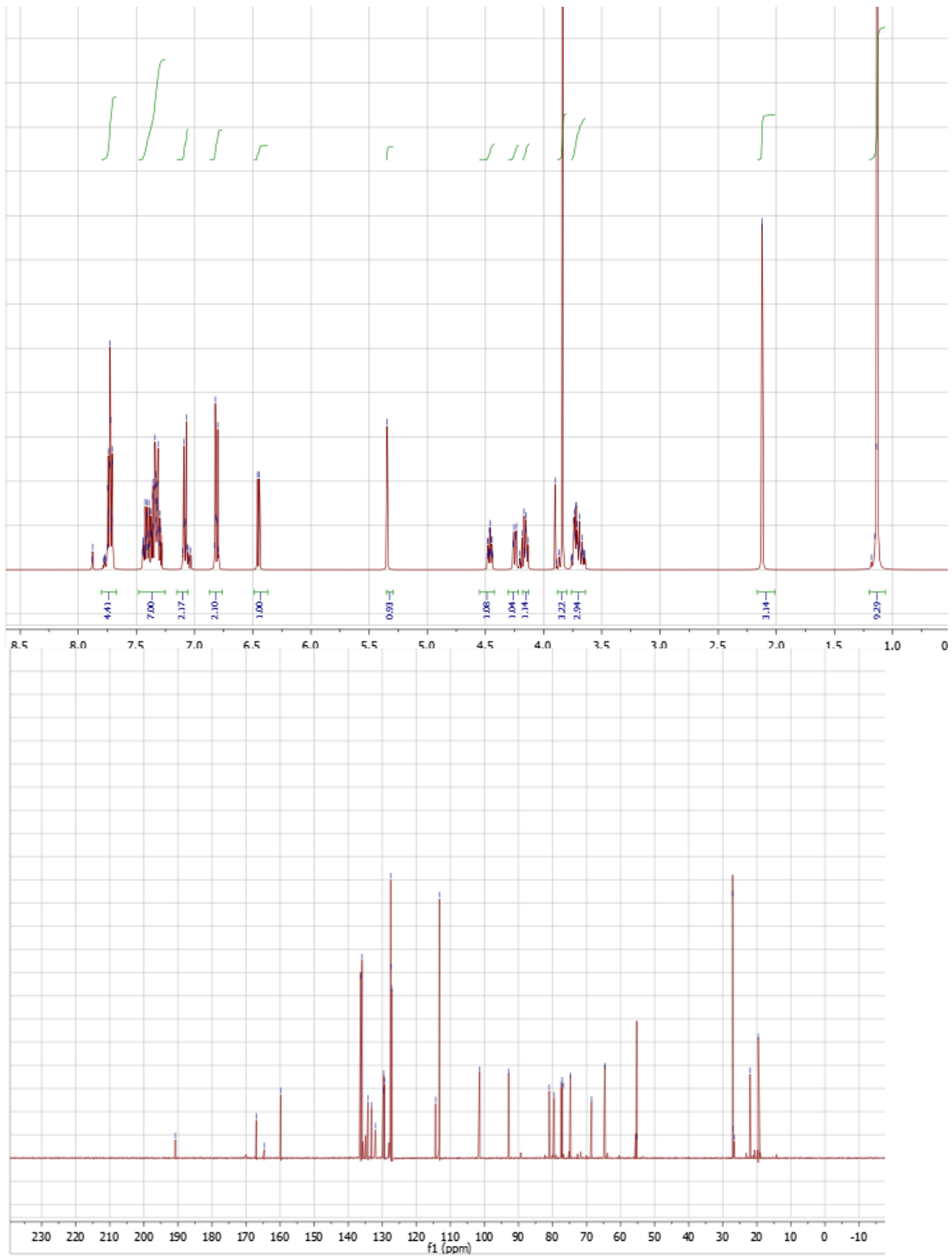


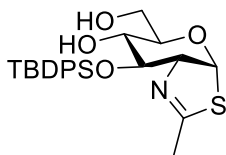
Compound 2 (Ritter, 2001). NAG-thiazoline (4.5 g, 20.5 mmol) was added to a 250 mL flame-dried round bottom flask under an atmosphere of argon. The compound was dissolved in anhydrous DMF (50 mL), then 4-methoxybenzaldehyde dimethyl acetal (4.2 mL, 24.6 mmol) and camphor sulfuric acid (950 mg, 4.1 mmol) was added and the reaction mixture was stirred for two hours at room temperature. The reaction mixture was transferred to a rotary vacuum evaporator and allowed to progress to completion during vacuum facilitated evaporation of methanol at 25 °C and 10 torr for 8 hours. Upon completion, ethyl acetate (300 mL) was added to the reaction and the mixture was washed five times with water, followed by back extraction of the aqueous layer with ethyl acetate. The combined organic layers were further washed eight times with water and brine to minimize residual DMF. The remaining solvent was dried over Na₂SO₄ before being filtered and concentrated *in vacuo* and the resulting residue was recrystallized from hot ethanol to afford 4,6-O-(4-methoxybenzylidene)-NAG-thiazoline as fine white crystals (4.07 g, 59%, decomposition at 187 – 192 °C). ¹H NMR (400 MHz, Chloroform-*d*) δ_H 7.41 (d, *J* = 9.2 Hz, 2H), 6.88 (d, *J* = 9.2 Hz, 2H), 6.50 (d, *J* = 7.1 Hz, 1H), 5.55 (s, 1H), 4.28 (m, 2H), 3.96 (td, *J* = 9.5, 4.8 Hz, 1H), 3.80 (s, 3H), 3.75 (q, *J* = 9.6 Hz, 2H), 3.56 (m, 2H), 2.21 (s, 3H). ¹³C NMR (100 MHz, Chloroform-*d*) δ_C 169.69, 160.26, 129.51, 127.80, 113.67, 101.96, 93.48, 79.02, 76.96, 73.66, 68.29, 64.62, 55.32, 22.49. HRMS (ESI⁺) *m/z*: [M+H]⁺ calcd for C₁₆H₂₀NO₅S 338.1062, found 338.1067.



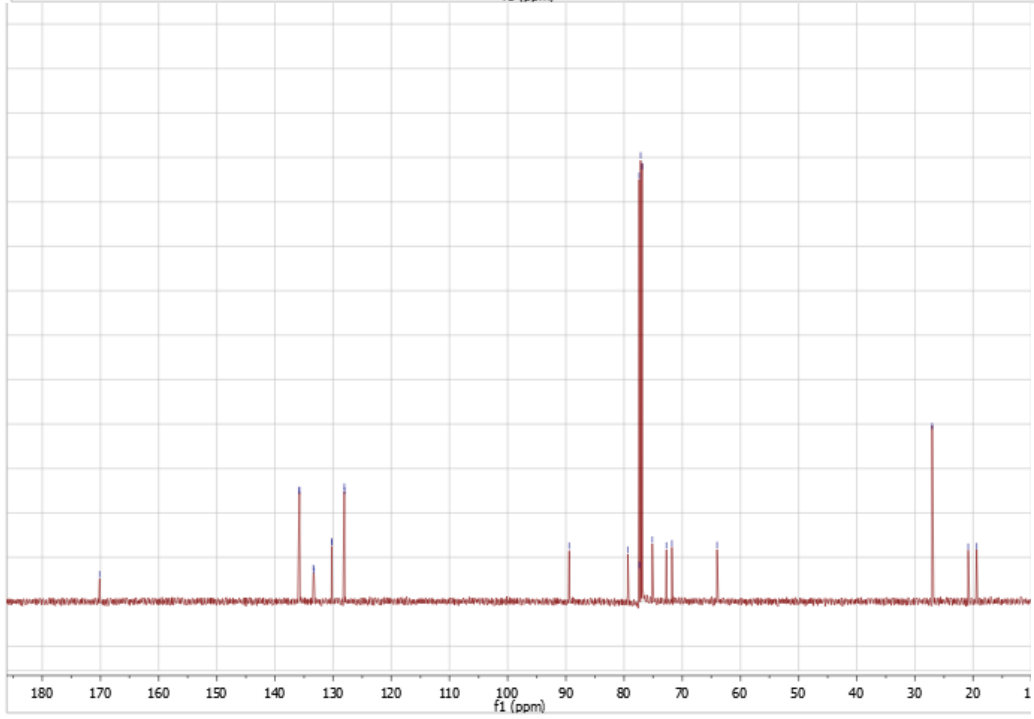
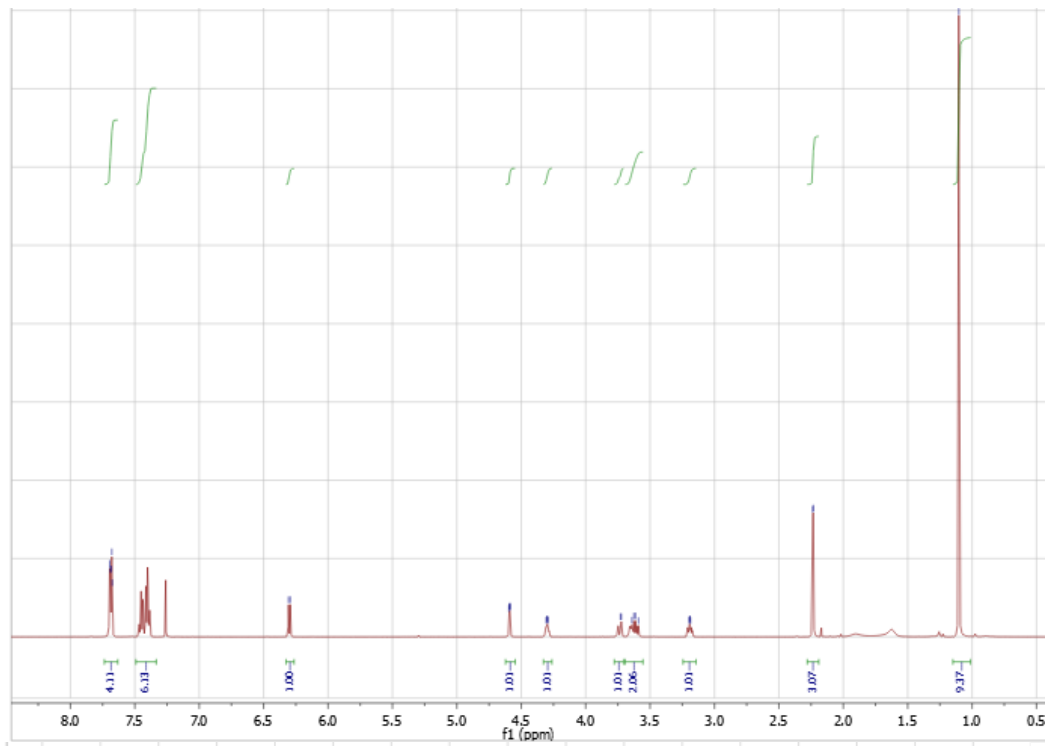


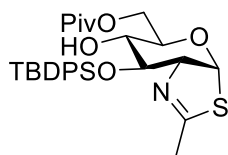
Compound 3. 4,6-O-(4-methoxybenzylidene)-NAG-thiazoline (8.54 g, 25.3 mmol) was added to a 500 mL flame-dried round bottom flask under an atmosphere of argon. The compound was dissolved in DCM (250 mL), then *tert*-butyl(chloro)diphenylsilane (9.8 mL, 37.9 mmol) and imidazole (3.78 g, 55.6 mmol) were added and the reaction mixture and stirred overnight at room temperature. Upon completion of the reaction, the solvent was removed under vacuum and the desired product was purified by silica gel flash column chromatography (1:5 ethyl acetate:hexanes) to afford 4,6-O-(4-methoxybenzylidene)-3-(*tert*-butyldiphenylsilyl)-NAG-thiazoline as a clear, colourless gum (14.0 g, 95%). ¹H NMR (400 MHz, Chloroform-*d*) δ_{H} 7.70 (m, 4H), 7.43-7.26 (m, 6H), 7.06 (dt, $J = 8.8, 2.0$ Hz, 2H), 6.79 (dt, $J = 8.9, 2.0$ Hz, 2H), 6.43 (d, $J = 7.4$ Hz, 1H), 5.32 (s, 1H), 4.44 (m, 1H), 4.22 (m, 1H), 4.13 (q, $J = 6.9$ Hz, 1H), 3.81 (s, 3H), 3.74-3.62 (m, 3H), 2.10 (d, $J = 1.3$ Hz, 3H), 1.11 (s, 9H). ¹³C NMR (100 MHz, Chloroform-*d*) δ_{C} 190.77, 166.97, 164.61, 159.80, 136.31, 135.93, 134.18, 133.14, 132.01, 129.63, 129.57, 129.35, 127.51, 127.37, 127.24, 114.35, 113.19, 101.40, 92.83, 80.99, 79.53, 74.74, 68.56, 64.61, 55.26, 27.10, 21.98, 19.60. HRMS (ESI⁺) m/z : [M+H]⁺ calcd for C₃₂H₃₈NO₅SSi 576.2240, found 576.2219.



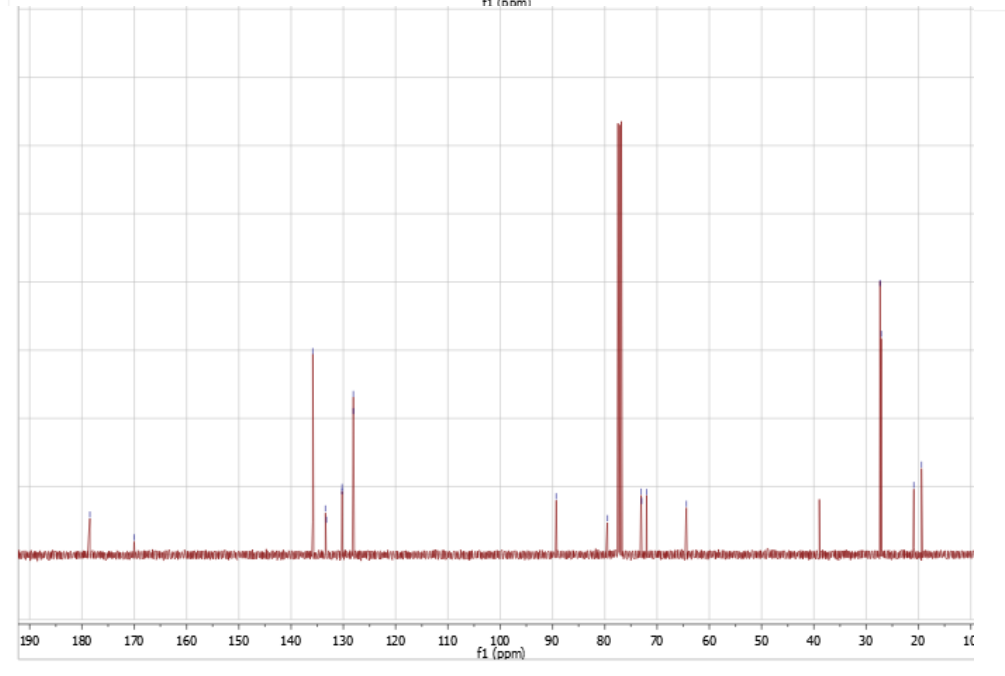
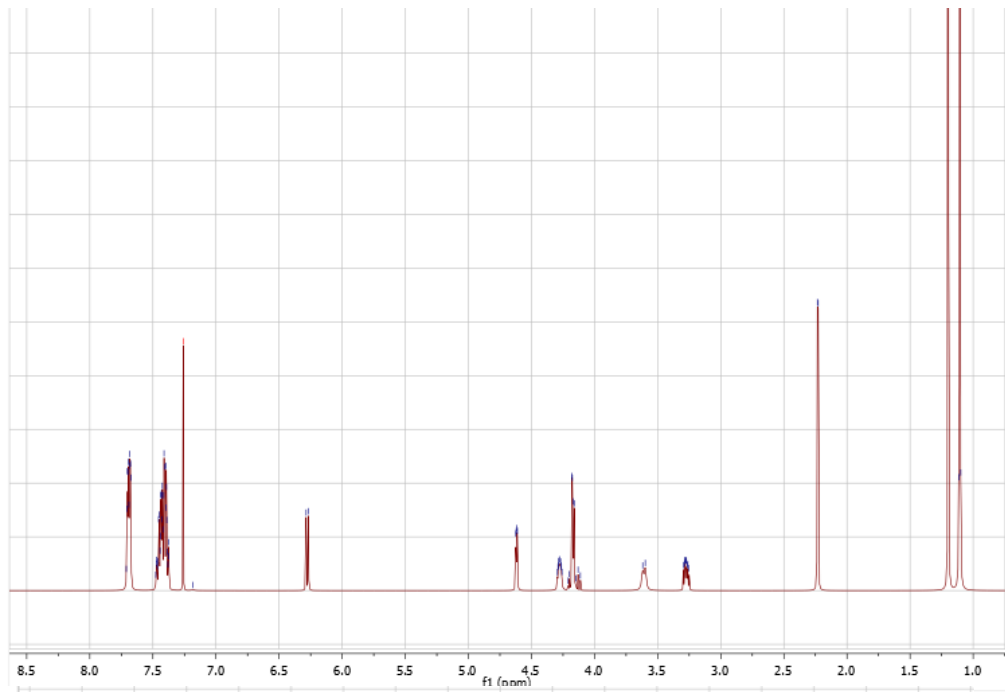


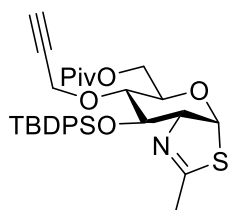
Compound 4. 4,6-O-(4-methoxybenzylidene)-3-(*tert*-butyldiphenylsilyl)-NAG-thiazoline (62.6 mg, 0.109 mmol) was added to a 50 mL flame-dried round bottom flask under an atmosphere of argon. The compound was dissolved in acetonitrile, then camphor sulfuric acid (25 mg, 0.109 mmol) and ethanedithiol (55 μ L, 0.654 mmol) was added and the reaction mixture was stirred for 90 minutes. The reaction was stopped by the addition of TEA to reach a pH value of approximately 8, followed by removal of solvent under vacuum. The resulting residue was dry loaded onto minimal silica gel and purified by flash column silica gel chromatography (1:4 acetone:hexanes to 1:3 acetone:hexanes) to yield 3-(*tert*-butyldiphenylsilyl)-NAG-thiazoline as a clear, colourless gum (47 mg, 94%). ^1H NMR (400 MHz, Chloroform-*d*) δ_{H} 7.68 (m, 4H), 7.47-7.38 (m, 6H), 6.30 (d, $J = 6.8$ Hz, 1H), 4.59 (dd, $J = 3.7, 1.2$ Hz, 1H), 4.30 (m, 1H), 3.74 (dd, $J = 12.0, 3.0$ Hz, 1H), 3.65 (d, $J = 8.0$ Hz, 1H), 3.61 (dd, $J = 11.7, 6.2$ Hz, 1H), 3.19 (m, 1H), 2.23 (d, $J = 2.3$ Hz, 3H), 1.10 (s, 9H). ^{13}C NMR (100 MHz, Chloroform-*d*) δ_{C} 170.11, 135.85, 135.80, 133.39, 133.29, 130.24, 130.22, 128.08, 128.03, 89.41, 79.35, 77.35, 75.15, 72.70, 71.77, 64.01, 27.04, 20.84, 19.41. HRMS (ESI $^+$) m/z : $[\text{M}+\text{H}]^+$ calcd for $\text{C}_{24}\text{H}_{32}\text{NO}_4\text{SSi}$ 458.1816, found 458.1828.



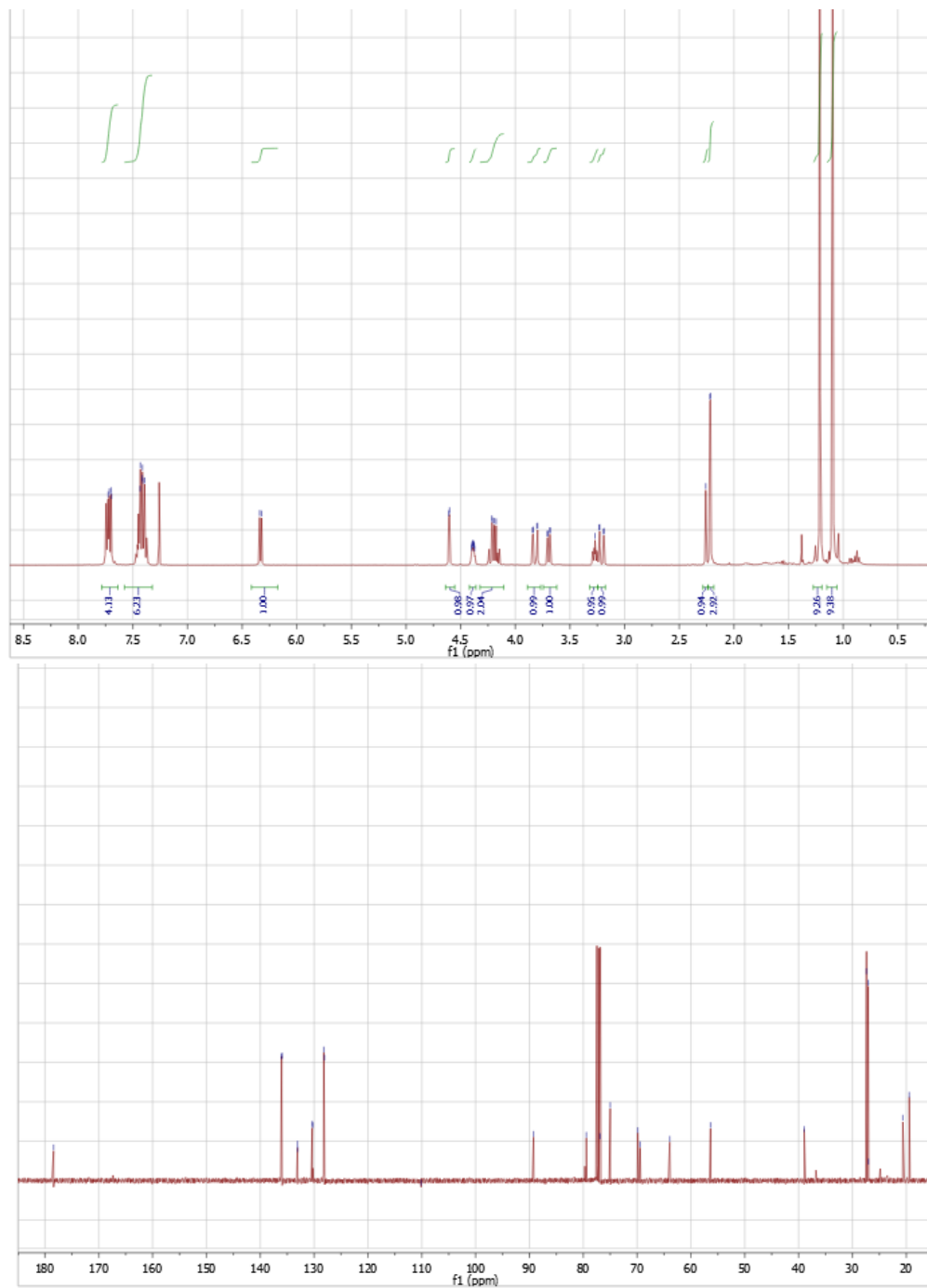


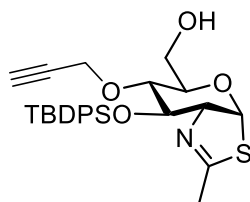
Compound 5. 3-(*tert*-butyldiphenylsilyl)-NAG-thiazoline (247 mg, 0.539 mmol) was added to a 25 mL flame dried round bottom flask under an atmosphere of argon. The compound was dissolved in pyridine (7 mL) and pivaloyl chloride (133 μ L, 1.08 mmol) was added. The mixture was stirred overnight at room temperature and upon completion, the reaction mixture was poured into ethyl acetate (100 mL) and washed five times with water. The resulting organic layer was washed with a saturated aqueous solution of potassium bisulfate until no pyridinium bisulfate precipitates were found. The organic layer was dried over sodium sulfate before being filtered and concentrated *in vacuo*. Purification by silica gel flash column chromatography (2:3:5 ethyl acetate:DCM:hexanes) yielded 6-pivaloyl-3-(*tert*-butyldiphenylsilyl)-NAG-thiazoline (252 mg, 86%) as a clear, colorless gum. ^1H NMR (400 MHz, Chloroform-*d*) δ_{H} 7.69 (m, 4H), 7.48-7.37 (m, 6H), 6.28 (d, J = 6.8 Hz, 1H), 4.62 (dd, J = 3.7, 1.2 Hz, 1H), 4.28 (m, 1H), 4.17 (m, 1H), 3.61 (d, J = 7.1 Hz, 1H), 3.28 (m, 1H), 2.23 (d, J = 2.0 Hz, 3H), 1.20 (s, 9H), 1.10 (s, 9H). ^{13}C NMR (100 MHz, Chloroform-*d*) δ_{C} 178.49, 170.03, 135.84, 133.42, 133.23, 130.26, 130.24, 128.09, 128.08, 89.28, 79.50, 73.06, 72.95, 72.00, 64.40, 38.95, 27.35, 27.10, 20.88, 19.44. HRMS (ESI $^+$) m/z : $[\text{M}+\text{H}]^+$ calcd for $\text{C}_{28}\text{H}_{36}\text{NO}_6\text{SSi}$ 542.2027, found 542.2020.



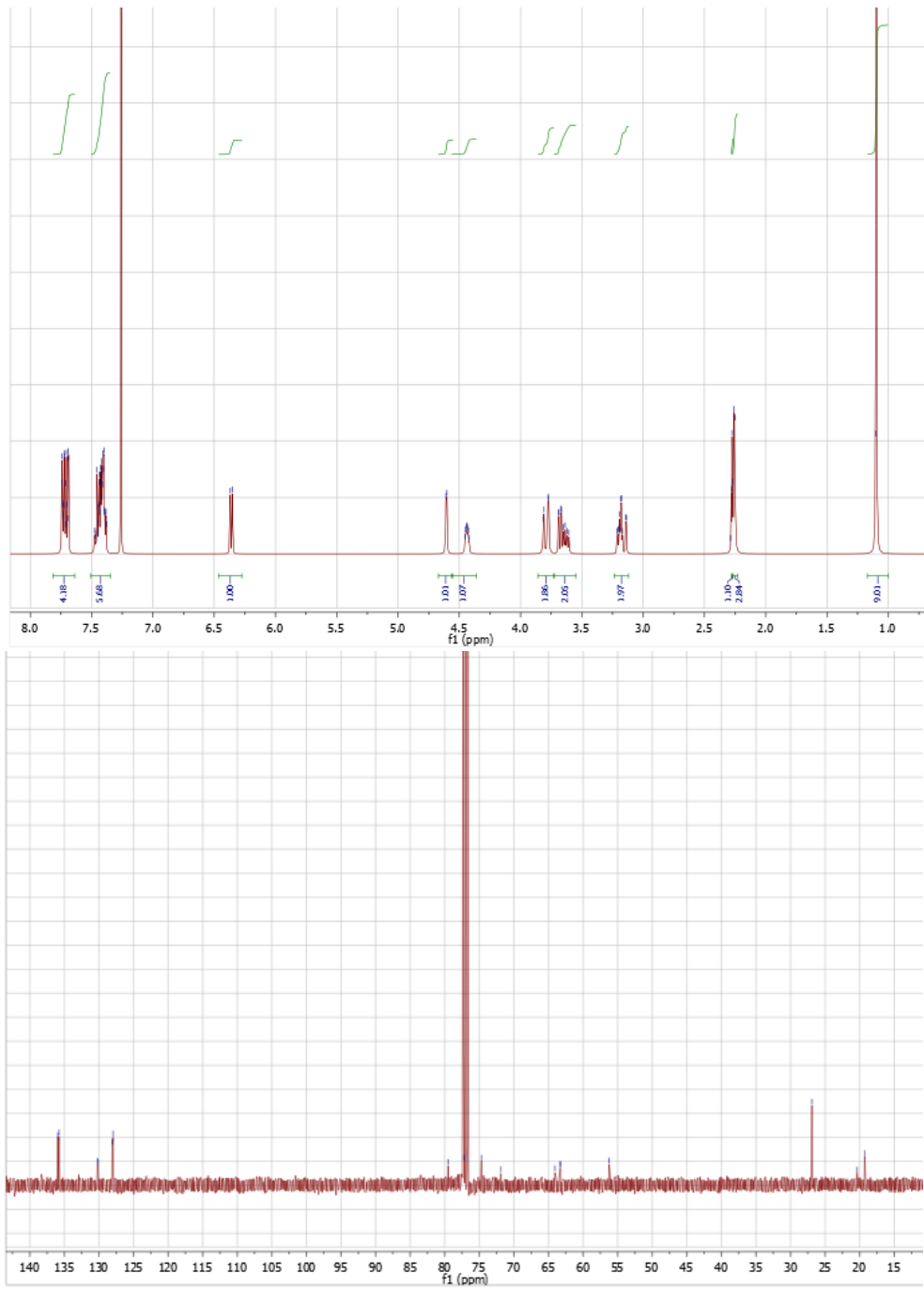


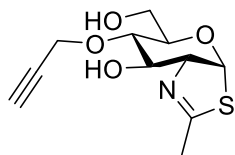
Compound 6. 6-O-pivaloyl-3-O-(*tert*-butyldiphenylsilyl)-NAG-thiazoline (188 mg, 0.348 mmol) was added to a 50 mL flame dried round bottom flask under an atmosphere of argon. The compound was dissolved in anhydrous DMF (3 mL) and barium oxide (62 mg, 0.404 mmol), barium hydroxide (76 mg, 0.404 mmol), tetrabutylammonium iodide (18 mg, 0.056 mmol) and propargyl bromide (29 μ L, 0.194 mmol) were added and the mixture was left stirring overnight at room temperature. Ethyl acetate (50 mL) was added to the mixture and washed thrice with water, back extracted with ethyl acetate, washed thrice more with water and brine before drying over sodium sulfate, concentrated, and purified using silica gel flash column chromatography (1:1:8 ethyl acetate:DCM:hexanes) to yield 6-O-pivaloyl-4-O-propargyl-3-O-(*tert*-butyldiphenylsilyl)-NAG-thiazoline as a clear, colorless gum (107 mg, 53%). ^1H NMR (400 MHz, Chloroform-*d*) δ_{H} 7.75-7.69 (m, 4H), 7.48-7.37 (m, 6H), 6.33 (d, J = 6.4 Hz, 1H), 4.61 (d, J = 4.0 Hz, 1H), 4.39 (m, 1H), 4.26-4.14 (m, 2H), 3.82 (dd, J = 15.9, 2.6 Hz, 1H), 3.69 (dd, J = 9.1, 1.5 Hz, 1H), 2.26 (t, J = 2.3 Hz, 1H), 2.21 (d, J = 2.3 Hz, 3H), 1.21 (s, 9H), 1.10 (s, 9H). ^{13}C NMR (100 MHz, Chloroform-*d*) δ_{C} 178.41, 136.05, 135.95, 133.09, 133.07, 130.35, 130.24, 128.20, 128.08, 89.24, 79.42, 76.90, 74.99, 69.89, 69.45, 63.94, 56.35, 38.96, 27.39, 27.07, 27.03, 20.64, 19.44. HRMS (ESI $^+$) m/z $[\text{M}+\text{H}]^+$ calcd for $\text{C}_{32}\text{H}_{41}\text{NO}_5\text{SSi}$ 580.2553, found 580.2574.



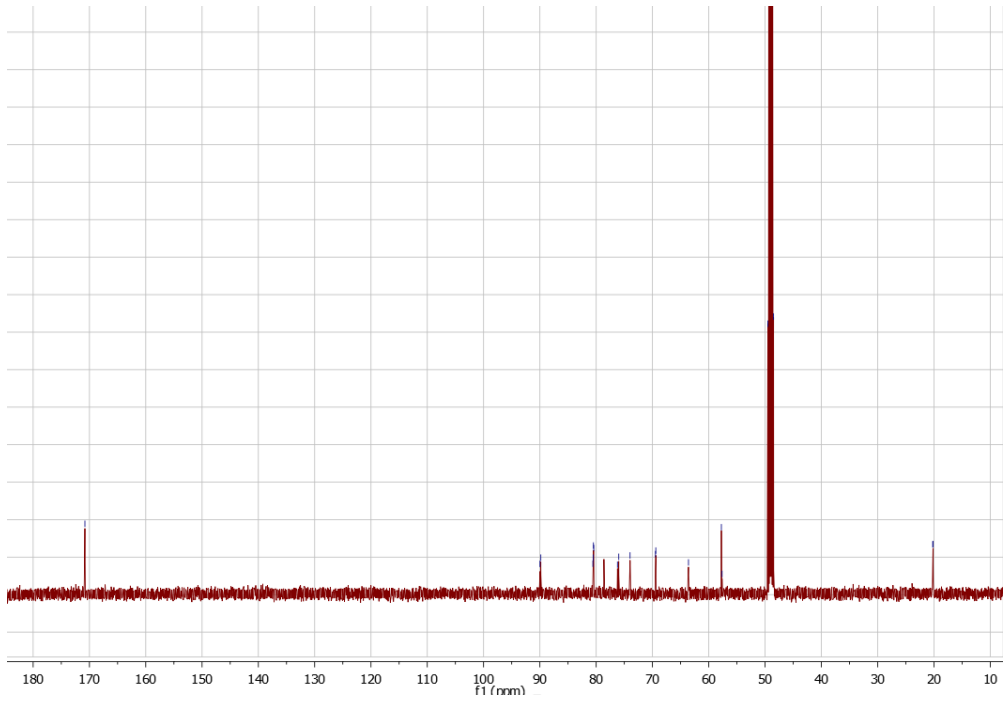
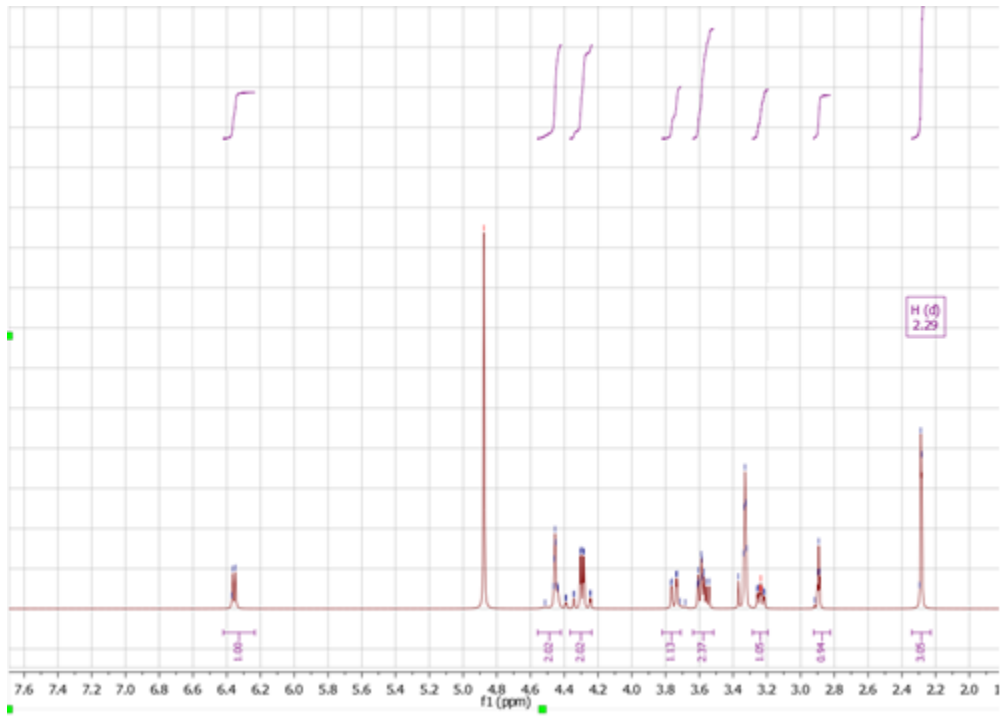


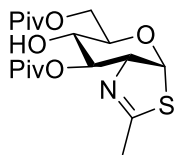
Compound 7. 6-pivaloyl-4-propargyl-3-(tert-butyldiphenylsilyl)-NAG-thiazoline (107 mg, 0.185 mmol) was added to a 50 mL flame dried round bottom flask under an atmosphere of argon. The compound was dissolved in methanol (3 mL) and a methanolic solution of sodium methoxide was added on ice until pH > 10. This solution was left stirring at room temperature for 3 days. The solution was neutralized by the addition of acetic acid until pH=7 and concentrated to 2 mL. Ethyl acetate (50 mL) was added and washed thrice with water and brine before being dried over sodium sulfate, concentrated and purified using silica gel flash column chromatography (3:7 ethyl acetate:hexanes) to yield 4-propargyl-3-(tert-butyldiphenylsilyl)-NAG-thiazoline as a clear, colorless gum (41 mg, 45%). ^1H NMR (400 MHz, Chloroform-*d*) δ_{H} 7.75-7.68 (m, 4H), 7.48-7.37 (m, 6H), 6.36 (d, J = 7.5 Hz, 1H), 4.61 (d, J = 3.3 Hz, 1H), 4.44 (m, 1H), 3.81 (m, 1H), 3.68 (dd, J = 8.1, 1.8 Hz, 1H), 3.63 (dd, J = 12.0, 6.0 Hz, 1H), 3.22-3.13 (m, 2H), 2.27 (t, J = 2.4 Hz, 1H), 2.25 (d, J = 2.0 Hz, 3H), 1.10 (s, 9H). ^{13}C NMR (100 MHz, Chloroform-*d*) δ_{C} 135.95, 135.77, 130.22, 130.13, 128.08, 127.95, 79.51, 77.23, 74.68, 71.89, 64.08, 63.29, 56.24, 26.91, 20.37. HRMS (ESI⁺) m/z [M+H]⁺ calcd for C₂₇H₃₄NO₄SSi 496.1978, found 496.1976.



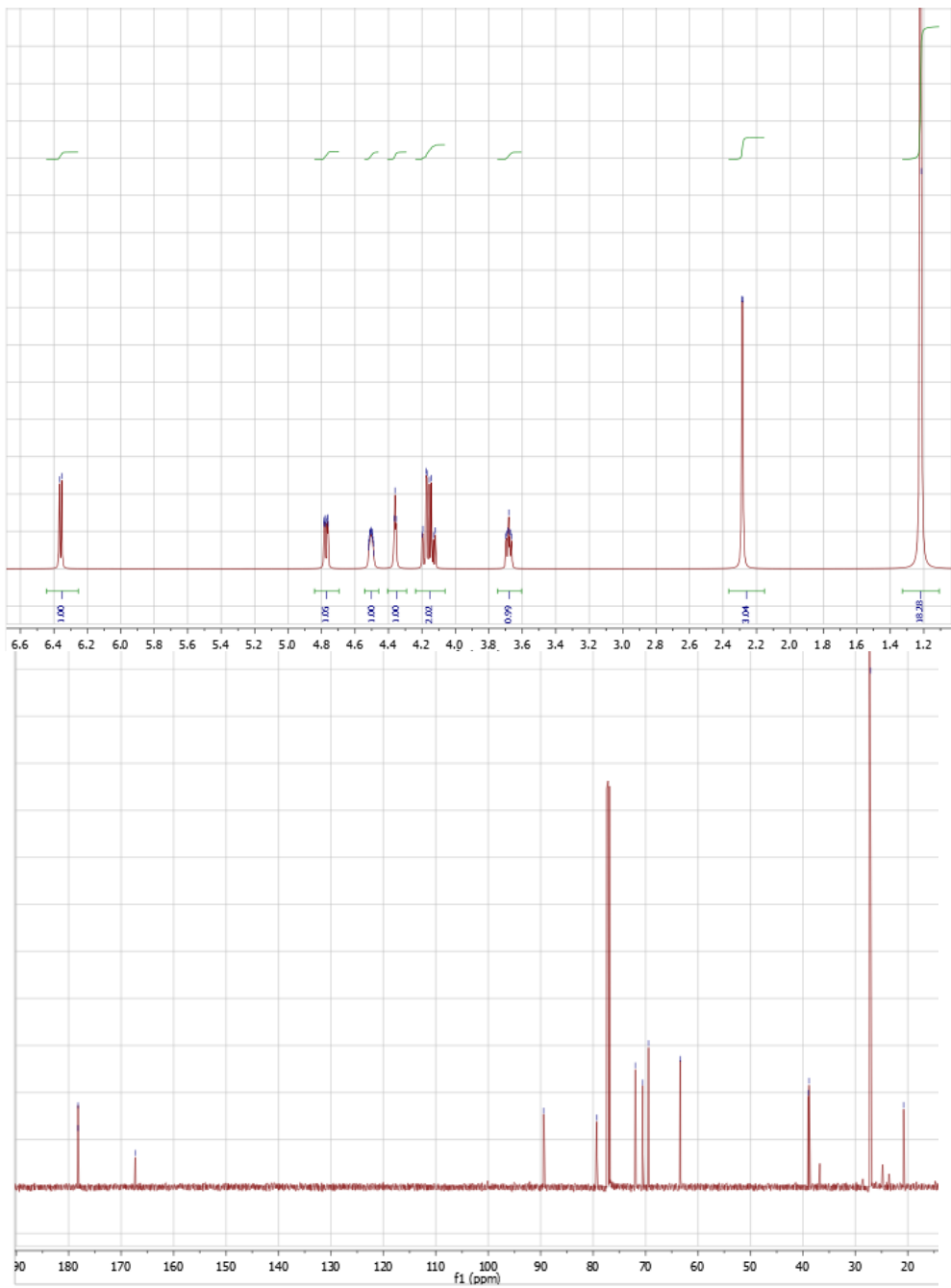


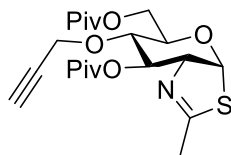
Compound 8. 3,6-*O*-dipivaloyl-4-*O*-propargyl-NAG-thiazoline was added to a 50 mL flame-dried round bottom flask under an atmosphere of argon. The compound was dissolved in methanol, then a 10% w/w methanolic solution of sodium methoxide was added and left stirring at room temperature overnight. The pH of the solution was checked to be approximately 10 and acetic acid diluted in methanol was added in an ice bath. Once neutralized, solvent was removed under vacuum and the residue was partially dissolved in DCM and filtered. The filtrate was concentrated and purified via silica gel flash column chromatography (1:19 methanol:DCM) to afford 4-*O*-propargyl-NAG-thiazoline as a white foam. ^1H NMR (400 MHz, Chloroform-*d*) δ_{H} 6.34 (d, $J = 6.0$ Hz, 1H), 4.45-4.40 (m, 2H), 4.31 (dd, $J = 16.1, 2.4$ Hz, 1H), 4.25 (dd, $J = 16.0, 2.4$ Hz, 1H), 3.73 (dd, $J = 12.2, 2.0$ Hz, 1H), 3.60-3.52 (m, 2H), 3.22 (m, 1H), 2.87 (t, $J = 3.1$ Hz, 1H), 2.27 (d, $J = 2.0$ Hz, 1H). ^{13}C NMR (126 MHz, Methanol-*d*) δ 170.81, 89.98, 89.83, 80.59, 80.54, 80.48, 80.43, 76.22, 75.99, 73.98, 69.47, 69.41, 63.61, 57.76, 57.64, 20.22, 20.18. HRMS (ESI $^+$) m/z : $[\text{M}+\text{H}]^+$ calcd for $\text{C}_{11}\text{H}_{16}\text{NO}_4\text{S}$ 258.0800, found 250.0789.



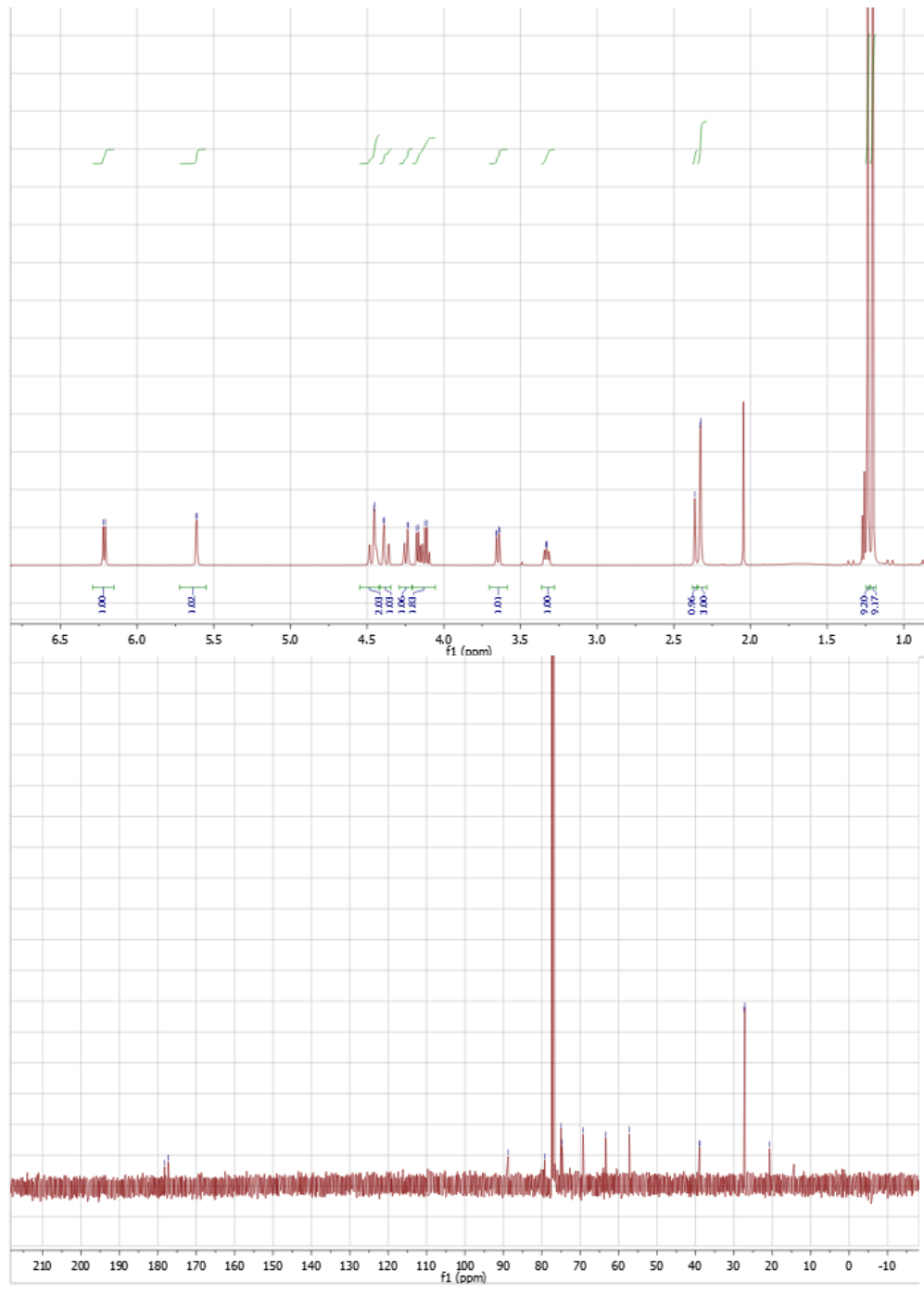


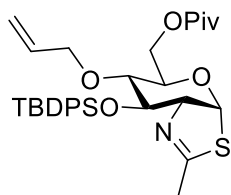
Compound 9. NAG-thiazoline (1.80 g, 8.66 mmol) was added to a 250 mL flame dried round bottom flask under an atmosphere of argon. The compound, along with DMAP (100 mg, 0.9 mmol), was dissolved in pyridine (100 mL) and pivaloyl chloride (2.1 mL, 17.0 mmol) was added dropwise at 0 °C. Once the addition was complete, the reaction mixture was allowed to warm to room temperature and left stirring overnight. Upon completion, the solution was concentrated to about 1/5 of the original volume with the addition of toluene under vacuum. Ethyl acetate (200 mL) was added and washed five times with water. The resulting organic layer was further washed with a saturated aqueous solution of potassium bisulfate until no pyridinium bisulfate precipitates were found and dried over sodium sulfate before being filtered and concentrated *in vacuo*. Purification by column chromatography (2:3 ethyl acetate:hexanes) yielded an equimolar amount of 3,6-O-dipivaloyl-NAG-thiazoline and 4,6-O-dipivaloyl-NAG-thiazoline as a clear, colorless gum (1.10 g for each, 33%) along with 6-O-pivaloyl-NAG-thiazoline. ¹H NMR (400 MHz, Chloroform-*d*) δ_H 6.33 (d, *J* = 7.3 Hz, 1H), 4.75 (ddd, *J* = 9.1, 2.7, 0.9 Hz, 1H), 4.48 (s(br), 1H), 4.33 (t, *J* = 3.1 Hz, 1H), 4.16 (dd, *J* = 12.0, 2.7 Hz, 1H), 4.11 (dd, *J* = 12.0, 6.1 Hz, 1H), 3.65 (ddd, *J* = 8.8, 6.0, 2.7 Hz, 1H), 2.26 (d, *J* = 2.0 Hz, 3H), 1.19 (s, 18H). ¹³C NMR (100 MHz, Chloroform-*d*) δ_C 178.23, 178.21, 167.29, 89.43, 79.31, 71.93, 70.56, 69.43, 63.39, 38.97, 38.83, 36.78, 27.29, 27.09, 24.81, 20.79. HRMS (ESI⁺) *m/z*: [M+H]⁺ calcd for C₁₈H₃₀NO₆S 388.1794, found 388.1817.



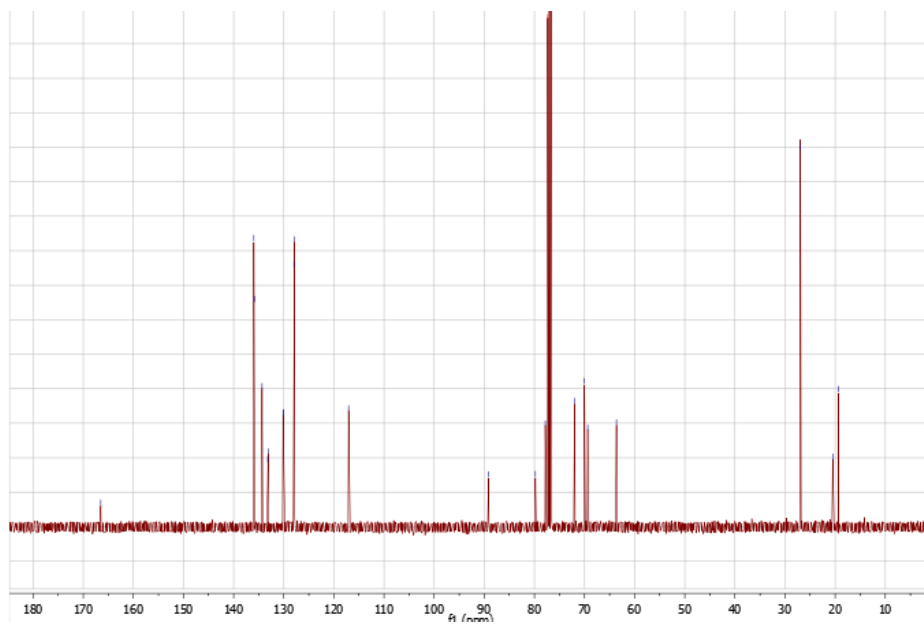
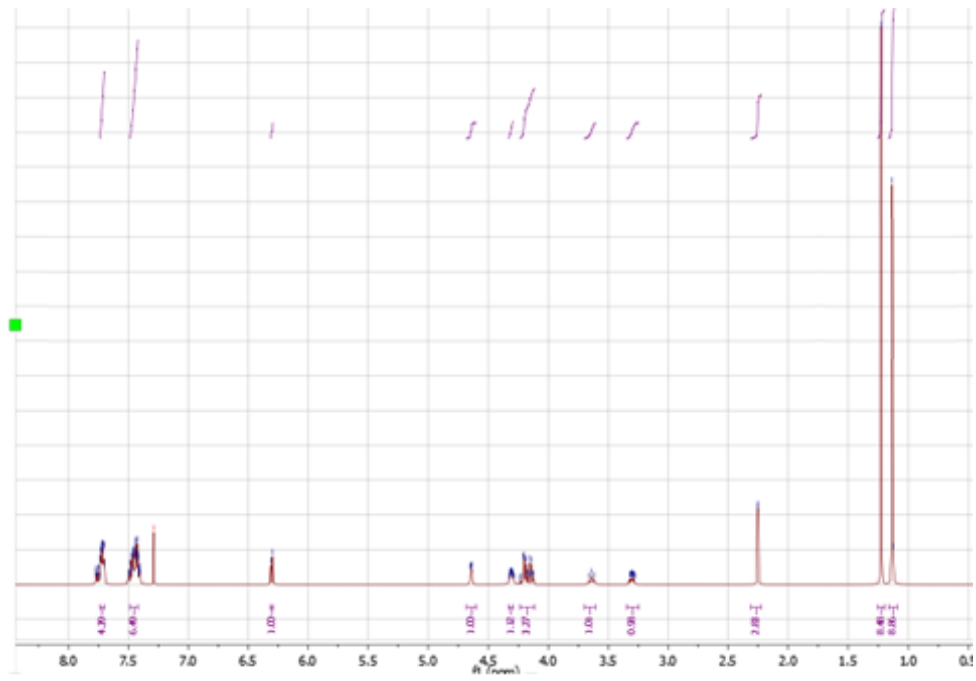


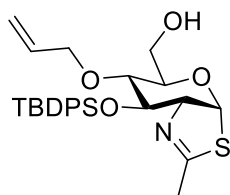
Compound 10. 3,6-O-dipivaloyl-NAG-thiazoline (200 mg, 0.516 mmol) was added to a 100 mL flame dried round bottom flask under an atmosphere of argon. The compound was dissolved in anhydrous DMF (25 mL) and cooled in a dry ice-brine bath at -20 °C. Sodium hydride (42 mg, 1.04 mmol, 60% dispersion in mineral oil) was slowly added in small portions over 5 minutes and left stirring for 10 minutes. Propargyl bromide (974 μ L, 1.04 mmol, 80% in toluene) was added dropwise and the reaction mixture was stirred at -20 °C for 6 hours and moved to an ice bath at 0 °C for 4 hours. Ethyl acetate was added to the mixture and washed five times with water, followed by back extraction of the aqueous layer with ethyl acetate. The combined organic layers were washed eight times with water and brine to minimize residual DMF. The remaining solvent was dried over Na_2SO_4 before being filtered and concentrated *in vacuo* and purified by silica gel flash column chromatography (1:4 ethyl acetate : hexanes) to afford 3,6-O-dipivaloyl-4-O-propargyl-NAG-thiazoline as a clear, colorless gum (129 mg, 59%). ^1H NMR (400 MHz, Chloroform-*d*) δ_{H} 6.27 (d, $J = 7.3$ Hz, 1H), 4.82 (d, $J = 8.0$ Hz, 1H), 4.54 (m, 1H), 4.41 (d, $J = 2.7$ Hz, 2H), 4.30 (m, 1H), 4.14 (dd, $J = 12.1, 2.5$ Hz, 1H), 4.03 (dd, $J = 12.0, 6.5$ Hz, 1H), 3.53 (ddd, $J = 8.9, 6.6, 2.3$ Hz 1H), 2.42 (t, $J = 2.1$ Hz, 1H), 2.27 (d, $J = 2.4$ Hz, 1H), 1.20 (s, 9H), 1.10 (s, 9H). ^{13}C NMR (100 MHz, Chloroform-*d*) δ_{C} 178.25, 177.28, 88.78, 79.24, 75.01, 74.76, 69.28, 63.36, 57.21, 38.96, 39.91, 27.35, 27.15, 20.72. HRMS (ESI⁺) m/z . $[\text{M}+\text{H}]^+$ calcd for $\text{C}_{21}\text{H}_{32}\text{NO}_6\text{S}$ 426.1950, found 426.1942.



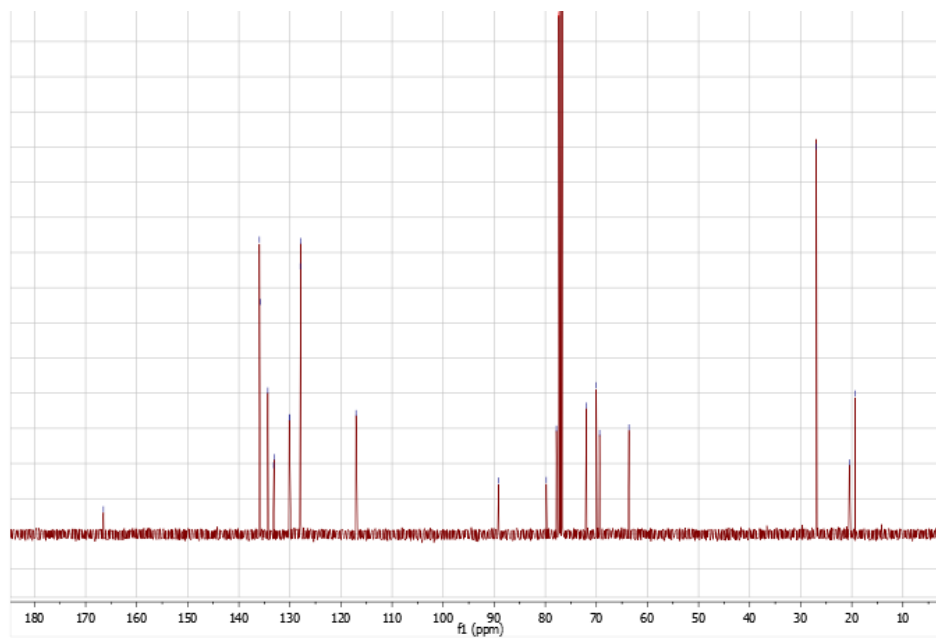
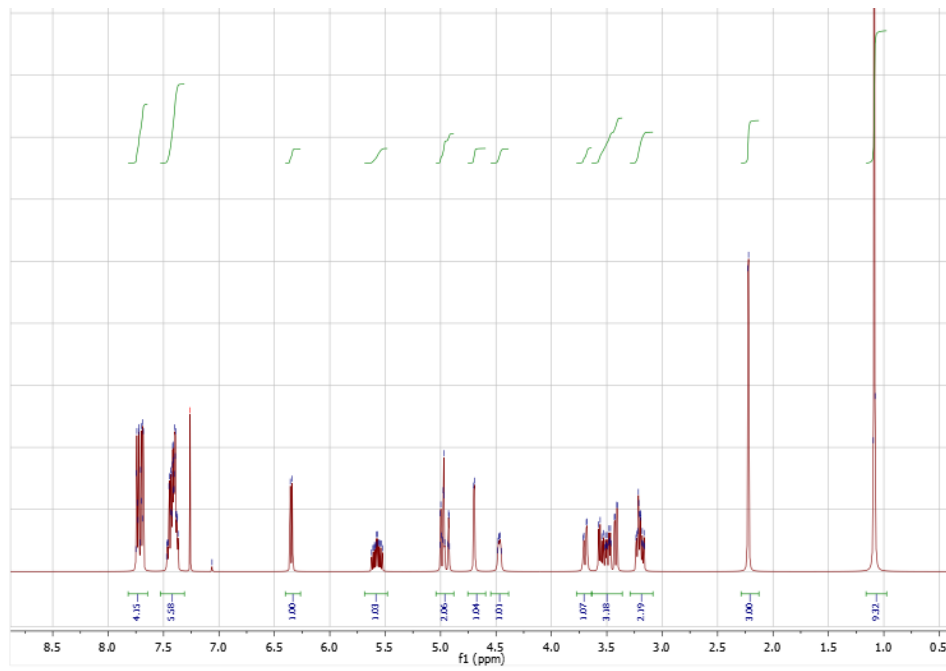


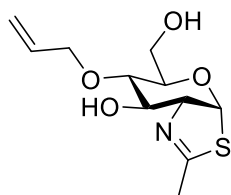
Compound 11. 6-pivaloyl-3-(*tert*-butyldiphenylsilyl)-NAG-thiazoline (490 mg, 0.904 mmol) was dissolved in DMF (10 mL) in a 50 mL flame-dried round bottom flask under an atmosphere of argon. Allyl bromide (153 μ L, 1.81 mmol) and TBAI (42 mg, 0.114 mmol) were added to the flask and cooled to -40 $^{\circ}$ C. Sodium hydride (40 mg, 0.995 mmol, 60% dispersion in mineral oil) was slowly added in three portions and left stirring at -40 $^{\circ}$ C for 6.5 hours. Ethyl acetate (100 mL) was added and the mixture was washed thrice with water and brine before drying over sodium sulfate, concentrated, and purified using silica gel flash column chromatography (1:9 ethyl acetate:hexanes) to yield 4-allyl-6-pivaloyl-3-(*tert*-butyldiphenylsilyl)-NAG-thiazoline as a clear, colorless gum (220 mg, 0.379 mmol). 1 H NMR (400 MHz, Chloroform-*d*) δ_{H} 7.72 (m, 4H), 7.47-7.37 (m, 6H), 6.32 (d, J = 7.2 Hz, 1H), 5.59 (m, 1H), 4.99 (m, 2H), 4.71 (d, J = 3.7 Hz, 1H), 4.42 (m, 1H), 4.12 (d, J = 5.0 Hz, 2H), 3.55 (dd, J = 12.9, 4.9 Hz, 1H), 3.39 (d, J = 9.5 Hz, 1H), 3.30 (m, 1H), 3.23 (dd, J = 12.5, 6.3, 1H), 2.22 (d, J = 1.8 Hz, 3H), 1.21 (s, 9H), 1.08 (s, 9H). 13 C NMR (100 MHz, Chloroform-*d*) δ_{C} 178.47, 136.06, 135.97, 134.33, 133.26, 133.21, 130.30, 130.24, 128.13, 128.06, 117.69, 89.28, 78.11, 70.25, 70.12, 69.74, 64.34, 38.97, 27.37, 27.08, 20.67, 19.51. HRMS (ESI $^{+}$) m/z : [M+H] $^{+}$ calcd for C₃₂H₄₄NO₅SSi 582.2704, found 582.2729.



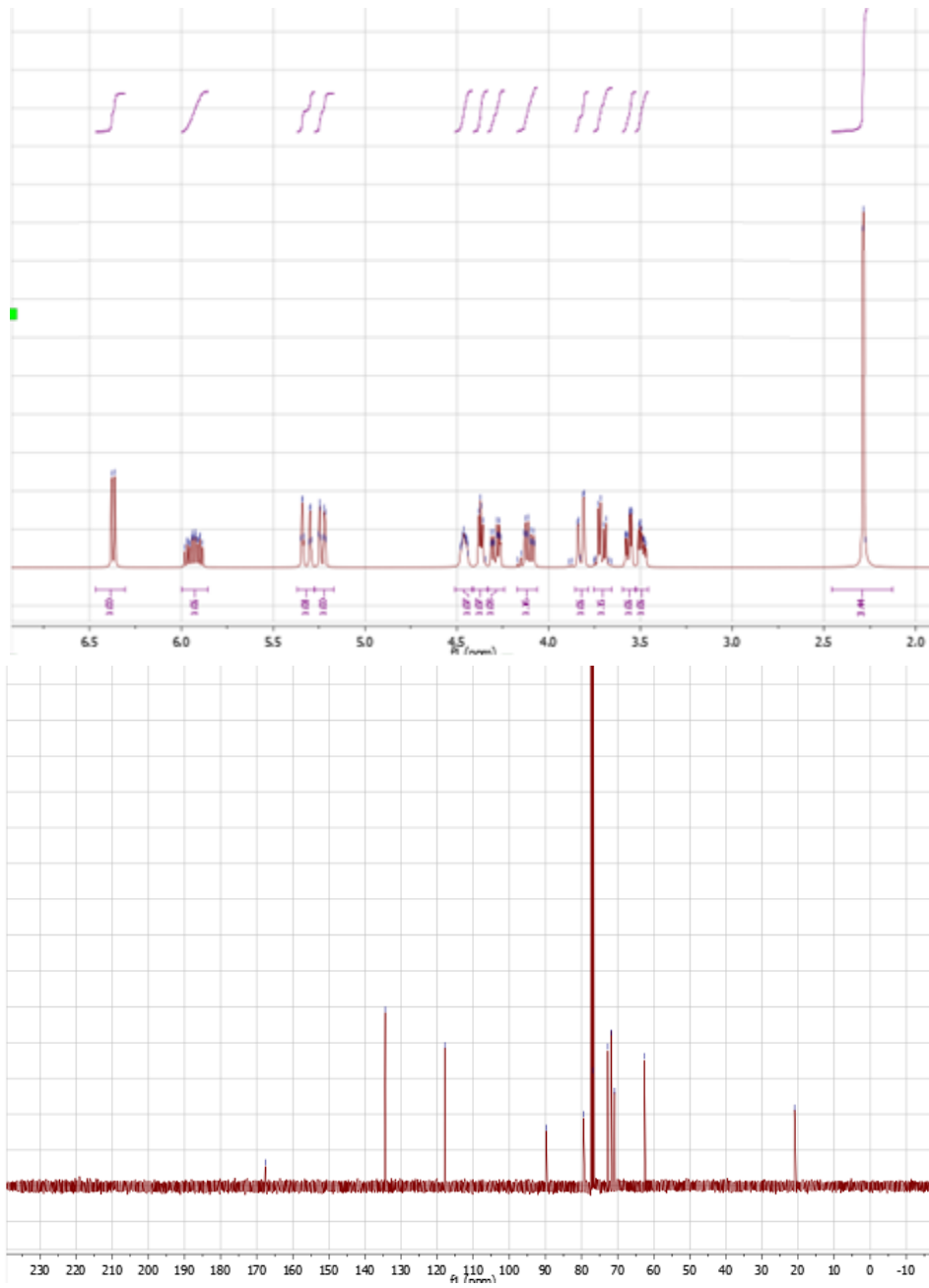


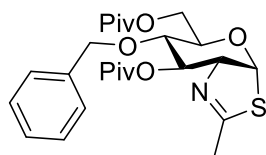
Compound 12. 4-O-allyl-6-O-pivaloyl-3-O-(*tert*-butyldiphenylsilyl)-NAG-thiazoline (88 mg, 0.151 mmol) was added to a 50 mL flame-dried round bottom flask and dissolved in methanol (2 mL). A methanolic solution of sodium methoxide was added until pH > 10. The solution was stirred overnight at room temperature and neutralized with acetic acid. After reducing the volume to 3mL via reduced pressure, ethyl acetate (100 mL) was added and washed thrice with water and brine. The organic layer was dried over sodium sulfate, concentrated and purified using silica gel flash column chromatography (3:7 ethyl acetate:hexanes) to afford 4-O-allyl-3-O-(*tert*-butyldiphenylsilyl)-NAG-thiazoline as a clear colorless gum (29 mg, 33%) ^1H NMR (400 MHz, Chloroform-*d*) δ_{H} 7.71 (m, 4H), 7.47-7.38 (m, 6H), 6.35 (d, $J = 7.2$ Hz, 1H), 5.58 (m, 1H), 4.98 (m, 2H), 4.71 (d, $J = 3.4$ Hz, 1H), 4.47 (m, 1H), 4.12 (d, $J = 5.0$ Hz, 2H), 3.70 (d, $J = 11.3$ Hz, 1H), 3.58-3.49 (m, 2H), 3.42 (d, $J = 8.2$ Hz, 1H), 3.20 (m, 2H), 2.25 (d, $J = 1.8$ Hz, 3H), 1.09 (s, 9H). ^{13}C NMR (100 MHz, Chloroform-*d*) δ_{C} 136.11, 135.96, 134.45, 130.32, 130.25, 128.14, 128.03, 117.28, 80.78, 77.82, 72.23, 70.18, 63.78, 27.07, 19.48. HRMS (ESI $^+$) m/z : $[\text{M}+\text{H}]^+$ calcd for $\text{C}_{27}\text{H}_{36}\text{NO}_4\text{SSi}$ 498.2134, found 498.2122.



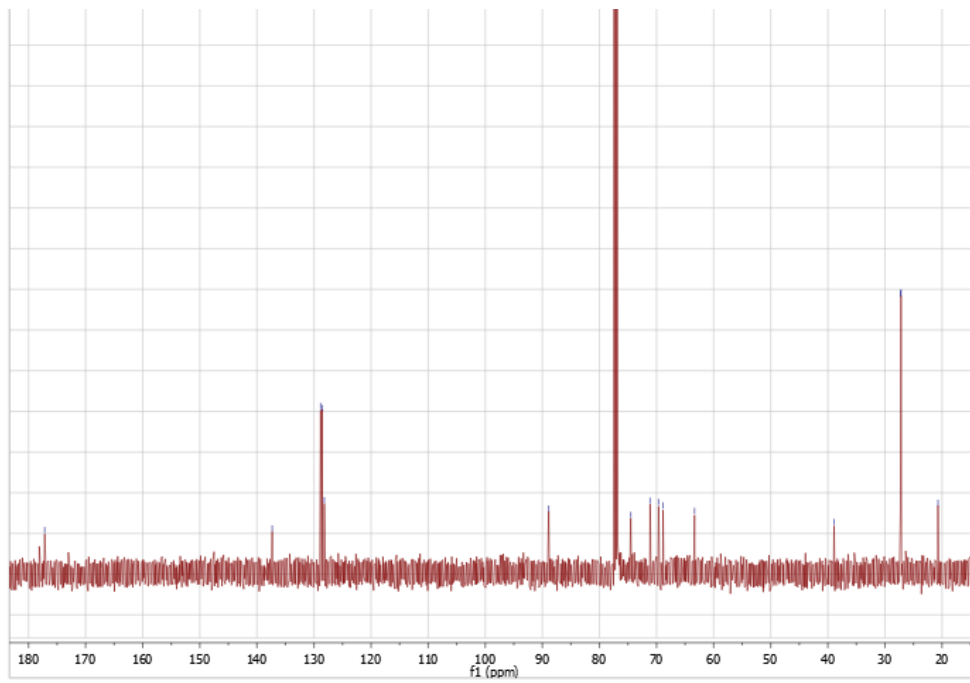
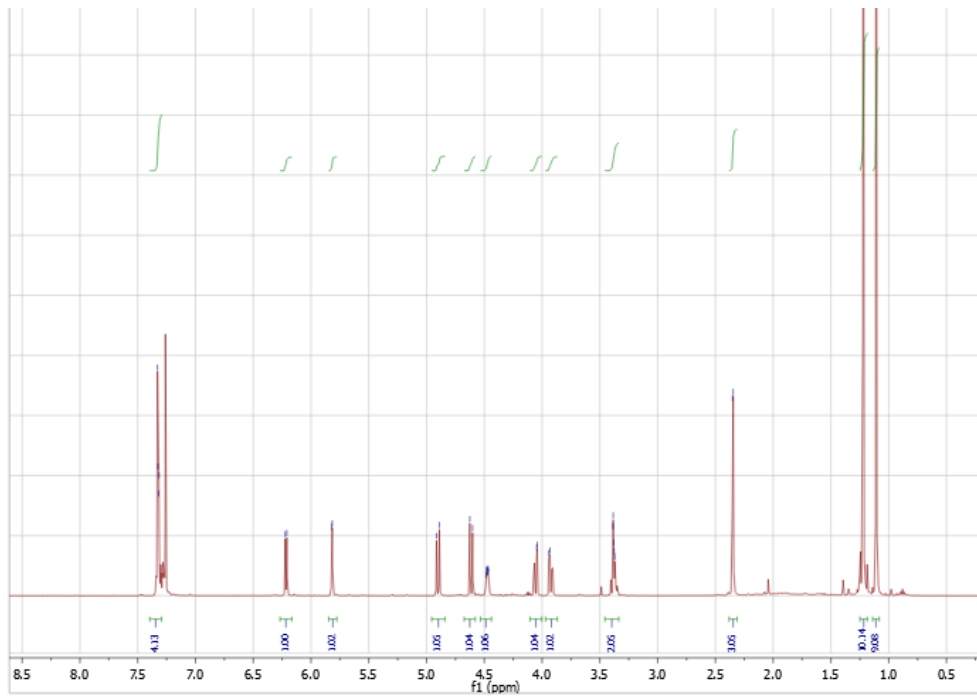


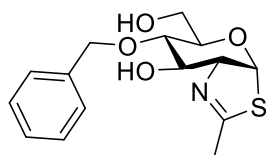
Compound 13. 4-O-allyl-3-O-(*tert*-butyldiphenylsilyl)-NAG-thiazoline (35 mg, 0.070 mmol) was added to a 50 mL flame-dried round bottom flask and dissolved in THF (3 mL) under an atmosphere of argon. TBAF (100 μ L, 1.0 M solution) was added and left stirring for 3 hours. When the reaction was complete, solvent was removed and purified on silica gel (1:19 methanol:DCM) to afford 4-O-allyl-NAG-thiazoline (18 mg, 99%) ^1H NMR (400 MHz, Chloroform-*d*) δ_{H} 6.32 (d, $J = 7.0$ Hz, 1H), 5.60 (m, 1H), 5.01 (d, $J = 11.5$ Hz, 1H), 4.97 (d, $J = 16.8$ Hz, 1H), 4.71 (d, $J = 3.4$ Hz, 1H), 4.47 (m, 1H), 4.12 (d, $J = 5.0$ Hz, 2H), 3.70 (d, $J = 11.3$ Hz, 1H), 3.58-3.49 (m, 2H), 3.42 (d, $J = 8.2$ Hz, 1H), 3.20 (m, 2H), 2.23 (d, $J = 1.8$ Hz, 3H). ^{13}C NMR (100 MHz, Chloroform-*d*) δ_{C} 178.37, 117.78, 89.51, 78.23, 70.11, 70.37, 69.69, 64.25, 38.88, 20.16. HRMS (ESI $^+$) m/z [M+H] $^+$ calcd for $\text{C}_{11}\text{H}_{18}\text{NO}_4\text{S}$ 260.0957, found 260.0949.



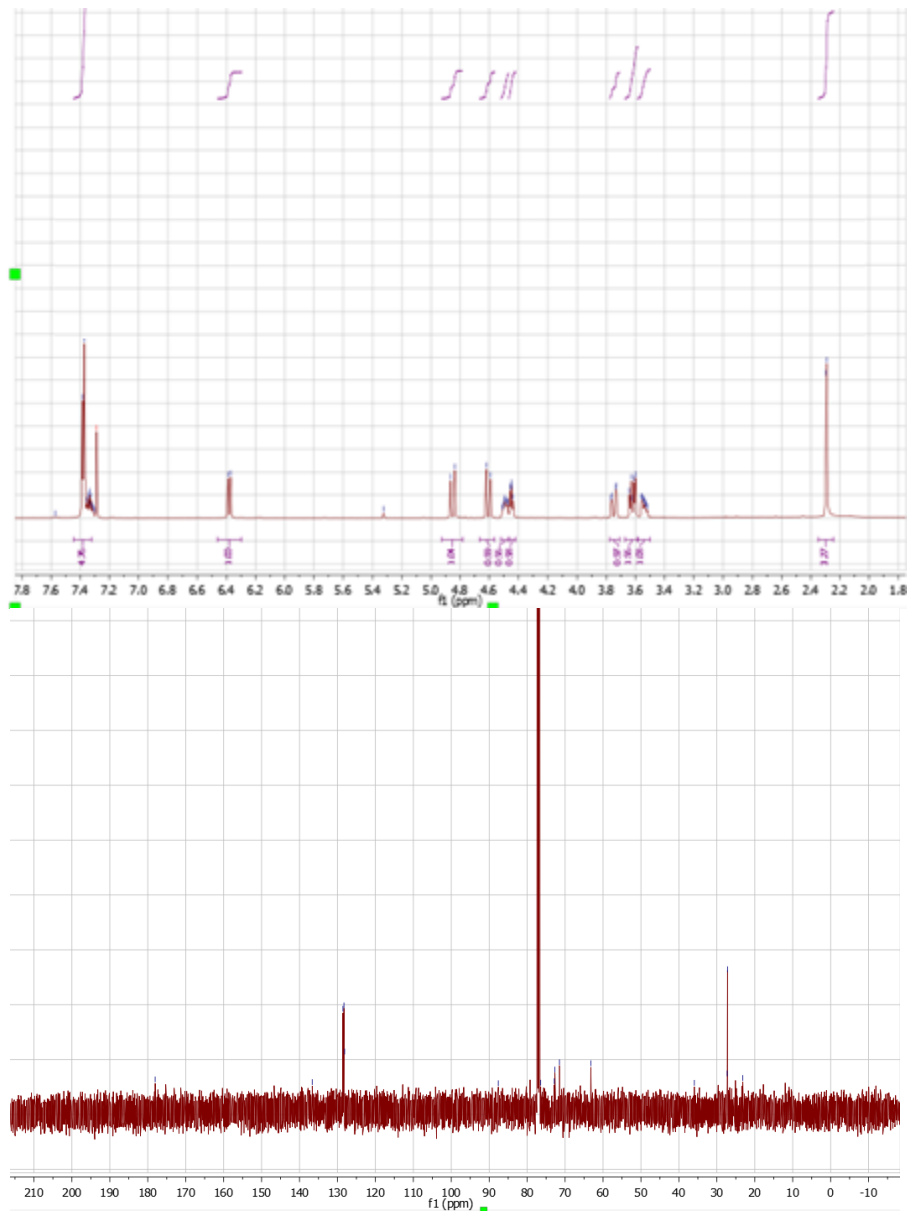


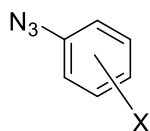
Compound 14. 3,6-di-O-pivaloyl-NAG-thiazoline (84 mg, 0.217 mmol) was added to a 50 mL flame dried round bottom flask under an atmosphere of argon. The compound was dissolved in DMF (5 mL) and cooled to -15 °C before adding sodium hydride (14 mg, 0.282 mmol, 60% dispersion in mineral oils). After stirring for 5 minutes, benzyl bromide (39 μ L, 0.325 mmol) was added and stirred for 4.5 hours at -15 °C. Upon completion of the reaction, ethyl acetate (30 mL) was added and the resulting solution was washed five times with water and brine before being dried over sodium sulfate and concentrated *in vacuo*. The resulting residue was purified using silica gel flash column chromatography (3:7 ethyl acetate:hexanes) to yield 4-O-benzyl-3,6-di-O-pivaloyl-NAG-thiazoline as a clear white foam (71 mg, 69%). ^1H NMR (400 MHz, Chloroform-*d*) δ_{H} 7.33 (m, 5H), 6.21 (d, $J = 8.0$ Hz, 1H), 5.82 (d, $J = 2.9$ Hz, 1H) 4.90 (d, $J = 12.5$ Hz, 1H), 4.61 (d, $J = 12.5$ Hz, 1H), 4.47 (m, 1H), 4.06 (dd, $J = 12.2, 1.5$ Hz, 1H), 3.93 (dd, $J = 12.2, 5.2$ Hz, 1H), 3.38 (m, 2H), 2.35 (d, $J = 2.2$ Hz, 3H), 1.22 (s, 9H), 1.11 (s, 9H). ^{13}C NMR (100 MHz, Chloroform-*d*) δ_{C} 177.16, 137.31, 128.83, 128.56, 128.18, 88.89, 74.52, 71.12, 69.64, 68.86, 63.36, 38.90, 27.27, 27.78, 20.70. HRMS (ESI⁺) m/z . $[\text{M}+\text{H}]^+$ calcd for $\text{C}_{25}\text{H}_{36}\text{NO}_6\text{S}$ 478.2263, found 478.2271.



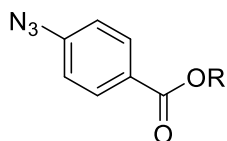


Compound 15. 4-O-benzyl-3,6-di-O-pivaloyl-NAG-thiazoline (71 mg, 0.149 mmol) was added to a 50 mL flame dried round bottom flask under an atmosphere of argon. The compound was dissolved in THF (3 mL) and water (1 mL). Lithium hydroxide (10.7 mg, 0.446 mmol) was added to this solution and left stirring overnight. After completion of the reaction, ammonium acetate (34 mg, 0.441 mmol) was added and solvent was removed under reduced pressure with the addition of ethanol. The resulting residue was purified using silica gel flash column chromatography (1:1 ethyl acetate:hexanes) to yield 4-O-benzyl-NAG-thiazoline as a clear white foam (29 mg, 63%). ^1H NMR (400 MHz, Methanol-*d*) δ_{H} 7.34 (m, 5H), 6.34 (d, $J = 7.4$ Hz, 1H), 4.78 (d, $J = 11.0$ Hz, 1H), 4.61 (d, $J = 12.5$ Hz, 1H), 4.57 (m, 1H), 4.50 (m, 2H), 4.00 (dd, $J = 10.8, 6.3$ Hz, 1H), 3.77 (d, $J = 10.8$ Hz, 1H), 3.51 (dt, $J = 7.5, 1.4$ Hz, 1H), 3.40 (ddd, $J = 9.0, 6.5, 2.3$ Hz, 1H), 2.28 (d, 2.3 Hz, 3H). ^{13}C NMR (100 MHz, Methanol-*d*) δ_{C} 177.01, 137.17, 128.68, 128.42, 128.04, 88.75, 74.33, 70.93, 69.49, 68.72, 63.21, 38.75, 27.12, 27.03, 20.96. HRMS (ESI⁺) m/z [M+H]⁺ calcd for C₁₅H₂₀NO₄S 310.1113, found 310.1108.





General procedure for halogenated azido benzenes: Halo-aniline (4 mmol) and sodium nitrite (276 mg, 4 mmol) was dissolved in an aqueous solution of hydrochloric acid (6 M, 15 mL) in a 50 mL round bottom flask and cooled to 0 °C. In a separate flask, sodium azide (325 mg, 5 mmol) was dissolved in water (6 mL), cooled to 0 °C, and added dropwise to the aniline solution and stirred for 3.5 hours at 0 °C. After completion of the reaction, ethyl acetate (30mL) was added to the reaction flask and washed three times with water and brine before being dried over sodium sulfate. Solvent was removed under vacuum to yield 1-azido-halo-benzene (40-65%) as a clear colorless liquid and used without further purification. Procedures and reference spectra were obtained from the laboratory of Prof. Peng Wu as pure compounds were not available for purchase due to long term stability.



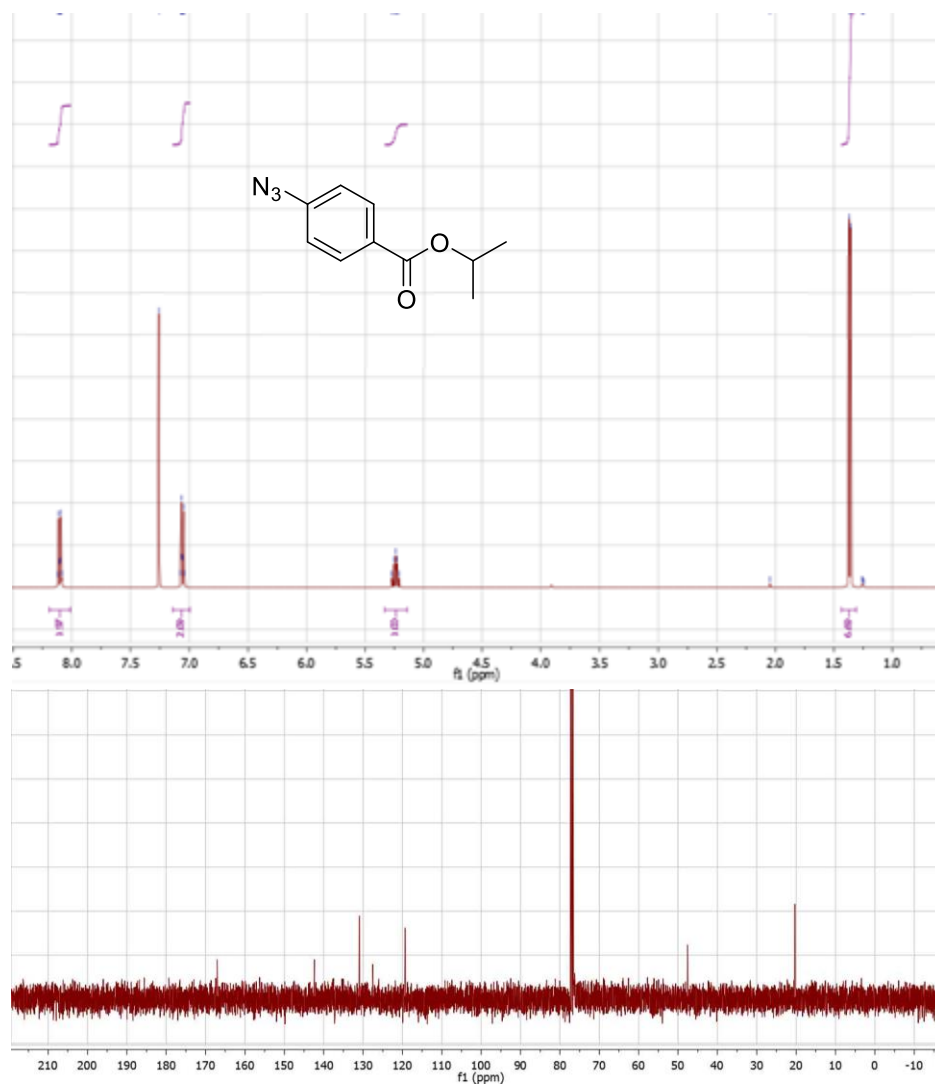
General procedure for 4-azido benzoates (Compounds 41 & 43): 4-azidobenzoic acid (50 mg, 0.31 mmol) was added to a 50 mL flame dried round bottom flask under an atmosphere of argon. The compound was dissolved in alcohol (10 mL), acidified with H₂SO₄ (50 μL, 0.95 mmol) and refluxed for 6 hours. Upon completion of the reaction, solvent was partially removed under vacuum until total volume amounted to approximately 3 mL. Ethyl acetate was added and washed thrice with saturated sodium bicarbonate, water and brine before drying over sodium sulfate. The resulting alkyl 4-azidobenzoate (22-96%) was obtained as a clear colorless liquid and used without further purification.

Compound 41.

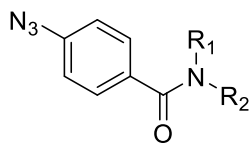


^1H NMR (500 MHz, Chloroform-*d*) δ 8.05 (dd, J = 8.5, 1.6 Hz, 2H), 7.08 (dd, J = 8.5, 1.6 Hz, 2H), 3.93 (d, J = 1.4 Hz, 3H). ^{13}C NMR (125 MHz, Chloroform-*d*) δ 166.73, 142.66, 130.95, 128.08, 119.02, 52.17.

Compound 43.

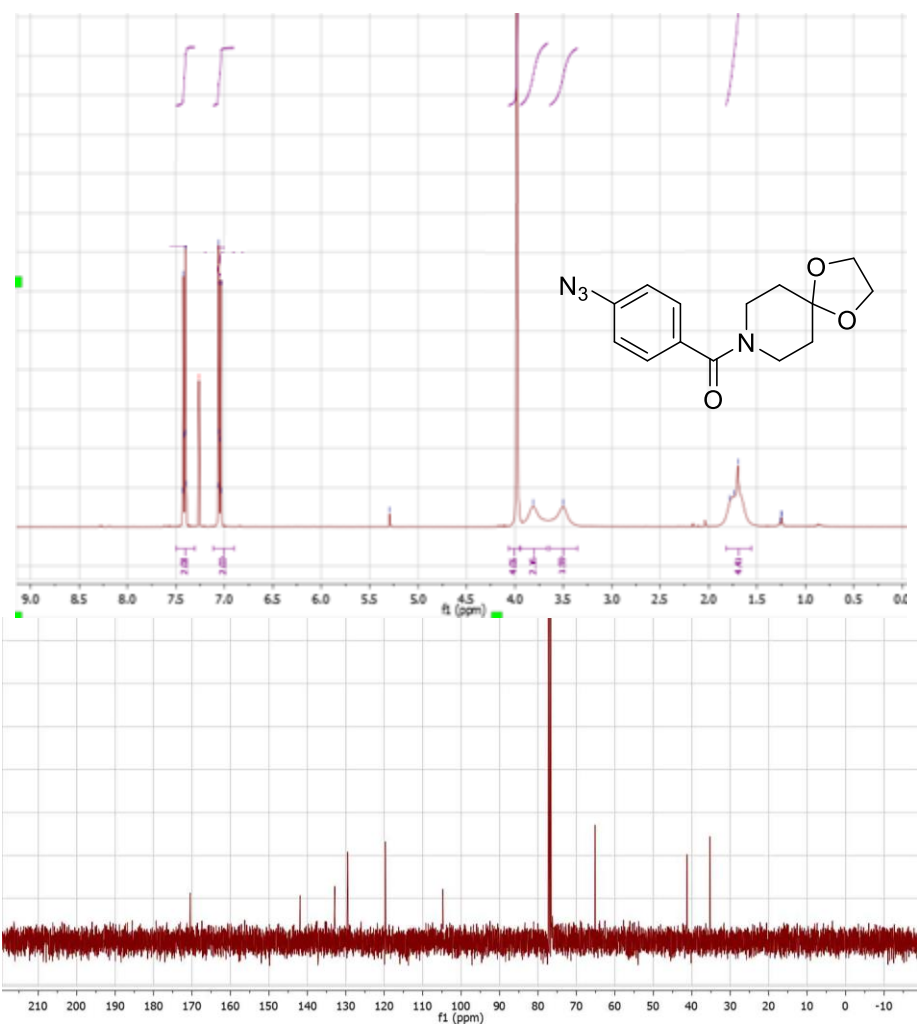


¹H NMR (400 MHz, Chloroform-*d*) δ 8.19 – 8.01 (m, 2H), 7.14 – 7.00 (m, 2H), 5.24 (p, *J* = 6.2 Hz, 1H), 1.36 (d, *J* = 6.2 Hz, 7H). ¹³C NMR (125 MHz, Chloroform-*d*) δ 167.83, 142.34, 131.24, 128.98, 119.27, 47.40, 20.12.



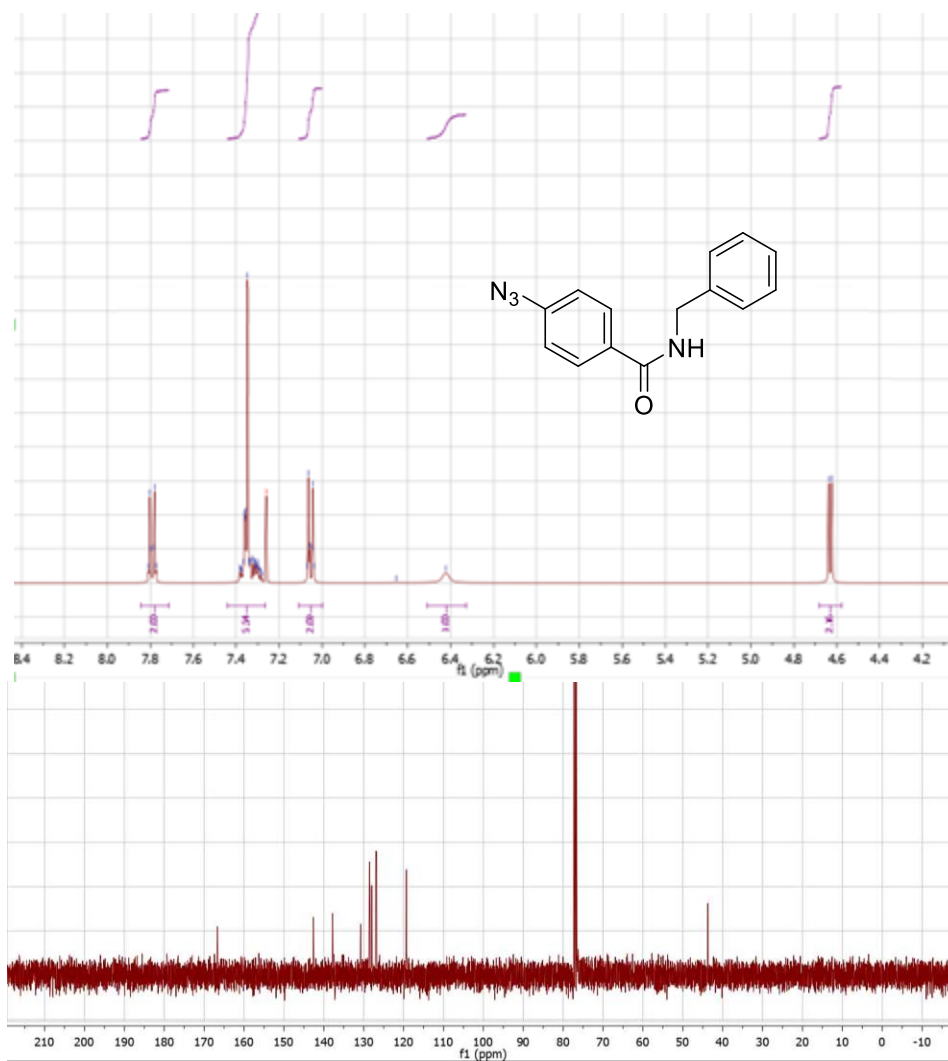
General procedure for 4-azido benzamides (Compounds 40, 42, & 44-50): 4-azidobenzoic acid (20 mg, 0.123 mmol) and EDCI (26 mg, 0.135 mmol) was added to a 50 mL flame-dried round bottom flask under an atmosphere of argon. The compounds were dissolved in chloroform (10 mL), then TEA (14 μ L, 0.135 mmol) and *N*-ethylamine (10 μ L of 2M solution in THF) was added. The reaction mixture was refluxed overnight. Upon completion, the solvent was removed under vacuum and purified by silica gel flash column chromatography (3:7 ethyl acetate:hexanes) to afford 4-azido-*N*-alkylbenzamide as a clear colorless liquid (50-90%).

Compound 40.



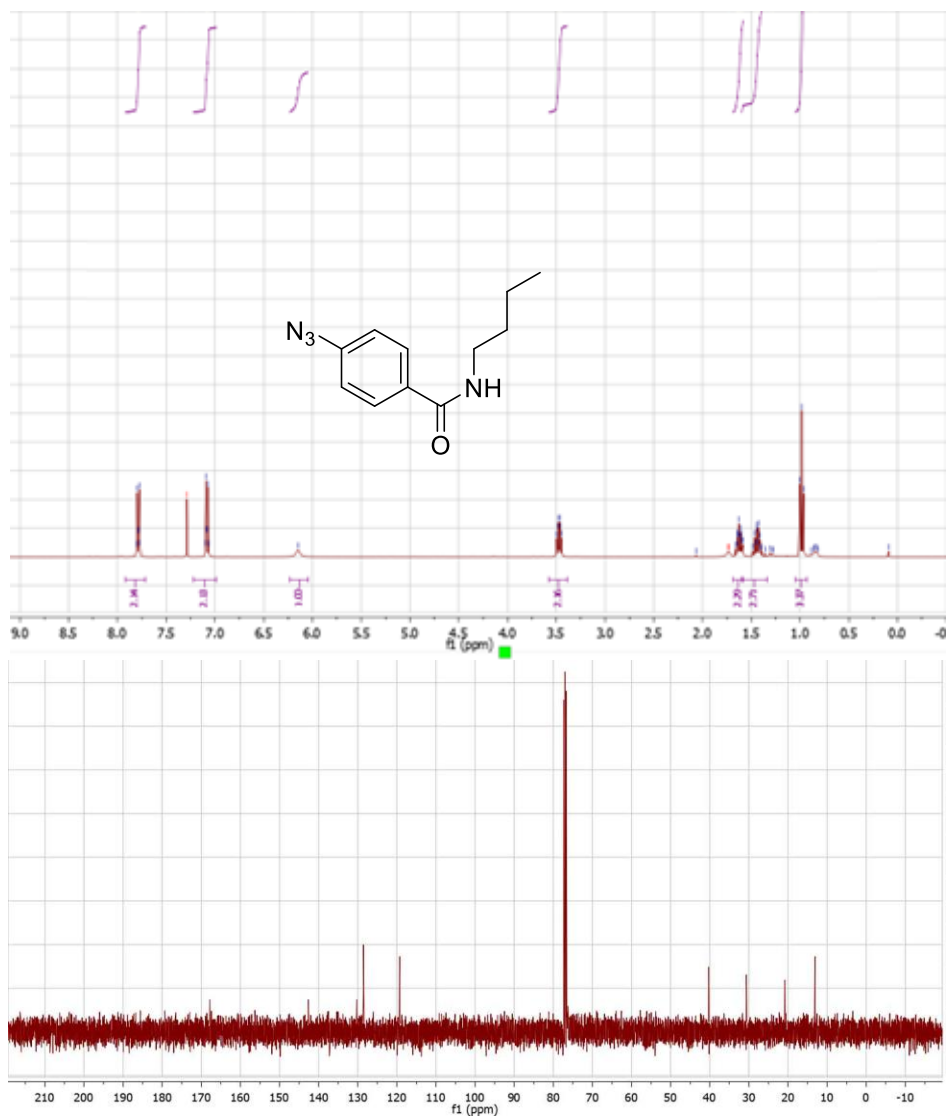
¹H NMR (400 MHz, Chloroform-*d*) δ 7.50 – 7.30 (m, 2H), 7.11 – 6.90 (m, 2H), 3.98 (s, 4H), 3.81 (s, 2H), 3.50 (s, 2H), 1.72 (m, 4H). ¹³C NMR (125 MHz, Chloroform-*d*) δ 170.77, 142.59, 133.16, 129.68, 119.40, 105.83, 64.40, 41.43, 35.21.

Compound 42.



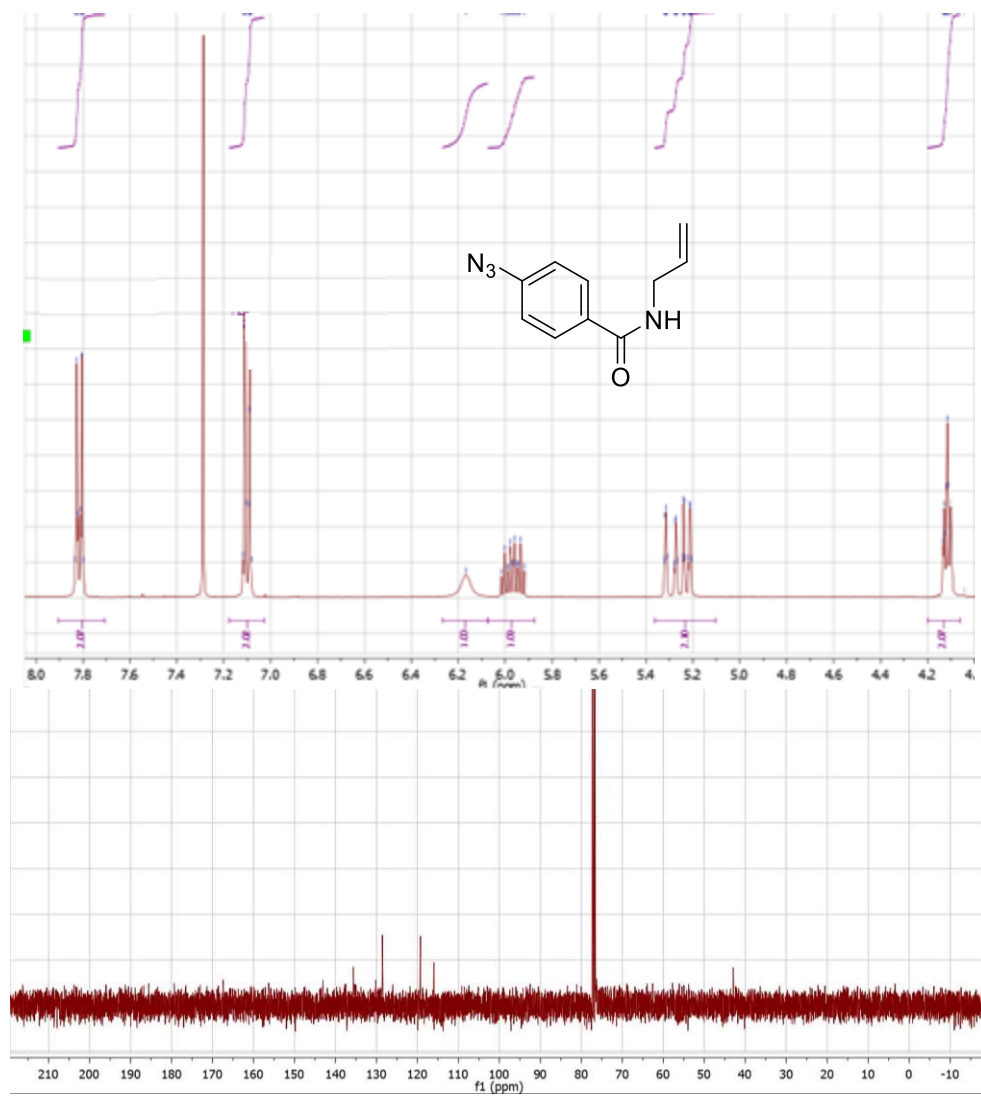
1H NMR (400 MHz, Chloroform-*d*) δ 7.84 – 7.71 (m, 2H), 7.44 – 7.26 (m, 5H), 7.11 – 7.00 (m, 2H), 6.42 (s, 1H), 4.63 (d, $J = 5.6$ Hz, 2H). ^{13}C NMR (125 MHz, Chloroform-*d*) δ 167.51, 142.34, 138.68, 131.26, 128.98, 128.40, 127.31, 127.17, 119.27, 43.74.

Compound 44.



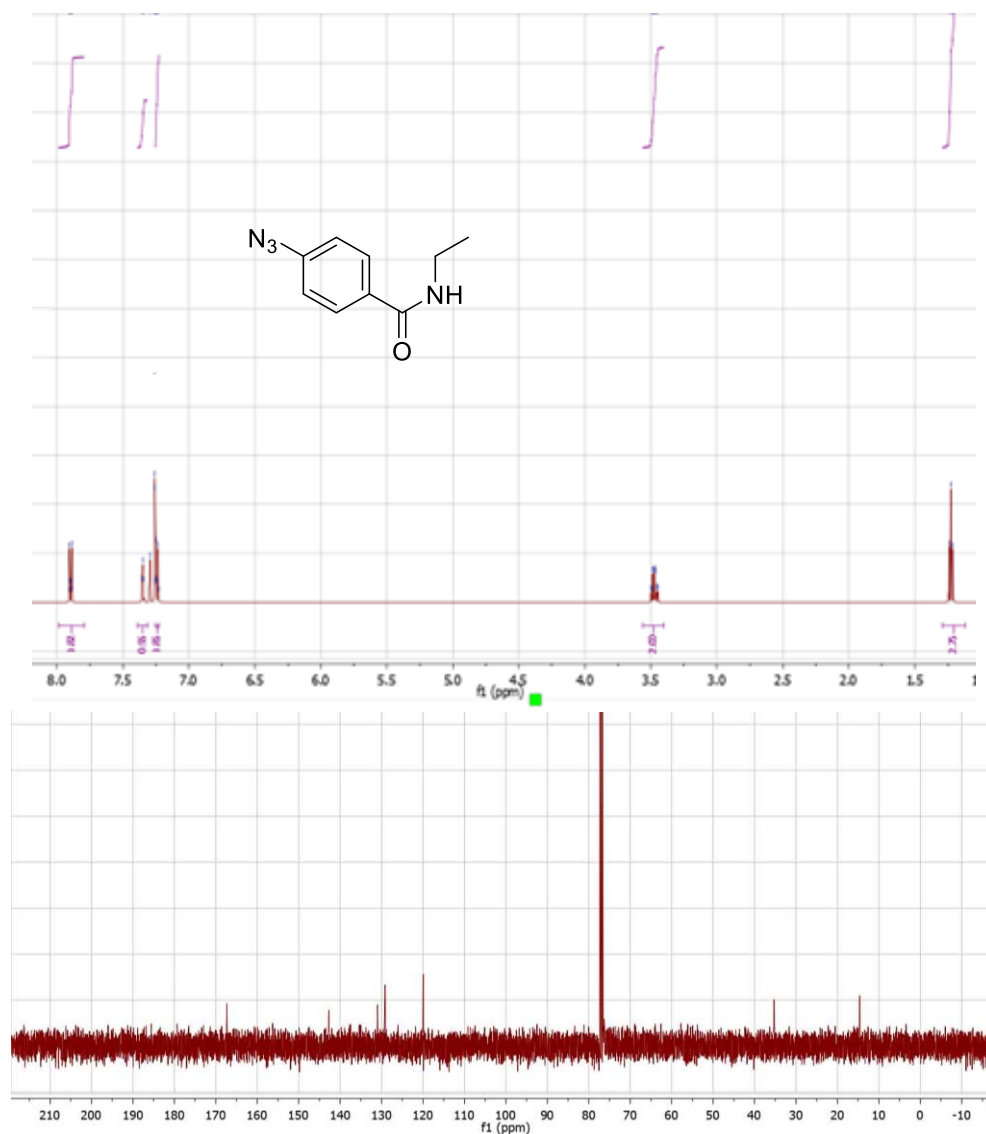
^1H NMR (400 MHz, Chloroform- d) δ 7.92 – 7.71 (m, 2H), 7.22 – 6.98 (m, 2H), 6.15 (s, 1H), 3.47 (td, $J = 7.2, 5.7$ Hz, 2H), 1.69 – 1.59 (m, 2H), 1.60 – 1.34 (m, 2H), 0.98 (t, $J = 7.3$ Hz, 3H). ^{13}C NMR (125 MHz, Chloroform- d) δ 168.71, 142.34, 130.79, 128.98, 119.27, 40.10, 30.74, 20.43, 13.74.

Compound 45.



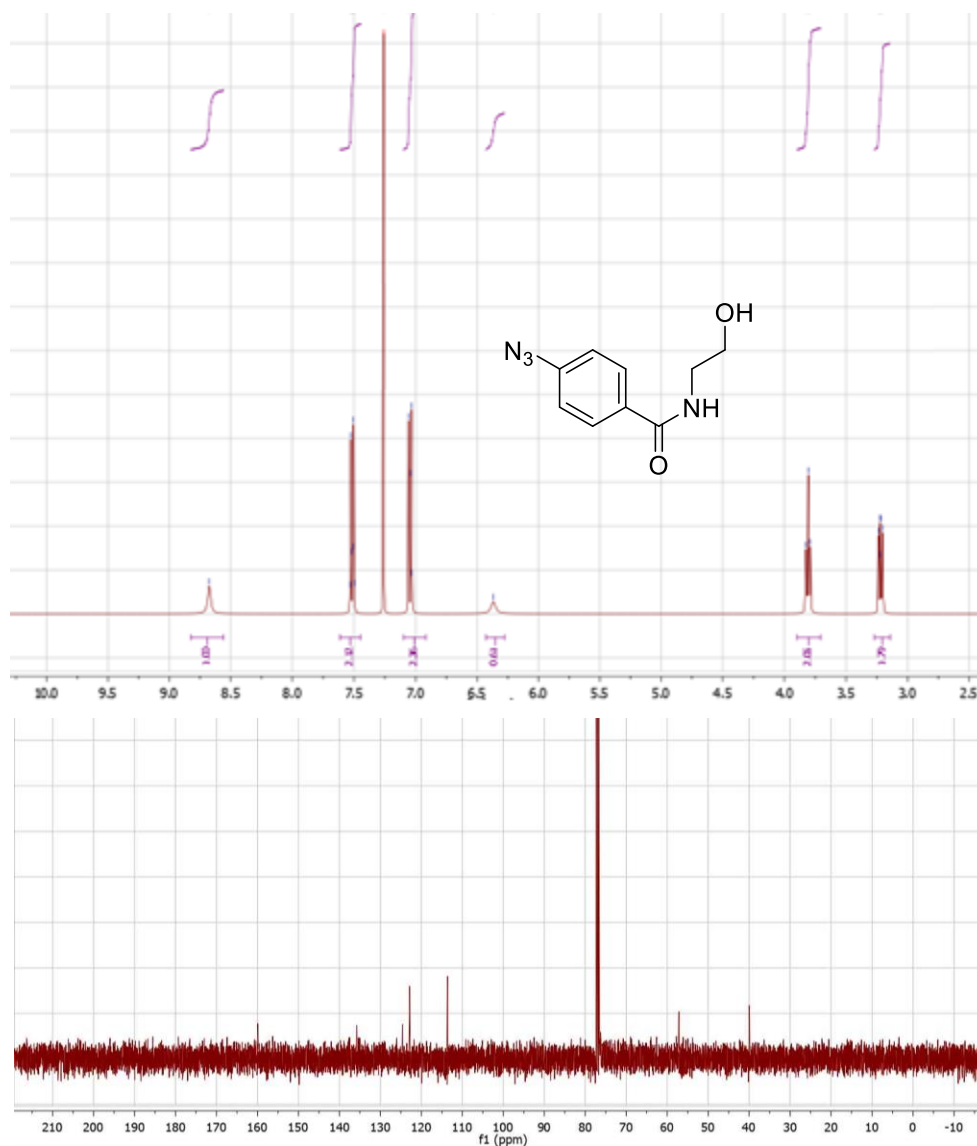
^1H NMR (400 MHz, Chloroform-*d*) δ 7.90 – 7.71 (m, 2H), 7.18 – 7.03 (m, 2H), 6.17 (s, 1H), 5.97 (dtd, $J = 17.1, 10.2, 5.7$ Hz, 1H), 5.36 – 5.10 (m, 2H), 4.12 (dt, $J = 5.8, 1.5$ Hz, 2H). ^{13}C NMR (125 MHz, Chloroform-*d*) δ 167.91, 142.45, 134.68, 130.67, 128.98, 119.27, 115.82, 43.23.

Compound 46.



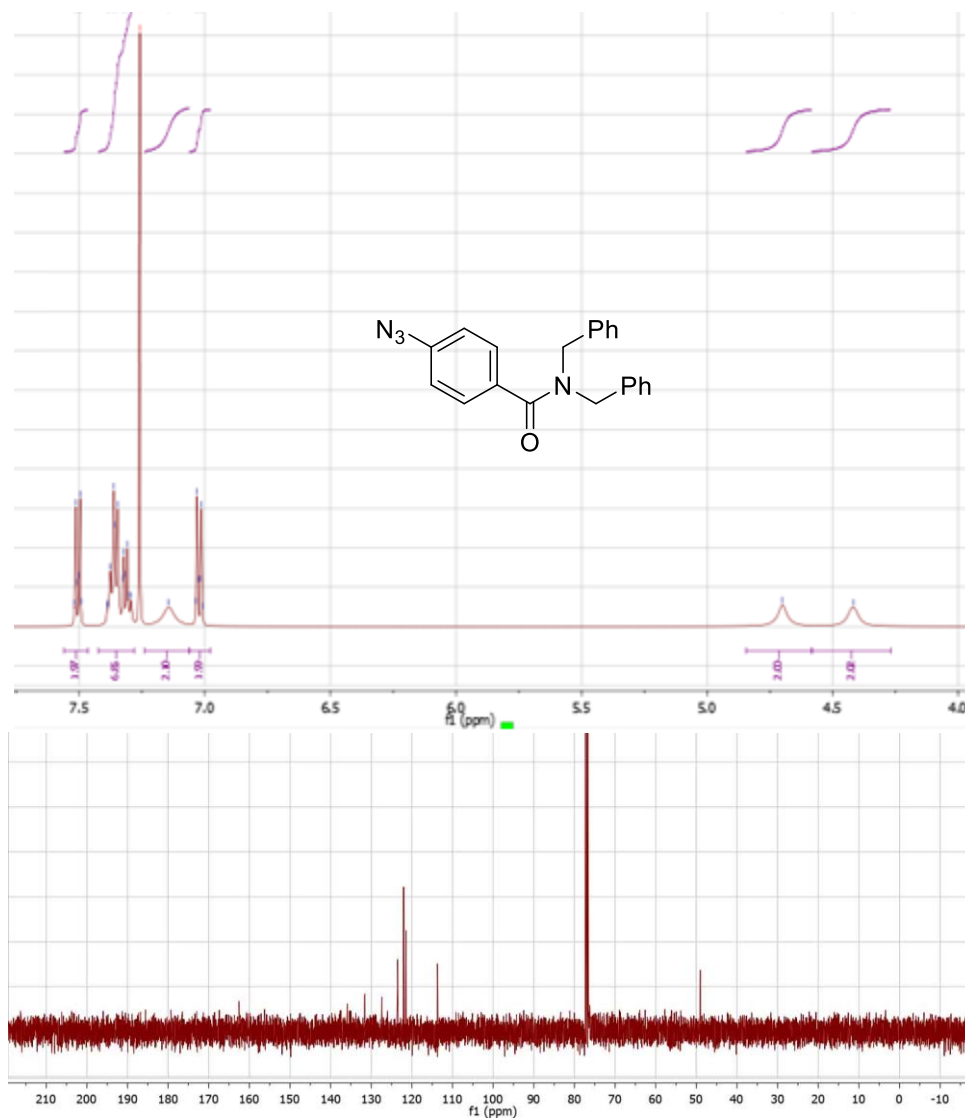
¹H NMR (500 MHz, Chloroform-*d*) δ 7.99 – 7.79 (m, 2H), 7.35 (t, J = 4.3 Hz, 1H), 7.25 – 7.22 (m, 2H), 3.47 (qd, J = 7.1, 4.3 Hz, 2H), 1.23 (t, J = 7.1 Hz, 3H). ¹³C NMR (125 MHz, Chloroform-*d*) δ 167.51, 142.45, 130.86, 128.98, 119.27, 35.96, 14.66.

Compound 47.

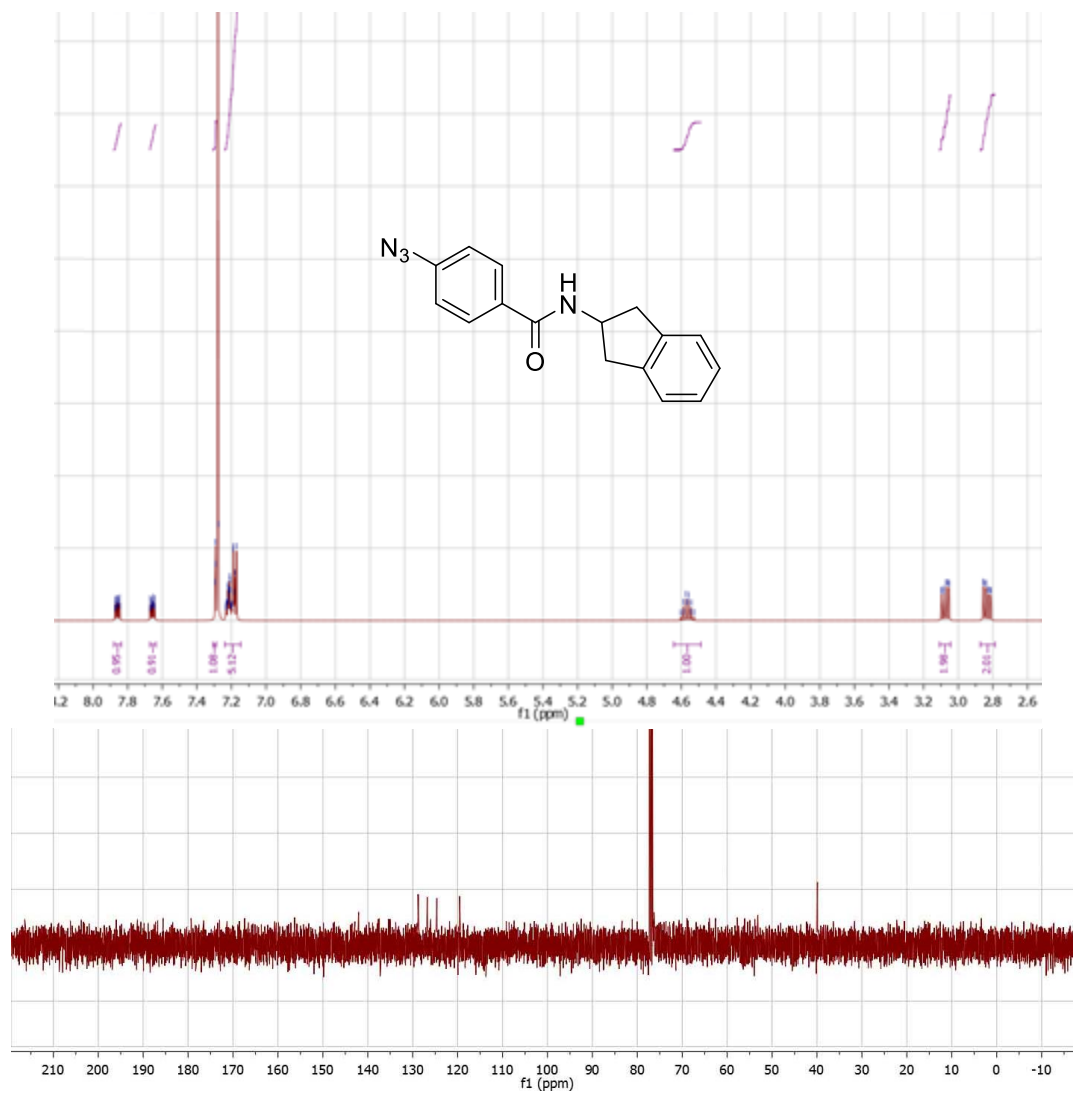


^1H NMR (400 MHz, Chloroform- d) δ 8.68 (s, 1H), 7.61 – 7.45 (m, 2H), 7.10 – 6.92 (m, 2H), 6.37 (s, 1H), 3.81 (t, $J = 6.7$ Hz, 2H), 3.27 – 3.14 (m, 2H). ^{13}C NMR (100 MHz, Chloroform- d) δ 167.75, 142.45, 130.79, 128.98, 119.27, 60.15, 42.22.

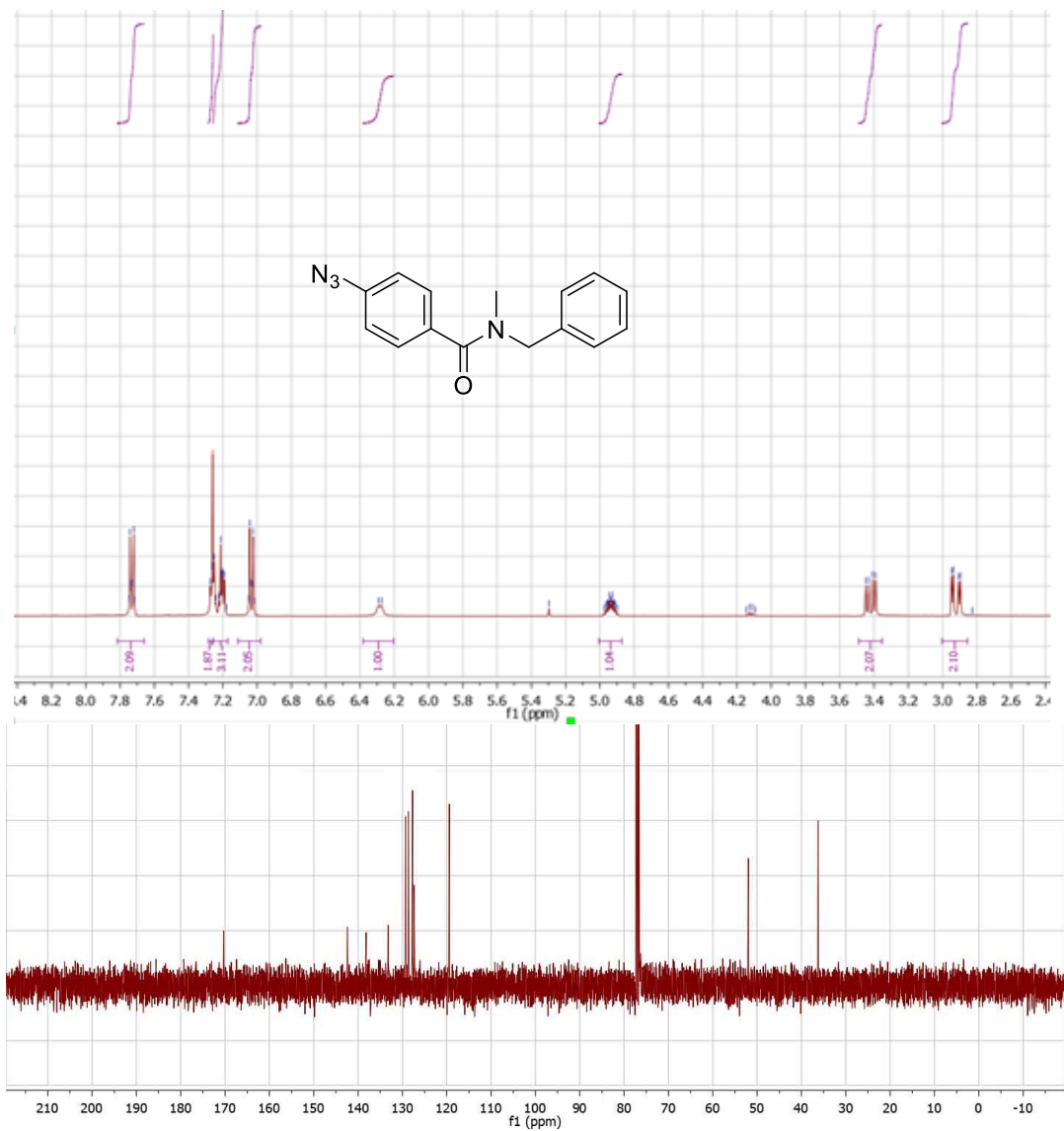
Compound 48.

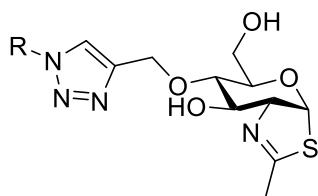


Compound 49.



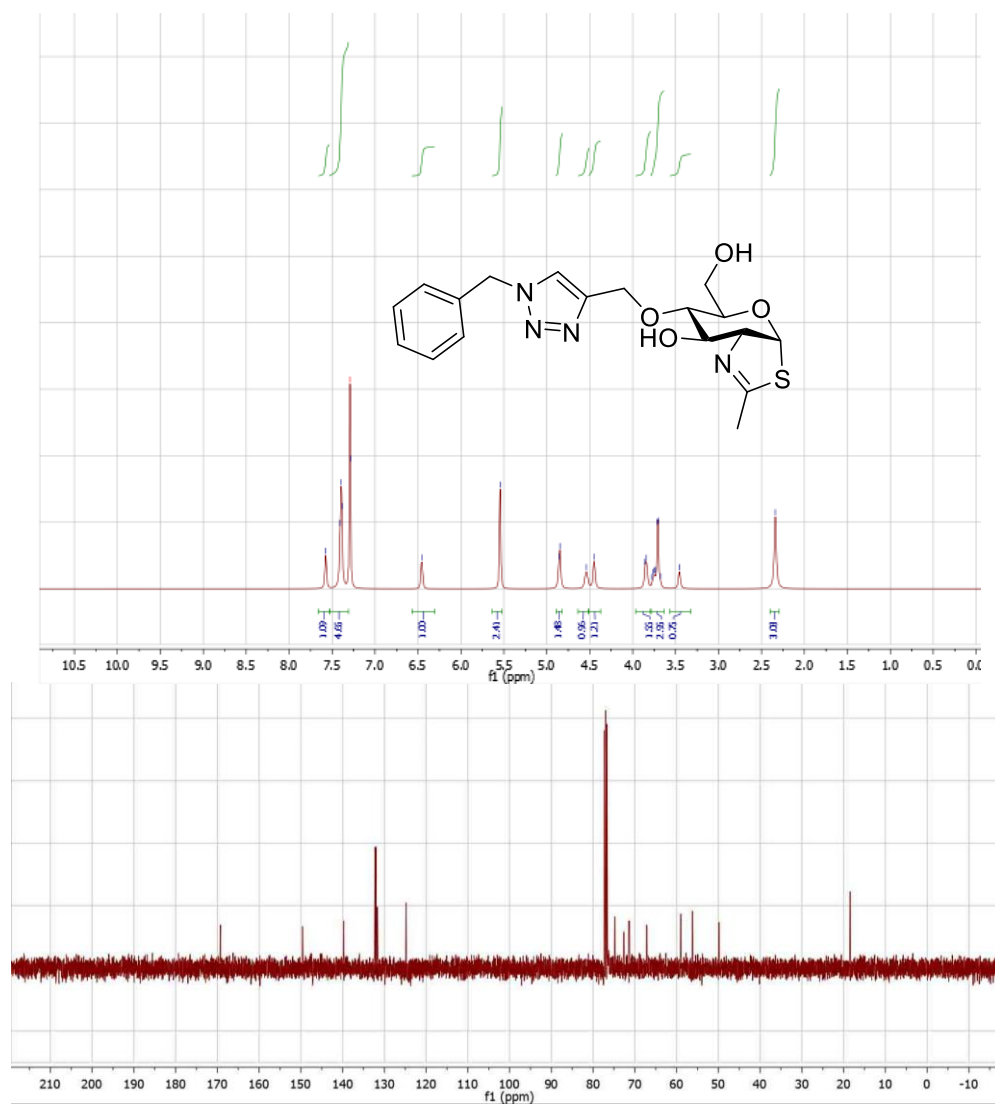
Compound 50.





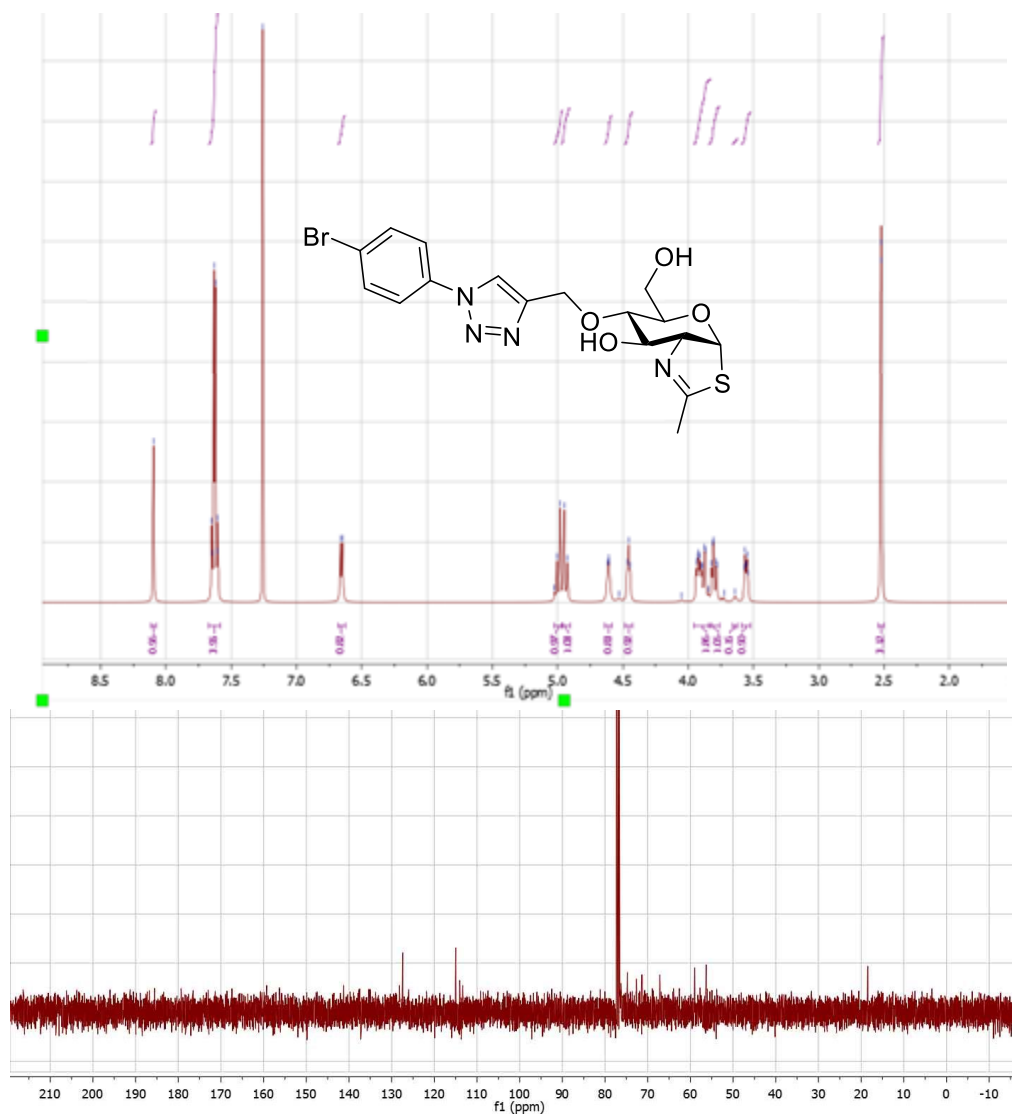
General procedure for compounds 16-39: 4-O-propargyl-NAG-thiazoline (13 mg, 0.0505 mmol), copper sulfate (8 mg, 0.032 mmol), sodium ascorbate (10 mg, 0.05 mmol), BTAA (1.0 mg, 2.3 μ mol), and azide (0.056 mmol) was added to a 50 mL round bottom flask and dissolved in *tert*-butanol (2 mL) and water (500 μ L). The reaction mixture was stirred for three hours. Upon completion, solvent was removed *in vacuo* with the addition of ethanol and purified using silica gel flash column chromatography (1:19 methanol:DCM) to afford 4-(aryl/alkyl-1-H-1,2,3-triazol-4-yl)methyl-NAG-thiazoline as a clear white foam (50-90%).

Compound 16.



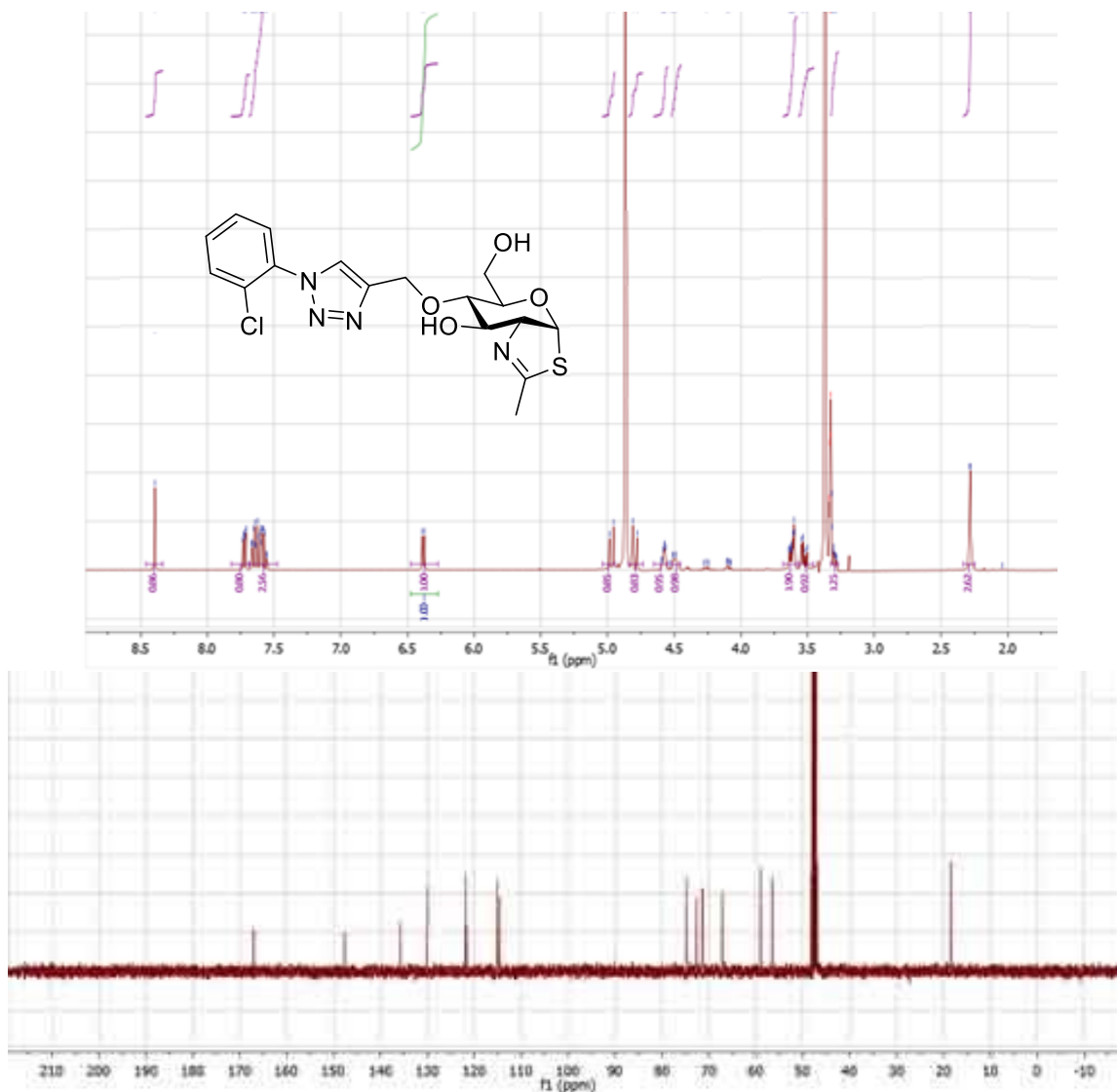
¹H NMR (500 MHz, Chloroform-*d*) δ 7.57 (s, 1H), 7.40 (t, *J* = 5.4 Hz, 5H), 6.46 (s, 1H), 5.54 (s, 2H), 4.85 (d, *J* = 6.8 Hz, 1H), 4.54 (s, 1H), 4.45 (s, 1H), 3.85 (d, *J* = 7.8 Hz, 2H), 3.73 (dd, *J* = 23.2, 5.1 Hz, 3H), 3.46 (s, 1H), 2.34 (s, 3H). ¹³C NMR (125 MHz, Chloroform-*d*) δ 169.07, 149.50, 139.18, 132.31, 132.07, 124.76, 120.53, 78.64, 76.41, 75.12, 75.00, 70.66, 62.12, 59.23, 52.53, 19.67. HRMS (ESI⁺) *m/z*: [M+H]⁺ calcd for C₁₈H₂₃N₄O₄S 391.1440, found 391.1438.

Compound 17.



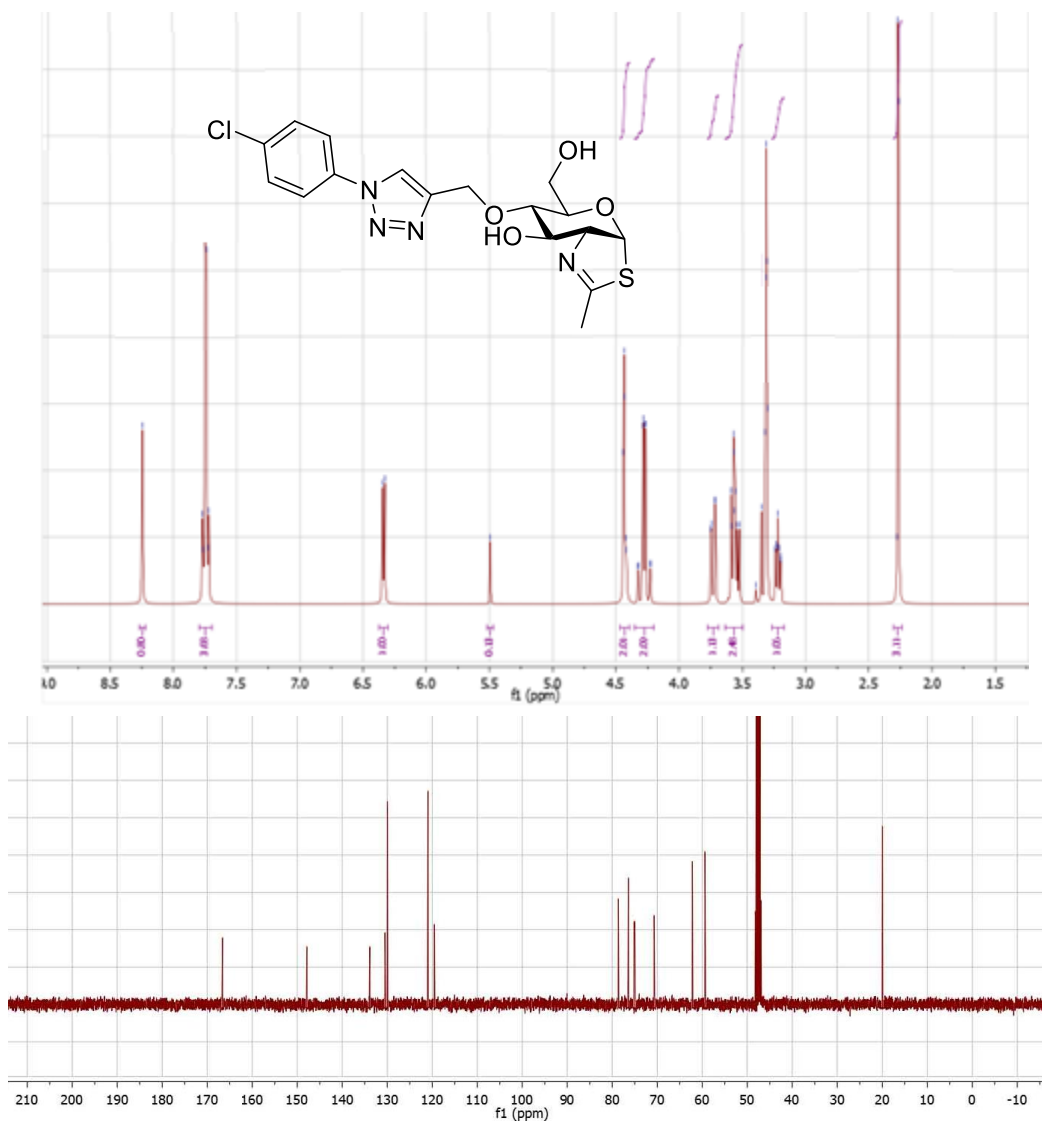
¹H NMR (500 MHz, Chloroform-*d*) δ 8.10 (s, 1H), 7.67 – 7.58 (m, 4H), 6.66 (d, *J* = 7.4 Hz, 1H), 4.99 (d, *J* = 12.8 Hz, 1H), 4.94 (d, *J* = 12.8 Hz, 1H), 4.64 – 4.58 (m, 1H), 4.46 (t, *J* = 5.3 Hz, 1H), 3.90 (m, 2H), 3.84 – 3.76 (m, 1H), 3.56 (dt, *J* = 9.1, 2.8 Hz, 1H), 2.52 (d, *J* = 1.5 Hz, 3H). ¹³C NMR (125 MHz, Chloroform-*d*) δ 167.07, 148.19, 134.50, 133.71, 120.69, 119.75, 118.98, 78.64, 76.41, 75.12, 75.00, 70.66, 62.12, 59.29, 19.67. HRMS (ESI⁺) *m/z*: [M+H]⁺ calcd for C₁₇H₂₀BrN₄O₄S 455.0389, found 455.0378.

Compound 18.

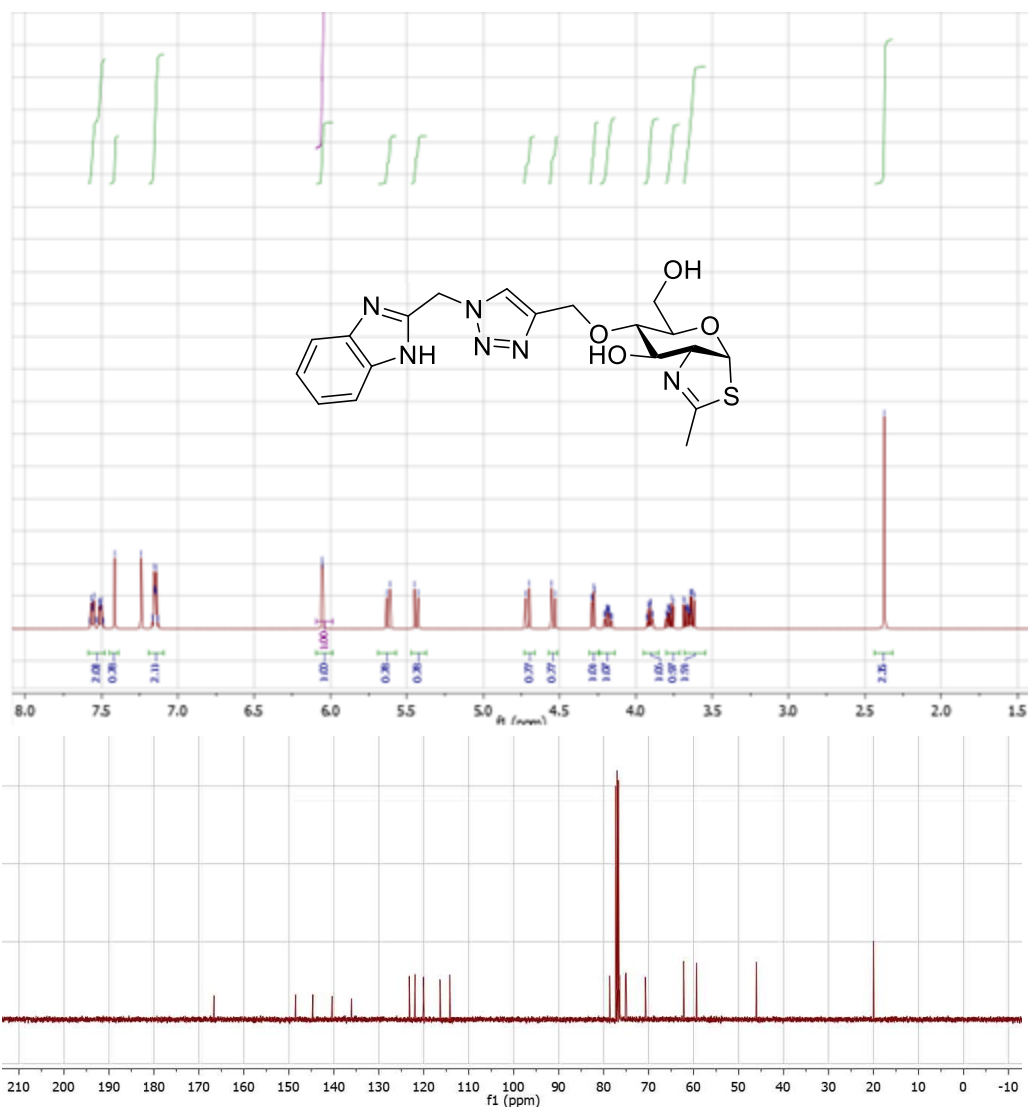


¹H NMR (400 MHz, Methanol-*d*₄) δ 8.39 (s, 1H), 7.82 – 7.69 (m, 1H), 7.69 – 7.48 (m, 3H), 6.38 (d, *J* = 7.0 Hz, 1H), 4.97 (d, *J* = 12.4 Hz, 1H), 4.79 (d, *J* = 12.4 Hz, 1H), 4.57 (dd, *J* = 3.7, 2.0 Hz, 1H), 4.52 – 4.45 (m, 1H), 3.68 – 3.58 (m, 2H), 3.57 – 3.45 (m, 1H), 3.32 – 3.27 (m, 1H), 2.28 (d, *J* = 2.1 Hz, 3H). ¹³C NMR (125 MHz, Methanol-*d*₄) δ 167.07, 148.31, 136.54, 131.86, 127.91, 127.88, 127.67, 120.89, 120.34, 78.64, 76.41, 75.12, 75.00, 70.66, 62.12, 59.51, 19.67. HRMS (ESI⁺) *m/z*: [M+H]⁺ calcd for C₁₇H₂₀ClN₄O₄S 411.0894, found 411.0891.

Compound 19.

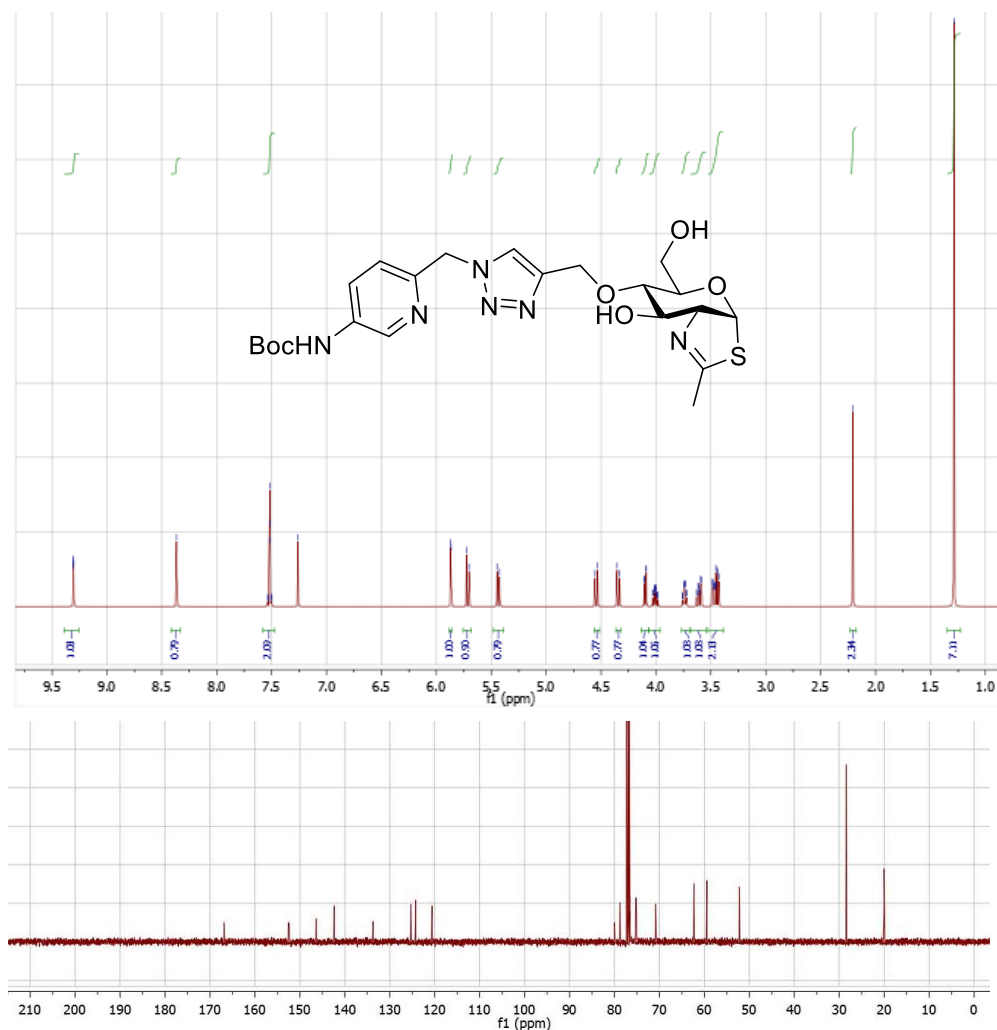


Compound 20.



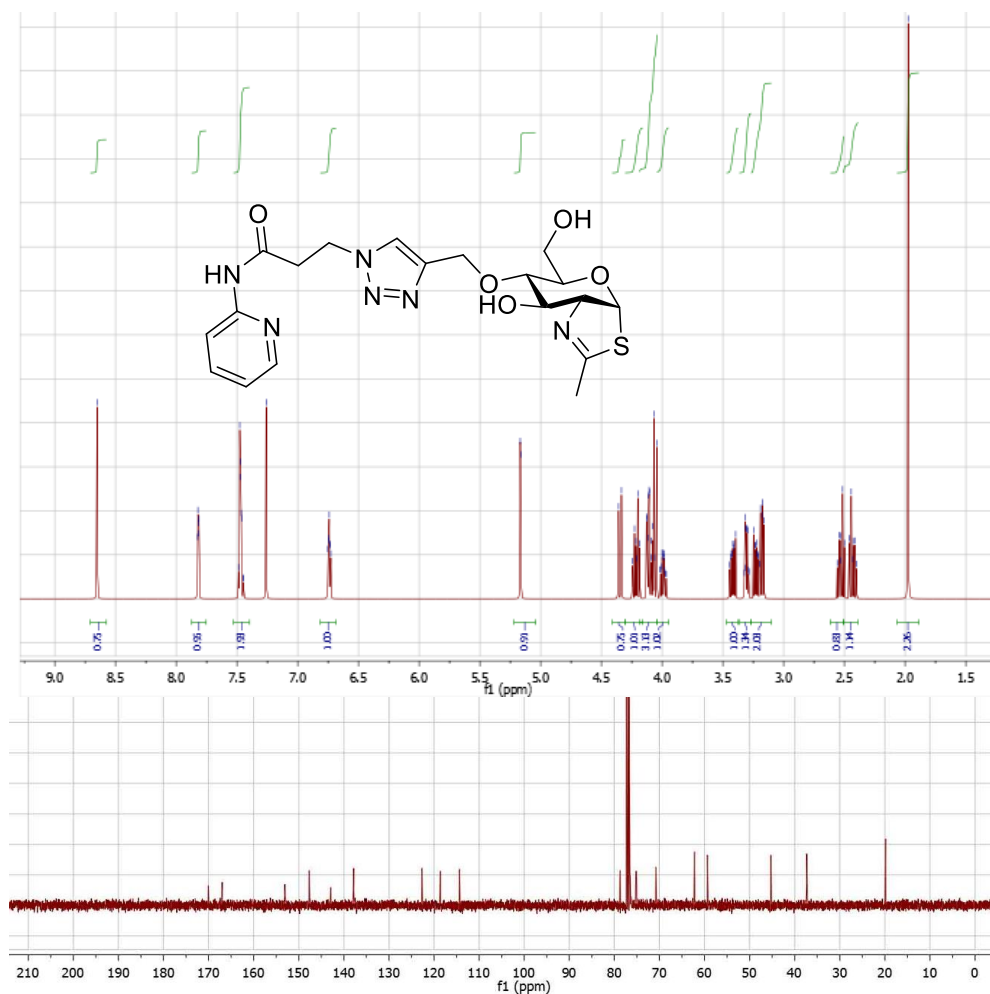
¹H NMR (500 MHz, Chloroform-*d*) δ 7.59 – 7.48 (m, 2H), 7.41 (s, 1H), 7.19 – 7.09 (m, 2H), 6.05 (d, $J = 2.4$ Hz, 1H), 5.62 (d, $J = 11.2$ Hz, 1H), 5.44 (d, $J = 11.2$ Hz, 1H), 4.71 (d, $J = 12.1$ Hz, 1H), 4.54 (d, $J = 11.9$ Hz, 1H), 4.28 (dd, $J = 8.2, 2.4$ Hz, 1H), 4.18 (m, 1H), 3.91 (m, 1H), 3.80 – 3.71 (m, 1H), 3.68 – 3.54 (m, 2H), 2.37 (d, $J = 1.5$ Hz, 3H). ¹³C NMR (125 MHz, Chloroform-*d*) δ 167.07, 148.88, 145.00, 140.68, 136.38, 123.42, 122.16, 120.27, 116.57, 114.38, 78.64, 76.41, 75.12, 75.00, 70.66, 62.12, 59.23, 45.87, 19.67. HRMS (ESI⁺) m/z : [M+H]⁺ calcd for C₁₉H₂₃N₆O₄S 431.1502, found 431.1509.

Compound 21.



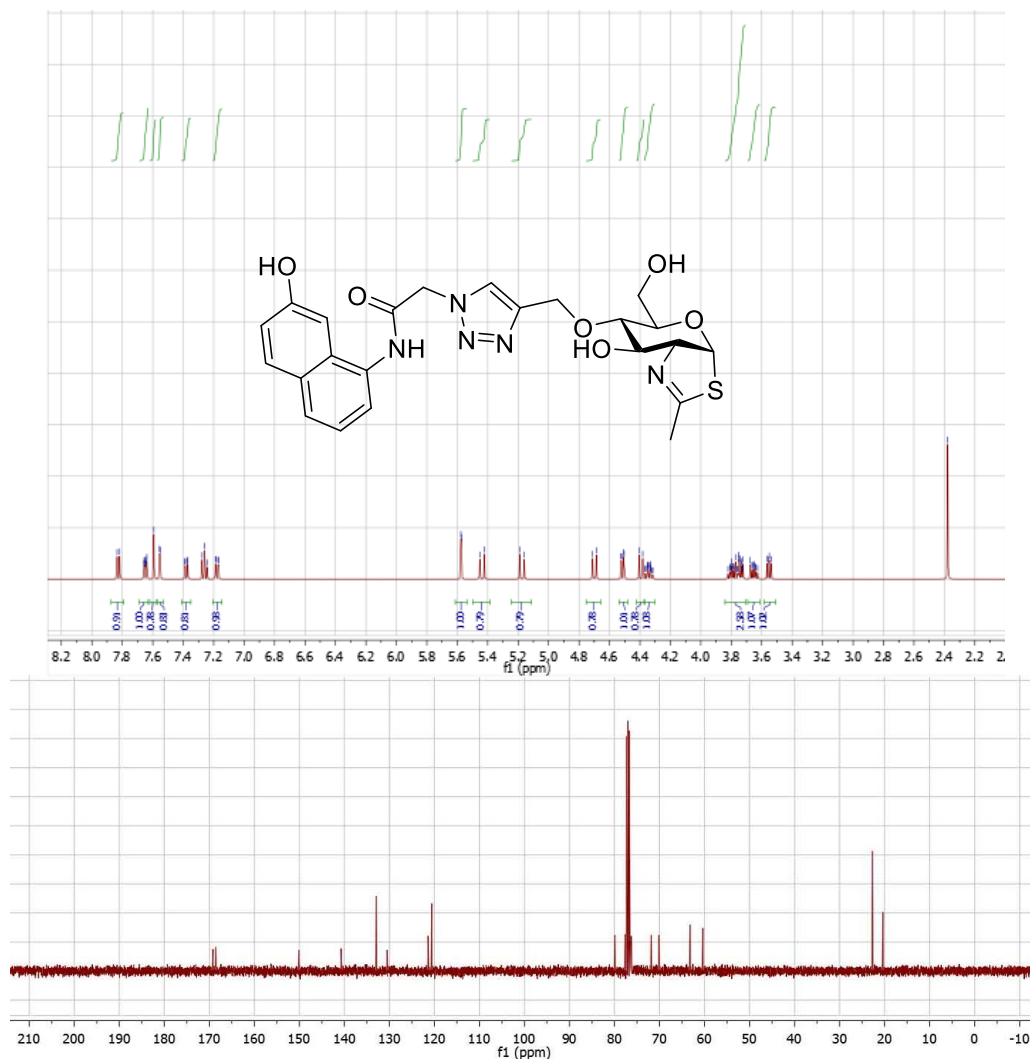
¹H NMR (500 MHz, Chloroform-*d*) δ 9.30 (dd, $J = 1.5, 0.7$ Hz, 1H), 8.37 (s, 1H), 7.58 – 7.47 (m, 2H), 5.87 (d, $J = 2.4$ Hz, 1H), 5.71 (d, $J = 11.3$ Hz, 1H), 5.44 (d, $J = 11.4$ Hz, 1H), 4.56 (d, $J = 11.9$ Hz, 1H), 4.32 (d, $J = 11.9$ Hz, 1H), 4.11 (dd, $J = 8.3, 2.4$ Hz, 1H), 4.06 – 3.96 (m, 1H), 3.71 (m, 1H), 3.61 (m, 1H), 3.53 – 3.39 (m, 2H), 2.21 (d, $J = 1.6$ Hz, 3H), 1.29 (s, 9H). ¹³C NMR (125 MHz, Chloroform-*d*) δ 167.07, 152.71, 152.58, 146.50, 142.46, 133.79, 125.34, 124.31, 120.61, 79.88, 78.64, 76.41, 75.12, 75.00, 70.66, 62.12, 59.23, 51.98, 28.11, 19.67. HRMS (ESI⁺) m/z : [M+H]⁺ calcd for C₂₂H₃₁N₆O₆S 507.2026, found 507.2022.

Compound 22.



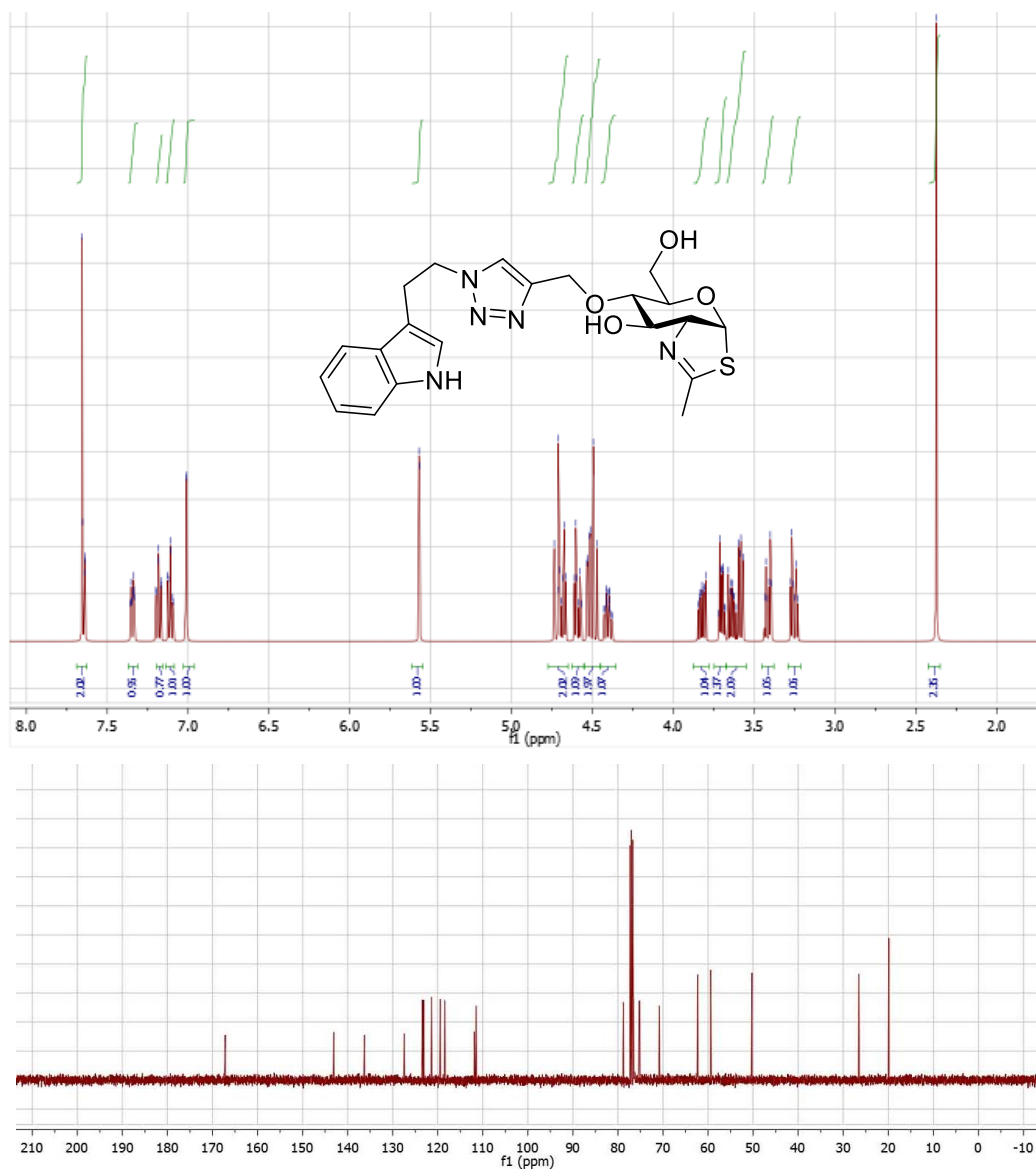
¹H NMR (500 MHz, Chloroform-*d*) δ 8.65 (s, 1H), 7.87 – 7.75 (m, 1H), 7.53 – 7.40 (m, 2H), 6.74 (m, 1H), 5.17 (d, *J* = 2.4 Hz, 1H), 4.35 (d, *J* = 12.1 Hz, 1H), 4.21 (m, 1H), 4.19 – 4.04 (m, 3H), 4.04 – 3.95 (m, 1H), 3.42 (m, 1H), 3.36 – 3.27 (m, 1H), 3.27 – 3.10 (m, 2H), 2.54 (dd, *J* = 14.1, 7.7 Hz, 1H), 2.51 – 2.39 (m, 1H), 1.97 (d, *J* = 1.5 Hz, 3H). ¹³C NMR (125 MHz, Chloroform-*d*) δ 170.12, 167.07, 153.15, 147.71, 142.95, 137.86, 122.68, 118.60, 114.33, 78.64, 76.41, 75.12, 75.00, 70.66, 62.12, 59.23, 45.14, 37.18, 19.67. HRMS (ESI⁺) *m/z*: [M+H]⁺ calcd for C₁₉H₂₅N₆O₅S 449.1607, found 449.1599.

Compound 23.



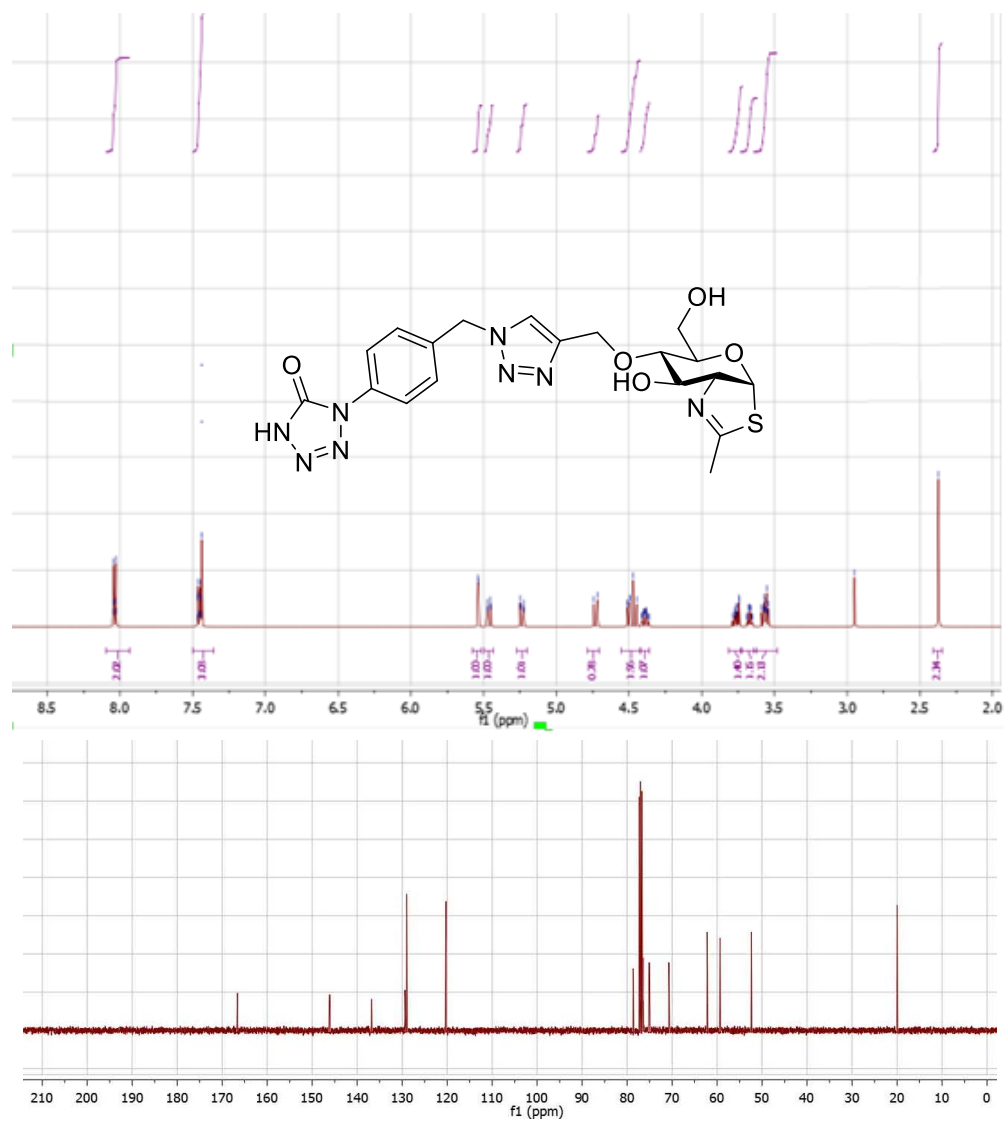
¹H NMR (500 MHz, Chloroform-*d*) δ 7.83 (d, $J = 8.4$ Hz, 1H), 7.69 – 7.63 (m, 1H), 7.59 (s, 1H), 7.55 (d, $J = 2.2$ Hz, 1H), 7.38 (dd, $J = 8.0, 1.5$ Hz, 1H), 7.18 (dd, $J = 8.4, 2.2$ Hz, 1H), 5.57 (d, $J = 2.4$ Hz, 1H), 5.44 (d, $J = 15.2$ Hz, 1H), 5.17 (d, $J = 15.2$ Hz, 1H), 4.70 (d, $J = 11.9$ Hz, 1H), 4.51 (dd, $J = 8.2, 2.4$ Hz, 1H), 4.39 (d, $J = 11.9$ Hz, 1H), 4.34 (m, 1H), 3.84 – 3.71 (m, 3H), 3.65 (m, 1H), 3.55 (dd, $J = 7.9, 6.0$ Hz, 1H), 2.38 (d, $J = 1.6$ Hz, 3H). ¹³C NMR (125 MHz, Chloroform-*d*) δ 168.96, 167.07, 155.75, 144.84, 137.75, 129.18, 128.67, 127.25, 125.81, 124.60, 121.19, 117.00, 114.90, 105.99, 78.64, 76.41, 75.12, 75.00, 70.66, 62.12, 59.23, 52.48, 19.67. HRMS (ESI+) m/z : [M+H]⁺ calcd for C₂₃H₂₆N₅O₆S 500.1604, found 500.1611.

Compound 24.



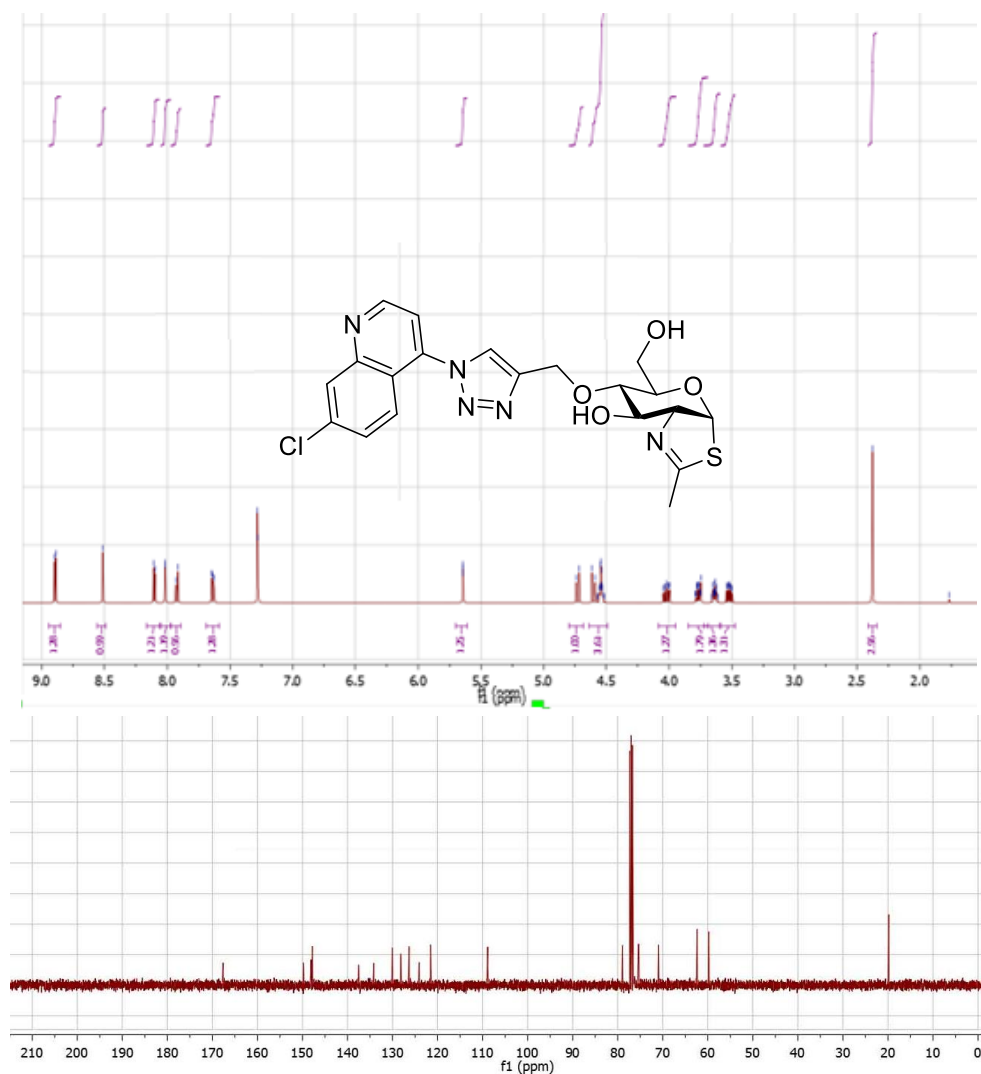
¹H NMR (500 MHz, Chloroform-*d*) 7.69 – 7.63 (m, 2H), 7.37 – 7.31 (m, 1H), 7.18 (dd, $J = 8.0, 1.1$ Hz, 1H), 7.11 (m, 1H), 7.01 (d, $J = 2.6$ Hz, 1H), 5.57 (d, $J = 2.4$ Hz, 1H), 4.78 – 4.65 (m, 2H), 4.59 (m, 1H), 4.55 – 4.45 (m, 2H), 4.40 (m, 1H), 3.82 (m, 1H), 3.75 – 3.67 (m, 1H), 3.67 – 3.55 (m, 2H), 3.41 (m, 1H), 3.25 (m, 1H), 2.37 (d, $J = 1.6$ Hz, 3H). ¹³C NMR (125 MHz, Chloroform-*d*) δ 167.07, 142.95, 136.16, 127.32, 123.25, 122.96, 121.24, 119.31, 118.29, 111.72, 111.33, 78.64, 76.41, 75.12, 75.00, 70.66, 62.12, 59.23, 50.08, 26.33, 19.67. HRMS (ESI⁺) m/z : [M+H]⁺ calcd for C₂₁H₂₆N₅O₄S 444.1706, found 444.1720.

Compound 25.



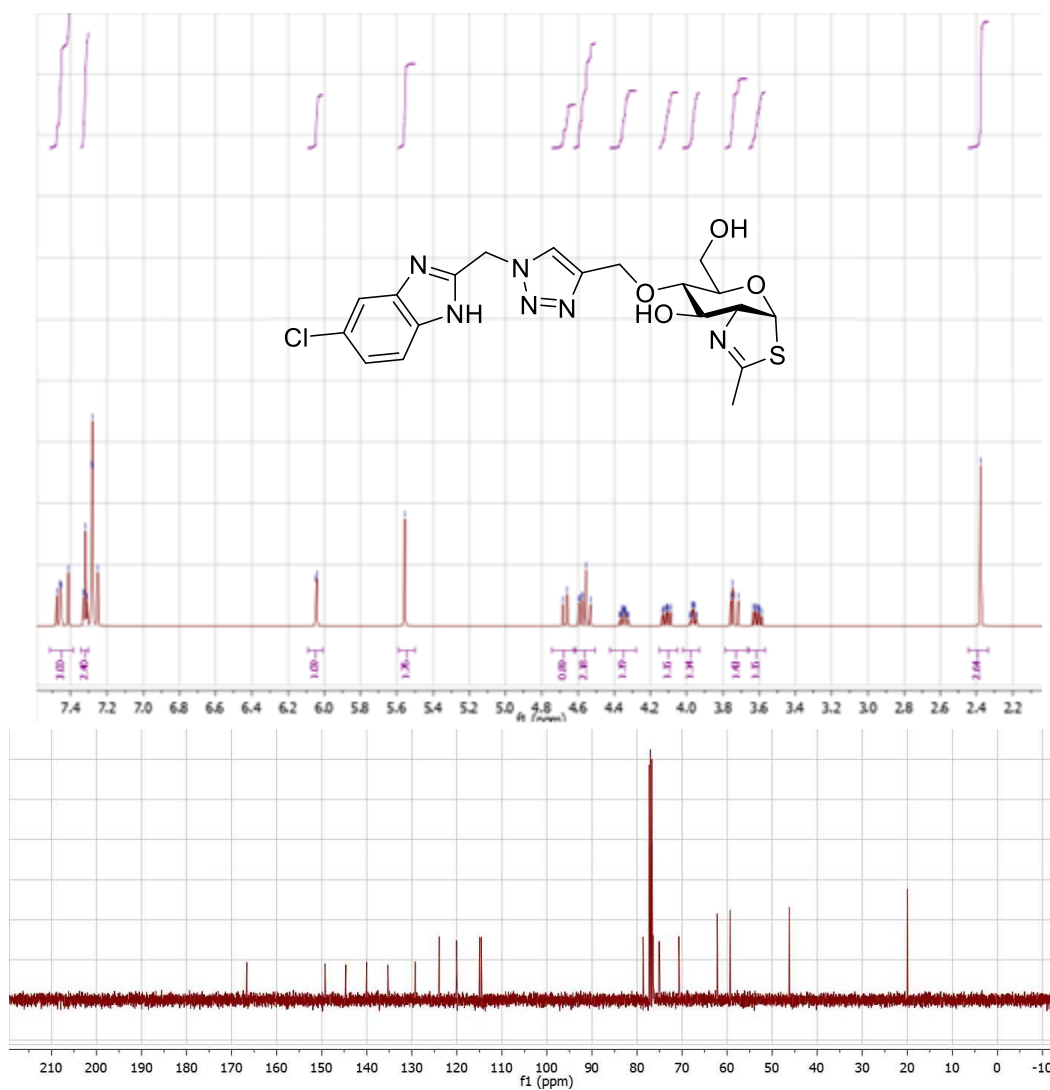
^1H NMR (500 MHz, Chloroform- d) δ 8.09 – 7.93 (m, 2H), 7.50 – 7.35 (m, 3H), 5.54 (d, $J = 2.4$ Hz, 1H), 5.46 (m, 1H), 5.24 (m, 1H), 4.73 (d, $J = 11.9$ Hz, 1H), 4.55 – 4.42 (m, 2H), 4.39 (m, 1H), 3.82 – 3.72 (m, 1H), 3.67 (m, 1H), 3.64 – 3.48 (m, 2H), 2.37 (d, $J = 1.5$ Hz, 3H). ^{13}C NMR (125 MHz, Chloroform- d) δ 167.07, 146.50, 146.37, 137.08, 129.62, 129.23, 120.53, 120.46, 78.64, 76.41, 75.12, 75.00, 70.66, 62.12, 59.23, 52.24, 19.67. HRMS (ESI $^+$) m/z : $[\text{M}+\text{H}]^+$ calcd for $\text{C}_{19}\text{H}_{23}\text{N}_8\text{O}_5\text{S}$ 475.1512, found 475.1516.

Compound 26.



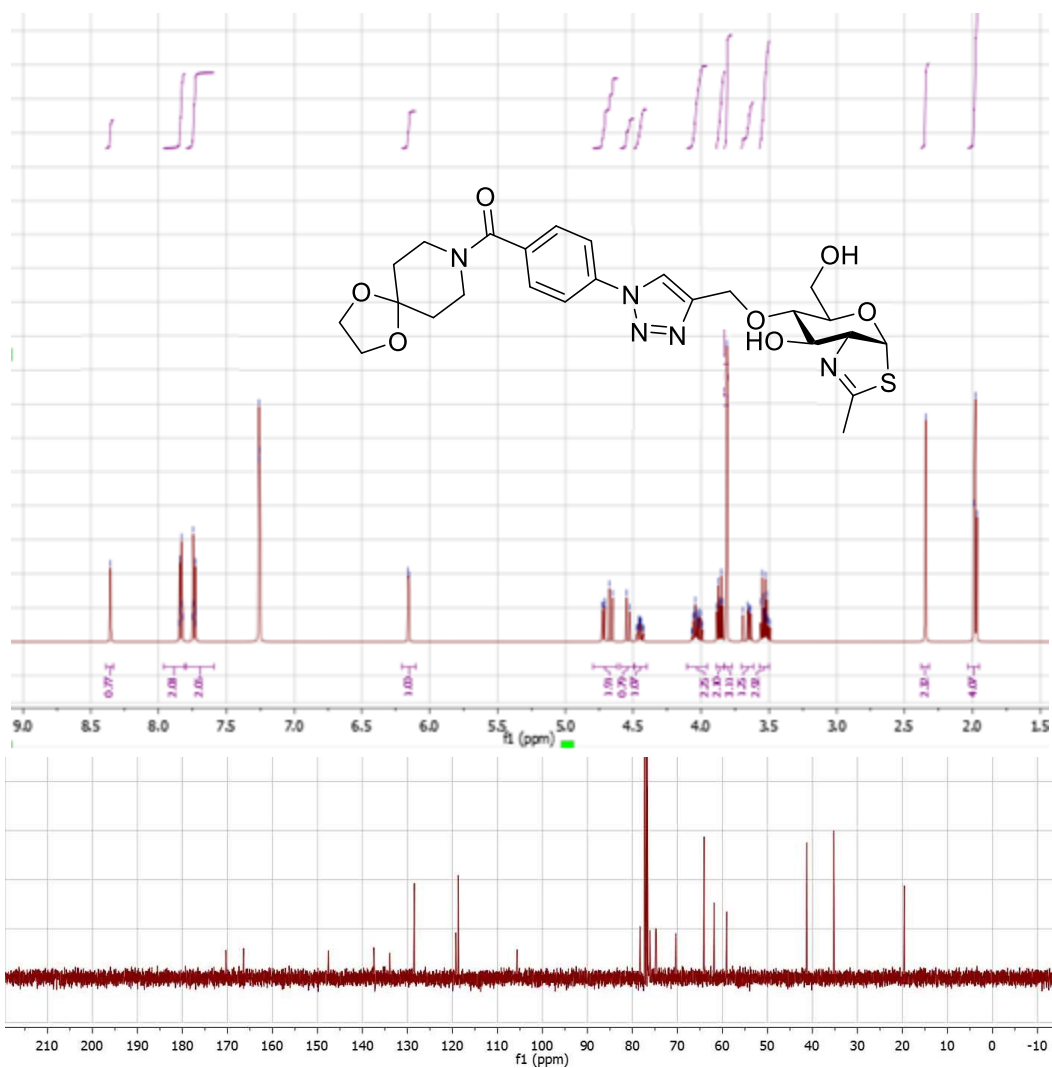
¹H NMR (500 MHz, Chloroform-*d*) δ 8.89 (d, J = 5.7 Hz, 1H), 8.51 (s, 1H), 8.10 (d, J = 5.7 Hz, 1H), 8.02 (d, J = 1.7 Hz, 1H), 7.92 (d, J = 8.6 Hz, 1H), 7.64 (dd, J = 8.4, 1.8 Hz, 1H), 5.70 – 5.61 (m, 1H), 4.73 (d, J = 12.1 Hz, 1H), 4.64 – 4.49 (m, 4H), 4.08 – 3.95 (m, 1H), 3.85 – 3.69 (m, 2H), 3.72 – 3.60 (m, 1H), 3.52 (m, 1H), 2.38 (d, J = 1.5 Hz, 3H). ¹³C NMR (125 MHz, Chloroform-*d*) δ 167.07, 149.26, 147.59, 147.29, 137.07, 133.72, 129.58, 127.71, 125.90, 123.65, 121.10, 108.47, 78.64, 76.41, 75.12, 75.00, 70.66, 62.12, 59.51, 19.67. HRMS (ESI⁺) m/z : [M+H]⁺ calcd for C₂₀H₂₁ClN₅O₄S 462.1003, found 462.1007.

Compound 27.



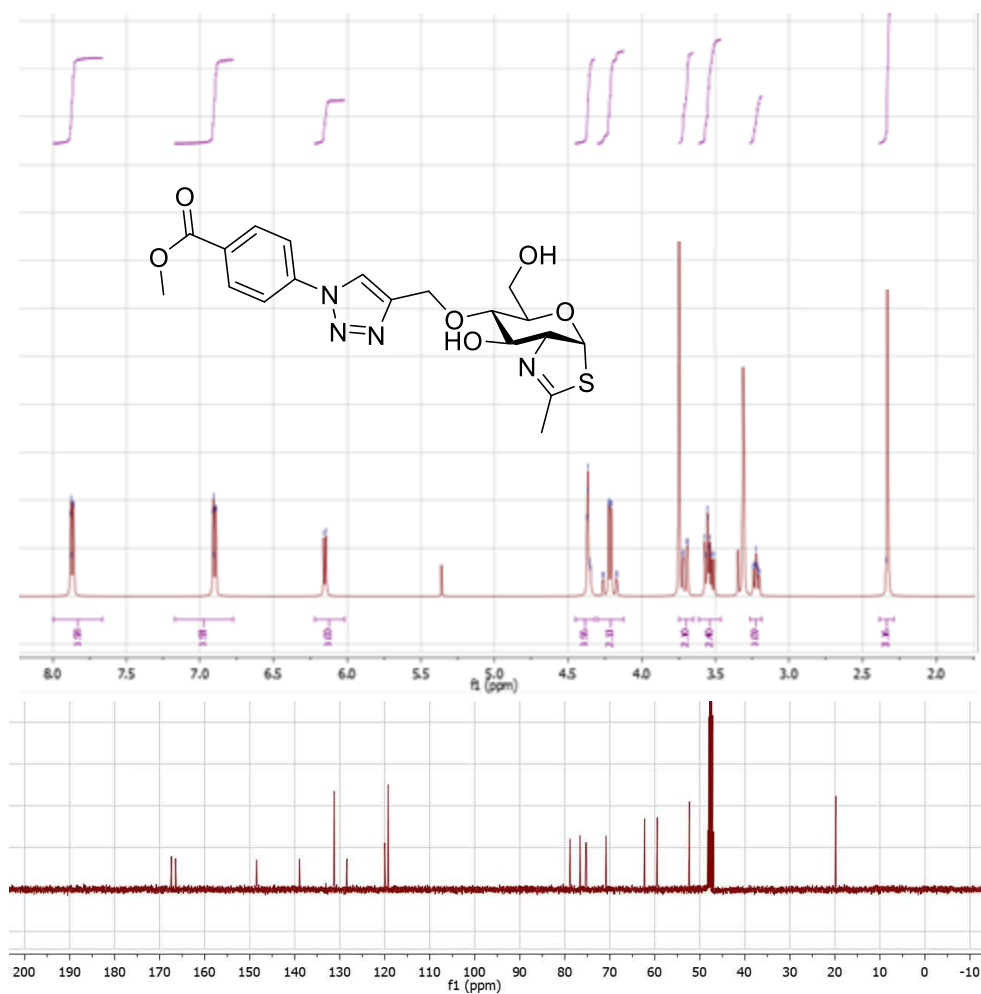
¹H NMR (500 MHz, Chloroform-*d*) δ 7.51 – 7.39 (m, 3H), 7.34 – 7.30 (m, 2H), 6.04 (d, $J = 2.5$ Hz, 1H), 5.56 (s, 2H), 4.67 (d, $J = 11.9$ Hz, 1H), 4.62 – 4.51 (m, 2H), 4.35 (m, 1H), 4.11 (ddd, $J = 11.9, 7.1, 5.7$ Hz, 1H), 3.96 (qd, $J = 5.7, 1.9$ Hz, 1H), 3.79 – 3.67 (m, 1H), 3.61 (ddd, $J = 11.9, 7.0, 5.6$ Hz, 1H), 2.38 (d, $J = 1.5$ Hz, 3H). ¹³C NMR (125 MHz, Chloroform-*d*) δ 164.19, 147.72, 146.66, 140.07, 137.07, 131.45, 122.61, 118.44, 117.66, 112.58, 77.14, 76.40, 75.00, 70.75, 62.13, 59.44, 47.15, 19.51. HRMS (ESI⁺) m/z : [M+H]⁺ calcd for C₁₉H₂₂ClN₆O₄S 465.1112, found 465.1122.

Compound 28.



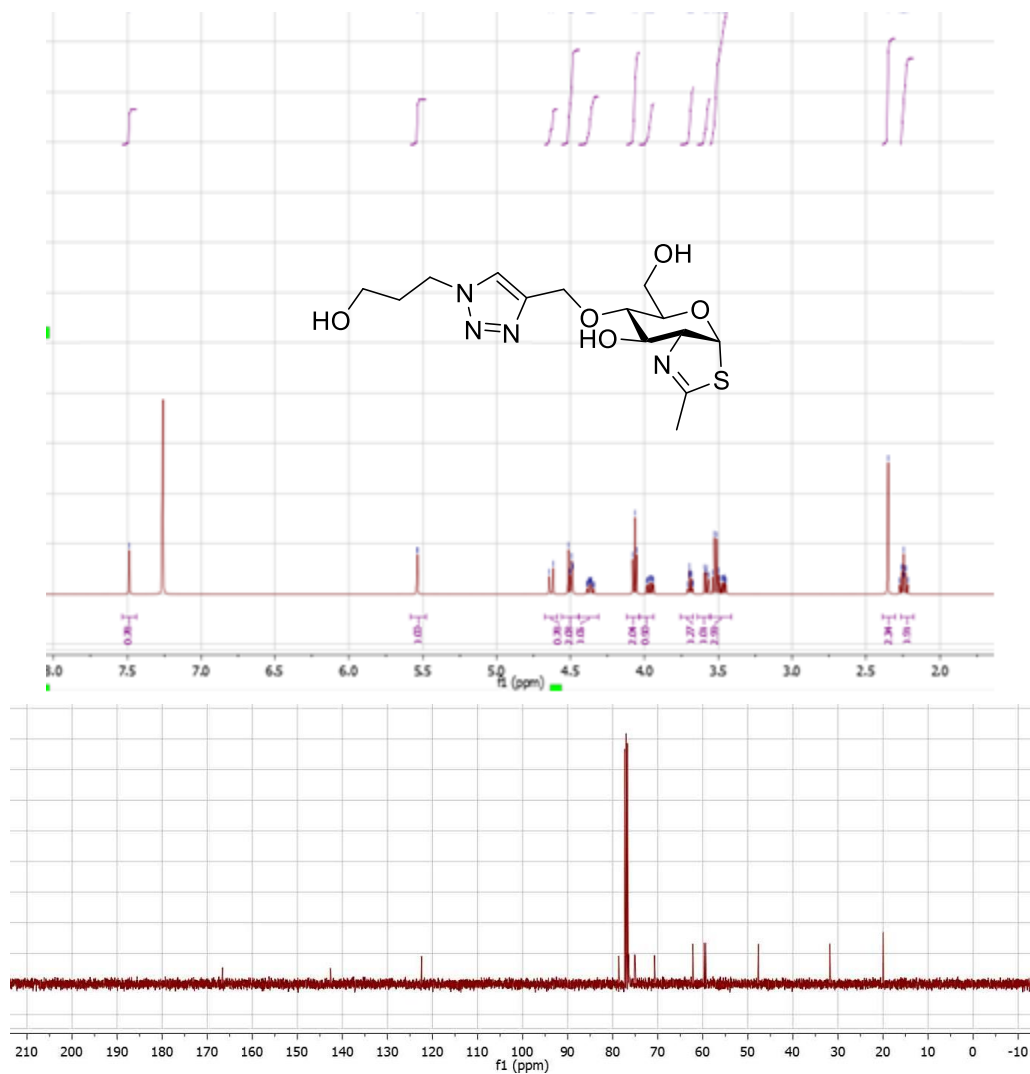
¹H NMR (500 MHz, Chloroform-*d*) δ 8.35 (s, 1H), 7.96 – 7.81 (m, 2H), 7.79 – 7.59 (m, 2H), 6.16 (d, $J = 2.4$ Hz, 1H), 4.80 – 4.62 (m, 2H), 4.54 (d, $J = 12.1$ Hz, 1H), 4.45 (tdd, $J = 8.0, 6.9, 1.9$ Hz, 1H), 4.10 – 3.96 (m, 2H), 3.86 (dt, $J = 12.1, 5.3$ Hz, 2H), 3.81 (s, 3H), 3.70 – 3.61 (m, 1H), 3.57 – 3.50 (m, 3H), 2.34 (d, $J = 1.5$ Hz, 3H), 1.98 (t, $J = 5.3$ Hz, 4H). ¹³C NMR (125 MHz, Chloroform-*d*) δ 171.03, 167.07, 148.19, 138.02, 134.47, 129.00, 119.75, 119.19, 106.05, 78.64, 76.41, 75.12, 75.00, 70.66, 64.33, 62.12, 59.29, 41.44, 35.38, 19.67. HRMS (ESI⁺) m/z : [M+H]⁺ calcd for C₂₅H₃₂N₅O₇S 546.2022, found 546.2021.

Compound 29.



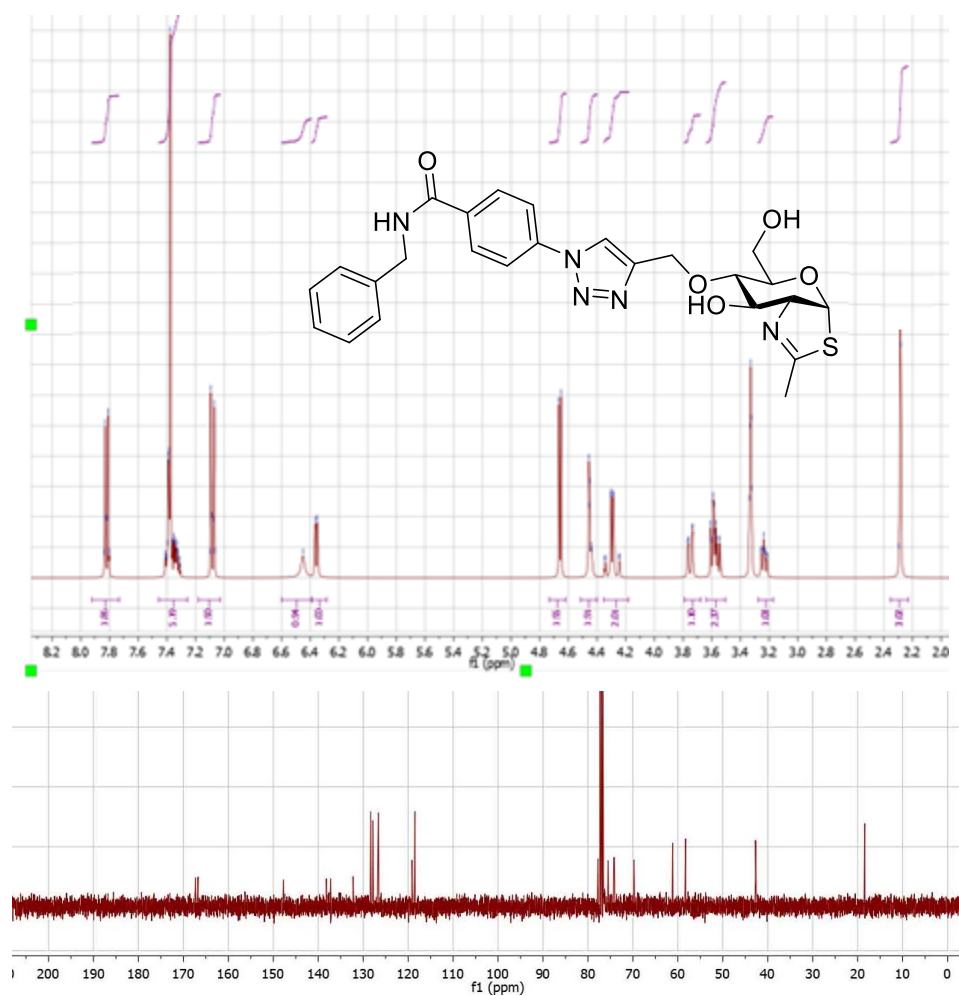
^1H NMR (500 MHz, Methanol-*d*) 7.87 (dd, $J = 8.5, 1.6$ Hz, 2H), 6.90 (dd, $J = 8.5, 1.6$ Hz, 2H), 6.15 (d, $J = 7.5$ Hz, 1H), 4.36 (q, $J = 4.6, 3.2$ Hz, 2H), 4.30 – 4.12 (m, 2H), 3.71 (dd, $J = 14.2, 2.7$ Hz, 2H), 3.62 – 3.46 (m, 2H), 3.22 (m, 1H), 2.33 (d, $J = 2.2$ Hz, 3H). ^{13}C NMR (125 MHz, Methanol-*d*) δ 167.07, 166.17, 148.19, 138.65, 130.97, 128.15, 119.75, 118.98, 78.64, 76.41, 75.12, 75.00, 70.66, 62.12, 59.29, 52.17, 19.67. HRMS (ESI⁺) m/z : $[\text{M}+\text{H}]^+$ calcd for $\text{C}_{19}\text{H}_{23}\text{N}_4\text{O}_6\text{S}$ 435.1338, found 435.1339.

Compound 30.



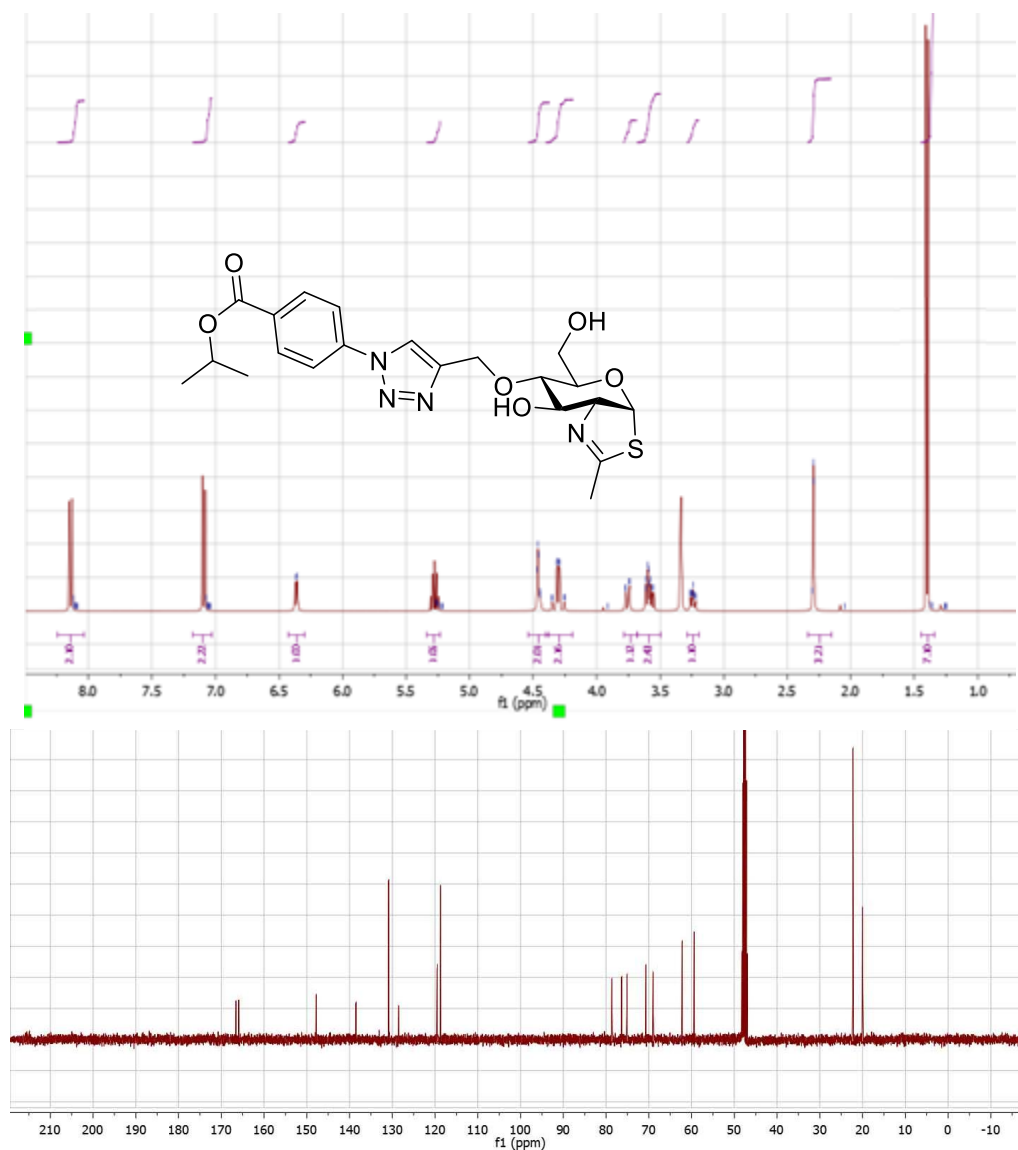
^1H NMR (500 MHz, Chloroform-*d*) δ 7.49 (s, 1H), 5.54 (d, J = 2.4 Hz, 1H), 4.63 (d, J = 12.1 Hz, 1H), 4.56 – 4.44 (m, 2H), 4.37 (td, J = 8.1, 6.9, 2.0 Hz, 1H), 4.07 (t, J = 6.3 Hz, 2H), 4.03 – 3.94 (m, 1H), 3.75 – 3.67 (m, 1H), 3.58 (dd, J = 7.9, 5.9 Hz, 1H), 3.56 – 3.41 (m, 3H), 2.35 (d, J = 1.5 Hz, 3H), 2.26 – 2.18 (m, 2H). ^{13}C NMR (125 MHz, Chloroform-*d*) δ 167.07, 142.95, 122.65, 78.64, 76.41, 75.12, 75.00, 70.66, 62.12, 59.59, 59.23, 47.50, 31.54, 19.67. HRMS (ESI⁺) m/z : [M+H]⁺ calcd for C₁₄H₂₃N₄O₅S 359.1389, found 359.1386.

Compound 31.



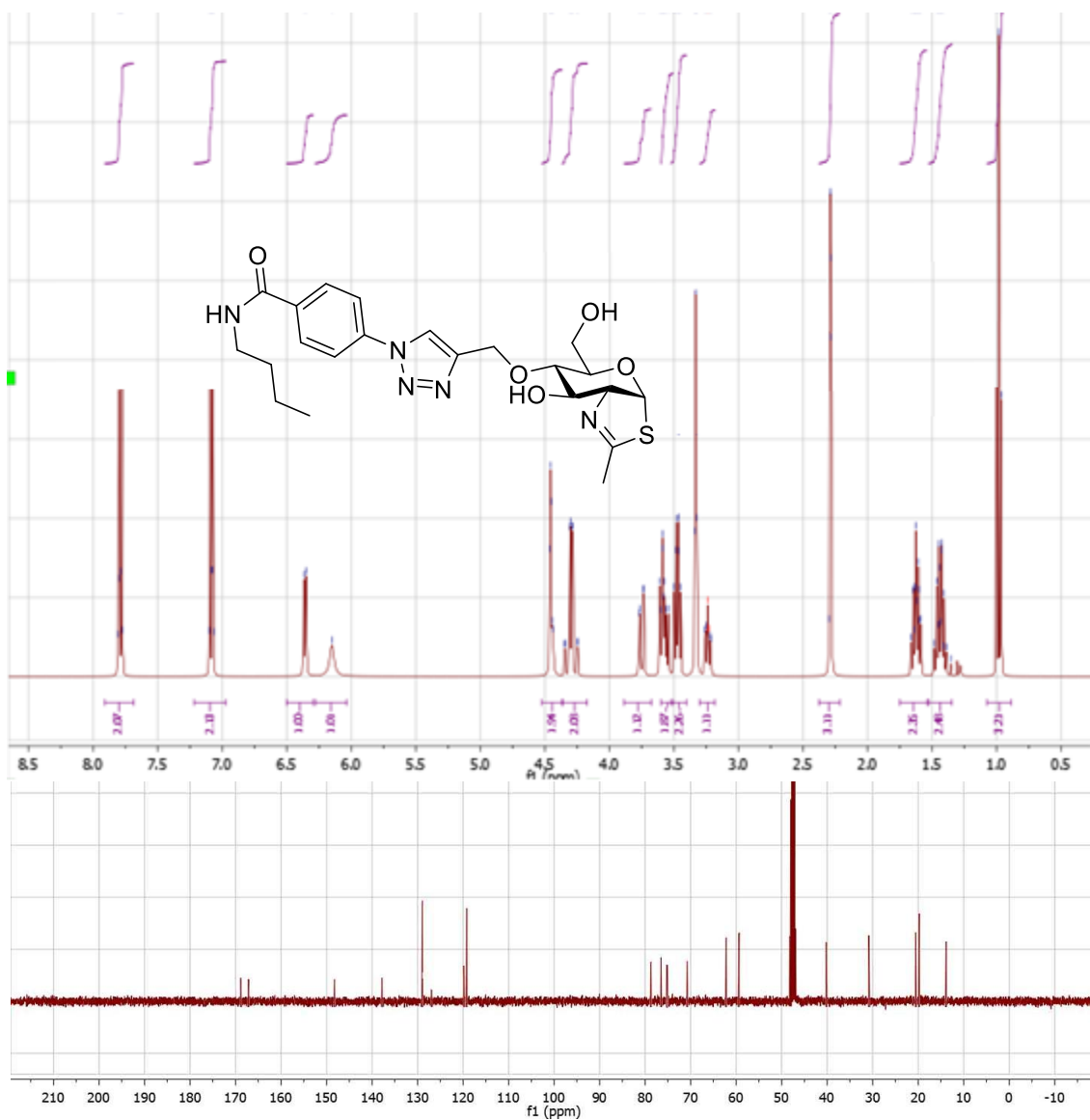
¹H NMR (400 MHz, Chloroform-*d*) δ 7.92 – 7.73 (m, 2H), 7.45 – 7.25 (m, 5H), 7.18 – 7.02 (m, 2H), 6.45 (s, 1H), 6.36 (d, *J* = 6.3 Hz, 1H), 4.66 (d, *J* = 5.6 Hz, 2H), 4.51 – 4.40 (m, 2H), 4.35 – 4.18 (m, 2H), 3.75 (dd, *J* = 12.1, 2.3 Hz, 1H), 3.64 – 3.50 (m, 2H), 3.24 (ddd, *J* = 9.0, 6.6, 2.3 Hz, 1H), 2.29 (d, *J* = 1.9 Hz, 3H). ¹³C NMR (125 MHz, Chloroform-*d*) δ 167.66, 167.07, 148.19, 138.71, 137.75, 132.77, 128.89, 128.40, 127.31, 127.17, 119.75, 119.13, 78.64, 76.41, 75.12, 75.00, 70.66, 62.12, 59.29, 43.79, 19.67. HRMS (ESI⁺) *m/z*: [M+H]⁺ calcd for C₂₅H₂₈N₅O₅S 510.1811, found 510.1818.

Compound 32.



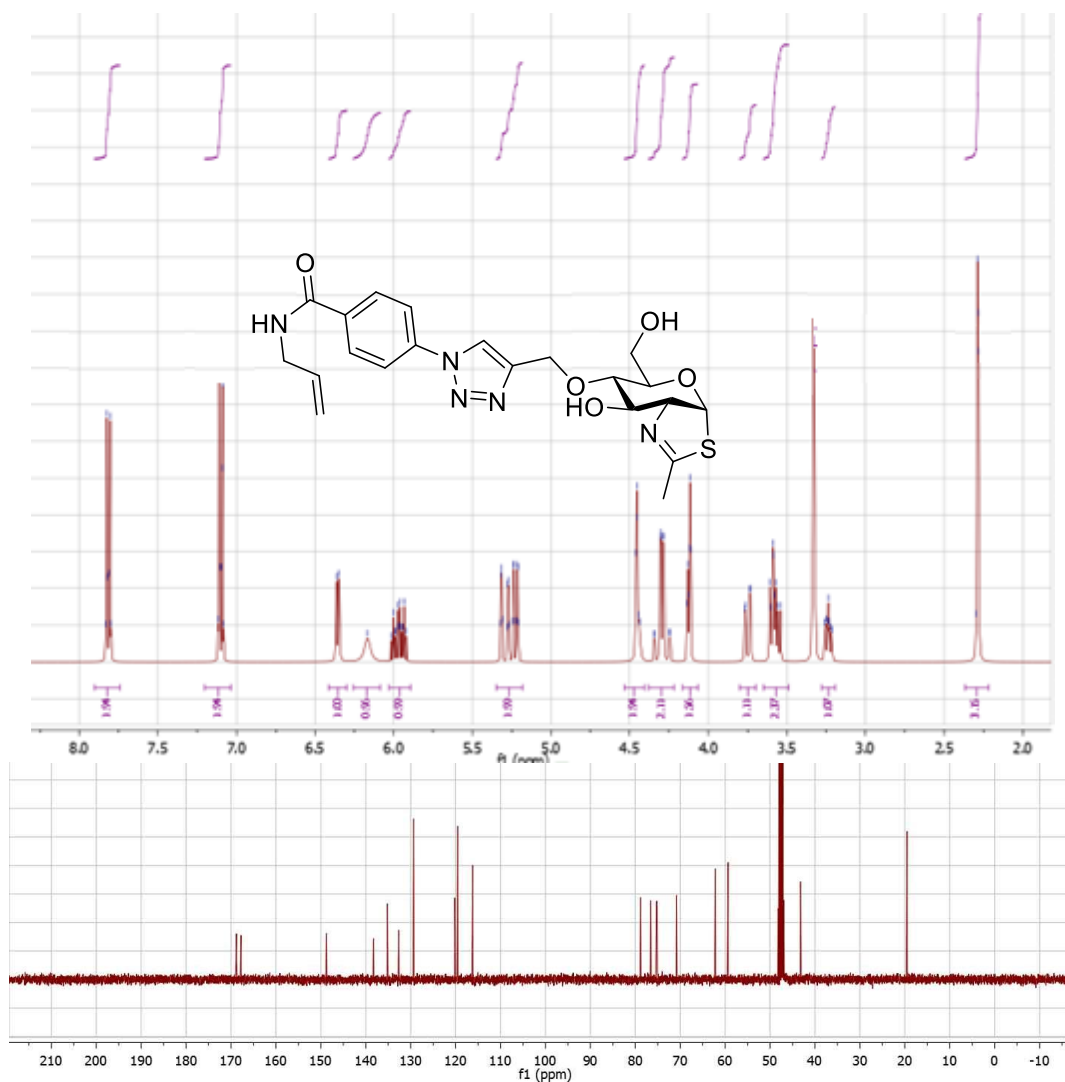
¹H NMR (400 MHz, Methanol-*d*) δ 8.24 – 8.03 (m, 2H), 7.18 – 7.03 (m, 2H), 6.38 (d, $J = 6.3$ Hz, 1H), 5.34 – 5.23 (m, 1H), 4.54 – 4.37 (m, 2H), 4.41 – 4.16 (m, 2H), 3.75 (dd, $J = 12.1, 2.3$ Hz, 1H), 3.68 – 3.50 (m, 2H), 3.24 (m, 1H), 2.28 (d, $J = 2.0$ Hz, 3H), 1.36 (d, $J = 6.2$ Hz, 7H). ¹³C NMR (125 MHz, Methanol-*d*) δ 167.07, 166.46, 148.19, 138.88, 131.16, 128.77, 119.75, 118.93, 78.64, 76.41, 75.12, 75.00, 70.66, 68.95, 62.12, 59.29, 21.98, 19.67. HRMS (ESI⁺) m/z . [M+H]⁺ calcd for C₂₁H₂₇N₄O₆S 463.1651, found 463.1663.

Compound 33.



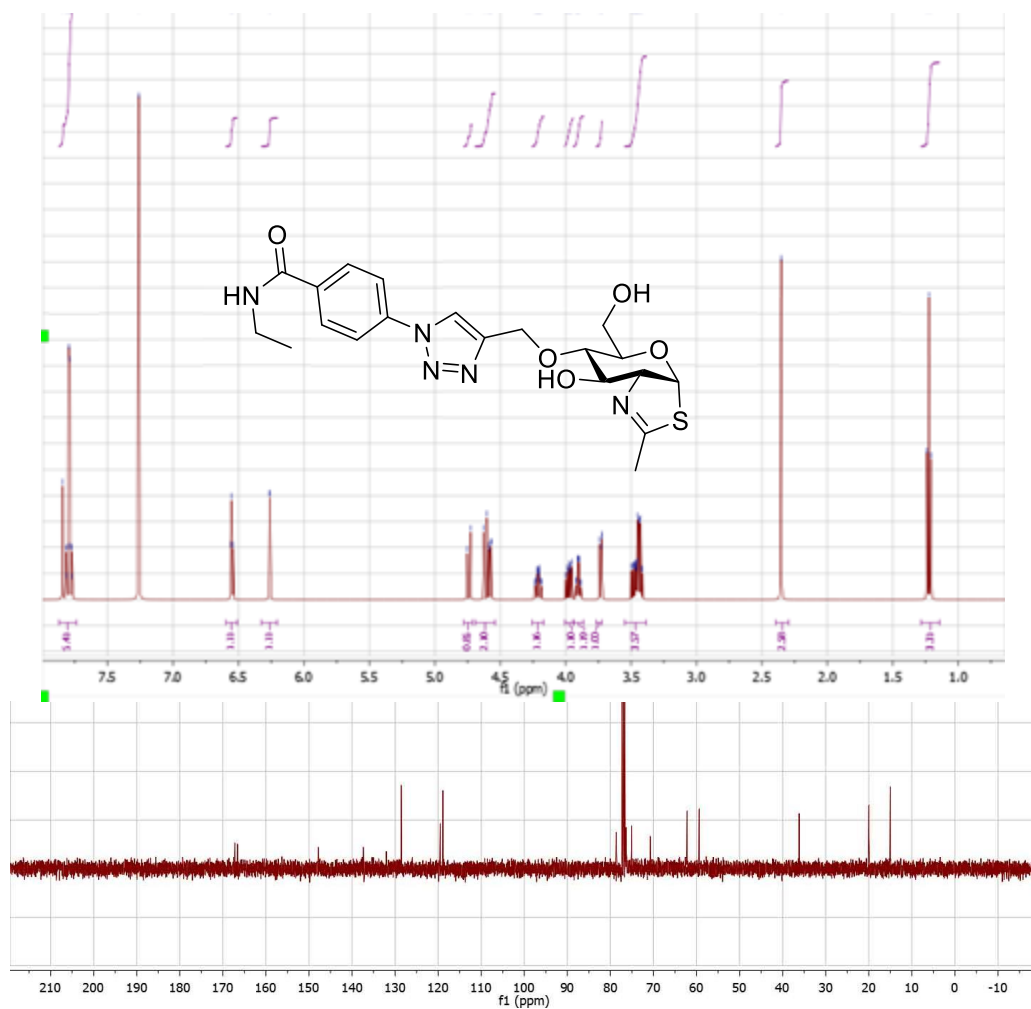
¹H NMR (400 MHz, Methanol-*d*) δ 7.90 – 7.68 (m, 2H), 7.21 – 6.97 (m, 2H), 6.36 (d, J = 6.4 Hz, 1H), 6.15 (s, 1H), 4.52 – 4.37 (m, 2H), 4.37 – 4.17 (m, 2H), 3.75 (dd, J = 12.1, 2.3 Hz, 1H), 3.60 – 3.51 (m, 2H), 3.47 (td, J = 7.2, 5.7 Hz, 2H), 3.24 (dd, J = 15.8, 2.3 Hz, 1H), 2.29 (d, J = 1.8 Hz, 3H), 1.62 (tt, J = 7.8, 6.4 Hz, 2H), 1.53 – 1.35 (m, 2H), 0.98 (t, J = 7.3 Hz, 3H). ¹³C NMR (125 MHz, Methanol-*d*) δ 168.77, 167.07, 148.19, 137.75, 128.89, 126.87, 119.75, 119.13, 78.64, 76.41, 75.12, 75.00, 70.66, 62.12, 59.29, 40.10, 30.74, 20.43, 19.67, 13.74. HRMS (ESI⁺) m/z : [M+H]⁺ calcd for C₂₂H₃₀N₅O₅S 476.1968, found 476.1964.

Compound 34.



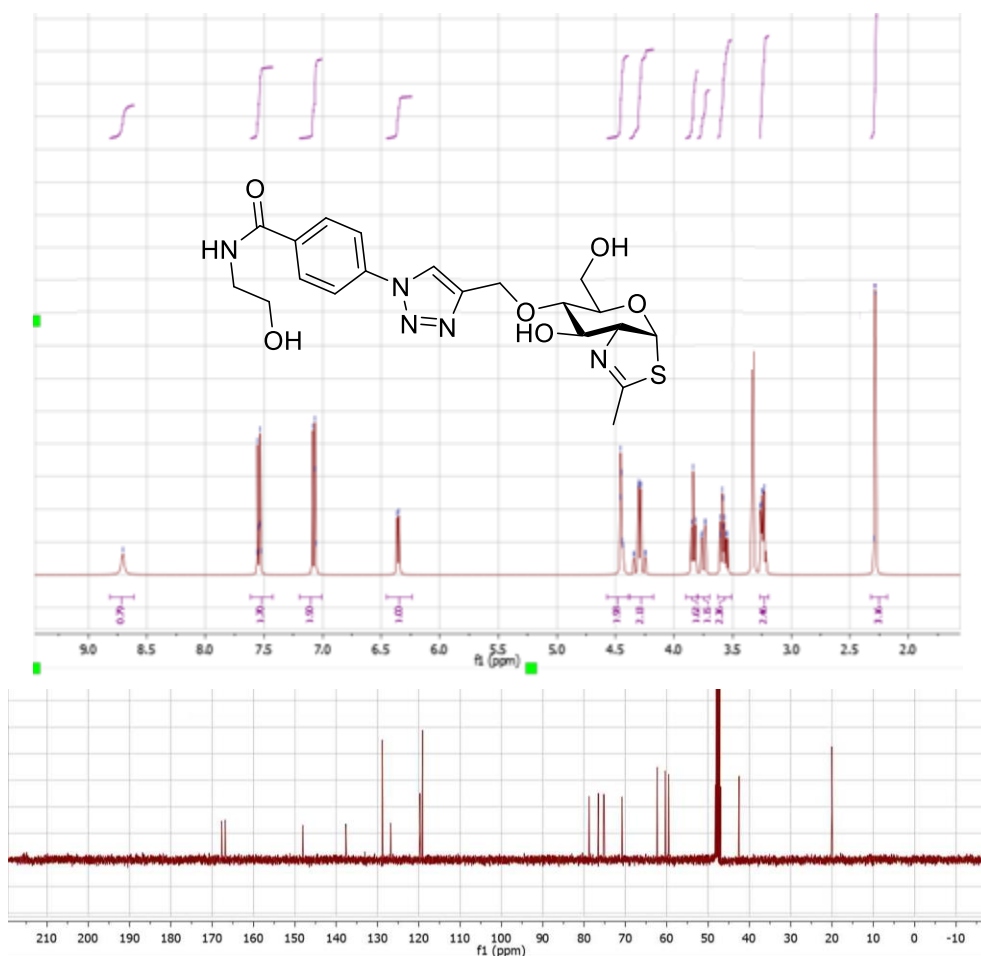
¹H NMR (400 MHz, Methanol-*d*) δ 7.90 – 7.74 (m, 2H), 7.20 – 7.04 (m, 2H), 6.36 (d, J = 6.4 Hz, 1H), 6.17 (s, 1H), 5.97 (ddt, J = 17.1, 10.2, 5.7 Hz, 1H), 5.35 – 5.19 (m, 2H), 4.53 – 4.41 (m, 2H), 4.38 – 4.22 (m, 2H), 4.12 (dt, J = 5.8, 1.5 Hz, 2H), 3.75 (dd, J = 12.1, 2.3 Hz, 1H), 3.66 – 3.49 (m, 2H), 3.25 (ddd, J = 9.0, 6.6, 2.3 Hz, 1H), 2.29 (d, J = 1.7 Hz, 3H). ¹³C NMR (125 MHz, Methanol-*d*) δ 168.11, 167.07, 148.19, 137.75, 134.68, 132.18, 128.89, 119.75, 119.13, 115.82, 78.64, 76.41, 75.12, 75.00, 70.66, 62.12, 59.29, 43.23, 19.67. HRMS (ESI⁺) m/z : [M+H]⁺ calcd for C₂₁H₂₆N₅O₅S 460.1655, found 460.1664.

Compound 35.



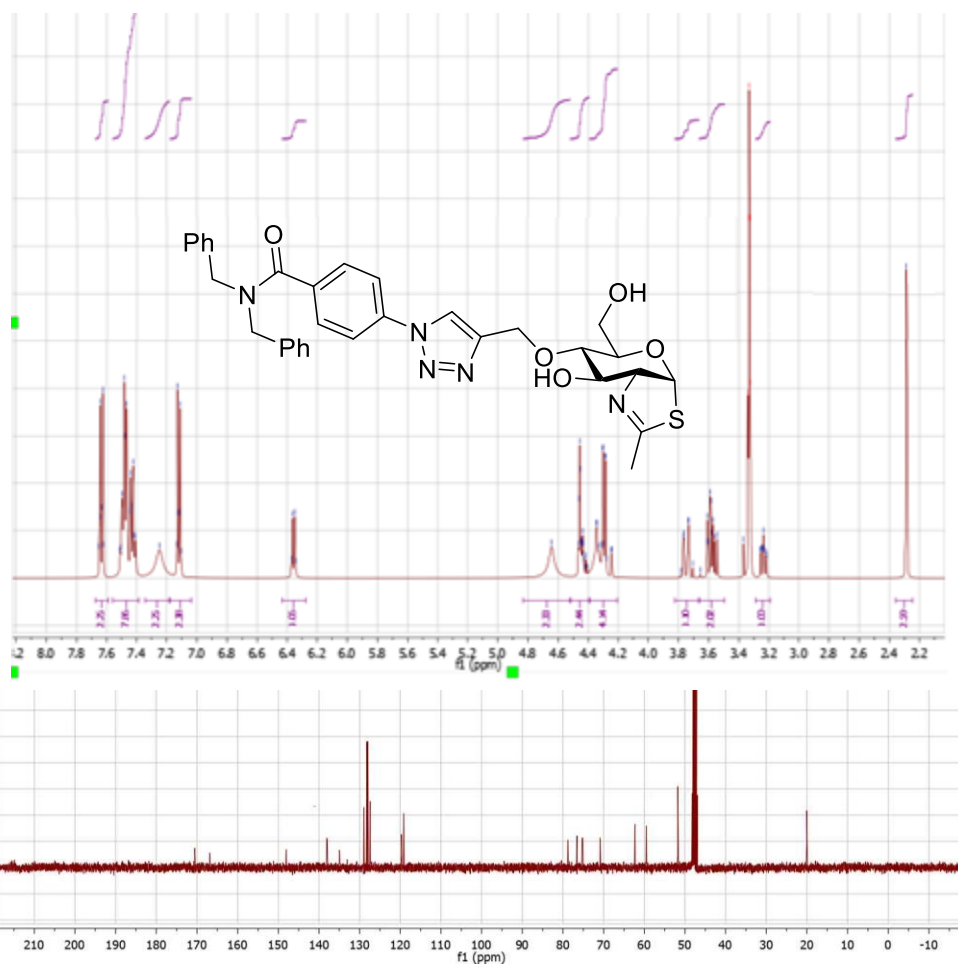
¹H NMR (500 MHz, Chloroform-*d*) δ 7.87 – 7.73 (m, 5H), 6.55 (t, J = 4.4 Hz, 1H), 6.26 (d, J = 2.4 Hz, 1H), 4.74 (d, J = 12.1 Hz, 1H), 4.69 – 4.54 (m, 2H), 4.21 (tdd, J = 8.3, 6.9, 2.0 Hz, 1H), 3.98 (ddd, J = 11.9, 7.1, 5.7 Hz, 1H), 3.90 (qd, J = 5.7, 2.0 Hz, 1H), 3.77 – 3.72 (m, 1H), 3.55 – 3.38 (m, 4H), 2.36 (s, 3H), 1.23 (t, J = 7.1 Hz, 3H). ¹³C NMR (125 MHz, Chloroform-*d*) δ 167.70, 167.07, 148.19, 137.75, 132.37, 128.89, 119.75, 119.13, 78.64, 76.41, 75.12, 75.00, 70.66, 62.12, 59.29, 35.96, 19.67, 14.66. HRMS (ESI⁺) m/z : [M+H]⁺ calcd for C₂₀H₂₆N₅O₅S 448.1655, found 448.1641.

Compound 36.



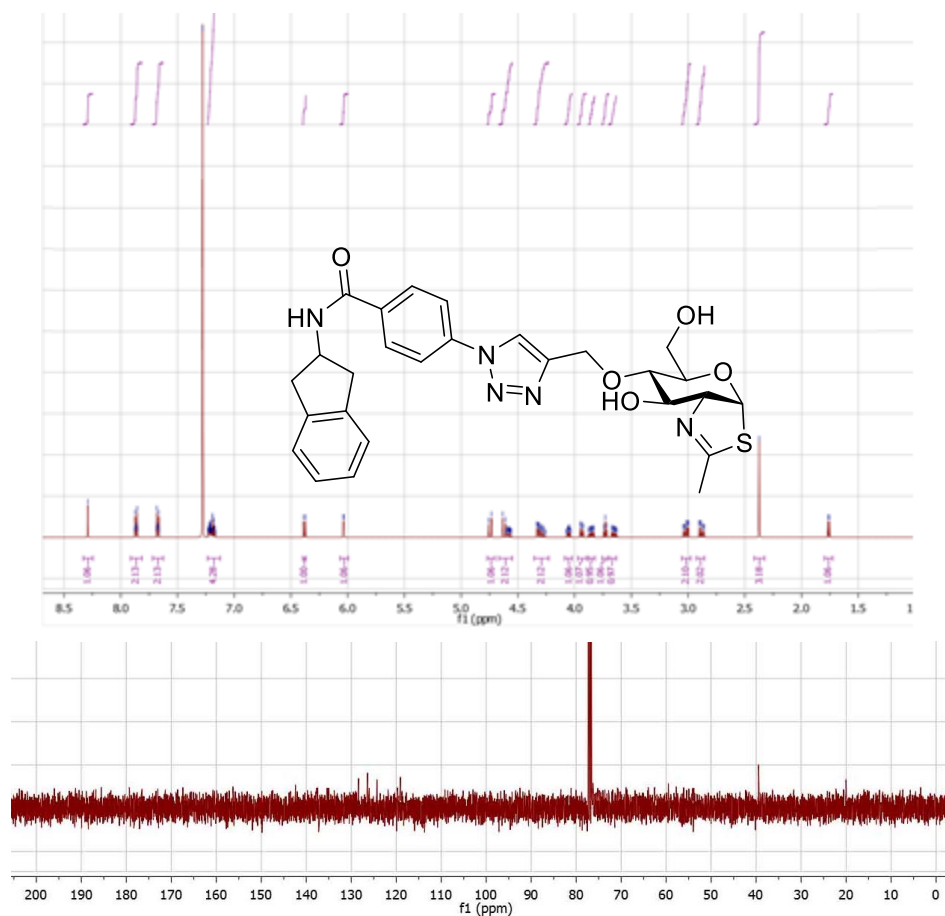
^1H NMR (400 MHz, Methanol-*d*) δ 8.71 (s, 1H), 7.61 – 7.42 (m, 2H), 7.20 – 7.01 (m, 2H), 6.36 (d, J = 6.4 Hz, 1H), 4.57 – 4.39 (m, 2H), 4.38 – 4.18 (m, 2H), 3.84 (t, J = 6.7 Hz, 2H), 3.75 (dd, J = 12.1, 2.4 Hz, 1H), 3.62 – 3.51 (m, 2H), 3.27 – 3.19 (m, 2H), 2.29 (d, J = 1.9 Hz, 3H). ^{13}C NMR (100 MHz, Methanol-*d*) δ 167.90, 167.07, 148.19, 137.75, 128.89, 126.87, 119.75, 119.13, 78.64, 76.41, 75.12, 75.00, 70.66, 62.12, 60.15, 59.29, 42.22, 19.67. HRMS (ESI⁺) m/z : [M+H]⁺ calcd for C₂₀H₂₆N₅O₆S 464.1604, found 464.1608.

Compound 37.



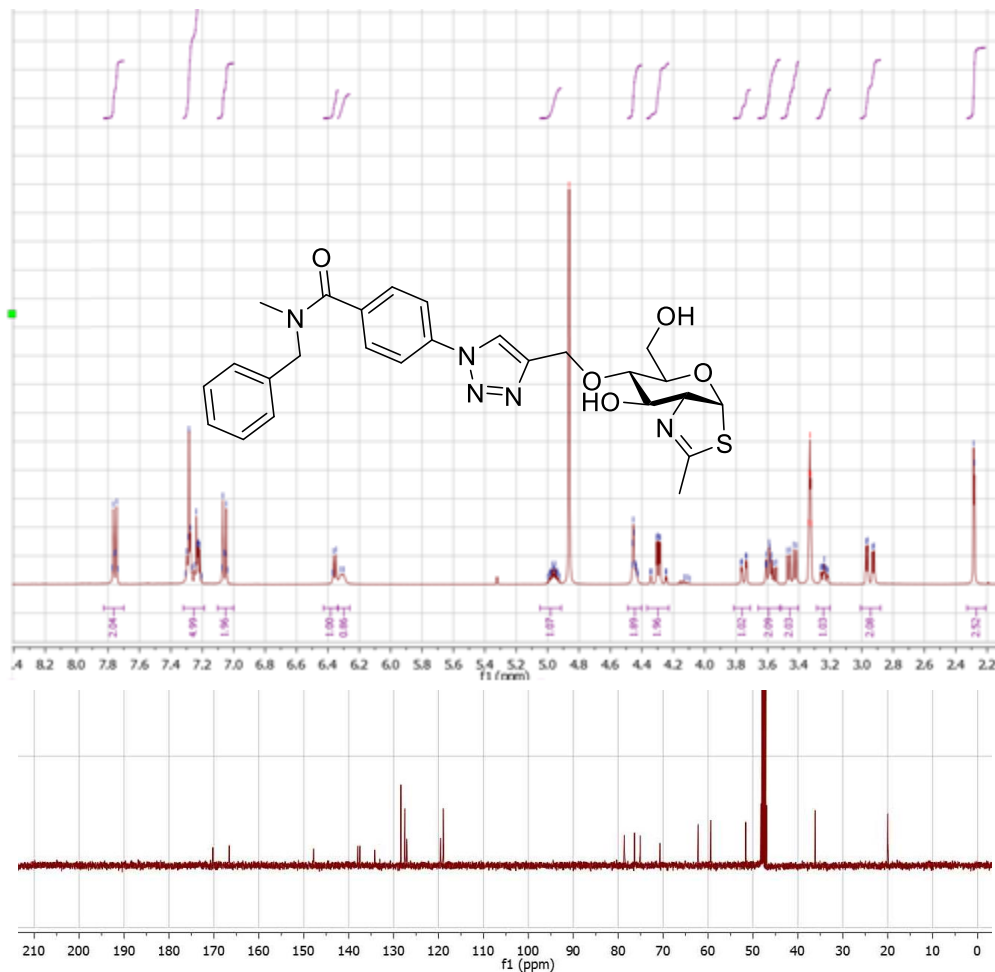
¹H NMR (400 MHz, Methanol-*d*) δ 7.67 – 7.59 (m, 2H), 7.56 – 7.38 (m, 8H), 7.25 (s, 2H), 7.18 – 7.04 (m, 2H), 6.36 (d, J = 6.3 Hz, 1H), 4.64 (s, 2H), 4.52 – 4.39 (m, 2H), 4.39 – 4.21 (m, 4H), 3.75 (dd, J = 12.1, 2.3 Hz, 1H), 3.66 – 3.49 (m, 2H), 3.24 (ddd, J = 9.0, 6.8, 2.3 Hz, 1H), 2.29 (d, J = 2.0 Hz, 3H). ¹³C NMR (125 MHz, Methanol-*d*) δ 170.77, 167.07, 148.19, 138.16, 138.02, 135.06, 129.00, 128.28, 128.04, 127.48, 119.75, 119.19, 78.64, 76.41, 75.12, 75.00, 70.66, 62.12, 59.29, 51.52, 19.67. HRMS (ESI⁺) m/z : [M+H]⁺ calcd for C₃₂H₃₄N₅O₅S 600.2281, found 600.2286.

Compound 38.



¹H NMR (500 MHz, Chloroform-*d*) δ 8.29 (s, 1H), 7.91 – 7.81 (m, 2H), 7.72 – 7.63 (m, 2H), 7.23 – 7.12 (m, 4H), 6.38 (d, $J = 9.2$ Hz, 1H), 6.04 (d, $J = 2.4$ Hz, 1H), 4.74 (d, $J = 11.9$ Hz, 1H), 4.67 – 4.55 (m, 2H), 4.36 – 4.23 (m, 2H), 4.05 (qd, $J = 5.7, 2.0$ Hz, 1H), 3.94 (dd, $J = 7.9, 6.0$ Hz, 1H), 3.88 – 3.82 (m, 1H), 3.73 (t, $J = 7.1$ Hz, 1H), 3.70 – 3.63 (m, 1H), 3.02 (ddd, $J = 15.0, 7.5, 0.9$ Hz, 2H), 2.88 (ddd, $J = 15.0, 7.5, 0.9$ Hz, 2H), 2.37 (d, $J = 1.6$ Hz, 3H), 1.76 (d, $J = 7.0$ Hz, 1H). ¹³C NMR (125 MHz, Chloroform-*d*) δ 167.07, 166.73, 148.19, 142.51, 137.98, 132.24, 128.43, 126.44, 124.31, 119.75, 119.09, 78.64, 76.41, 75.12, 75.00, 70.66, 62.12, 59.29, 53.87, 39.17, 19.67. HRMS (ESI⁺) m/z : [M+H]⁺ calcd for C₂₇H₃₀N₅O₅S 536.1968, found 536.1966.

Compound 39.



¹H NMR (400 MHz, Methanol-*d*) δ 7.83 – 7.70 (m, 2H), 7.32 – 7.19 (m, 5H), 7.10 – 7.00 (m, 2H), 6.36 (d, J = 6.4 Hz, 1H), 6.31 (d, J = 7.7 Hz, 1H), 4.96 (qt, J = 7.2, 4.3 Hz, 1H), 4.45 (dp, J = 6.0, 2.0 Hz, 2H), 4.37 – 4.23 (m, 2H), 3.75 (dd, J = 12.1, 2.3 Hz, 1H), 3.66 – 3.52 (m, 2H), 3.44 (dd, J = 16.3, 7.1 Hz, 2H), 3.24 (ddd, J = 9.0, 6.6, 2.3 Hz, 1H), 2.95 (dd, J = 16.2, 4.4 Hz, 2H), 2.28 (d, J = 2.0 Hz, 3H). ¹³C NMR (100 MHz, Methanol-*d*) δ 170.79, 167.07, 148.19, 138.30, 137.84, 134.58, 128.70, 127.77, 127.41, 119.75, 119.22, 78.64, 76.41, 75.12, 75.00, 70.66, 62.12, 59.29, 51.48, 35.93, 19.67. HRMS (ESI⁺) m/z : [M+H]⁺ calcd for C₂₆H₃₀N₅O₅S 524.1968, found 524.1966.

2.6.3. Gene expression and enzyme purification

Gene expression and protein purification of SpGH85: SpGH85 was produced according to previous literature (Abbott 2009) in *Escherichia coli* BL21 Star (DE3) cells using Lysogeny broth (LB medium) with 50 µg/mL of kanamycin incubated for 8 hours at 37 °C, or until they reached an absorbance of 0.6 using 600 nm wavelength light. Protein production was induced with 0.5mM isopropyl β-D-1-thio-galactopyranoside (IPTG) for 4 hours at 37 °C. The cells were harvested by centrifugation, resuspended in loading buffer, frozen overnight at -80 °C, ruptured by the addition of 0.2 mg of lysozyme per mL of resuspended *E. coli*, and sonicated on ice. SpGH85 was purified on a Ni²⁺ His tag column, dialyzed, and concentrated. Final concentration of SpGH85 was determined by Nanodrop₂₀₀₀. SpGH85 plasmid, along with transfected *E. coli* BL21 Star (DE3) cells were obtained from Melissa Cid from the laboratory of Prof. Alisdair Boraston at the University of Victoria.

Gene expression and protein purification of Endo D: Endo D was produced according to previous literature (Abbott 2009) in *Escherichia coli* BL21 Star (DE3) cells using LB media with 50 µg/mL of kanamycin incubated for 8 hours at 37 °C, or until they reached an absorbance of 0.6 using 600 nm wavelength light. Protein production was induced with 0.5mM IPTG for 4 hours at 37 °C. The cells were harvested by centrifugation, resuspended in loading buffer, frozen overnight at -80 °C, ruptured by the addition of 0.2 mg of lysozyme per mL of resuspended *E. coli*, and sonicated on ice. Endo D was purified on a Ni²⁺ His tag column, dialyzed, and concentrated. Purified Endo D was obtained from Dr. Joanne Hobbs from the laboratory of Prof. Alisdair Boraston at the University of Victoria.

Gene expression and protein purification of FlgJ: FlgJ was transfected by adding plasmid DNA into *Escherichia coli* BL21 Gold cells and heat shocking them at 42 °C for one minute and allowing them to grow for 30 minutes in LB media before plating on an agar plate infused with kanamycin. A single colony was taken and incubated in LB media with 50 µg/mL of kanamycin overnight. 1 mL of this culture was added to 1L of LB media with 50 µg/mL of kanamycin and incubated at 37 °C until they reached an absorbance of 0.6 using 600 nm wavelength light. Protein production was induced with 0.2mM IPTG for 4 hours at 28 °C. The cells were harvested by centrifugation, resuspended

in loading buffer, frozen overnight at -80 °C, ruptured by the addition of 0.2 mg of lysozyme per mL of resuspended *E. coli*, and sonicated on ice. FlgJ was purified on a Ni²⁺ His tag column, dialyzed, and concentrated. Final concentration of FlgJ was determined by Nanodrop₂₀₀₀. The plasmid for FlgJ with an excised inhibitory helix was obtained from Patryk Zaloba from the laboratory of Prof. Brian Mark at the University of Manitoba.

Protein purification of Auto: *E. coli* cell lysate containing Auto was purified on a Ni-NTA column, followed by overnight incubation with HRV3C protease to remove the GST and His tag. The tags were removed using a GST bind resin and the filtrate was further purified over Superdex 75 resin before being dialyzed and concentrated. Purified Auto was obtained from Dr. Veronica Larmour from the laboratory of Prof. Brian Mark at the University of Manitoba.

2.6.4. Kinetic analysis of enzymes

Kinetic analysis of Endo D: All assays were carried out in Greiner 384-well low volume plates in 50mM citrate, 50mM CHES, 50mM phosphate, and 100mM NaCl pH 7.5 buffer in quadruplicate for 20 minutes. A continuous assay procedure was performed in which the reactions were initiated by the addition of 3,4-DNP-GlcNAc substrate (8 µL via multichannel pipette). The total assay volume was 10 µL.

2.6.5. Standard analysis of water content

NMR analysis of water content in 3,4-dinitrophenol standard. The commercial 3,4-dinitrophenol available is moistened with 15 to 25% water as anhydrous 3,4-dinitrophenol is highly explosive. Due to this explosive nature, elemental analysis or thermogravimetric analysis was not suitable for water determination. Quantitative NMR analysis was used with a 99.7% ± 0.2% pure methyl 3,5-dinitrobenzoate standard in homogenized deuterated DMSO on the Bruker AVANCE II 600 MHz NMR spectrometer. From these experiments, it was deduced that the commercial sample is 76.4% ± 0.2% pure.

Chapter 3.

Rational design and synthesis of an inhibitor of HexD to explore enzyme function

3.1. Contributions

This work builds off of previous research done by Matthew Alteen from the Vocadlo Lab in collaboration with Prof. Tracey Gloster at the University of St. Andrews. X-Ray structures of HexD were solved by Prof. Tracey Gloster. Design and synthesis of inhibitors were done by Matthew Alteen and Isaac Seo. Kinetic inhibition studies were performed by Matthew Alteen.

3.2. Abstract

Hex D is a mammalian *N*-acetylgalactosaminidase that hydrolyzes *O*-GalNAc substrates. Although the mechanism and substrate selectivity of this enzyme is known, the exact biological substrates and functions of this enzyme are unknown. Gal-thiazoline is known to inhibit Hex D competitively ($K_i = 420$ nM) and a recent co-crystal structure of Gal-thiazoline bound to Hex D showed a pocket near the 3-OH position of the inhibitor. To further study the physiological role of Hex D, more potent and selective inhibitors with modifications at the 3-OH position of Gal-thiazoline were synthesized and tested for inhibitory potential. Unfortunately, modifications at this position resulted in decreased inhibition. We hypothesize that the 3-OH position is responsible for a key hydrogen bonding interaction that is compromised upon alkylation.

3.3. Introduction

Four mammalian *N*-acetyl hexosaminidases are known; these are responsible for cleaving terminal GlcNAc or GalNAc residues off proteins or gangliosides (Suzuki, 2003). However, only three of these *N*-acetyl hexosaminidases (Hex A, Hex B, and Hex C, which was renamed OGT) have known functions (Gloster, 2010). Hex D was only recently characterized mechanistically, but the natural substrates and functions are still unknown (Alteen, 2016). Previous studies indicate that Hex D is selective towards *O*-GalNAc, but can still hydrolyze *O*-GlcNAc (Gutternigg, 2009). This would indicate that GalNAc containing glycoconjugates may be involved in cellular processes in the cytosol, but enzymes responsible for installation of GalNAc in the cytosol are currently unknown, though conflicting studies suggests that OGT may or may not be able to tolerate UDP-GalNAc as a substrate in transferring GalNAc onto serine or threonine residues of proteins (Ma, 2013; Lazarus, 2012).

Recently, the mechanism of Hex D was confirmed as using a substrate assisted catalysis mechanism by synthesizing a series of *p*-nitrophenyl *N*-acetylgalactosamine substrates having varying number of fluorine substitutions on the acetamido group. Further validation was found in the effective inhibition of Hex D by Gal-thiazoline, with a K_i value of 420 nM (Alteen, 2016). Variants of Gal-thiazoline with modifications at the 2-position were synthesized, but little or no inhibition was observed using these. The reason for the lack of inhibition when making extensions at the 2 position were realized when the co-crystal structure of Gal-thiazoline bound to the active site of Hex D was elucidated and showed no room for modifications at this position. However, a large binding pocket was found near the 3 position of Gal-thiazoline, illustrated in Figure 3.1. To develop a potent and selective inhibitor of Hex D, analogs of Gal-thiazoline with modifications at the 3 position were developed and tested for inhibition with the goal of eventually using these to understand the role of Hex D in cells.

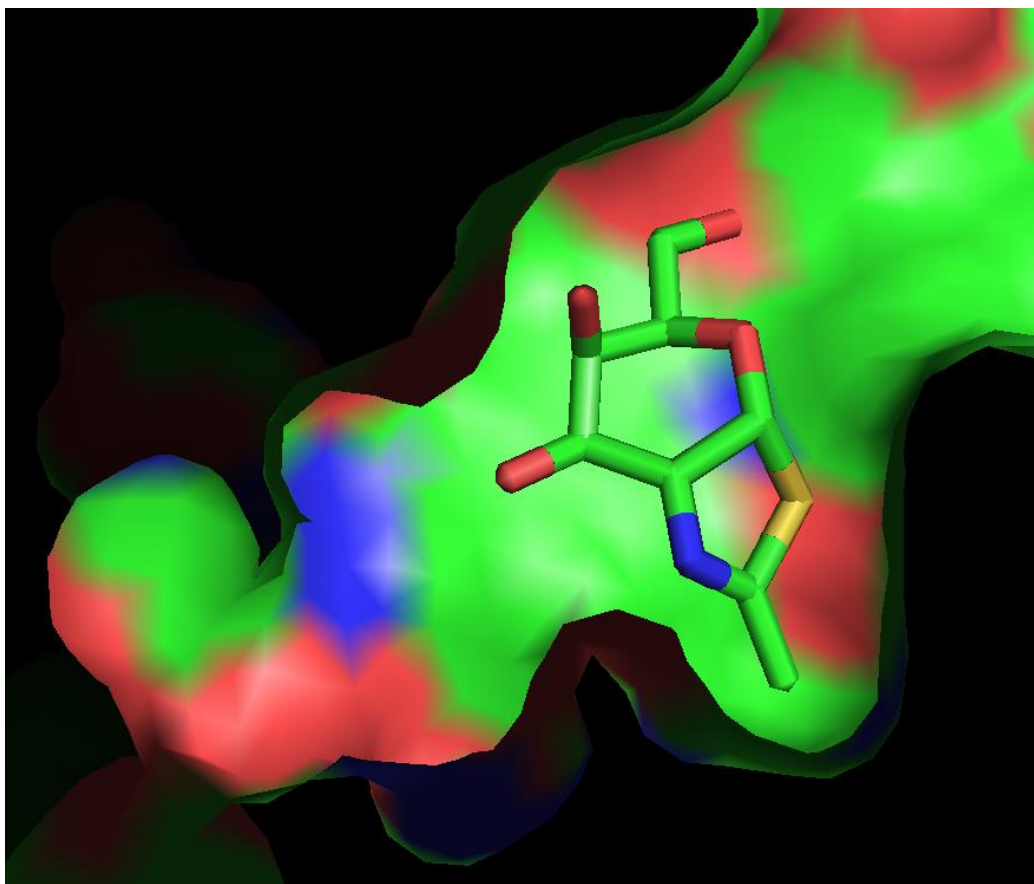
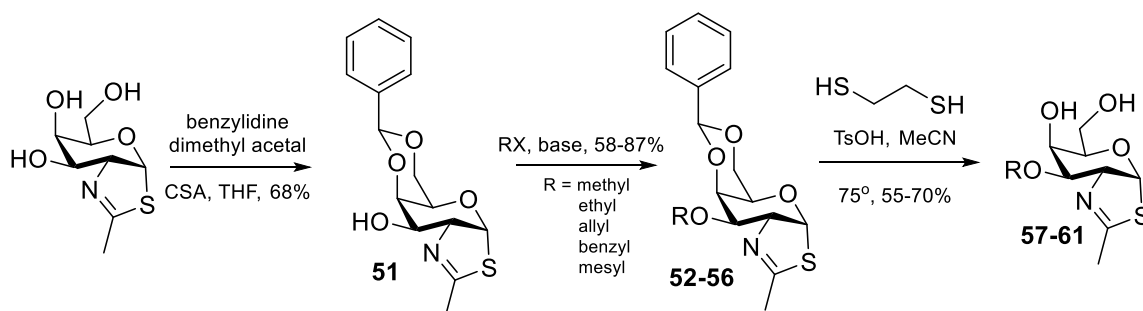


Figure 3.1. Co-crystal structure of Gal-thiazoline bound to Hex D shows a large binding pocket vicinal to the 3-OH position of Gal-thiazoline

3.4. Results and discussion

3.4.1. Design and synthesis of 3-OH modified galactose-thiazoline

Building on previous knowledge regarding the chemical reactivity of gluco-configured thiazolines as outlined in Chapter 2, Gal-thiazoline was synthesized according to reported methods (Alteen, 2016) and selectively protected at the 4 and 6-OH positions using benzaldehyde dimethyl acetal in the presence of catalytic camphorsulfonic acid. The sole free hydroxyl group was then alkylated at low temperature by addition of sodium hydride and appropriate alkyl halides to form the corresponding 3-O-alkyl-4,6-O-*p*-methoxybenzylidene-Gal-Thiazoline. The benzylidene protecting group was removed using ethane dithiol, catalytic amounts of *p*TSA, and gentle heating to afford the 3-O-alkyl-Gal-thiazoline.



Scheme 3.1. Synthesis of 3-OH functionalized Gal-thiazoline.

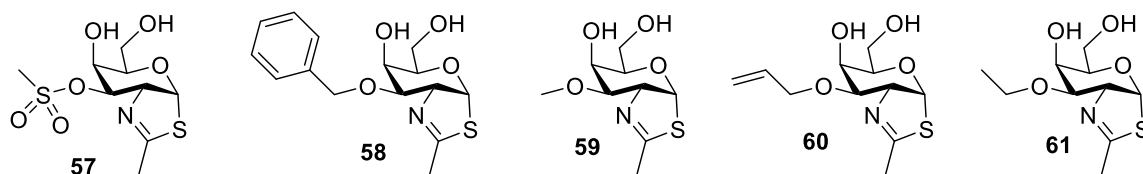


Figure 3.2. Synthesized Gal-thiazoline inhibitors of Hex D.

3.4.2. Inhibition assays of Hex D shows loss of inhibition potential

3-OH functionalized Gal-thiazoline derivatives were tested with Hex D using *p*-nitrophenyl *N*-acetylgalactosamine as a substrate. These inhibitors showed poor inhibition compared to the parent Gal-thiazoline with K_i values that were 200 to 4000 fold greater. These results showcase the often unpleasant truth that crystal structures in solid form do not always have the same conformation in solution. Should the pocket exist in solution, other possibilities that may account for these observations include the presence of hydrophilic residues around the pocket, thereby disfavoring hydrophobic molecules, or the alkylation of the 3-OH position acting to disrupt an essential hydrogen bond required for proper binding. The area surrounding the pocket is rich in polar moieties such as lysine, histidine, aspartic acid, glutamic acid, and glutamine. This may explain why the methyl sulfonate ester is the most potent of the modified inhibitors.

Table 3.1. K_i values of inhibitors developed for Hex D

Inhibitor	K_i
Gal-thiazoline	420 nM
3-O-methanesulfonyl-Gal-thiazoline	87 μ M
3-O-methyl -Gal-thiazoline	259 μ M
3-O-benzyl-Gal-thiazoline	878 μ M
3-O-allyl-Gal-thiazoline	1.67 mM
3-O-ethyl-Gal-thiazoline	n.d. ¹

¹ Not determined. This compound was not sent for inhibition testing as it would not lead to more potent inhibitors

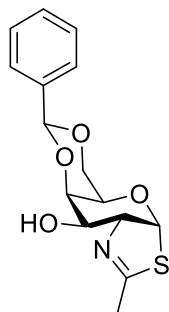
3.5. Conclusions and future prospects

A handful of Gal-thiazoline derivatives were synthesized and tested for inhibition against Hex D. Several of these compounds (51, 53 & 61) will need to be revisited for complete characterization to obtain melting points or ^{13}C spectra. Although all 3-O-alkyl-Gal-thiazolines showed worse inhibition than the parent Gal-thiazoline inhibitor, comparative studies between these inhibitors indicates the hydrophilic nature of the binding pocket near the 3 position may be important. It is possible that inhibitors based on Gal-thiazolines with an alkyl amine at the 3 position can be developed as a potent inhibitor of Hex D.

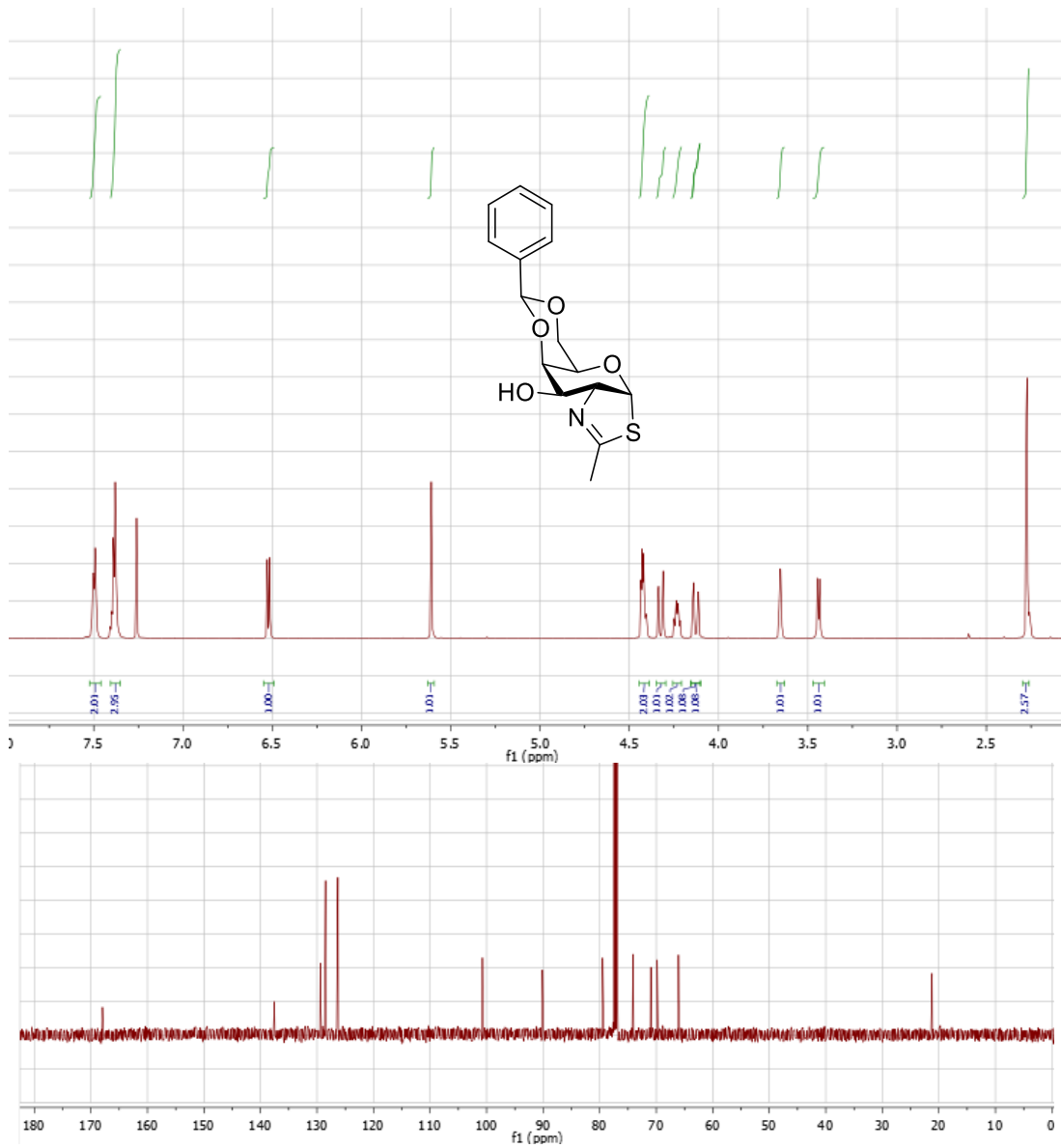
Hex D remains an interesting enzyme as it is conserved in mammals and found in all cell types and appears to act on a sugar substrate for which no biological information pertaining to its hydrolysis is known. The development of 3-amino galacto-configured inhibitors possessing a secondary amine at the 3 position that could enable hydrogen bonding with a vicinal hydrogen bond acceptor could be a potent and selective inhibitor. In the future, 3-OH functionalized Gal-PUGNAc, which is a more potent inhibitor scaffold, could be developed to yield potential inhibitors of Hex D.

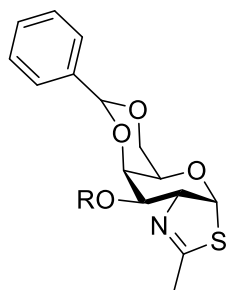
3.6. Experimental

3.6.1. Synthetic procedures for chemical compounds



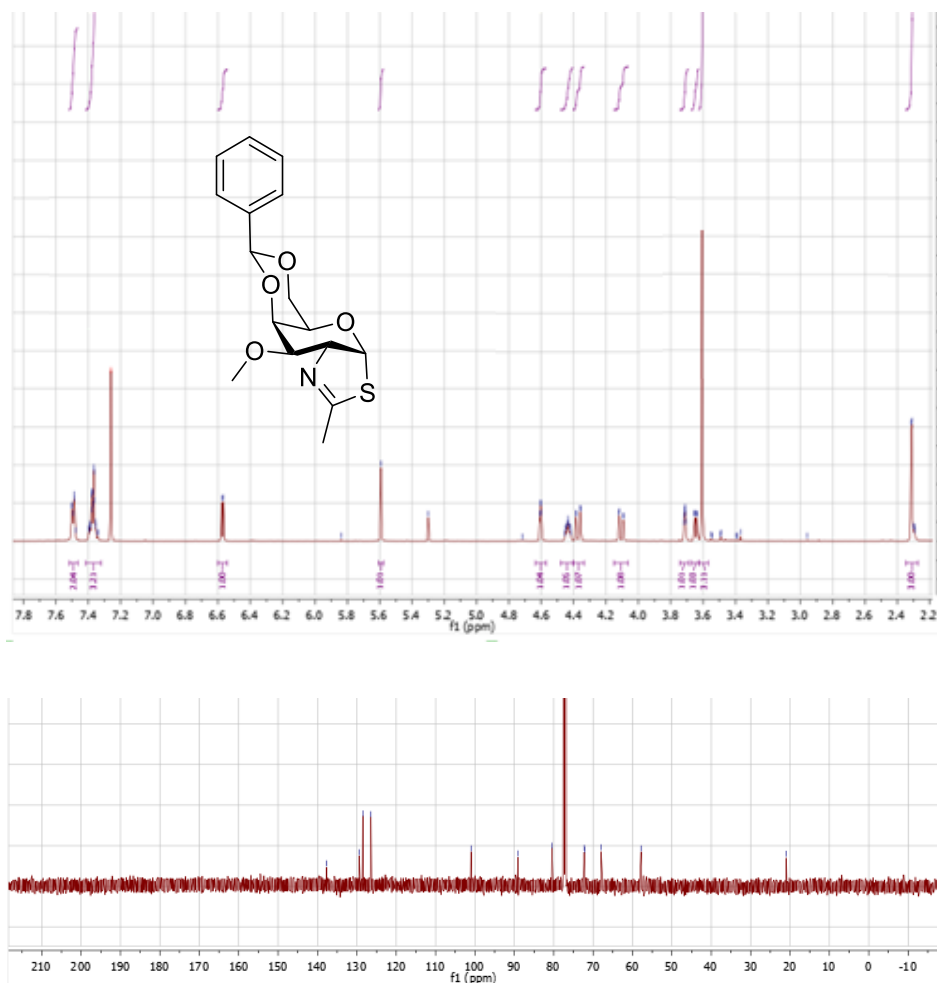
Compound 51: Gal-thiazoline (30 mg, 0.137 mmol) was added to a flame-dried 50 mL round bottom flask in an atmosphere of argon. The compound was dissolved in THF (6 mL) before the addition of benzaldehyde dimethyl acetal (83 μ L, 0.548 mmol) and camphor sulfonic acid (6.4 mg, 0.027 mmol). This mixture was heated to 50°C for 3 hours and transferred to a rotary evaporator where solvent volume was reduced to 1 mL. Dichloromethane was added and the solution was filtered through a silica plug and recrystallized with ethyl acetate and cold hexanes to yield 4,6-O-benzylidene-Gal-thiazoline as a white solid (28.8 mg, 62%). ^1H NMR (500 MHz, Chloroform-*d*) δ 7.52 – 7.46 (m, 2H), 7.38 (qd, J = 4.7, 1.5 Hz, 3H), 6.52 (d, J = 6.2 Hz, 1H), 5.61 (s, 1H), 4.44 – 4.39 (m, 2H), 4.32 (dd, J = 12.9, 1.3 Hz, 1H), 4.23 (td, J = 6.4, 3.8 Hz, 1H), 4.13 (dd, J = 13.0, 2.4 Hz, 1H), 3.65 (q, J = 2.1 Hz, 1H), 3.44 (d, J = 6.0 Hz, 1H), 2.27 (d, J = 1.9 Hz, 3H). ^{13}C NMR (126 MHz, Chloroform-*d*) δ 167.94, 137.54, 129.43, 128.48, 126.31, 100.76, 90.13, 79.49, 77.40, 77.15, 76.90, 74.10, 70.95, 69.83, 66.06, 21.22. HRMS (ESI+) m/z : $[\text{M}+\text{H}]^+$ calcd for $\text{C}_{15}\text{H}_{20}\text{NO}_4\text{S}$ 310.0951, found 310.0966.





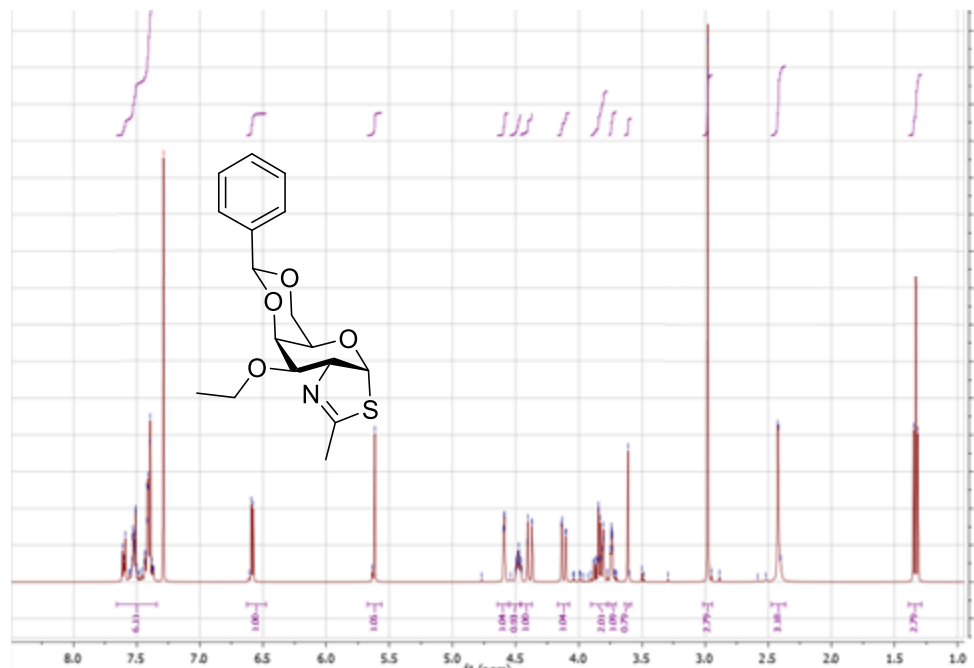
General procedure for Compounds 52-56: 4,6-*O*-benzylidene-Gal-thiazoline (50 mg, 0.163 mmol) was added to a flame-dried 50 mL round bottom flask in an atmosphere of argon. The compound was dissolved in DMF (2 mL) before the addition of alkyl halide (0.326 mmol) and cooled to 0°C. Sodium hydride (13 mg, 0.326 mmol, 60% dispersion in mineral oil) was added in portions and stirred on ice for 3 hours. Cold ethyl acetate was added and the mixture was washed thrice with water and brine before being dried on sodium sulfate and concentrated *in vacuo*. Purification by silica gel flash column chromatography (1:1 ethyl acetate : hexanes) gave 4,6-*O*-benzylidene-3-*O*-alkyl-Gal-thiazoline as a clear, white foam (58-87%).

Compound 52.



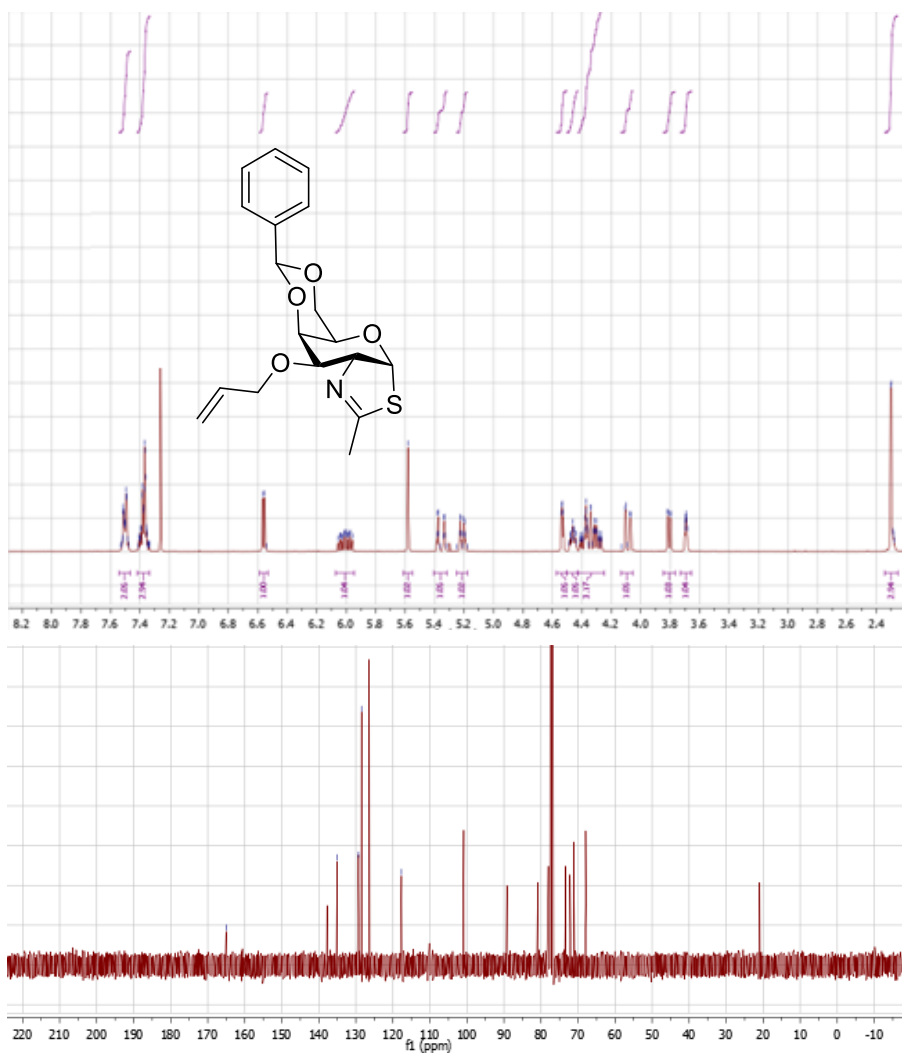
^1H NMR (500 MHz, Chloroform-*d*) δ 7.52 – 7.47 (m, 2H), 7.42 – 7.32 (m, 3H), 6.57 (d, $J = 5.5$ Hz, 1H), 5.59 (s, 1H), 4.60 (dd, $J = 3.1, 2.1$ Hz, 1H), 4.44 (ddd, $J = 7.7, 5.6, 2.0$ Hz, 1H), 4.37 (dd, $J = 12.8, 1.3$ Hz, 1H), 4.11 (dd, $J = 12.9, 2.1$ Hz, 1H), 3.71 (ddd, $J = 3.2, 2.1, 1.2$ Hz, 1H), 3.65 (dd, $J = 7.6, 2.1$ Hz, 1H), 3.61 (s, 3H), 2.31 (d, $J = 2.0$ Hz, 3H). ^{13}C NMR (126 MHz, Chloroform-*d*) δ 137.66, 129.36, 128.49, 126.42, 101.00, 89.08, 80.48, 72.26, 72.11, 67.97, 57.84, 20.93. HRMS (ESI⁺) m/z : $[\text{M}+\text{H}]^+$ calcd for $\text{C}_{16}\text{H}_{20}\text{NO}_4\text{S}$ 322.1108, found 322.1118.

Compound 53.



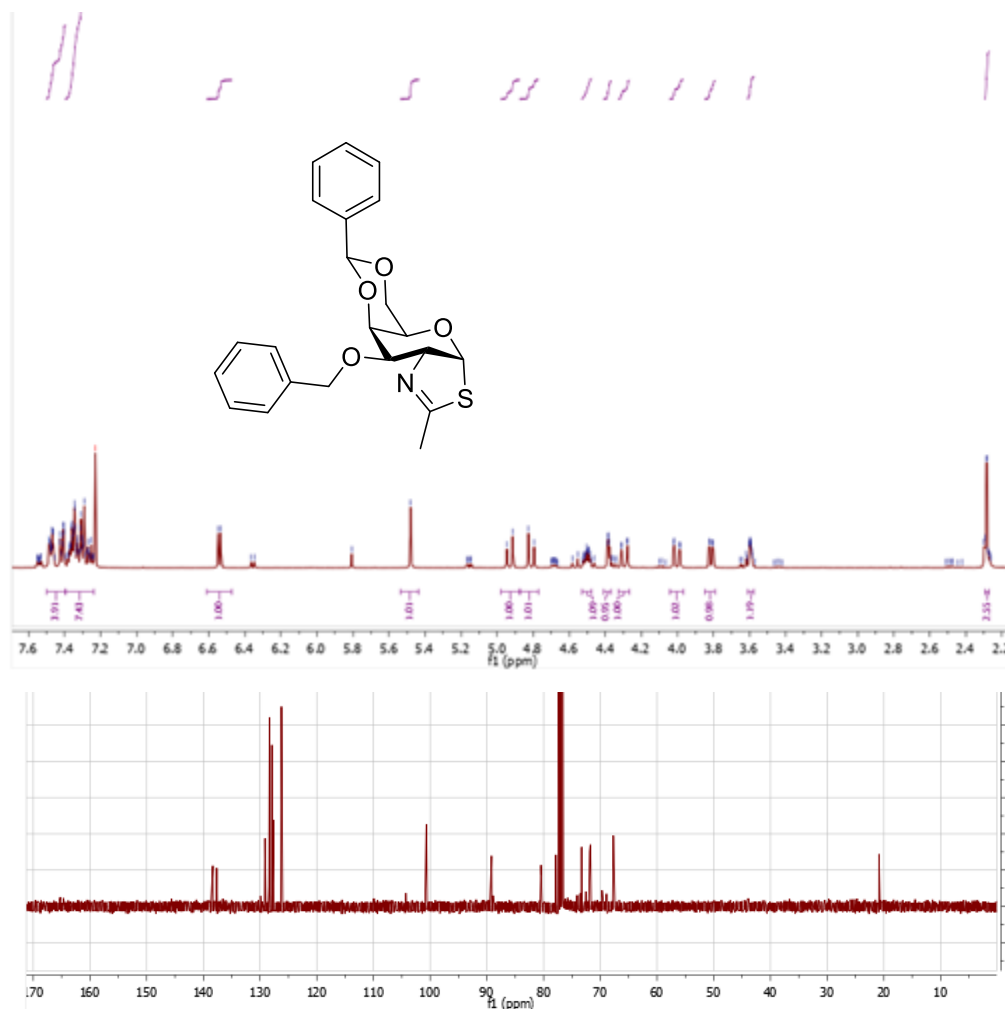
^1H NMR (400 MHz, Chloroform-*d*) δ 7.66 – 7.34 (m, 6H), 6.59 (d, J = 5.5 Hz, 1H), 5.62 (s, 1H), 4.59 (dd, J = 3.0, 2.1 Hz, 1H), 4.48 (ddt, J = 7.5, 3.4, 1.9 Hz, 1H), 4.46 – 4.37 (m, 1H), 4.12 (dd, J = 12.9, 2.1 Hz, 1H), 3.90 – 3.78 (m, 2H), 3.74 (ddd, J = 3.2, 2.1, 1.3 Hz, 1H), 3.61 (s, 1H), 2.98 (d, J = 0.5 Hz, 3H), 2.42 (d, J = 2.0 Hz, 3H), 1.33 (t, J = 7.0 Hz, 3H). HRMS (ESI⁺) m/z . $[\text{M}+\text{H}]^+$ calcd for $\text{C}_{17}\text{H}_{22}\text{NO}_4\text{S}$ 336.1270, found 336.1272.

Compound 54.



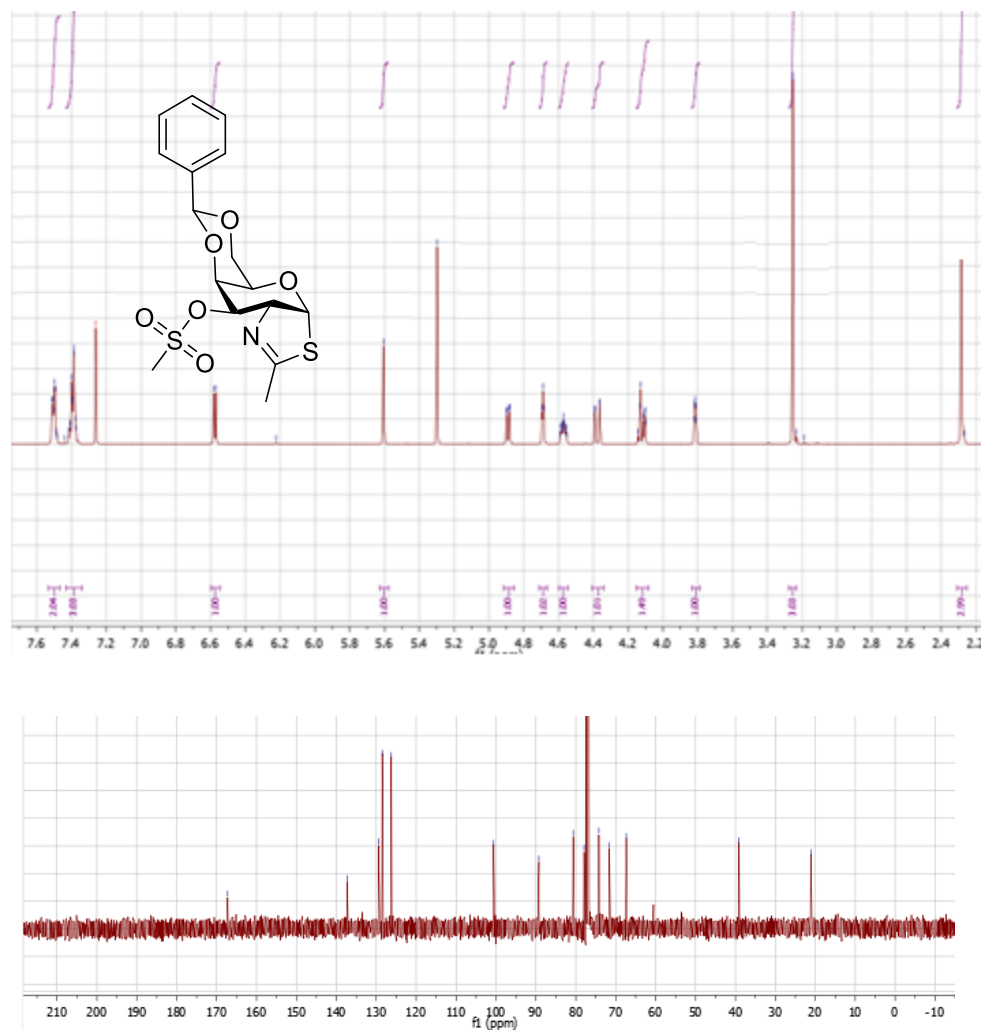
¹H NMR (400 MHz, Chloroform-*d*) δ 7.54 – 7.47 (m, 2H), 7.42 – 7.33 (m, 3H), 6.56 (d, $J = 5.5$ Hz, 1H), 6.01 (dddd, $J = 17.3, 10.3, 6.1, 5.4$ Hz, 1H), 5.58 (s, 1H), 5.36 (dq, $J = 17.3, 1.6$ Hz, 1H), 5.21 (dq, $J = 10.4, 1.4$ Hz, 1H), 4.53 (dd, $J = 3.0, 2.2$ Hz, 1H), 4.46 (ddt, $J = 7.6, 6.0, 2.1$ Hz, 1H), 4.43 – 4.25 (m, 3H), 4.09 (dd, $J = 12.8, 2.1$ Hz, 1H), 3.81 (dd, $J = 7.6, 2.2$ Hz, 1H), 3.69 (ddd, $J = 3.3, 2.1, 1.3$ Hz, 1H), 2.30 (d, $J = 2.1$ Hz, 3H). ¹³C NMR (101 MHz, Chloroform-*d*) δ 165.04, 135.06, 129.30, 128.45, 126.40, 117.70, 100.88, 89.20, 80.86, 78.02, 77.48, 77.36, 77.16, 76.84, 73.34, 72.17, 71.19, 67.96, 20.96. HRMS (ESI⁺) m/z : [M+H]⁺ calcd for C₁₈H₂₂NO₄S 348.1264, found 348.1267.

Compound 55.

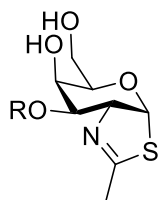


¹H NMR (400 MHz, Chloroform-*d*) δ 7.50 – 7.40 (m, 4H), 7.40 – 7.24 (m, 7H), 6.54 (d, $J = 5.5$ Hz, 1H), 5.48 (s, 1H), 4.93 (d, $J = 12.4$ Hz, 1H), 4.81 (d, $J = 12.4$ Hz, 1H), 4.53 – 4.48 (m, 1H), 4.38 (dd, $J = 3.0, 2.2$ Hz, 1H), 4.29 (dd, $J = 12.8, 1.4$ Hz, 1H), 4.00 (dd, $J = 12.8, 2.1$ Hz, 1H), 3.81 (dd, $J = 7.6, 2.2$ Hz, 1H), 3.59 (ddt, $J = 3.2, 2.4, 1.1$ Hz, 1H), 2.28 (d, $J = 2.0$ Hz, 3H). ¹³C NMR (101 MHz, Chloroform-*d*) δ 138.34, 137.64, 129.14, 128.35, 128.33, 128.30, 127.92, 127.75, 127.66, 127.47, 126.23, 100.67, 89.19, 80.48, 77.84, 73.30, 71.88, 71.75, 67.71, 20.86. HRMS (ESI⁺) m/z : [M+H]⁺ calcd for C₂₂H₂₄NO₄S 398.1421, found 398.1413.

Compound 56.

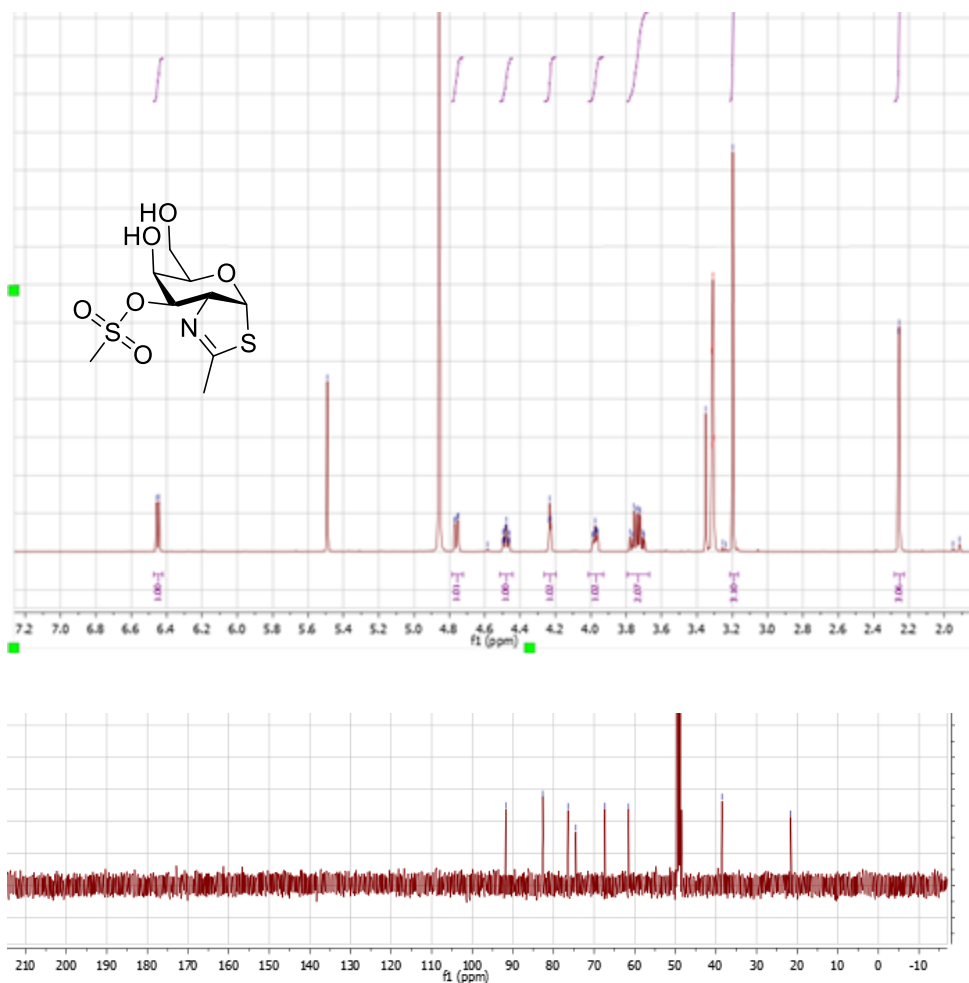


¹H NMR (500 MHz, Chloroform-*d*) δ 7.53 – 7.47 (m, 2H), 7.43 – 7.34 (m, 3H), 6.58 (d, J = 5.7 Hz, 1H), 5.61 (s, 1H), 4.89 (dd, J = 8.1, 2.3 Hz, 1H), 4.69 (t, J = 2.7 Hz, 1H), 4.57 (ddt, J = 7.9, 5.8, 1.9 Hz, 1H), 4.38 (dd, J = 13.0, 1.3 Hz, 1H), 4.15 – 4.08 (m, 1H), 3.81 (dt, J = 3.0, 1.7 Hz, 1H), 3.25 (s, 3H), 2.28 (d, J = 1.9 Hz, 3H). ¹³C NMR (126 MHz, Chloroform-*d*) δ 167.23, 137.30, 129.43, 128.50, 126.23, 100.59, 89.26, 80.65, 77.94, 74.23, 71.59, 67.35, 39.10, 21.11. HRMS (ESI⁺) m/z : [M+H]⁺ calcd for C₁₆H₂₀NO₆S₂ 386.0727, found 386.0741.



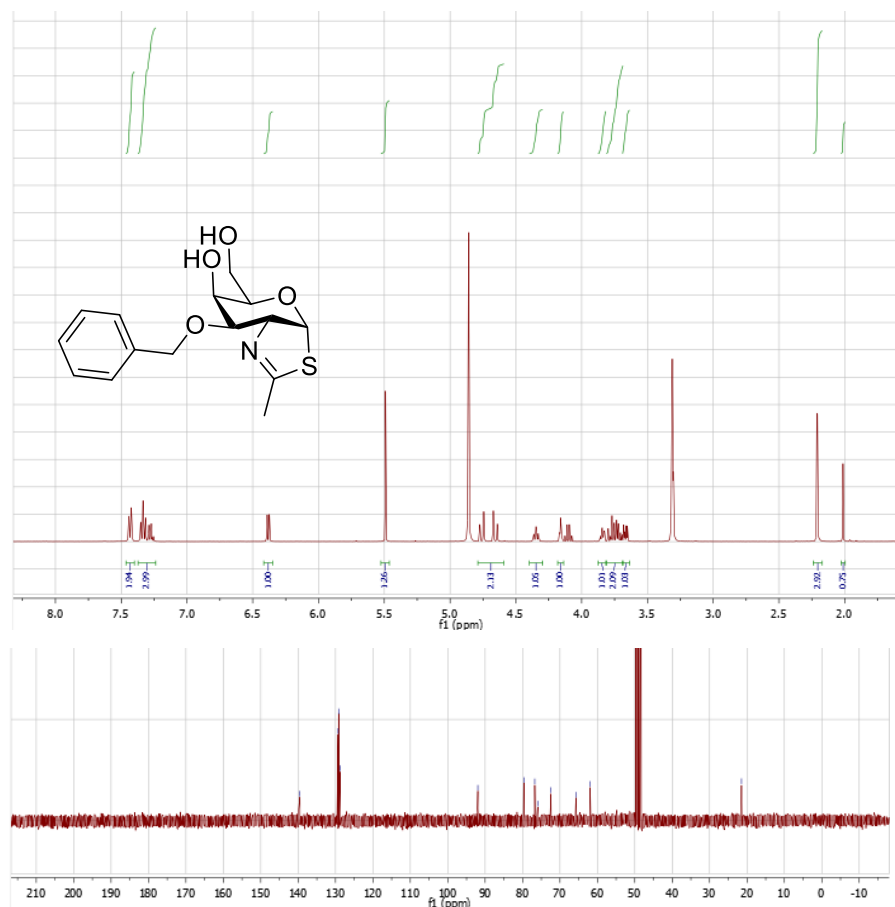
General procedure for Compounds 57-61: 4,6-*O*-benzylidene-3-*O*-alkyl-Gal-thiazoline (23.4 mg, 0.070 mmol) was added to a flame-dried 50 mL round bottom flask in an atmosphere of argon. The compound was dissolved in acetonitrile (2 mL). *p*-Toluenesulfonic acid (2.6 mg, 0.014 mmol) and ethanedithiol (35 μ L, 0.417 mmol) were added and the reaction was heated to 75 $^{\circ}$ C for 40 minutes before being concentrated and purified by silica gel flash column chromatography (1:19 methanol : dichloromethane) to yield 3-*O*-alkyl-Gal-thiazoline as a clear, white foam (55- 81%).

Compound 57.



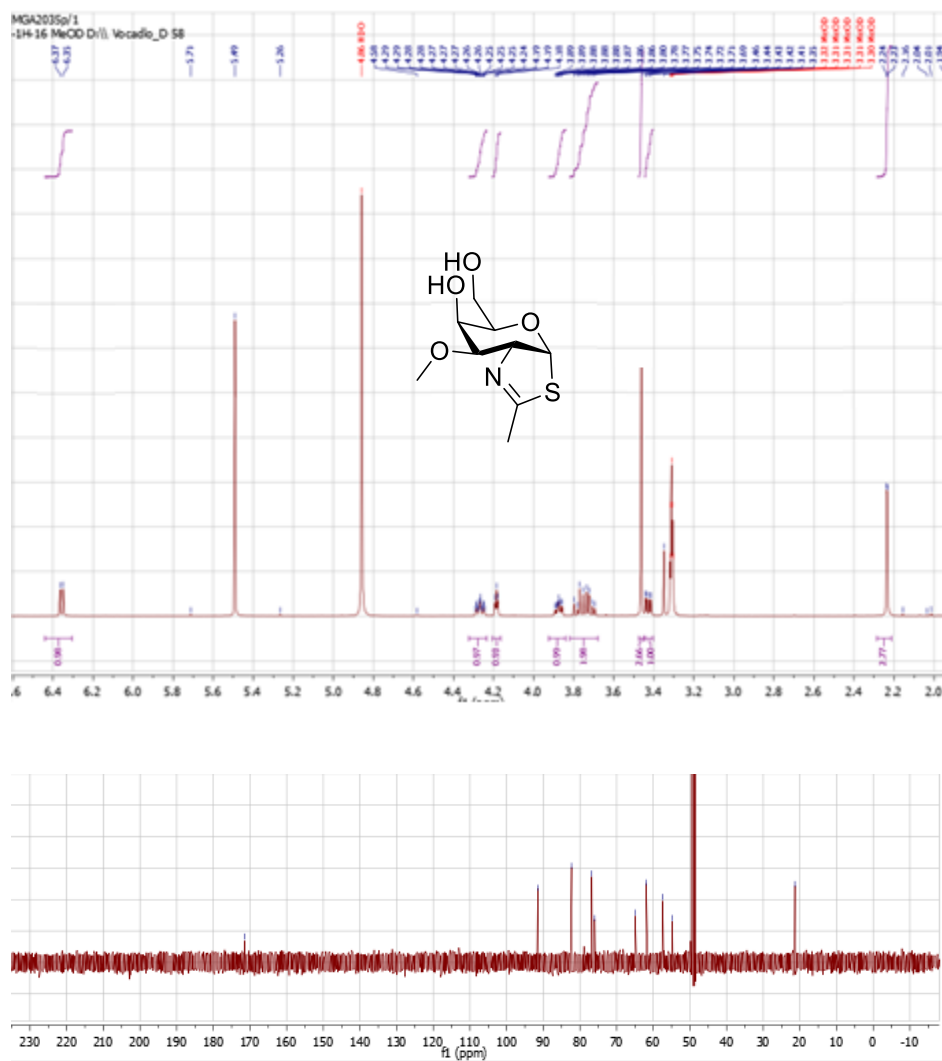
¹H NMR (500 MHz, Methanol-*d*₄) δ 6.45 (d, J = 6.5 Hz, 1H), 4.76 (dd, J = 8.3, 3.1 Hz, 1H), 4.48 (tq, J = 8.0, 1.4 Hz, 1H), 4.23 (t, J = 2.9 Hz, 1H), 3.97 (ddd, J = 7.4, 5.2, 2.5 Hz, 1H), 3.74 (qd, J = 11.7, 6.1 Hz, 2H), 3.20 (s, 3H), 2.26 (d, J = 1.4 Hz, 3H). ¹³C NMR (126 MHz, Methanol-*d*₄) δ 91.76, 82.65, 76.44, 74.50, 67.33, 61.52, 38.52, 21.59. HRMS (ESI⁺) m/z : [M+H]⁺ calcd for C₉H₁₁NO₆S₂ 298.0414, found 298.0422.

Compound 58.



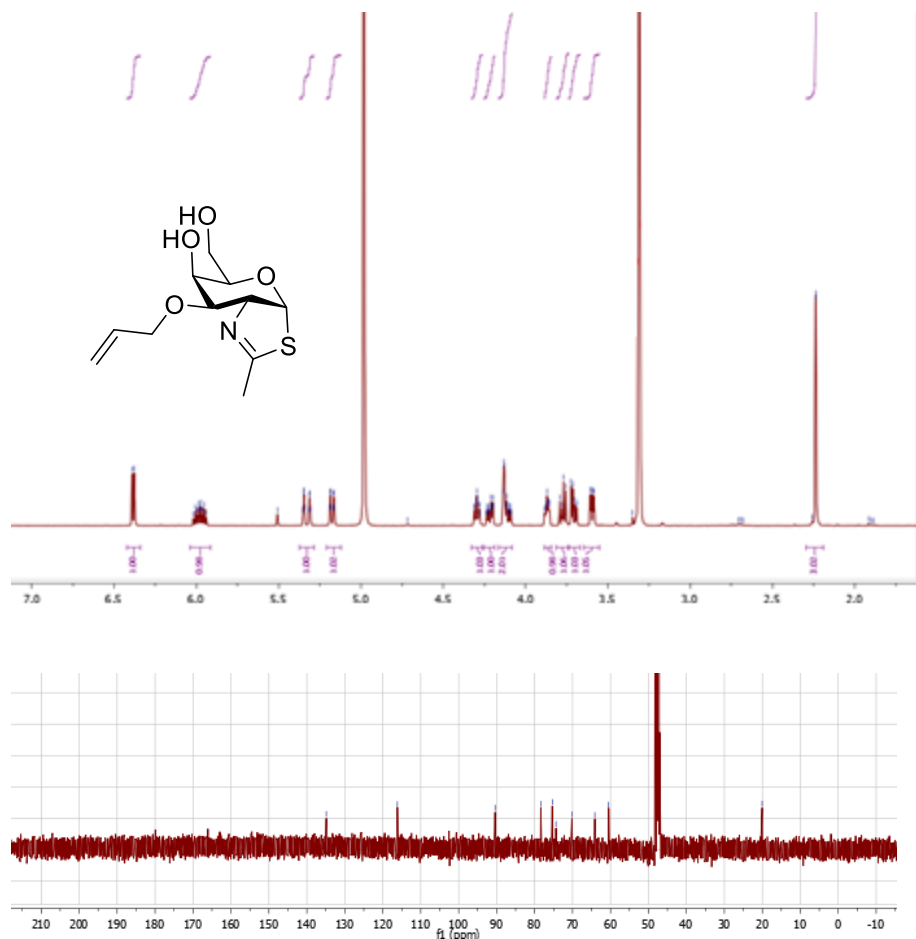
¹H NMR (400 MHz, Methanol-*d*₄) δ 7.46 – 7.40 (m, 2H), 7.37 – 7.24 (m, 3H), 6.38 (d, *J* = 6.4 Hz, 1H), 5.49 (s, 1H), 4.79 – 4.59 (m, 2H), 4.35 (ddq, *J* = 7.9, 6.4, 1.4 Hz, 1H), 4.16 (t, *J* = 2.8 Hz, 1H), 3.84 (ddd, *J* = 7.1, 4.9, 2.4 Hz, 1H), 3.81 – 3.69 (m, 2H), 3.67 (dd, *J* = 8.0, 3.1 Hz, 1H), 2.21 (d, *J* = 1.4 Hz, 3H), 2.01 (s, 1H). ¹³C NMR (101 MHz, Methanol-*d*₄) δ 129.01, 128.90, 128.44, 91.68, 79.38, 76.44, 75.63, 65.42, 49.21, 49.00, 48.79, 21.19. HRMS (ESI⁺) *m/z* [M+H]⁺ calcd for C₁₅H₁₉NO₄S 310.1113, found 310.1124.

Compound 59.



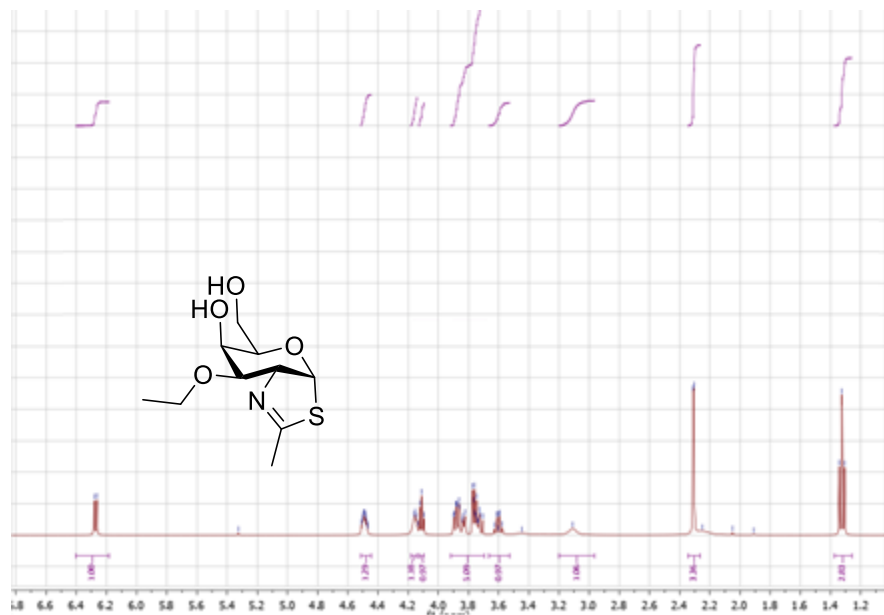
¹H NMR (400 MHz, Methanol-*d*₄) δ 6.36 (d, *J* = 6.5 Hz, 1H), 4.27 (ddq, *J* = 8.0, 6.5, 1.5 Hz, 1H), 4.19 (t, *J* = 2.8 Hz, 1H), 3.88 (ddd, *J* = 7.2, 5.0, 2.5 Hz, 1H), 3.82 – 3.68 (m, 2H), 3.46 (s, 3H), 3.43 (dd, *J* = 8.0, 3.0 Hz, 1H), 2.23 (d, *J* = 1.5 Hz, 3H). ¹³C NMR (101 MHz, Methanol-*d*₄) δ 171.49, 91.49, 82.29, 76.79, 76.00, 64.93, 61.93, 57.43, 54.80, 21.36. HRMS (ESI⁺) *m/z* [M+H]⁺ calcd for C₉H₁₆NO₄S 234.0795, found 234.0805.

Compound 60.



¹H NMR (500 MHz, Methanol-*d*₄) δ 6.38 (d, *J* = 6.5 Hz, 1H), 5.98 (ddt, *J* = 17.3, 10.4, 5.7 Hz, 1H), 5.33 (dq, *J* = 17.3, 1.7 Hz, 1H), 5.18 (dq, *J* = 10.4, 1.4 Hz, 1H), 4.30 (ddd, *J* = 8.0, 6.5, 1.5 Hz, 1H), 4.22 (ddt, *J* = 12.7, 5.5, 1.5 Hz, 1H), 4.16 – 4.08 (m, 2H), 3.87 (ddd, *J* = 7.3, 4.9, 2.4 Hz, 1H), 3.77 (dd, *J* = 11.7, 7.3 Hz, 1H), 3.71 (dd, *J* = 11.7, 4.9 Hz, 1H), 3.60 (dd, *J* = 8.1, 3.0 Hz, 1H), 2.24 (d, *J* = 1.4 Hz, 3H). ¹³C NMR (126 MHz, Methanol-*d*₄) δ 134.88, 116.16, 90.41, 78.37, 75.35, 70.17, 64.13, 60.48, 20.05. HRMS (ESI⁺) *m/z*: [M+H]⁺ calcd for C₁₁H₁₈NO₄S 260.0951, found 260.0954.

Compound 61.



¹H NMR (400 MHz,) δ 6.27 (d, J = 6.6 Hz, 1H), 4.49 (ddq, J = 6.1, 3.8, 2.0 Hz, 1H), 4.18 – 4.14 (m, 1H), 4.11 (t, J = 5.1 Hz, 1H), 3.92 – 3.69 (m, 5H), 3.67 – 3.53 (m, 1H), 3.11 (s, 1H), 2.31 (d, J = 2.1 Hz, 3H), 1.32 (t, J = 7.0 Hz, 3H). HRMS (ESI⁺) m/z [M+H]⁺ calcd for C₁₀H₁₈NO₄S 248.0951, found 248.0961.

References

- Abbott, D. W., Macauley, M. S., Vocadlo, D. J., & Boraston, A. B. (2009). Streptococcus pneumoniae endohexosaminidase D, structural and mechanistic insight into substrate-assisted catalysis in family 85 glycoside hydrolases. *Journal of Biological Chemistry*, 284(17), 11676-11689.
- Ahmad, I., & Aqil, F. (Eds.). (2008). *New strategies combating bacterial infection*. John Wiley & Sons.
- Aldridge, S., & Sturchio, J.L. (1999). *The discovery and development of penicillin*. Royal Society of Chemistry & American Chemical Society.
- Alharbi, S. A., Wainwright, M., Alahmadi, T. A., Salleeh, H. B., Faden, A. A., & Chinnathambi, A. (2014). What if Fleming had not discovered penicillin. *Saudi Journal of Biological Sciences*, 21(4), 289-293.
- Alteen, M. G., Oehler, V., Nemčovičová, I., Wilson, I. B., Vocadlo, D. J., & Gloster, T. M. (2016). Mechanism of Human Nucleocytoplasmic Hexosaminidase D. *Biochemistry*, 55(19), 2735-2747.
- Amblard, F., Cho, J. H., & Schinazi, R. F. (2009). Cu (I)-catalyzed Huisgen azide-alkyne 1, 3-dipolar cycloaddition reaction in nucleoside, nucleotide, and oligonucleotide chemistry. *Chemical Reviews*, 109(9), 4207-4220.
- Anthony, R. M., & Nimmerjahn, F. (2011). The role of differential IgG glycosylation in the interaction of antibodies with FcγRs in vivo. *Current Opinion in Organ Transplantation*, 16(1), 7-14.
- Anthony, R. M., & Ravetch, J. V. (2010). A novel role for the IgG Fc glycan: the anti-inflammatory activity of sialylated IgG Fcs. *Journal of Clinical Immunology*, 30(1), 9-14.
- Anthony, R. M., Wermeling, F., & Ravetch, J. V. (2012). Novel roles for the IgG Fc glycan. *Annals of the New York Academy of Sciences*, 1253(1), 170-180.
- Beckham, K. S., & Roe, A. J. (2015). From screen to target: insights and approaches for the development of anti-virulence compounds. *Host-adapted metabolism and its regulation in Bacterial Pathogens*.
- Berg, J. M., Tymoczko, J. L., & Stryer, L. (2006). Biochemistry. *Carbohydrates*, 11.
- Bertozzi, C. R., & Kiessling, L. L. (2001). Chemical glycobiology. *Science*, 291(5512), 2357-2364.

- Besanceney-Webler, C., Jiang, H., Zheng, T., Feng, L., Soriano del Amo, D., Wang, W., & Wu, P. (2011). Increasing the efficacy of bioorthogonal click reactions for bioconjugation: a comparative study. *Angewandte Chemie International Edition*, 50(35), 8051-8056.
- Bond, M.R. & Hanover, J.A. (2015) A little sugar goes a long way: The cell biology of O-GlcNAc. *Journal of Cell Biology*, 208(7), 869.
- Brands, M., Grande, Y. C., Endermann, R., Gahlmann, R., Krüger, J., & Raddatz, S. (2003). Pyrimidinone antibiotics—heterocyclic analogues with improved antibacterial spectrum. *Bioorganic & Medicinal Chemistry Letters*, 13(16), 2641-2645.
- Brandt, A. M., & Gardner, M. (2013). The golden age of medicine. *Companion to Medicine in the Twentieth Century*, 21-38.
- Brown, A. J. (1902). XXXVI.—Enzyme action. *Journal of the Chemical Society, Transactions*, 81, 373-388.
- Bublitz, M., Polle, L., Holland, C., Heinz, D. W., Nimtz, M., & Schubert, W. D. (2009). Structural basis for autoinhibition and activation of Auto, a virulence-associated peptidoglycan hydrolase of *Listeria monocytogenes*. *Molecular Microbiology*, 71(6), 1509-1522.
- Burlingham, B. T., & Widlanski, T. S. (2003). An intuitive look at the relationship of K_i and IC50: A more general use for the Dixon plot. *Journal of Chemical Education*, 80(2), 214.
- Cabanes, D., Dussurget, O., Dehoux, P., & Cossart, P. (2004). Auto, a surface associated autolysin of *Listeria monocytogenes* required for entry into eukaryotic cells and virulence. *Molecular Microbiology*, 51(6), 1601-1614.
- Cegelski, L., Marshall, G. R., Eldridge, G. R., & Hultgren, S. J. (2008). The biology and future prospects of antivirulence therapies. *Nature Reviews Microbiology*, 6(1), 17-27.
- Cekic, N., Heinonen, J. E., Stubbs, K. A., Roth, C., He, Y., Bennet, A. J., & Vocadlo, D. J. (2016). Analysis of transition state mimicry by tight binding aminothiazoline inhibitors provides insight into catalysis by human O-GlcNAcase. *Chemical Science*, 7(6), 3742-3750.
- Çetinbaş, N., Macauley, M. S., Stubbs, K. A., Drapala, R., & Vocadlo, D. J. (2006). Identification of Asp174 and Asp175 as the key catalytic residues of human O-GlcNAcase by functional analysis of site-directed mutants. *Biochemistry*, 45(11), 3835-3844.

- Chaudhuri, S., Gantner, B. N., Richard, D. Y., Cianciotto, N. P., & Freitag, N. E. (2013). The *Listeria monocytogenes* ChiA chitinase enhances virulence through suppression of host innate immunity. *MBio*, *4*(2), e00617-12.
- Chen, H., Ma, Y., Yang, J., O'Brien, C. J., Lee, S. L., Mazurkiewicz, J. E., & Zhang, J. R. (2008). Genetic requirement for pneumococcal ear infection. *PLoS One*, *3*(8), e2950.
- Chen, L., Zhou, Y., Qu, M., Zhao, Y., & Yang, Q. (2014). Fully deacetylated chitooligosaccharides act as efficient glycoside hydrolase family 18 chitinase inhibitors. *Journal of Biological Chemistry*, *289*(25), 17932-17940.
- Cheng, Y-C, & Prusoff, W. H. (1973). Relationship between the inhibition constant (K_i) and the concentration of inhibitor which causes 50 per cent inhibition (IC₅₀) of an enzymatic reaction. *Biochemical Pharmacology*, *22*(23), 3099-3108.
- Costerton, J. W., Irvin, R. T., & Cheng, K. J. (1981). The bacterial glycocalyx in nature and disease. *Annual Reviews in Microbiology*, *35*(1), 299-324.
- Craig, D. A. (1993). The Cheng-Prusoff relationship: something lost in the translation. *Trends in Pharmacological Sciences*, *14*(3), 89-91.
- Csermely, P., Korcsmáros, T., Kiss, H. J., London, G., & Nussinov, R. (2013). Structure and dynamics of molecular networks: a novel paradigm of drug discovery: a comprehensive review. *Pharmacology & Therapeutics*, *138*(3), 333-408.
- Dixon, M. (1953). The determination of enzyme inhibitor constants. *Biochemical Journal*, *55*(1), 170.
- Dorfmueller, H. C., Borodkin, V. S., Schimpl, M., Shepherd, S. M., Shpiro, N. A., & van Aalten, D. M. (2006). GlcNAcstatin: a picomolar, selective O-GlcNAcase inhibitor that modulates intracellular O-glcNAcylation levels. *Journal of the American Chemical Society*, *128*(51), 16484-16485.
- Dowd, J. E., & Riggs, D. S. (1965). A comparison of estimates of Michaelis-Menten kinetic constants from various linear transformations. *Journal of Biological Chemistry*, *240*(2), 863-869.
- Eisenthal, R., & Danson, M. J. (2002). *Enzyme Assays: A Practical Approach* (No. 257). Oxford University Press, USA.
- Eliopoulos, G. M., Cosgrove, S. E., & Carmeli, Y. (2003). The impact of antimicrobial resistance on health and economic outcomes. *Clinical Infectious Diseases*, *36*(11), 1433-1437.

- Fang, J., Richardson, J., Du, Z., & Zhang, Z. (2016). Effect of Fc-glycan structure on the conformational stability of IgG revealed by hydrogen/deuterium exchange and limited proteolysis. *Biochemistry*, 55(6), 860-868.
- Fenical, W., & Jensen, P. R. (2006). Developing a new resource for drug discovery: marine actinomycete bacteria. *Nature Chemical Biology*, 2(12), 666-673.
- Fleming, A. (1945). Penicillin, *1945 Nobel Lecture*, 83.
- Frederiksen, R. F., Paspaliari, D. K., Larsen, T., Storgaard, B. G., Larsen, M. H., Ingmer, H., & Leisner, J. J. (2013). Bacterial chitinases and chitin-binding proteins as virulence factors. *Microbiology*, 159(5), 833-847.
- Freeze, H. H., & Kranz, C. (2008). Endoglycosidase and Glycoamidase Release of N-Linked Glycans. *Current Protocols in Immunology*, 8-15.
- Fujita, K., Sato, R., Toma, K., Kitahara, K., Suganuma, T., Yamamoto, K., & Takegawa, K. (2007). Identification of the Catalytic Acid–Base Residue of *Arthrobacter* Endo- β -N-Acetylglucosaminidase by Chemical Rescue of an Inactive Mutant. *Journal of Biochemistry*, 142(3), 301-306.
- Ganem, B. (1996). Inhibitors of carbohydrate-processing enzymes: design and synthesis of sugar-shaped heterocycles. *Accounts of Chemical Research*, 29(7), 340-347.
- Gaumont, A. C., Gulea, M., & Levillain, J. (2009). Overview of the Chemistry of 2-Thiazolines. *Chemical Reviews*, 109(3), 1371-1401.
- Gillespie, S. H. (2001). Antibiotic resistance in the absence of selective pressure. *International Journal of Antimicrobial Agents*, 17(3), 171-176.
- Gloster, T. M. (2012). Development of inhibitors as research tools for carbohydrate-processing enzymes. *Biochemical Society Transactions*, 40(5), 913-928.
- Gloster, T. M., & Vocadlo, D. J. (2010). Mechanism, structure, and inhibition of O-GlcNAc processing enzymes. *Current Signal Transduction Therapy*, 5(1), 74-91.
- Gloster, T. M., & Vocadlo, D. J. (2012). Developing inhibitors of glycan processing enzymes as tools for enabling glycobiology. *Nature Chemical Biology*, 8(8), 683-694.
- Greenfield, N. J. (2006). Using circular dichroism spectra to estimate protein secondary structure. *Nature Protocols*, 1(6), 2876-2890.
- Gründling, A., Burrack, L. S., Bower, H. A., & Higgins, D. E. (2004). *Listeria monocytogenes* regulates flagellar motility gene expression through MogR, a transcriptional repressor required for virulence. *Proceedings of the National Academy of Sciences of the United States of America*, 101(33), 12318-12323.

- Guo, Y., Cai, S., Gu, G., Guo, Z., & Long, Z. (2015). Recent progress in the development of sortase A inhibitors as novel anti-bacterial virulence agents. *RSC Advances*, 5(62), 49880-49889.
- Gutternigg, M., Rendić, D., Voglauer, R., Iskratsch, T., & Wilson, I. B. (2009). Mammalian cells contain a second nucleocytoplasmic hexosaminidase. *Biochemical Journal*, 419(1), 83-90.
- Gutternigg, M., Rendić, D., Voglauer, R., Iskratsch, T., & Wilson, I. B. (2009). Mammalian cells contain a second nucleocytoplasmic hexosaminidase. *Biochemical Journal*, 419(1), 83-90.
- Hanover, J. A., Krause, M. W., & Love, D. C. (2010). The hexosamine signaling pathway: O-GlcNAc cycling in feast or famine. *Biochimica et Biophysica Acta (BBA)-General Subjects*, 1800(2), 80-95.
- Hart, G. W., Housley, M. P., & Slawson, C. (2007). Cycling of O-linked β -N-acetylglucosamine on nucleocytoplasmic proteins. *Nature*, 446(7139), 1017-1022.
- Harvey, A. L., Edrada-Ebel, R., & Quinn, R. J. (2015). The re-emergence of natural products for drug discovery in the genomics era. *Nature Reviews Drug Discovery*, 14(2), 111-129.
- Hauser, S., Song, H., Li, H., & Wang, L. X. (2005). A novel fluorescence-based assay for the transglycosylation activity of endo- β -N-acetylglucosaminidases. *Biochemical and Biophysical Research Communications*, 328(2), 580-585.
- Hava, D. L., & Camilli, A. (2002). Large-scale identification of serotype 4 *Streptococcus pneumoniae* virulence factors. *Molecular Microbiology*, 45(5), 1389-1406.
- Hein, J. E., & Fokin, V. V. (2010). Copper-catalyzed azide-alkyne cycloaddition (CuAAC) and beyond: new reactivity of copper (I) acetylides. *Chemical Society Reviews*, 39(4), 1302-1315.
- Herlihey, F. A., Moynihan, P. J., & Clarke, A. J. (2014). The essential protein for bacterial flagella formation FlgJ functions as a β -N-acetylglucosaminidase. *Journal of Biological Chemistry*, 289(45), 31029-31042.
- Himo, F., Lovell, T., Hilgraf, R., Rostovtsev, V. V., Noodleman, L., Sharpless, K. B., & Fokin, V. V. (2005). Copper (I)-catalyzed synthesis of azoles. DFT study predicts unprecedented reactivity and intermediates. *Journal of the American Chemical Society*, 127(1), 210-216.
- Horn, S. J., Sørbotten, A., Synstad, B., Sikorski, P., Sørлие, M., Vårum, K. M., & Eijsink, V. G. (2006). Endo/exo mechanism and processivity of family 18 chitinases produced by *Serratia marcescens*. *FEBS Journal*, 273(3), 491-503.

- Horsch, M., Mayer, C., Sennhauser, U., & Rast, D. M. (1997). β -N-acetylhexosaminidase: a target for the design of antifungal agents. *Pharmacology & Therapeutics*, 76(1), 187-218.
- Huisgen, R. (1963). Kinetics and mechanism of 1, 3-dipolar cycloadditions. *Angewandte Chemie International Edition in English*, 2(11), 633-645.
- Iseli, B., Armand, S., Boller, T., Neuhaus, J. M., & Henrissat, B. (1996). Plant chitinases use two different hydrolytic mechanisms. *FEBS letters*, 382(1-2), 186-188.
- Jackson, A. L., & Linsley, P. S. (2010). Recognizing and avoiding siRNA off-target effects for target identification and therapeutic application. *Nature Reviews Drug Discovery*, 9(1), 57-67.
- Johnson, K. A., & Goody, R. S. (2011). The original Michaelis constant: translation of the 1913 Michaelis–Menten paper. *Biochemistry*, 50(39), 8264-8269.
- Joung, J. K., & Sander, J. D. (2013). TALENs: a widely applicable technology for targeted genome editing. *Nature Reviews Molecular Cell Biology*, 14(1), 49-55.
- Juhas, M. (2015). Horizontal gene transfer in human pathogens. *Critical Reviews in Microbiology*, 41(1), 101-108.
- Kardos, N., & Demain, A. L. (2011). Penicillin: the medicine with the greatest impact on therapeutic outcomes. *Applied Microbiology and Biotechnology*, 92(4), 677-687.
- King, D. T., King, A. M., Lal, S. M., Wright, G. D., & Strynadka, N. C. (2015). Molecular mechanism of avibactam-mediated β -lactamase inhibition. *ACS Infectious Diseases*, 1(4), 175-184.
- Knapp, S., & Myers, D. S. (2002). Synthesis of α -GalNAc Thioconjugates from an α -GalNAc Mercaptan. *The Journal of Organic Chemistry*, 67(9), 2995-2999.
- Knapp, S., Abdo, M., Ajayi, K., Huhn, R. A., Emge, T. J., Kim, E. J., & Hanover, J. A. (2007). Tautomeric modification of GlcNAc-thiazoline. *Organic Letters*, 9(12), 2321-2324.
- Knapp, S., Vocadlo, D., Gao, Z., Kirk, B., Lou, J., & Withers, S. G. (1996). NAG-thiazoline, an N-acetyl- β -hexosaminidase inhibitor that implicates acetamido participation. *Journal of the American Chemical Society*, 118(28), 6804-6805.
- Kolb, H. C., Finn, M. G., & Sharpless, K. B. (2001). Click chemistry: diverse chemical function from a few good reactions. *Angewandte Chemie International Edition*, 40(11), 2004-2021.

- Kong, H., Chen, W., Lu, H., Yang, Q., Dong, Y., Wang, D., & Zhang, J. (2015). Synthesis of NAG-thiazoline-derived inhibitors for β -N-acetyl-d-hexosaminidases. *Carbohydrate Research*, 413, 135-144.
- Krejzová, J., Šimon, P., Kalachova, L., Kulik, N., Bojarová, P., Marhol, P., & Křen, V. (2014). Inhibition of GlcNAc-processing glycosidases by C-6-azido-NAG-thiazoline and its derivatives. *Molecules*, 19(3), 3471-3488.
- Lazarus, M. B., Jiang, J., Gloster, T. M., Zandberg, W. F., Whitworth, G. E., Vocadlo, D. J., & Walker, S. (2012). Structural snapshots of the reaction coordinate for O-GlcNAc transferase. *Nature Chemical Biology*, 8(12), 966-968.
- Lee, C. G., Da Silva, C. A., Cruz, C. S. D., Ahangari, F., Ma, B., Kang, M. J., & Elias, J. A. (2011). Role of chitin and chitinase/chitinase-like proteins in inflammation, tissue remodeling, and injury. *Annual Review of Physiology*, 73.
- Lenardon, M. D., Munro, C. A., & Gow, N. A. (2010). Chitin synthesis and fungal pathogenesis. *Current Opinion in Microbiology*, 13(4), 416-423.
- Lenski, R. E. (2010). Bacterial evolution and the cost of antibiotic resistance. *International Microbiology*, 1(4), 265-270.
- Lenzen, S. (2008). The mechanisms of alloxan-and streptozotocin-induced diabetes. *Diabetologia*, 51(2), 216-226.
- Lillelund, V. H., Jensen, H. H., Liang, X., & Bols, M. (2002). Recent developments of transition-state analogue glycosidase inhibitors of non-natural product origin. *Chemical Reviews*, 102(2), 515-554.
- Lineweaver, H., & Burk, D. (1934). The determination of enzyme dissociation constants. *Journal of the American Chemical Society*, 56(3), 658-666.
- Love, D. C., & Hanover, J. A. (2005). The hexosamine signaling pathway: deciphering the "O-GlcNAc code". *Science Signaling*, 2005(312), re13-re13.
- Lynd, L. R., Cushman, J. H., Nichols, R. J., & Wyman, C. E. (1991). Fuel ethanol from cellulosic biomass. *Science*, 251(4999), 1318-1323.
- Ma, X., Liu, P., Yan, H., Sun, H., Liu, X., Zhou, F., & Wang, P. G. (2013). Substrate specificity provides insights into the sugar donor recognition mechanism of O-GlcNAc transferase (OGT). *PloS One*, 8(5), e63452.
- Macauley, M. S., & Vocadlo, D. J. (2009). Enzymatic characterization and inhibition of the nuclear variant of human O-GlcNAcase. *Carbohydrate Research*, 344(9), 1079-1084.

- Macauley, M. S., Shan, X., Yuzwa, S. A., Gloster, T. M., & Vocadlo, D. J. (2010). Elevation of Global O-GlcNAc in rodents using a selective O-GlcNAcase inhibitor does not cause insulin resistance or perturb glucohomeostasis. *Chemistry & Biology*, 17(9), 949-958.
- Macauley, M. S., Whitworth, G. E., Debowski, A. W., Chin, D., & Vocadlo, D. J. (2005). O-GlcNAcase uses substrate-assisted catalysis Kinetic analysis and development of highly selective mechanism-inspired inhibitors. *Journal of Biological Chemistry*, 280(27), 25313-25322.
- Macdonald, J. M., Tarling, C. A., Taylor, E. J., Dennis, R. J., Myers, D. S., Knapp, S., & Withers, S. G. (2010). Chitinase inhibition by chitobiose and chitotriose thiazolines. *Angewandte Chemie International Edition*, 49(14), 2599-2602.
- Mark, B. L., Vocadlo, D. J., Knapp, S., Triggs-Raine, B. L., Withers, S. G., & James, M. N. (2001). Crystallographic evidence for substrate-assisted catalysis in a bacterial β -hexosaminidase. *Journal of Biological Chemistry*, 276(13), 10330-10337.
- McCarter, J. D., & Withers, G. S. (1994). Mechanisms of enzymatic glycoside hydrolysis. *Current Opinion in Structural Biology*, 4(6), 885-892.
- McKay, C. S., & Finn, M. G. (2014). Click chemistry in complex mixtures: bioorthogonal bioconjugation. *Chemistry & Biology*, 21(9), 1075-1101.
- McNaught, A. D. (1996). Nomenclature of carbohydrates (IUPAC Recommendations 1996). *Pure and Applied Chemistry*, 68(10), 1919-2008.
- Merzendorfer, H., & Zimoch, L. (2003). Chitin metabolism in insects: structure, function and regulation of chitin synthases and chitinases. *Journal of Experimental Biology*, 206(24), 4393-4412.
- Michaelis, L., & Menten, M. L. (1913). Die kinetik der invertinwirkung. *Biochemische Zeitschrift*, 49(333-369), 352.
- Molohon, K. J., Blair, P. M., Park, S., Doroghazi, J. R., Maxson, T., Hershfield, J. R., & Mitchell, D. A. (2016). Plantazolicin is an ultranarrow-spectrum antibiotic that targets the Bacillus anthracis membrane. *ACS Infectious Diseases*, 2(3), 207-220.
- Mühlen, S., & Dersch, P. (2015). Anti-virulence strategies to target bacterial infections. *Current Topics in Microbiology and Immunology*, 398, 147-183.
- Munkley, J., Mills, I.G., & Elliott, D.J. (2016) The role of glycans in the development and progression of prostate cancer. *Nature Reviews Urology*, 13, 324.

- Muramatsu, H., Tachikui, H., Ushida, H., Song, X. J., Qiu, Y., Yamamoto, S., & Muramatsu, T. (2001). Molecular cloning and expression of endo- β -N-acetylglucosaminidase D, which acts on the core structure of complex type asparagine-linked oligosaccharides. *Journal of Biochemistry*, 129(6), 923-928.
- Nambu, T., Minamino, T., Macnab, R. M., & Kutsukake, K. (1999). Peptidoglycan-Hydrolyzing Activity of the FlgJ Protein, Essential for Flagellar Rod Formation in *Salmonella typhimurium*. *Journal of Bacteriology*, 181(5), 1555-1561.
- Nelson, D. L., & Cox, M. M. (2008). Glycolysis, gluconeogenesis, and the pentose phosphate pathway. *Lehninger, Principles of Biochemistry*, 521-559.
- Noguchi, M., Kobayashi, A., & Shoda, S. I. (2015). The One-step Preparation of Sugar Oxazoline Enables the Synthesis of Glycoprotein Having a Definite Structure. *Trends in Glycoscience and Glycotechnology*, 27(158), E35-E42.
- Nuermberger, E. L., & Bishai, W. R. (2004). Antibiotic resistance in *Streptococcus pneumoniae*: what does the future hold?. *Clinical Infectious Diseases*, 38(Supplement 4), S363-S371.
- Orihuela, C. J., Radin, J. N., Sublett, J. E., Gao, G., Kaushal, D., & Tuomanen, E. I. (2004). Microarray analysis of pneumococcal gene expression during invasive disease. *Infection and Immunity*, 72(10), 5582-5596.
- Oudar, J. (1980). Sulfur adsorption and poisoning of metallic catalysts. *Catalysis Reviews—Science and Engineering*, 22(2), 171-195.
- Perez, S. (2016). Glycopedia. <http://www.glycopedia.eu/e-chapters/the-symbolic-representation-of/article/at-the-instigation-of-glycobiology>, accessed on April 10, 2017.
- Pérez-Dorado, I., Galan-Bartual, S., & Hermoso, J. A. (2012). Pneumococcal surface proteins: when the whole is greater than the sum of its parts. *Molecular Oral Microbiology*, 27(4), 221-245.
- Piszkiewicz, D., & Bruice, T. C. (1967). Glycoside hydrolysis. I. Intramolecular acetamido and hydroxyl group catalysis in glycoside hydrolysis. *Journal of the American Chemical Society*, 89(24), 6237-6243.
- Piszkiewicz, D., & Bruice, T. C. (1968a). Glycoside hydrolysis. II. Intramolecular carboxyl and acetamido group catalysis in β -glycoside hydrolysis. *Journal of the American Chemical Society*, 90(8), 2156-2163.
- Piszkiewicz, D., & Bruice, T. C. (1968b). Glycoside hydrolysis. III. Intramolecular acetamido group participation in the specific acid catalyzed hydrolysis of methyl 2-acetamido-2-deoxy- β -D-glucopyranoside. *Journal of the American Chemical Society*, 90(21), 5844-5848.

- Rasko, D. A., & Sperandio, V. (2010). Anti-virulence strategies to combat bacteria-mediated disease. *Nature Reviews Drug Discovery*, 9(2), 117-128.
- Reardon, S. (2014). Antibiotic resistance sweeping developing world. *Nature*, 509(7499), 141.
- Rico-Lastres, P., Díez-Martínez, R., Iglesias-Bexiga, M., Bustamante, N., Aldridge, C., Heseck, D., & García, P. (2015). Substrate recognition and catalysis by LytB, a pneumococcal peptidoglycan hydrolase involved in virulence. *Scientific Reports*, 5.
- Ritter, T. K., & Wong, C. H. (2001). Synthesis of N-acetylglucosamine thiazoline/lipid II hybrids. *Tetrahedron Letters*, 42(4), 615-618.
- Robb, M., Hobbs, J. K., Woodiga, S. A., Shapiro-Ward, S., Suits, M. D., McGregor, N., & Boraston, A. B. (2017). Molecular Characterization of N-glycan Degradation and Transport in *Streptococcus pneumoniae* and Its Contribution to Virulence. *PLoS Pathogens*, 13(1), e1006090.
- Robb, M., Robb, C. S., Higgins, M. A., Hobbs, J. K., Paton, J. C., & Boraston, A. B. (2015). A second β -hexosaminidase encoded in the *Streptococcus pneumoniae* genome provides an expanded biochemical ability to degrade host glycans. *Journal of Biological Chemistry*, 290(52), 30888-30900.
- Round, J. L., & Mazmanian, S. K. (2009). The gut microbiota shapes intestinal immune responses during health and disease. *Nature Reviews Immunology*, 9(5), 313-323.
- Roure, S., Bonis, M., Chaput, C., Ecobichon, C., Mattox, A., Barrière, C., & Labigne, A. (2012). Peptidoglycan maturation enzymes affect flagellar functionality in bacteria. *Molecular Microbiology*, 86(4), 845-856.
- Santana, A. G., Vadlamani, G., Mark, B. L., & Withers, S. G. (2016). N-Acetyl glycals are tight-binding and environmentally insensitive inhibitors of hexosaminidases. *Chemical Communications*.
- Schramm, V. L. (1998). Enzymatic transition states and transition state analog design. *Annual Review of Biochemistry*, 67(1), 693-720.
- Seeberger, P. H., & Rademacher, C. (2014). *Carbohydrates as Drugs* (Vol. 12). Springer.
- Shaikh, F. A., & Withers, S. G. (2008). Teaching old enzymes new tricks: engineering and evolution of glycosidases and glycosyltransferases for improved glycoside synthesis. *Biochemistry and Cell Biology*, 86(2), 169-177.

- Shi, Y. (2014). A glimpse of structural biology through X-ray crystallography. *Cell*, 159(5), 995-1014.
- Siemieniuk, R. A., Gregson, D. B., & Gill, M. J. (2011). The persisting burden of invasive pneumococcal disease in HIV patients: an observational cohort study. *BMC Infectious Diseases*, 11(1), 314.
- Slémové, K., & Kien, V. (2013). BN-Acetylhexosaminidases: group-specific inhibitors wanted. *Carbohydrate Chemistry*, 39, 102.
- Soderberg, T. (2016). *Organic Chemistry with a Biological Emphasis* (Vol. 1). University of Minnesota, Morris Creative Commons.
- Soriano del Amo, D., Wang, W., Jiang, H., Besanceney, C., Yan, A. C., Levy, M., & Wu, P. (2010). Biocompatible copper (I) catalysts for in vivo imaging of glycans. *Journal of the American Chemical Society*, 132(47), 16893-16899.
- Spiteri, C., & Moses, J. E. (2010). Copper-Catalyzed Azide–Alkyne Cycloaddition: Regioselective Synthesis of 1, 4, 5-Trisubstituted 1, 2, 3-Triazoles. *Angewandte Chemie International Edition*, 49(1), 31-33.
- Stubbs, K. A., Balcewich, M., Mark, B. L., & Vocadlo, D. J. (2007). Small molecule inhibitors of a glycoside hydrolase attenuate inducible AmpC-mediated β -lactam resistance. *Journal of Biological Chemistry*, 282(29), 21382-21391.
- Suzuki, K., Iseki, E., Katsuse, O., Yamaguchi, A., Katsuyama, K., Aoki, I., & Kosaka, K. (2003). Neuronal accumulation of α - and β -synucleins in the brain of a GM2 gangliosidosis mouse model. *Neuroreport*, 14(4), 551-554.
- Terwisscha van Scheltinga, A. C., Armand, S., Kalk, K. H., Isogai, A., Henrissat, B., & Dijkstra, B. W. (1995). Stereochemistry of chitin hydrolysis by a plant chitinase/lysozyme and x-ray structure of a complex with allosamidin evidence for substrate assisted catalysis. *Biochemistry*, 34(48), 15619-15623.
- Uttamapinant, C., Tangpeerachaikul, A., Grecian, S., Clarke, S., Singh, U., Slade, P., & Ting, A. Y. (2012). Fast, Cell-Compatible Click Chemistry with Copper-Chelating Azides for Biomolecular Labeling. *Angewandte Chemie*, 124(24), 5954-5958.
- Varki, A. (1993). Biological roles of oligosaccharides: all of the theories are correct. *Glycobiology*, 3(2), 97-130.
- Varki, A., Cummings, R., Esko, J., Freeze, H., Hart, G., & Marth, J. (1999). Essentials of Glycobiology, 1999. *Cold Spring Harbor Laboratory Press, New York*.
- Varki, A., Cummings, R.D., Esko, J.D., Freeze, H.H., Stanley, P., Marth, J.D., Bertozzi, C.R., Hart, G.W., & Etzler, M.E. (2009). Symbol nomenclature for glycan representation. *Proteomics*, 9(24), 5398.

- Vocadlo, D. J. (2012). O-GlcNAc processing enzymes: catalytic mechanisms, substrate specificity, and enzyme regulation. *Current Opinion in Chemical Biology*, 16(5), 488-497.
- Vocadlo, D. J., & Withers, S. G. (2005). Detailed comparative analysis of the catalytic mechanisms of β -N-acetylglucosaminidases from families 3 and 20 of glycoside hydrolases. *Biochemistry*, 44(38), 12809-12818.
- Vocadlo, D. J., Withers, S. G., Ernst, B., Hart, G. W., & Sinaý, P. (2000). Glycosidase-catalysed oligosaccharide synthesis. *Carbohydrates in Chemistry and Biology*, 724-844.
- Weiss, W. A., Taylor, S. S., & Shokat, K. M. (2007). Recognizing and exploiting differences between RNAi and small-molecule inhibitors. *Nature Chemical Biology*, 3(12), 739-744.
- Whitworth, G. E., Macauley, M. S., Stubbs, K. A., Dennis, R. J., Taylor, E. J., Davies, G. J., & Vocadlo, D. J. (2007). Analysis of PUGNAc and NAG-thiazoline as transition state analogues for human O-GlcNAcase: mechanistic and structural insights into inhibitor selectivity and transition state poise. *Journal of the American Chemical Society*, 129(3), 635-644.
- Wilkinson, G. N. (1961). Statistical estimations in enzyme kinetics. *Biochemical Journal*, 80(2), 324.
- Withers, S. (2016). Anomeric centre (alpha and beta). CAZypedia. [https://www.cazypedia.org/index.php/Absolute-_configuration_\(D/L_nomenclature\)](https://www.cazypedia.org/index.php/Absolute-_configuration_(D/L_nomenclature)), accessed on 4/10/2017.
- Wuts, P. G., & Greene, T. W. (2006). *Greene's protective groups in organic synthesis*. John Wiley & Sons.
- Yagi, T., Hisada, R., & Shibata, H. (1989). 3, 4-Dinitrophenyl N-acetyl- β -d-glucosaminide, a synthetic substrate for direct spectrophotometric assay of N-acetyl- β -d-glucosaminidase or N-acetyl- β -d-hexosaminidase. *Analytical Biochemistry*, 183(2), 245-249.
- Yamamoto, S., Muramatsu, H., & Muramatsu, T. (2005). Mutational studies on endo- β -N-acetylglucosaminidase D which hydrolyzes core portion of asparagine-linked complex type oligosaccharides. *Glycoconjugate Journal*, 22(1-2), 35-42.
- Yang, H., Wang, H., Shivalila, C. S., Cheng, A. W., Shi, L., & Jaenisch, R. (2013). One-step generation of mice carrying reporter and conditional alleles by CRISPR/Cas-mediated genome engineering. *Cell*, 154(6), 1370-1379.

- Yuzwa, S. A., Macauley, M. S., Heinonen, J. E., Shan, X., Dennis, R. J., He, Y., & Vocadlo, D. J. (2008). A potent mechanism-inspired O-GlcNAcase inhibitor that blocks phosphorylation of tau in vivo. *Nature Chemical Biology*, 4(8), 483-490.
- Yuzwa, S. A., & Vocadlo, D. J. (2014). O-GlcNAc and neurodegeneration: biochemical mechanisms and potential roles in Alzheimer's disease and beyond. *Chemical Society Reviews*, 43(19), 6839-6858.
- Yuzwa, S. A., Cheung, A. H., Okon, M., McIntosh, L. P., & Vocadlo, D. J. (2014). O-GlcNAc modification of tau directly inhibits its aggregation without perturbing the conformational properties of tau monomers. *Journal of Molecular Biology*, 426(8), 1736-1752.
- Yuzwa, S. A., Macauley, M. S., Heinonen, J. E., Shan, X., Dennis, R. J., He, Y., & Vocadlo, D. J. (2008). A potent mechanism-inspired O-GlcNAcase inhibitor that blocks phosphorylation of tau in vivo. *Nature Chemical Biology*, 4(8), 483-490.
- Zaloba, P., Bailey-Elkin, B. A., Derksen, M., & Mark, B. L. (2016). Structural and Biochemical Insights into the Peptidoglycan Hydrolase Domain of FlgJ from *Salmonella typhimurium*. *PloS One*, 11(2), e0149204.
- Zasloff, M. (2002). Antimicrobial peptides of multicellular organisms. *Nature*, 415(6870), 389-395.
- Zhou, G. Q., & Zhong, W. Z. (1982). Diffusion-Controlled Reactions of Enzymes. *European Journal of Biochemistry*, 128(2-3), 383-387.
- Zhu, Y., Liu, T. W., Cecioni, S., Eskandari, R., Zandberg, W. F., & Vocadlo, D. J. (2015). O-GlcNAc occurs cotranslationally to stabilize nascent polypeptide chains. *Nature Chemical Biology*, 11(5), 319-325.
- zur Wiesch, P. S., Engelstädter, J., & Bonhoeffer, S. (2010). Compensation of fitness costs and reversibility of antibiotic resistance mutations. *Antimicrobial Agents and Chemotherapy*, 54(5), 2085-2095.